ERRATUM

Substitute in Figures II.4 and II.5 the word "Composite sand body" by "Reservoir unit" and the word " Single sand body" by "Genetic unit".

C.A.Hartkamp-Bakker

STELLINGEN

1) Het is opmerkelijk dat het percentage van geïnterpreteerde rechtkammige ribbels in kernen van fluviatiele zandsteenreservoirs vele malen hoger ligt dan hun voorkomen in outcrops van fluviatiele zanden.
(log-interpretaties bij RGD en NAM kernen)

2) Lage opbrengst uit distributary channel-fills zal, naast andere heterogeniteiten, veroorzaakt kunnen worden door baffles (clay-draping) op sedimentaire-structuren schaal.
(Hoofdstuk I & II van dit proefschrift)

3) Het feit dat het publiceren van werk waarbij gebruik gemaakt is van de minipermeameter, een uitgebreide verhandeling over de werking, accuratesse en calibratie vereist, terwijl de eveneens gebruikte binoculaire microscoop geen uitleg behoeft, geeft aan dat na ruim twintig jaar de minipermeameter binnen de wetenschap nog geen volwassen status heeft.
(Hoofdstuk III A & B van dit proefschrift)

4) De kwaliteit van resultaten van een simulatie van vloeistofstroming door een geologische formatie, uitgevoerd door een reservoir engineer, wordt vooral bepaald door de terugkoppeling van deze resultaten naar de geoloog.
(Kortekaas, T.F.M., 1985, Water/oil displacement characteristics in cross-bedded reservoir zones., Soc. of Petrol. Eng. Journ., December, 917-926)

5) Iedere heterogeniteit in een reservoir, waarbij een contrast in permeabiliteit bestaat, heeft een invloed op het achterblijven van winbare olie tijdens water/olie verdringing.
(Hoofdstuk V van dit proefschrift)

6) Bij een studie naar water/olie verdringing door een geologisch complexe heterogeniteit kan men uit een eenvoudig numeriek model meer concluderen dan uit een model dat de werkelijkheid nastreeft.
(Hoofdstuk V van dit proefschrift)

7) Opschalen van het effect van cross-beds op water/olie verdringing is alleen dan mogelijk als alle facetten die een rol spelen bij het proces van capillair achterblijven van winbare olie in cross-beds door experimentele en numerieke modellen onderzocht zijn en de tijdseffecten voor een reservoir met bepaalde contrasten in permeabiliteit bekend zijn.

8) Scheef-gelaagde sets in fossiele rivierafzettingen in sterk vervuilde delen van de Nederlandse ondergrond kunnen op grond van de in dit proefschrift beschreven principes, bij sanering door uitspoeling met te geringe tijdsduur, leiden tot het achterblijven van vervuiling in de rivierafzettingen.

9) Conclusies die niet het eigen werk reflecteren maar zijn gebaseerd op een foute interpretatie van andermans werk zijn wetenschappelijk gezien van nul en gener waarde.

10) Het is niet bevorderlijk voor de aanvraag van een promotie indien de aanvraag zelf te goed opgeborgen ligt in een kastje van de promotor.

11) De verkeersproblematiek van de steeds drukkere Haagse binnenstad leidt tot een voortdurend groter wordende agressie en anarchie bij de automobilist en zal uiteindelijk alleen beheerst kunnen worden door het vervangen van stoplichten door slagbomen.

12) Om de toekenning van subsidies, bedoeld om de Nederlandse binnensteden leefbaar te houden, met de zelfde voortvarendheid te laten geschieden als de subsidies van bedrijven aan dit promotie onderzoek dient de slagvaardigheid van de desbetreffende overheden met tenminste een factor 10 vergroot te worden.

Permeability heterogeneity in cross-bedded sandstones
Impact on water/oil displacement in fluvial reservoirs

Proefschrift

ter verkrijging van de graad van doctor
aan de Technische Universiteit Delft,
op gezag van de Rector Magnificus, Prof. ir. K.F. Wakker,
in het openbaar te verdedigen ten overstaan van
een commissie aangewezen door het College van Dekanen
op dinsdag 7 september 1993 te 10.00 uur

door

Christel Alexandra Hartkamp-Bakker
geboren te Harderwijk
doctorandus in de wis- en natuurwetenschappen

Dit proefschrift is goedgekeurd door de promotor:

Prof. ir. K.J. Weber

Published by:
Krips repro meppel
Postbus 1106
7940 KC Meppel
The Netherlands

English corrector:
T. van de Graaff-Trouwborst (THEMA GEOLOGICA)
Sir W. Churchilllaan 1009a
2286 AD Rijswijk
The Netherlands

ISBN 90-9006383-8

Voor Ria en Ada.

Cover page: Drawing based on outcrops of a cross-bedded low-sinuosity channel fill near Huete, Loranca Basin, Central Spain. The drawing represents a model of a cross-bedded fluvial channel-fill reservoir with an imaginary bore hole and permeability profile.

TABLE OF CONTENTS

ABSTRACT

Reservoir heterogeneity is a major control on the non-uniform distribution of unrecovered oil after water flooding. In fluvial sandstone reservoirs, high percentages of movable oil remain to be recovered after passing of a flood front. The objective of this study is to increase the understanding of one specific type of heterogeneity: cross-bedding, and the effect of this sedimentary structure and its internal fabrics exert on by-passing of movable oil.

Fluvial deposits are commonly extensively cross-bedded. In cross-beds, bottomsets are invariably finer grained and better sorted than the bulk of the foreset. Adjacent foreset laminae show remarkably sharp contacts in distinctive grain size and sorting. On average the grain size of finer-grained and coarser-grained foreset laminae differs a factor 1.5 with the latter being more poorly sorted. The contrasting grain size, sorting and framework composition of adjacent foreset laminae in combination with the bottomsets result in a considerable permeability heterogeneity.

Studies were done by measuring permeabilities in outcrop and on cores by minipermeameter. The outcrop measurements of permeabilities in fluvial sandstones ranged from 0.5 to 20 Darcy. Permeabilities measured on reservoir cores of Dutch gas fields yielded values ranging from 10 millidarcy up to several hundreds of millidarcy. Average permeability contrasts between bottomset layers and those foreset laminae that are coarser grained were found to vary a factor 2 in outcrop and between a factor 2 to 30 in reservoir cores. The higher contrasts in reservoir cores are the result of different proportions of pore-filling minerals (kaolinite) and cement (anhydrite) in the foreset laminae and the bottomset.

Grain size and sorting determine the pore size and pore-size distribution and hence, define capillary-pressure characteristics in separate laminae and bottomsets. In a water-wet oil reservoir, the influence of capillary pressure is most apparent at the water/oil front under a weak water drive. Adjoining zones of contrasting capillary-pressure characteristics determine both initial and residual water/oil saturations. Computer simulations and laboratory experiments show that movable oil is initially trapped in coarser-grained laminae when the surrounding finer-grained laminae and bottomsets are flushed to approximately maximum water saturations in a non-zero capillary-pressure situation. Sorting of the sand and the

related pore-size distributions in the different sub-facies defines water/oil saturation in the coarser-grained foreset laminae at the moment entrapment is initiated.

In the physical and numerical models, a permeability contrast of a factor 25 was modelled between bottomsets and coarser-grained laminae. In the laboratory experiments, almost identical viscosities for oil and water were selected to create a smooth flood front. Initial entrapment occurred after injection of 0.77 pore volumes of water. The initially trapped movable oil was ultimately flooded to residual oil saturation. Five to seven pore volumes of water were needed to reach this ultimate situation. Flooding direction or geometrical characteristics of the cross-bedded region did not affect initial entrapment behaviour under non-gravity model conditions. A higher flooding rate increased the displacement of initially trapped movable oil.

INTRODUCTION

Increasing oil recovery

Oil is a finite resource, as is presently most evident in the USA and Rumania where the history of oil industry is longest. Of particular concern is that on average less than half of the oil originally present in a reservoir is normally recovered. Maximising recovery of this precious but finite resource is therefore of critical importance to our industrial society. Research at the Faculty of Mining and Petroleum Engineering at the Delft University of Technology focuses on ways to improve development and recovery of the oil and gas resources. This thesis forms part of this overall effort and describes the small scale geological characteristics of a common type of sandstone reservoir: fluvial channel fills. Description of the geological characteristics of reservoirs is important since the geological features of a reservoir largely determine the way oil and gas flow through the reservoir rock towards the wells. Understanding these flow characteristics is an essential basis for optimising oil and gas recovery from a subsurface reservoir.

Reservoir heterogeneity and oil recovery

Oil is recovered from the subsurface by drilling wells into porous rocks in which oil and gas have accumulated over geological time. The recovery efficiency of oil from a reservoir depends on a combination of technical and economic factors. The essential technical factors are: 1) reservoir heterogeneity, 2) recovery processes and 3) well trajectory and spacing. The most common recovery process is displacement of the oil by water, either through natural expansion of water in an aquifer or by an artificial water drive. The importance of reservoir heterogeneity as a prime control on oil recovery by water drive has been shown by e.g. Tyler (1988). Using well-documented Texas oil fields as examples, Tyler demonstrated that the more heterogeneous a reservoir, the lower the recovery. A heterogeneous reservoir typically results in a nonuniform distribution of

unrecovered oil after water drive (Weber 1986).

Reservoir heterogeneity occurs over a scale range from kilometres to micrometres. At reservoir scale, large faults and boundaries between genetic sediment bodies largely determine areal sweep. After the oil has been produced unswept zones, which were either areally by-passed or originally disconnected, are left. Macroscopic heterogeneities such as permeability zonation and baffles in genetic sediment bodies affect both vertical and horizontal sweep and commonly result in vertically by-passed zones. At a sedimentary-structure scale, cross-bedding, laminations, and small fractures control the by-passed of oil in a water-swept rock volume. Microscopic heterogeneity is the variability on pore and pore-throat scale and determines the residual-oil saturation within the swept zones. Such residual oil is not movable in a water/oil displacement process. By-passed oil determined by non-microscopic heterogeneities is non-residual and hence movable at reservoir conditions. It is this movable oil, left in incompletely drained reservoirs that forms an immediately available resource for infield re-development.

Tyler (1988) demonstrated for Texas fields that in typical fluvial reservoirs 43% and in fluvial-dominated deltaic reservoirs 27% of the originally present movable oil is left. Many important oil fields in the world produce from fluvial reservoirs, such as the Bolivar Coast and Lake Maracaibo in Venezuela, the Llanos area in Colombia, the Niger delta, Alaska North Slope and the North Sea, these fields contain a total of several tens of billions of barrels of oil-in-place. Thus the scope for increasing recovery from fluvial reservoirs is very large. Our immediate research objective is therefore to increase our understanding of the internal architecture of such fluvial reservoirs and the way the geological characteristics control retention of movable oil.

Heterogeneity of fluvial channel sand reservoirs

The most common types of heterogeneities that affect recovery from fluvial channel-fill reservoirs are: 1) On a reservoir scale; the degree of interconnectedness of stacked fluvial channel-fill sand bodies, 2) On a macroscopic scale; compartmentalization of channel-fills by permeability barriers such as mud drapes deposited during channel migration or clay

plugs deposited during channel abandonment, 3) On a sedimentary-structure scale at which this study focuses; trough cross-bedding occurring abundantly in the channel-fill sands. After water flooding, channel-fill reservoirs are typically well-swept in the lower parts of the channel-fill where porosity and permeability are highest. By contrast, by-passing of oil in reservoir compartments typically occurs in the upper parts of the channel-fills in which clay drapes, silt and fine-grained sand streaks form obstacles to flow and cause predominantly vertical by-passing of oil. In the well-swept lower parts of the channel fills, a significant volume of unrecovered movable oil nevertheless remains (e.g. Xue Peihua 1986). As cross-bedding occurs ubiquitously in the lower parts of channel-fills to the near exclusion of other heterogeneity types, a quantification of the effect of cross-bedding on water/oil displacement is needed to model oil recovery from such reservoirs.

Cross-beds form through the migration of large-scale ripple bed forms on the floor of the river channel. A cross-bed set consists of two genetically different facies, the foreset and the bottomset. A foreset consists of alternating inclined laminae of contrasting grain sizes. Bottomsets are typically finer grained than the overlying foreset. Fluvial channel-fill sand bodies typically consist of stacked cross-beds (Fig. 1). The bottomsets of these cross-beds are spoon shaped and usually interconnected in three dimensions. As a result, these poorly permeable bottomsets can effectively compartmentalize channel fills. The geometry of cross-beds as well as the typical laminae-scale contrasts in grain size between the different sub-facies is thought to have a significant influence on water/oil displacement (Kortekaas 1985).

Water/oil displacement through cross-beds

In a natural or artificial water drive, oil is displaced towards the producer wells under the influence of a pressure gradient. In addition to the pressure gradient, capillary pressure characteristics affect the efficiency of the recovery process. Capillary pressure is a function of the surface tensions existing between the reservoir rock and the contained fluids. Capillary pressure is determined by pore scale characteristics (pore-throat

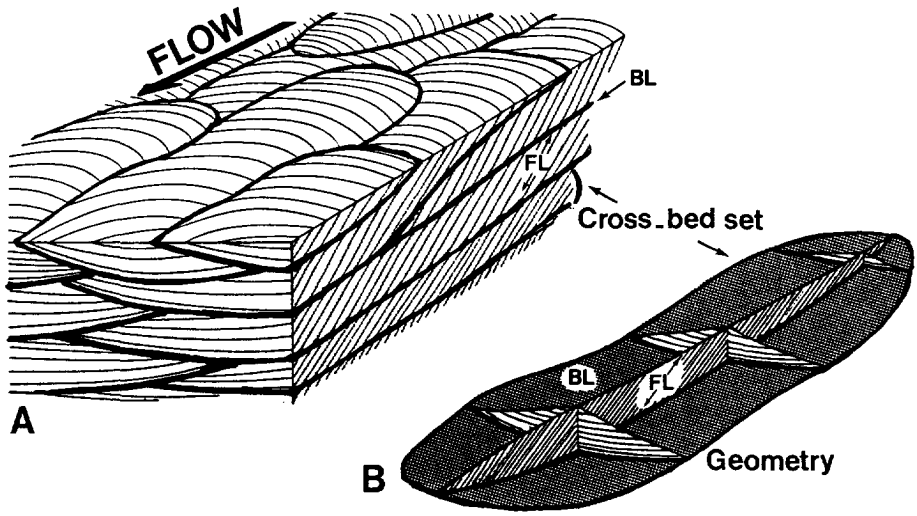

Fig. 1 A) Three dimensional model of vertically stacked trough cross-beds with distinctive bottomset (BL) and foreset (FL) facies, note the inclined laminae (indicated by small arrows) in the foreset. Thick arrow indicates the palaeo flow direction of the river. B) Typical geometry of a trough cross-bed set (modified from Weber 1982).

distribution), the oil/water/rock interaction (wettability) and the surface tension of the oil/water interface (interfacial tension). The surface forces are strongest in sediments that have small pore spaces (small capillaries). Pore sizes in clastic rocks are primarily determined by grain size and sorting. Grain-size contrasts between laminae in foresets and between foresets and bottomsets result in zones with contrasting capillary-pressure characteristics. Especially at the water/oil front under a weak water drive, capillary forces tend to imbibe water into the finer-grained parts, initially by-passing the coarser-grained laminae.

Experimental investigations of capillary-pressure effects on water/oil displacement confirm that water is imbibed faster through a finer-grained zone (Dawe *et al.* 1992). Simulation studies by Kortekaas (1985) based on cross-bed models showed that this effect

might trap oil in the coarser-grained foreset laminae. This model was based on assumed permeability distributions. It is therefore of interest to investigate the permeability contrasts occurring in nature in cross-bedded reservoirs.

Permeability is primarily controlled by pore size and pore connectedness. In clastic reservoirs, these parameters are basically controlled by grain size and sorting. Hence the regular and systematic pattern of inclined foreset laminae of alternating grain size and adjacent finer-grained bottomsets forms regions of contrasting permeability. Because capillary pressure and permeability are both related to pore size, measured contrasts in permeability directly indicate zones of contrasting capillary pressure characteristics. The relative ease of measuring permeability at small scale by minipermeameter provides a technique to characterize both permeability and capillary pressure contrasts of cross-bed laminae and associated bottomset layers. The research described in this thesis focuses on measuring permeability contrasts in fluvial channel fills at outcrop and core scale.

Study objectives

The main objective of this study is to define the influence of zones of contrasting capillary-pressure characteristics in trough cross-beds on water/oil displacement in fluvial sandstone channel-fill reservoirs. The study is restricted to displacement processes under conditions of equal mobility of oil and water. The following are addressed as part of this thesis:

1- How does the geometry of the sedimentary structure influence trapping behaviour?

2- What textural and compositional characteristics of foreset laminae and bottomsets determine permeability and capillary pressure conditions?

3- What actual permeability contrasts are likely to occur in cross-bedded sets in fluvial reservoirs? Is there a critical limit before capillary entrapment occurs at a boundary of zones of contrasting permeability?

4- What is the likelihood that the initially trapped movable oil is flooded before the economic limits of the reservoir are reached?

5- Is it possible to quantify the amounts of movable oil initially trapped in cross-

bedding?

Outline of this thesis

This study focuses on quantitatively defining the permeability/capillary-pressure characteristics in a number of well-exposed reservoir analogues and cored reservoirs by minipermeametry. Average contrasts in permeability are determined for fluvial cross-bedding and combined with thin-section studies to characterize the grain size, sorting and compositional characteristics that determine permeability contrasts. In addition capillary pressure experiments of laminated samples were carried out to study the contrasting capillary-pressure characteristics between the laminae. Water/oil displacement through cross-bedding by numerical and physical modelling were performed in close corporation with reservoir engineers to increase our understanding of the geological and physical conditions under which movable-oil entrapment occurs. Finally, the likely percentages of movable oil that are initially trapped in a cross-bedded reservoir are estimated.

CHAPTER I
FLUVIAL SANDSTONE DEPOSITS

I.1 INTRODUCTION

There is a vast literature on fluvial sandstones, however for the purpose of introducing the subject for petroleum engineers a summary of the major features has been compiled.

Fluvial channel patterns and their associated sedimentary deposits have been studied extensively for many years. Rivers are of economic importance because of the transport opportunities they provide and because their deposits are host rocks of hydrocarbons, uranium and placer minerals, e.g. gold (Galloway & Hobday 1983). Production of hydrocarbons from fluvial sands has given a new impetus to sedimentological-, geometrical-, architectural- and petrophysical studies of fluvial deposits.

Miall (1978) reviews the history of publications on geological interpretation of fluvial deposits. One of the most important works from the early days of the science of geology is Principles of Geology by Charles Lyell (1837). Lyell described river meander processes on the basis of field observations on Tertiary fluvial deposits in France. He was probably the first geologist who recognized and described fluvial cross-bedding. He notes that "the same phenomenon" is exhibited in older strata of all ages.

Many other publications on fluvial deposits followed. Most describe ancient and recent river processes and deposits. Books on fluvial sedimentology were written by e.g. Leopold and Miller (1964), Schumm (1977), Miall (1978), Collinson & Lewin (1983). Several papers described the development and deposition of sedimentary structures in fluvial deposits in detail. Joplin (1965 and 1967) studied the processes of development of current ripples in laboratory experiments.

In the first part of this chapter, details on fluvial systems, channel types and channel-fill deposits including the development of sedimentary structures are introduced. Next, several outcrop case studies are described as examples of fossil fluvial deposits.

This introductory chapter aims at giving general rules for the occurrence of cross-bedded sedimentary structures in different types of fluvial deposits.

I.2 FLUVIAL SYSTEMS; SETTING AND PATTERNS

Fluvial deposits are found in association with deposits of deserts, lakes, sabkhas and glaciers or in combination with near-shore marine deposits. Continental to near-shore deposits may be part of the basin fill of intracratonic-, rift-, foreland- and strike-slip basins (Allen & Allen 1990). Flowing from mountain ranges down to delta plains, fluvial systems may show a variety of river patterns (Fig. I.1). River patterns can be classified on the basis of the type of load transport (Schumm 1977), channel sinuosity (Leopold & Wolman 1957), or the existence of a single or multiple thalweg for braided systems (Rust 1978).

The four principal river patterns that can be distinguished according to Allen and Allen (1990) are: A) meandering, B) braided, C) straight and D) anastomosing. Channel patterns are determined by the type of load, the discharge, the slope and the vegetation.

The channel type is best classified using the degree of curvature of the channel pattern, or sinuosity, defined by Leopold & Miller (1964) as the ratio of the actual channel length to the direct down-valley length. Straight channels have essentially no curvature and hence a sinuosity of 1. Low-sinuosity channels are defined as having a sinuosity of less than 1.5, whereas high-sinuosity channels have a sinuosity equal to or greater than 1.5.

A meandering channel pattern basically consists of a single channel of high sinuosity. Local channel configurations are not consistent, and patterns may change within very short distances. Within a meander belt, channel type may vary from low- to high-sinuosity due to variations in slope or discharge.

In a braided fluvial system, low- and high-sinuousity channels occur but may vary in place and time (Olsen 1989). A braided system is characterized by a dense interweaving system of multiple channels within the depositional system. Braided channels are commonly formed in the upper parts of alluvial plains, whereas meandering channels

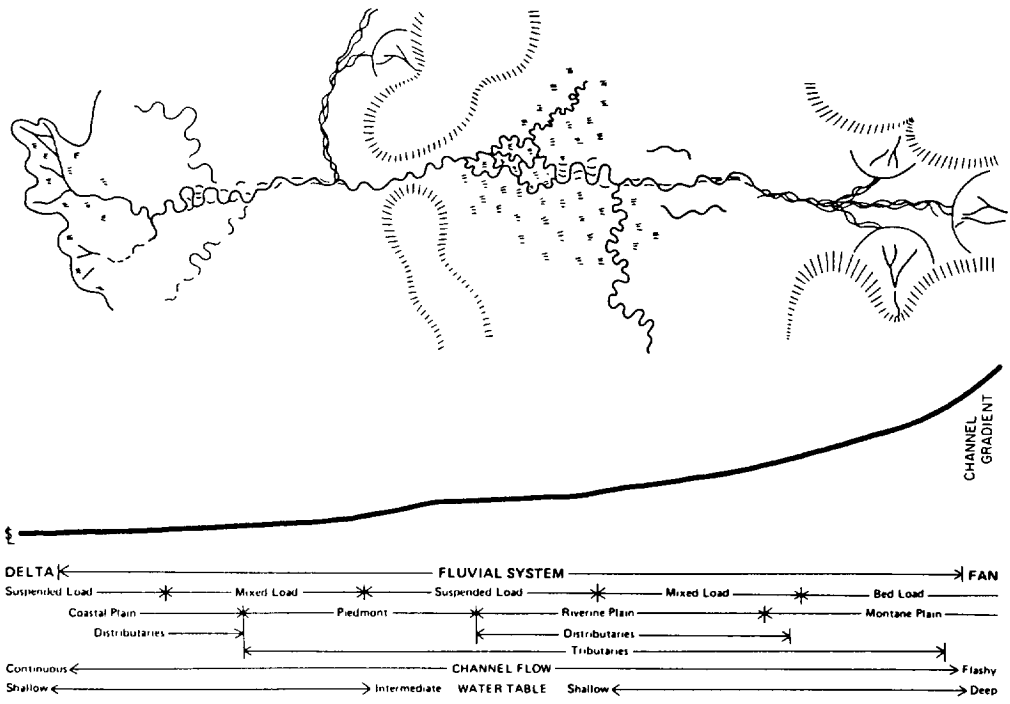

Fig. I.1 Hypothetical fluvial system and its variety in channel patterns from mountain range to delta plain (from Galloway and Hobday 1983).

generally occur in the lower parts of alluvial plains. The term anastomosing pattern is occasionally used as a synonym for braided pattern, but preferably describes a more broadly branched and joined system of channels rather than the intricate interweaving of a single channel (Schumm 1968). Anastomosing rivers usually develop in coastal lowland areas.

The pattern of multiple branching- and splaying channels that do not rejoin in a

downstream direction is generally termed a distributary system and may form on a delta plain and the upper part of an alluvial fan. The pattern typically formed on the lower part an alluvial fan is called a tributary system and is characterized by joining of multiple channels in a downstream direction.

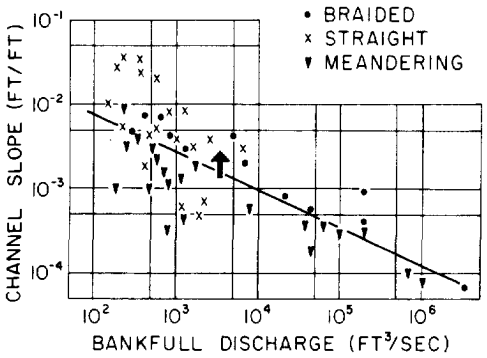

Fig. I.2 Channel patterns as function of slope and discharge in modern streams (from Leopold and Wolman 1957).

Channel patterns are classified as a function of slope and discharge by Leopold and Wolman (1957) (Fig. I.2). From this graph, they concluded that slope and discharge primarily control braided and meandering channel patterns, whereas straight channels are basically determined by geological- or geomorphological features. Figure I.3 shows the various channel patterns with a number of associated variables.

I.3 FLUVIAL CHANNEL FILLS; FACIES AND ARCHITECTURE

Fluvial depositional systems comprise a large variety of genetic facies, including channel-fill, channel-margin and flood-basin deposits. The channel-fill facies is the

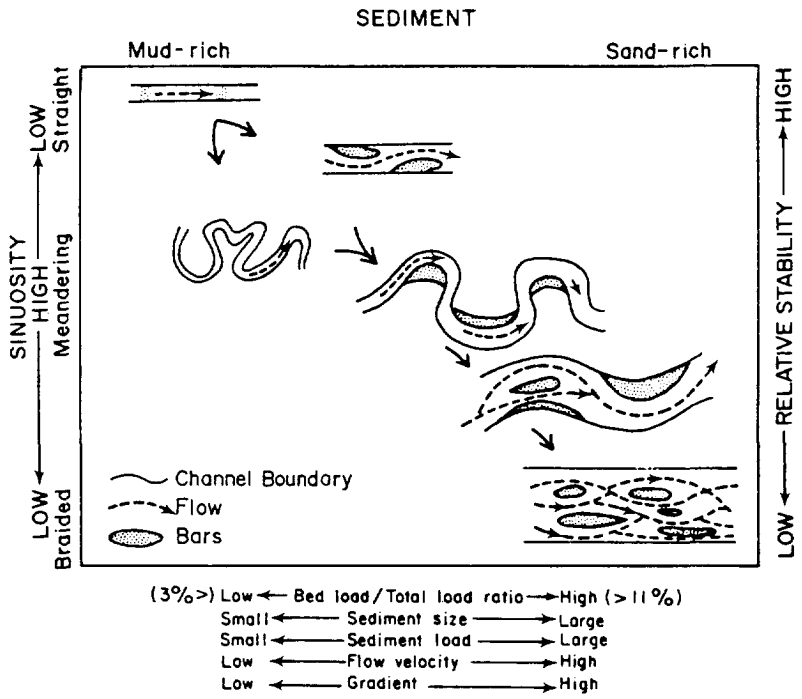

Fig. I.3 Channel patterns displayed by single-channel segments and associated variables (from Galloway and Hobday 1983).

component of the fluvial depositional system that has been studied most extensively. This facies is especially important as a potential hydrocarbon reservoir. The channel-fill facies and geometry is defined by channel patterns and associated variables. The general architecture and interconnectedness of channel-fill sand bodies depends on aggradation rate and basin subsidence (Alexander & Leeder 1987; Leeder & Alexander 1987). Stacking of subsequent channel sand bodies is related to the behaviour of the fluvial system, apart from aggradation rate and basin subsidence, it depends on the behaviour of the channels in time and size of the transported sediment (Friend 1983). River flow conditions, channel

type and the related sand-body shape is demonstrated in Fig. I.4. In this Figure I.4, typical examples of high- and low-sinuosity channel-fill and sheet sandbodies are presented. Sheet sandbodies are characteristically formed by sheet floods that do not develop incised channels (Olsen 1989). Controversially, the term "fluvial sheet sandbody" is often related to overbank deposits (crevasse) or to a complex of multilateral and multistorey high- and low-sinuosity channel deposits (Marzo *et al.* 1988).

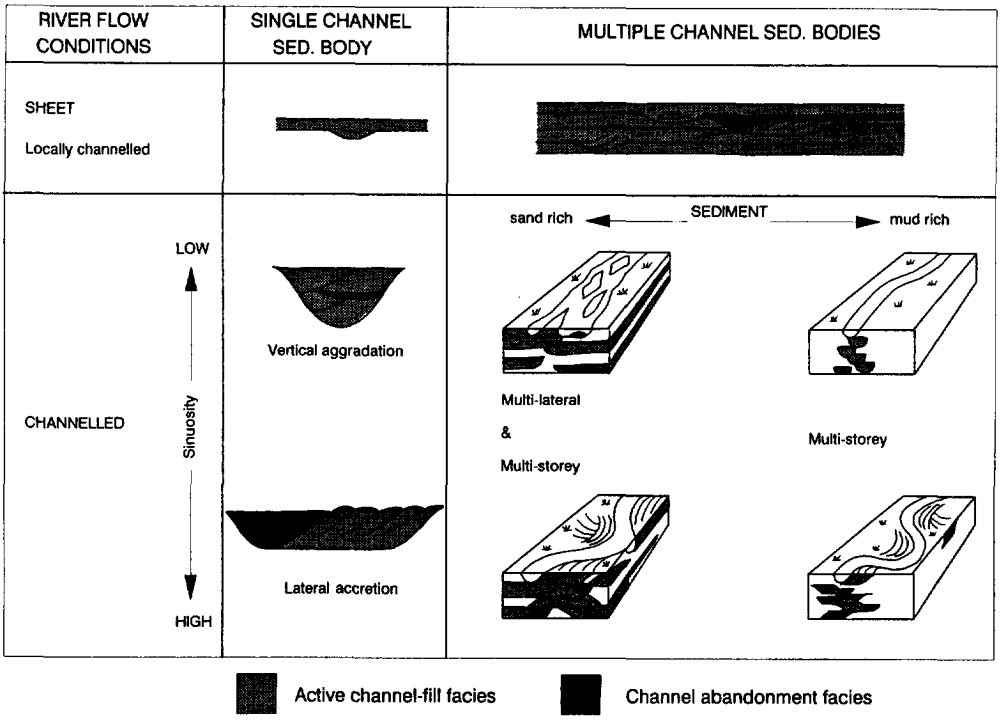

Fig. I.4 Classification of distinctive types of river flow conditions, channel type and related single and multiple channel-fill sediment bodies (modified from Friend 1983, Nio and Hussain 1984, Marzo *et al.* 1988, Olsen 1989).

I.3.1 High-sinuosity river facies model

I.3.1.1 Sand-rich, high-sinuosity channels

In a sand-rich environment, meandering rivers continuously deposit sediments in their inside bends, building out into point-bar deposits. On the outside of the river bends, cut banks are eroded continuously, resulting in lateral displacement of the channel. The channel floor commonly consists of a coarse lag of pebbles that are transported only at maximum flood velocities as bed-load sediment. As meander loops migrate laterally, point-bar deposits develop from sediment transported by helical flow within the channel. The direction of net sediment transport depends on the bed shear-stress vector (Leeder 1982). As bed shear stress decreases from point-bar toe to point-bar top, sediment size decreases upwards. This results in a classical fining-upward sequence.

Variations in bed shear stress lead to the development of distinct bed forms on the point-bar surface. Current ripples, dunes and bars are the most common bed forms. The lateral-accretion units commonly result in an upward sequence from coarse lag through trough-cross-stratified to ripple-cross-laminated deposits (Fig. I.5).

Seasonal variations in discharge and deposition of fine-grained sediment may result in the preservation of a number of point-bar slopes, dipping towards the channel axis or thalweg. These preserved surfaces form lateral accretion surfaces in point-bar deposits, called "epsilon cross-bedding" by some authors (Allen 1963). The term "epsilon cross-bedding" is a descriptive term and is not related to the process of ripple or dune deposition and the formation of cross-bedding as such and is therefore not used in this thesis. Clay drapes covering the depositional slopes are common in the upper part of the point bar but may extend into the middle, or even, rarely, into the lower part.

Individual meander-loop extensions are eventually deserted by the river either by chute cut-off or by neck cut-off. In the first type of cut-off gradual abandonment of the channel results in the deposition of thick ripple-cross-laminated sand. In the second type of cut-off (avulsion), the increased flow cutting through the narrow neck causes sudden abandonment of the channel and forms the typical ox-bow lakes in which deposition is dominated by muddy sediments forming a clay plug on top of the channel deposit.

In three dimensions the sand body may show point-bar sheets, elongated in the

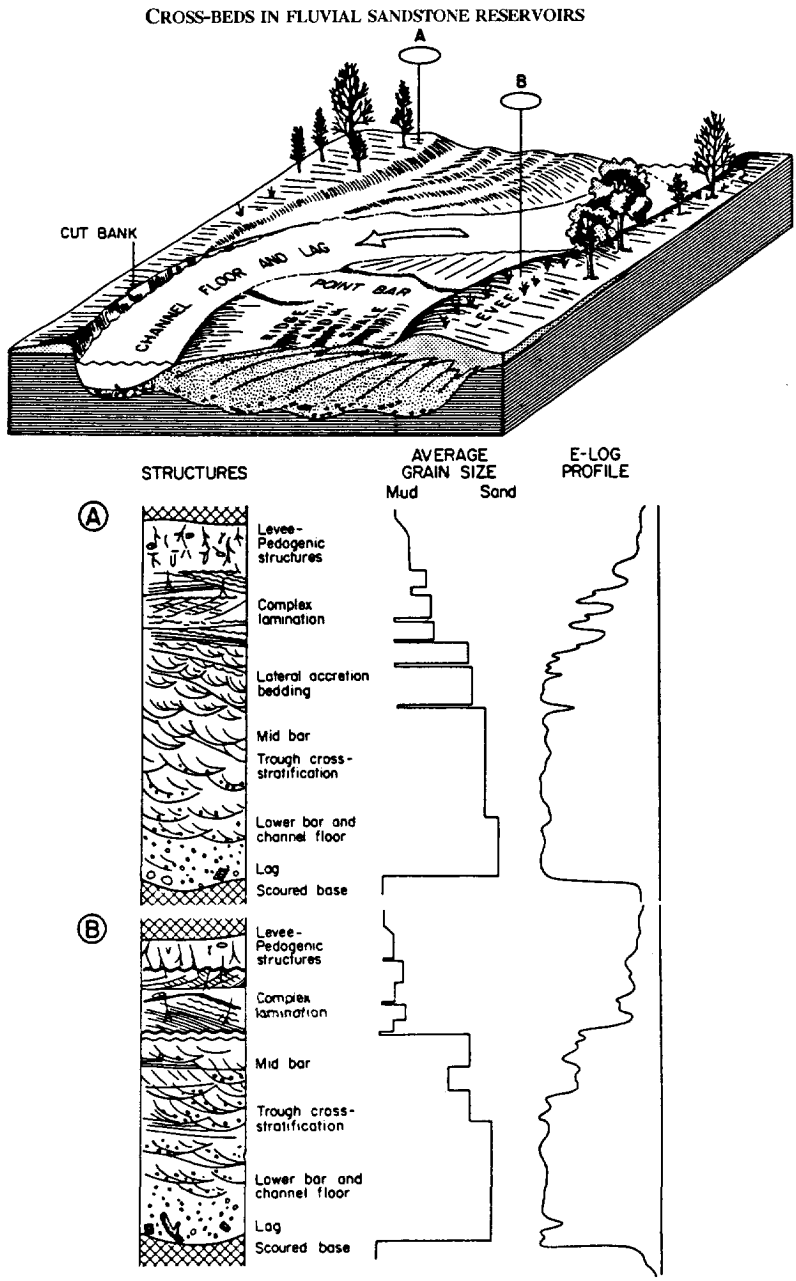

Fig. I.5 Generalized depositional model, vertical sequences of grain size and sedimentary structures, and electric (SP) log profiles of a point-bar deposit produced by a high-sinuosity channel. Sequence A illustrates a complete fining-upward sequence typical of a mid or down-stream point bar. Sequence B represents the truncated vertical sequence commonly found in the up-stream end of the bar (from Galloway and Hobday 1983). Vertical scale of the sections is generally between 10 and 30 meters (see Fig. II.10).

longitudinal direction (Fig. I.4). In the transverse direction, their extent is controlled by the rate of lateral migration of the meander loops and the duration of steady lateral migration in between abandonment phases (Allen & Allen, 1990).

I.3.1.2 Mud-rich, high-sinuosity channels

In a mudrich environment, shoestring-like channels occur as low- or high sinuosity channels (Fig. I.4). Typical examples are the delta-plain distributary-channel model and the anastomosing river model (Schumm 1968, Smith & Smith 1980).

Channels are relatively short lived. Although lateral accretion is initiated, broad point bars are rare (Kirschbaum & McCabe 1992) (Fig. I.6). Mud plugs are formed during channel abandonment. Grain size characteristically fines upward, depending on the range of grain sizes available. Large to small-scale trough cross-stratification dominates the internal structures. Structures resulting from soft-sediment deformation are common.

I.3.2 Low-sinuosity river facies model

I.3.2.1 Sand-rich, low-sinuosity channels

Sand-rich, low-sinuosity channels include a variety of specific depositional features, including lateral, transverse and longitudinal bars. Lateral bars or alternating sand bars form along the margins of low-sinuosity channel segments. Primary structures include planar and low-angle accretionary foreset bedding (Fig. I.7). Transverse bars are downstream-migrating sand bars oriented transverse to flow. During flood stages, sediment moves up the stoss side of the bar and avalanches down the lee side of the bar, where tabular cross bedding forms. The long axis of longitudinal bars is parallel to the flow. Depositional structures include horizontal stratification and low- to-moderate-angle cross stratification. The occurrence of trough cross-bedding ranges from rare to common.

Channel fills form broad, tabular, dip-oriented, multilateral sand belts (Fig. I.4). Channel-fill sequences consist predominantly of sand and are commonly conglomeratic. Vertical sequences are usually very poorly developed within bed-load channel facies. A succession of local scour surfaces, discontinuous lags, and diffuse pebble sheets may

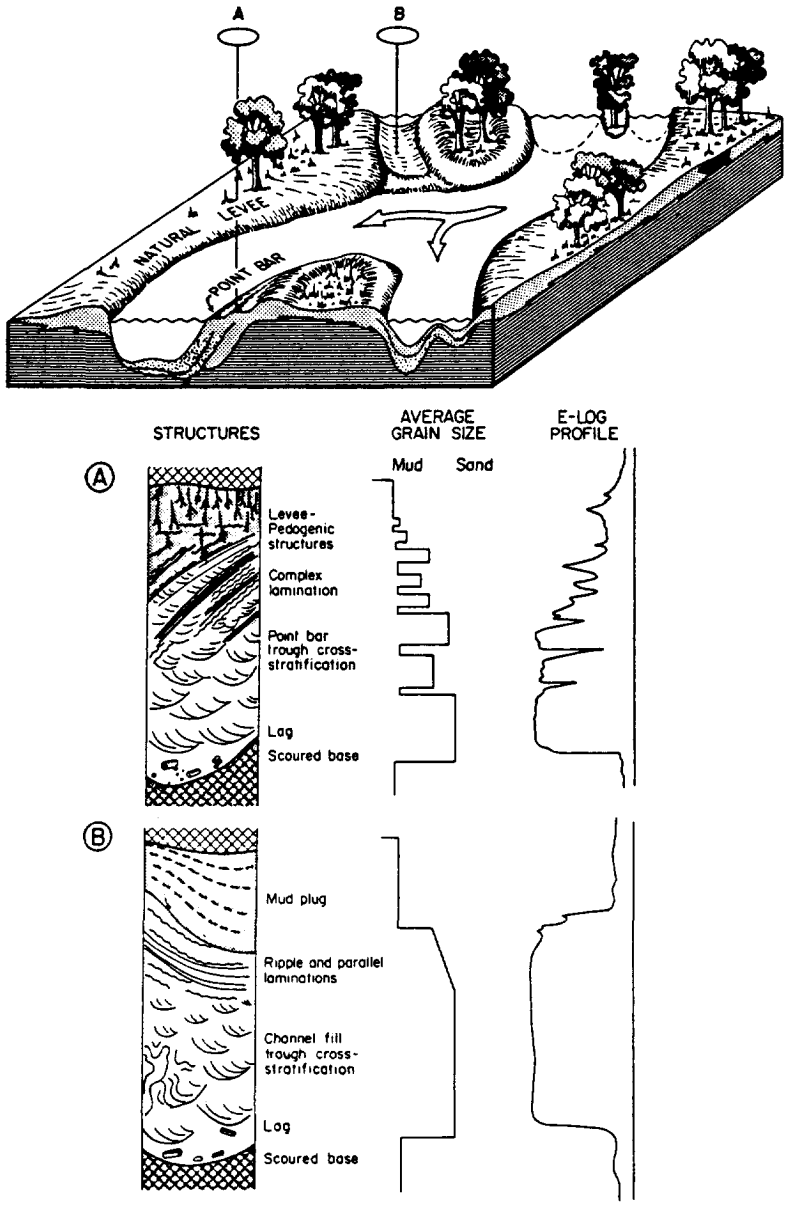

Fig. I.6 Generalized depositional model, vertical sequences of grain size and sedimentary structures, and electric (SP) log profiles of a sand-rich low-sinuosity channel deposit. Sequence A is dominated by migration of a gravelly longitudinal bar. Sequence B records deposition of successive transverse bar cross-bed sets (from Galloway and Hobday 1983). Vertical scale of the sections is generally between 3 and 45 meters (see Fig. II.10).

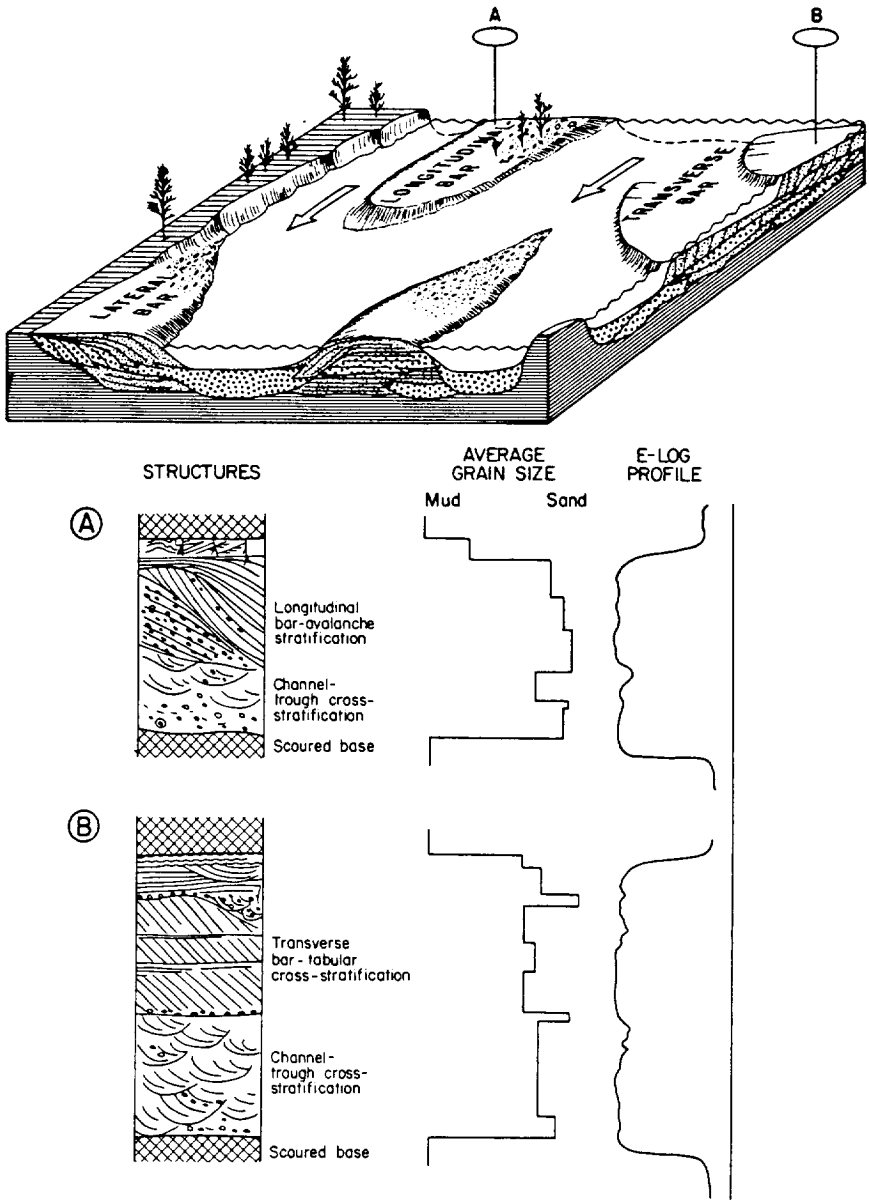

Fig. I.7 Generalized depositional model, vertical sequences of grain size and sedimentary structures, and electric (SP) log profiles of a mud-rich high-sinuosity channel deposit. Sequence A shows a profile through a lateral-accretion sand body. Sequence B represents an abandoned-channel sequence (from Galloway and Hobday 1983). Vertical scale of the sections is generally between 3 and 45 meters (see Fig. II.10).

occur within a single sand body.

I.3.2.2 Mud-rich, low-sinousity channels

Mud-rich low-sinuosity channel deposits typically show highly convex and symmetrical cross-sections (Fig. I.4). Channel-fill sequences form dip-elongated, narrow, lenticular units (shoestring sandbodies). Coarse material is typically sparse, but may include gravel and intraclasts. The channels are predominantly filled by vertical aggradation. Sediments are typically fining upwards. Cross-bedding is usually present.

I.3.3 Fluvial interaction

Fluvial systems occur in combination with other depositional environments such as aeolian, lacustrine or near-shore marine environments. Deposition may have been controlled or altered by non-fluvial influences. Details on fluvial interaction and the consequences for reservoir heterogeneity can be found in Allen & Allen (1990). North (1989) described an example of the fluvial-aeolian interaction from the Cutler Formation, Utah, U.S.A. In section I.5.3 of the present thesis, characteristics of cross-bedded sedimentary structures of fluvial deposits of tidal-fluvial interaction are described.

I.4 CROSS-BED STRUCTURES

Cross-beds originate from large-scale dunes moving along the river bed. Dunes are very common in recent rivers and so are cross-bedded sedimentary structures in fossil fluvial sandbodies.

The processes involved in dune sedimentation are demonstrated in Fig. I.8 (Joplin 1965). Cross-beds consist of two genetically different facies, the foreset and the bottomset (Fig. I.9). Avalanches of sediment over the lee side of the dune develop inclined laminae (foreset laminae) of well sorted sediment. This sediment is transported either by bed load or suspended load over the dune crest. In front of the dune, fall-out sediment and sediment out of suspension develop a bottomset layer over which the succeeding dune migrates (Fig. I.8). The sediment in the bottomset layer below the slope break is finer grained than that in the foresets deposited from avalanches (Allen 1970). The inclined avalanche laminae of the foreset often pinch out in the finer grained bottomset sediments. The boundaries between the laminae in the foreset and between the toes of the foreset laminae and the bottomset is commonly very sharp.

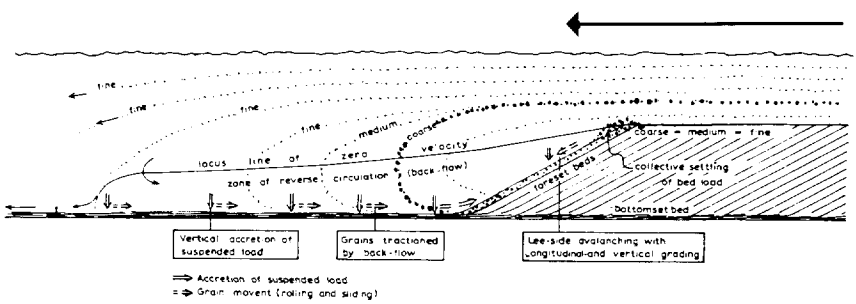

Fig. I.8 Processes involved in dune sedimentation. Arrow indicates direction of water movement (modified from Joplin 1965).

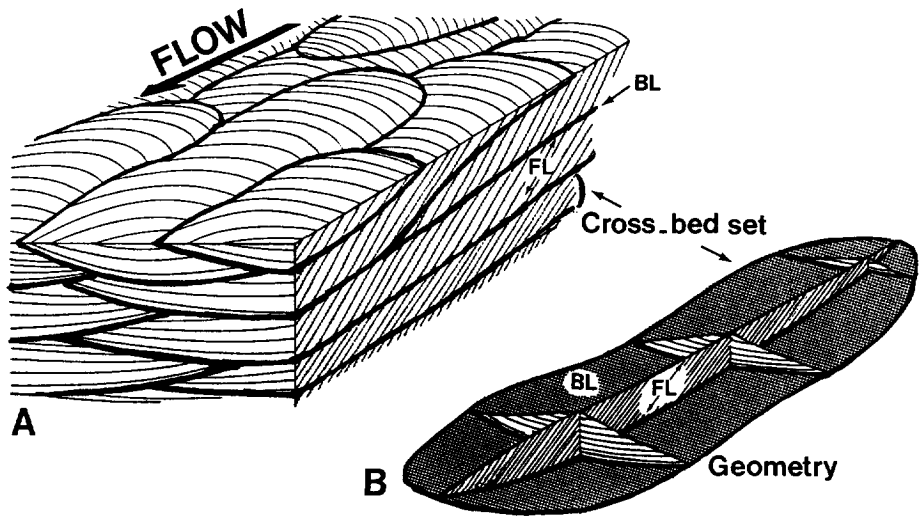

Fig. I.9 A) Three dimensional model of vertically stacked trough cross-beds with distinctive bottomset (BL) and foreset (FL) facies, note the inclined laminae (indicated by small arrows) in the foreset. Thick arrow indicates the palaeo flow direction of the river. B) Typical geometry of a trough cross-bed set (modified from Weber 1982).

Cross-strata of the foreset of a dune can be described by two principal shapes in profile parallel to flow. Cross-strata are called angular if they meet the unit's base at a sharp, acute angle. In this case, the bottomset is not preserved in the cross-bed set. Cross-strata are called tangential when the lower contact is asymptotic and extends down only as far as the slope break.

The grain size and other characteristics of foreset and bottomset of cross-bed sets form the subject of the present thesis. In view of the importance of cross-bedding and related permeability heterogeneity in the context of this thesis, special attention is given to the mineralogical composition of these sedimentary structures.

In the next sections classification, development, sedimentary characteristics and occurrence of cross-bed sets will be explained.

I.4.1 Classification

The origin of sedimentary structures can be studied in the laboratory by flume experiments (Joplin 1965, 1967) or by computer modelling (Rubin 1987; Myrow & Southard 1990). Experimental studies on sedimentary structures resulting from current action were performed as early as 1850 by Henry Sorby (see Allen 1970), the first scientist who used experimental results for environmental and palaeogeographical interpretation. It is not until the 1960s that sedimentologists began classifying bed-form morphology. Subaqueous bed forms were interpreted according to their environments of deposition (the fluvial, tidal and shallow-marine environment). As a consequence, the terminology contains a multiplicity of names and descriptions.

Table I.I, Classification scheme recommended by the SEPM Bed forms and Bedding Structures Research Symposium (after Ashley 1990).

First-order descriptors (necessary)				
Size: Spacing =	small 0.6-5 m;	medium 5-10 m;	large 10-100 m;	very large > 100 m
Height =	0.075-0.4 m;	0.4-0.75 m;	0.75-5 m;	> 5 m
Shape:	2-dimensional			
	3-dimensional			
Second-order descriptors (important)				
- Superposition:	Simple or compound (sizes and relative orientation)			
- Sediment characteristics:	Size and sorting			
Third-order descriptors (useful)				
- Bed-form profile (stoss- and lee-slope lengths and angles)				
- Fullbeddedness (fraction of bed covered by bedforms)				
- Flow structure (time-velocity characteristics)				
- Relative strengths of opposing flows				
- Dune behaviour-migration history (vertical and horizontal accretion)				

In 1987, a Symposium entitled "Classification of Large-Scale Flow-Transverse Bed

forms" (Ashley 1990) was held, with the purpose of examining the problems involved in classifying large subaqueous bed forms in the fluvial, tidal and shallow-marine environments.

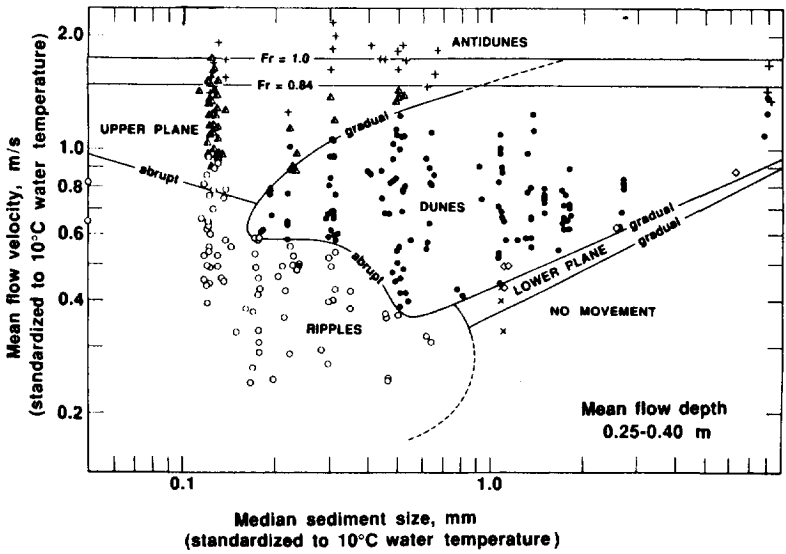

Fig. I.10 Bed-form types in a plot of median sediment size versus mean flow velocity (from Ashley 1990).

Figure I.10 shows bed-form types in a plot of the median sediment size versus the mean flow velocity (Southard & Boguchwal, 1990). The term "dunes" is used for large-scale bed forms, which can be subdivided into two groups: two-dimensional (2D) bed forms, which occur at lower water velocities, and three-dimensional (3D) bed forms, which occur at higher water velocities for a given grain size. The flow-transverse bed forms appear to act as an element resisting the flow. Consequently these bed forms migrate as a result of the shear stress imparted on the bed by the moving fluid (Ashley 1990). If the flow pattern persists relatively unchanged perpendicular to flow and strong

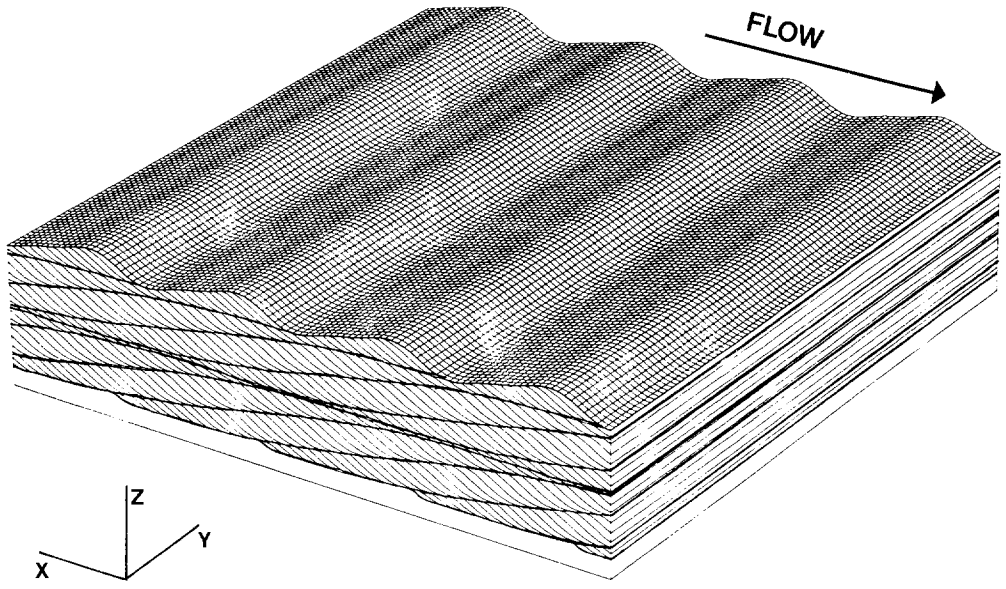

Fig. I.11 Model of 2D (planar or tabular) bed forms in a block diagram with surface view of ripples. Arrow indicates flow direction (modified from Rubin 1987).

eddies and vortices are absent, the bed form produced is straight-crested (2D). A typical example is planar (or tabular) cross-stratification (Fig. I.11). If the flow structure varies significantly in the third dimension and vortices capable of scouring depressions are present, this will be reflected in the resulting bed form (3D). A typical example is trough (or festoon) cross-stratification (Fig. I.12 A & B).

Bed forms are classified according to their size and shape (see Table I.I). The nomenclature is principally based on heights and wavelengths of the current ripples during deposition. Maximum heights and wavelengths of fossil bed forms depend on the erosional forces of the vortex eddy after deposition. The dimensions of fossil bed forms are outlined in section I.4.3 and a more detailed description is given in section I.5.1.2.

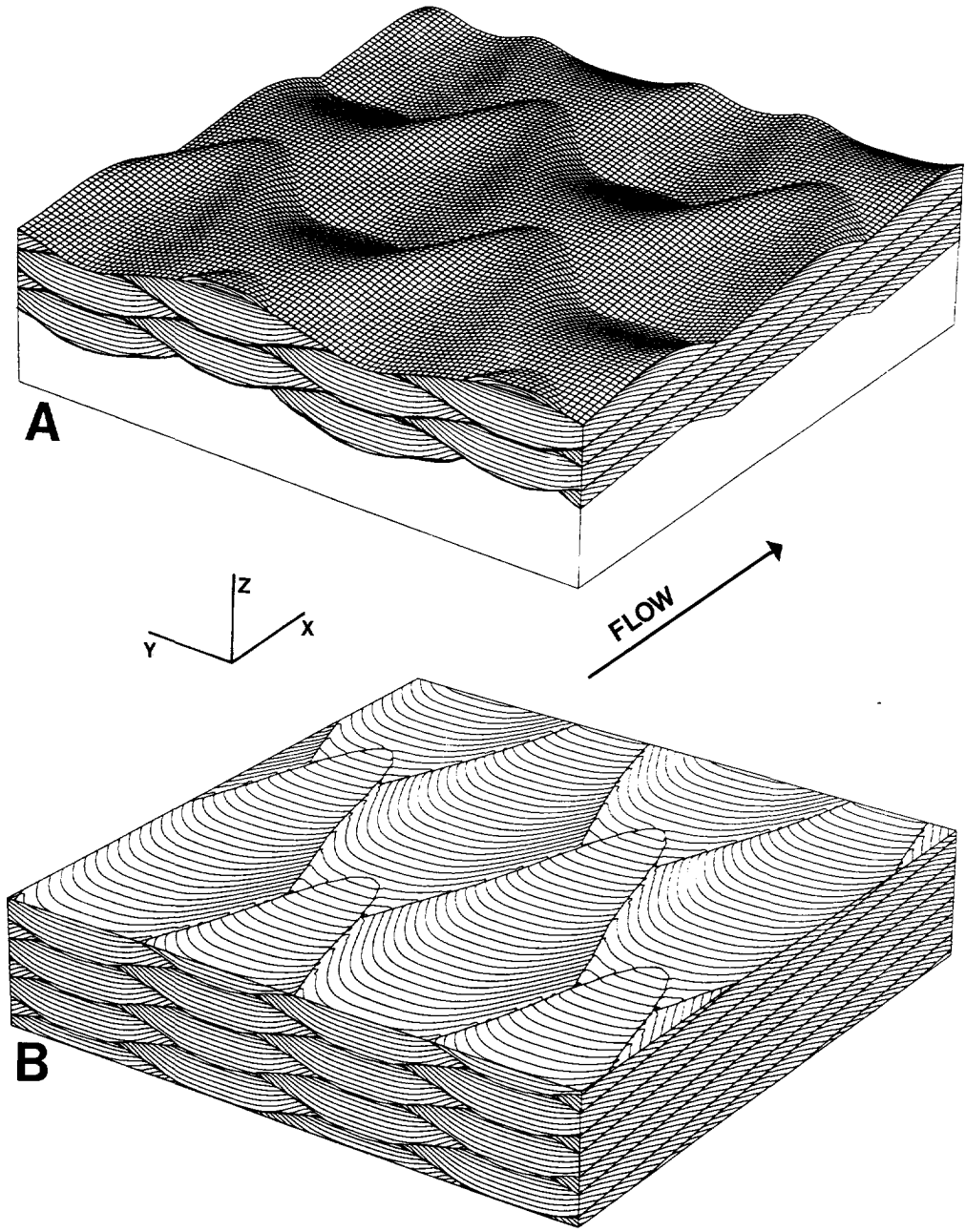

Fig. I.12 Model of 3D (trough or festoon) bed forms: A) Block diagram with surface view of ripples. B) Block diagram with 3D representation of ripple-laminae geometry. Arrow indicates flow direction (modified from Rubin 1987).

I.4.2 Grain size

Since ripples and dunes travel in the direction of flow, inclined layers or cross-strata preserved in sequence are a record of successive earlier positions of their leesides. The inclined layers or cross-laminae in large-scale dunes are relatively thick (5-15 mm) (Allen 1970). The cross-strata are formed by a continuous process of grains discharged over the wave crest and settling on the leeside. The settling increases the slope of the leeside and hence decreases the leeside slope stability. The moment the slope reaches its critical angle, an avalanche of grains slides down the leeside of the ripple. The grains avalanching down the leeside are automatically sorted according to size. Avalanching is intermittent at small sediment transport rates, but at sufficiently large sediment transport rates a continuous, general sliding of sediment occurs down the leeside. However, sorting becomes progressively poorer and under conditions of continuous sliding the internal structure of cross-strata may disappear completely.

Usually, there is a regular and systematic pattern of variation in medium grain size with respect to the successive cross-strata (Figs. I.13, A to C). This pattern is grossly rhythmic, although the periodicity of the rhythm might be somewhat irregular (Basumallick 1966). Jordan & Pryor (1992) presented thickness, sorting and grain size of foreset laminae. They find an average grain size contrast of coarse silt to very fine sand between the laminae. The very-fine grained laminae are on average worse sorted than the coarse silt laminae. The thickness of the laminae vary between a 0.2 and 2 cm. According to Basumallick (1966), a significant variation in medium grain size within a single lamina is absent.

The bottomset material which underlies the base of the foresets is invariably much finer grained than the bulk of cross-laminae succeeding it (Basumallick 1966). Bottomsets are primarily formed by suspension-load material.

I.4.3 Dimensions of cross-bed sets

Much has been written about the original dimensions of large-scale cross-bed sets,

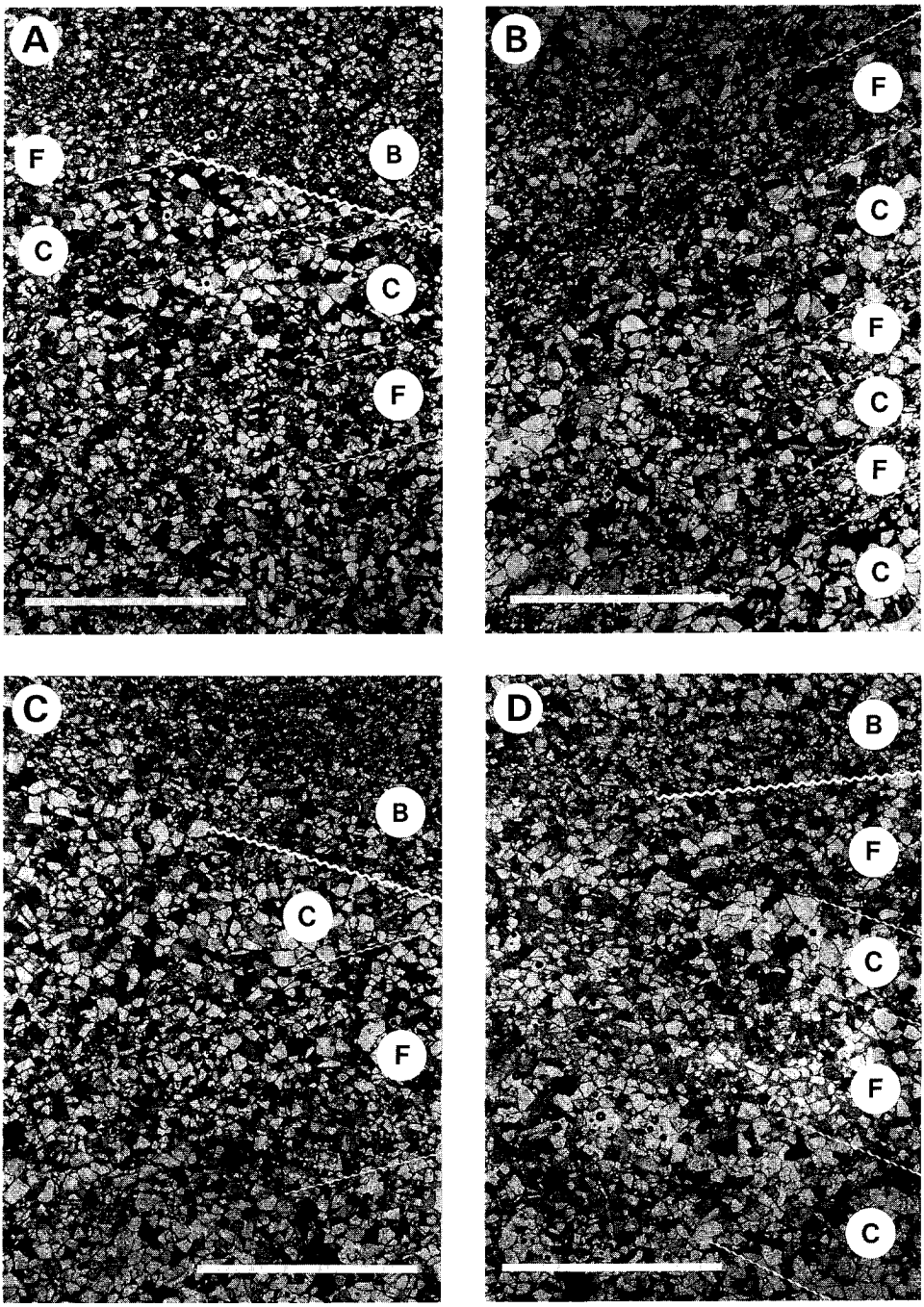
A
F
B
C
C
F
B
F
C
F
C
F
C
C
B
C
F
D
B
F
C
F
C

Fig. I.13 Photo-micrographs of features in cross-beds. Shown are coarser-grained (C) and finer-grained (F) foreset laminae and bottomset (B). Scale bar is 0.5 cm. Boundaries between foreset laminae are partially indicated by a fine wiggly line, boundaries between foreset and bottomset are partially indicated by a thick wiggly line. Note the sharp boundaries between the different units. A) Sample 90.XIII.2; B) Sample 90.XIII.2; C) Sample 90.IX.1; and D) Sample 90.XI.1.

but very little is known about their geologically preserved dimensions. Harms *et al.* (1963) presented width-thickness-length ratios for large-scale and small-scale trough (3D) cross-bed sets, based on measurements in point bars of a recent meandering river. Table I.II, lists the results of this study, together with those of other studies (Weber *et al.* 1972, Olsen 1988) and of my own observations in outcrops of point-bar deposits near Huete, Central Spain (discussed in section I.5.1.2). All thickness-to-width ratios are in good agreement.

Harms *et al.* (1963) noted that the lengths of the large-scale trough cross-bed sets probably do not exceed 30 m. This is in agreement with the maximum average lengths measured at outcrops in Central Spain, which ranged from 15 to 20 m. Weber *et al.* (1972) presented an approximate thickness-width-length ratio of 1 : 7 : 25 of trough cross-bed sets. The difference in ratios measured at outcrop may be a result of different measured heights (actual maximum height versus outcrop-apparent maximum height).

Dimensions of large-scale planar (2D) cross-bed sets were not found in literature, although Harms *et al.* (1963) measured small-scale planar cross-bed sets with a thickness of 7.5 - 10 cm and a width of 122 cm (approximate T:W ratio of 1:15). Smith (1990) describes very large-scale planar cross-bedded conglomerates, the thickness of which ranges from 1 to 3 m and the width may be up to 60 m (approximate T:W ratio of 1:20). Smith (1990) describes the occurrence of conglomeratic foresets as a result of gravel clasts rolling down a migrating slip-face of a gravel bar. The authentic term "cross-bedding" is not valid for conglomeratic deposits (see Fig. 10, dunes are characteristically formed in sediment between 0.2 and 2 mm). Cross-bedding in conglomeratic deposits may also result from imbrication of pebbles (Gustavson 1978).

Table I.II, Dimensions of fossil trough cross-beds.

	Large-scale trough cross-bed sets
Harms *et al.* (1963)	
Thickness:	45.75 cm
Width:	228.75 cm
Approximate T:W ratio:	1 : 5
Olsen (1988)	
Thickness:	20 cm - 1 m
Width:	1 - 5 m
Approximate T:W ratio:	1 : 5
Weber *et al.* (1972)	
Approximate T:W:L ratio:	1 : 7 : 25 (T:W ranges between 4 and 16)
Own observations (Huete, 1989-1990)	
Thickness:	20 - 40 cm
Width:	80 - 200 cm
Approximate T:W:L ratio:	1 : 6.5 : 20 (T:W ranges between 4 and 16)

I.4.4 Occurrence of cross-bed sets

The active channel fill of a fluvial deposit is characterized by a fining-upward sequence of coarse- to medium-grained sand, and an abundance of large-scale sedimentary structures. In order to give an approximation of the abundance of large-scale cross-bedding in the sandy part of high- and low-sinuosity channel deposits, volume percentages were obtained from sedimentary logs presented in literature and from own observations. The resulting probability curve is displayed in Fig. I.14. This graph shows that the probability of cross-bedded sedimentary structures occurring in high-sinuosity channel deposits is significantly higher than in low-sinuosity channel deposits.

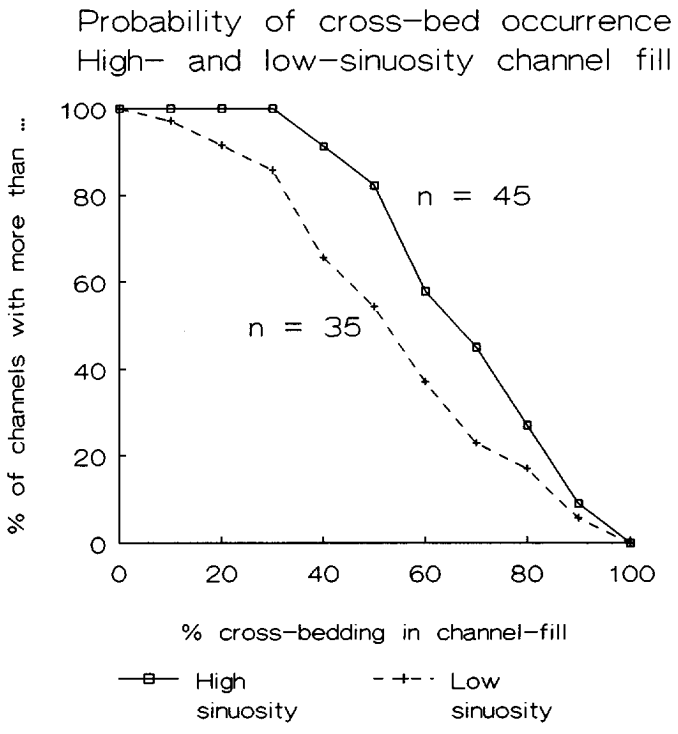

Fig. 1.14 Probability curves of frequency of large-scale cross-bedding in the sandy part of high- and low-sinuosity channel deposits.

I.5 OUTCROP CASE STUDIES

During the research for this thesis, several field trips were made to study different types of fluvial deposits and associated sedimentary structures and permeability heterogeneity. In addition to the literature study of different types of fluvial channel-fill deposits, a selection of the studied outcrops of distinctive types of fluvial architecture (Fig. I.4, multistorey and multilateral complex channel sandbodies) as well as outcrops of rocks that show fluvial-tidal interaction are outlined. Referred to Fig. I.1, these examples represent fluvial deposits in alluvial-fan setting, river-plain setting and coastal-plain setting. In the first example, Tertiary sand-rich high- and low-sinuosity river deposits of inland-basin alluvial fans in Central Spain showed typical lateral-accretion and vertical-aggradation sand-bodies with an abundance of cross-bedding. High porosities and permeabilities made these outcrops very suitable for detailed minipermeameter studies (chapter III). In the second example, the Lower Triassic Solling Formation near Kassel in Germany was chosen as an representative example of sand-rich, braided-meandering river systems in a fluvial plain setting. The outcrops show, in contrast with the first example, low percentages of cross-bedding. Very low porosities and permeabilities made these outcrops unsuitable for further investigations with the minipermeameter. As a third example, tidally influenced coastal plain deposits of the Capella Formation in North Spain exhibit low- and high sinuosity channel deposits that are influenced by tidal action. This example shows that although sediments are dominantly laid by river currents, their internal structures may be influenced by tidal action. Cross-beds of this type of deposits differ from the former, pure fluvial, examples in the occurrence of potential permeability barriers in foreset and bottomset.

I.5.1 LORANCA BASIN, CENTRAL SPAIN

AN EXAMPLE OF HIGH- AND LOW-SINUOSITY CHANNEL DEPOSITS

The Tertiary fluvial sediments of the Loranca Basin, Central Spain (Fig. I.15), were deposited from the Late Oligocene to Early Miocene. Many different examples of

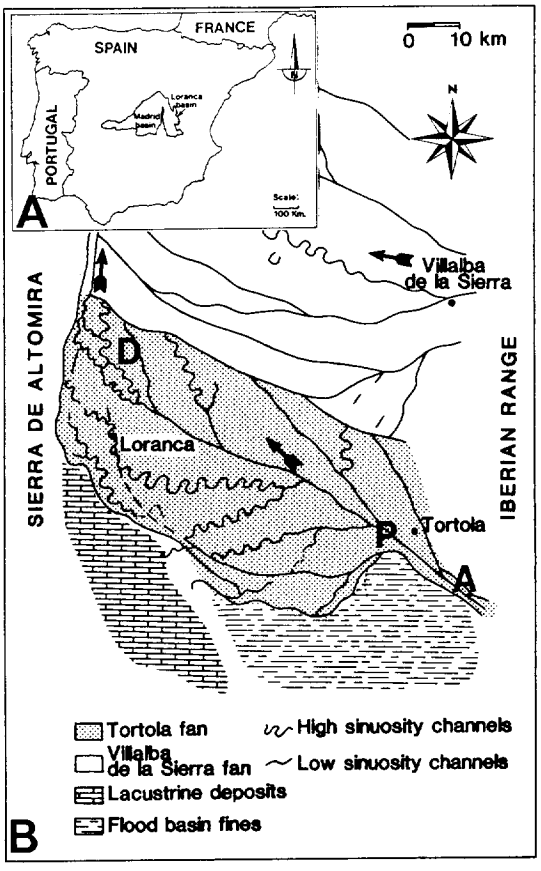

Fig. I.15 A) Location map of the Loranca Basin in Central Spain. B) The Tertiary fluvial fan deposits of the Loranca Basin, Central Spain. The basin is bordered by mountain ranges, to the west by the Sierra de Altomira and to the east by the Iberian mountain range, which acted as a source area for both fluvial fans. A = apex feeder channels, P = proximal area and D = distal area of the Tórtola fluvial fan. (modified from Diaz Molina *et al.* 1989).

low- and high-sinuosity channel deposits are excellently exposed. All accumulate in two coalescing fluvial fans, which formed during a major compressional tectonic phase (Díaz Molina, 1989). Details about the geological setting are discussed in Díaz Molina *et al.*

(1985), Díaz Molina *et al.* (1989) and Díaz Molina (1991). A summary of the setting and facies description is presented in chapter IIIA and IIIB of this thesis.

The Tertiary fluvial fans of the Loranca Basin were wet systems (Schumm 1977) in a generally dry, subtropical climate interrupted by humid periods (Daams & van der Meulen 1984; Álvarez *et al.* 1987). The Tertiary fluvial fans are similar to the recently deposited Kosi river fan in India. Both show a predominance of individual channels that are part of a multiple channel system. The multiple channel pattern consists of tributary and distributary areas (Díaz Molina *et al.* 1989).

I.5.1.1 Channel types and characteristics

High-sinuosity channels

The remnants of high-sinuosity rivers are point-bar and meander-loop complexes (Díaz Molina *et al.* 1989). During individual lateral-accretion episodes a fining-upward sequence usually developed. Large-scale bed forms are well preserved in the lower part of the point-bar deposits, whereas lateral-accretion surfaces are better preserved in the upper part. Point-bar sedimentary structures usually moved up the erosional surface and as a consequence bottomsets are parallel to the lateral-accretion surface. The heterogeneities in permeability occurring in these large-scale sedimentary structures are described in detail in chapter IIIA and IIIB. In the meander-loop deposits of the Loranca Basin, laterally stacked sequences deposited by adjacent point bars and separated by reactivation surfaces occur frequently. The heterogeneity caused by reactivation surfaces in sand bodies was studied in detail and results are presented in chapter IIIA.

Low-sinuosity channels

Channel fills of low-sinuosity channels are characterized by vertical aggradation. They are believed to have formed by backfilling ribbon-type channels (Friend 1983). Reactivation surfaces may be present in the channel fills. Internally, they lack any sequence of sedimentary structures or any geometric characteristics in which side bars and riffle- and-pool bed-form patterns can be recognised. Sedimentary structures, if present,

are dominated by large-scale trough cross-bed sets and water escape structures. Multiple low-sinuosity-channel fills form stacked sequences. The superimposed units are separated by flat surfaces.

I.5.1.2 Sedimentary structures and heterogeneities

Cross-bedded sedimentary structures

Pebbly coarse- to medium-grained sandstones occur in the proximal areas (Fig. I.15). The apex feeder channels are truly conglomeratic. The distal parts (Fig. I.15) of the fans are characterized by medium- to fine-grained sandstones. The sandstones are of a very friable nature and have a high porosity (30-35%) and permeability (0.5-20 D).

The characteristics of cross-beds have been studied in the Tórtola fan in a number of different types of channel deposits ranging from proximal to distal. Frequency distributions of length, width and thickness, measured at outcrop, are presented in Fig. I.16, A and B. The approximate L:T ratio is 20 (ranging from 10 to 30). The approximate W:T ratio is 6.5 (ranging from 4 to 16). The maximum thickness and average grain size of the cross-bed sets decreases from proximal to distal. The largest sets were observed near Villanueva de los Escuderos (half way between Tórtola and Loranca) with an average apparent vertical thickness of 70 to 90 cm (Fig. I.17). The conglomeratic feeder channels were not included in the study. The total percentage of dunes occurring in the sand bodies decreases from approximately 85% to 75% going from proximal to distal.

Bottomsets make up more or less 10 to 30% of the cross-bed set. The ratio of cross-bed thickness to bottomset thickness is presented in Fig. I.16C. This T:B ratio is approximately 10 (ranging from 5 to 25). Bottomsets are laterally continuous and interconnect with bottomsets of laterally and vertically stacked cross-beds. This results in a compartmentalization of the cross-bedded channel-fill.

The thickness of foreset laminae varies between 0.1 and 1.2 cm, with the thickest laminae developed in the coarser-grained deposits (0.5 and 1.2 cm). As a measure to characterize foreset laminae thickness one can use the ratio of coarse grained foreset laminae thickness (CFL) versus fine grained foreset laminae thickness (FFL) (Fig. I.16D).

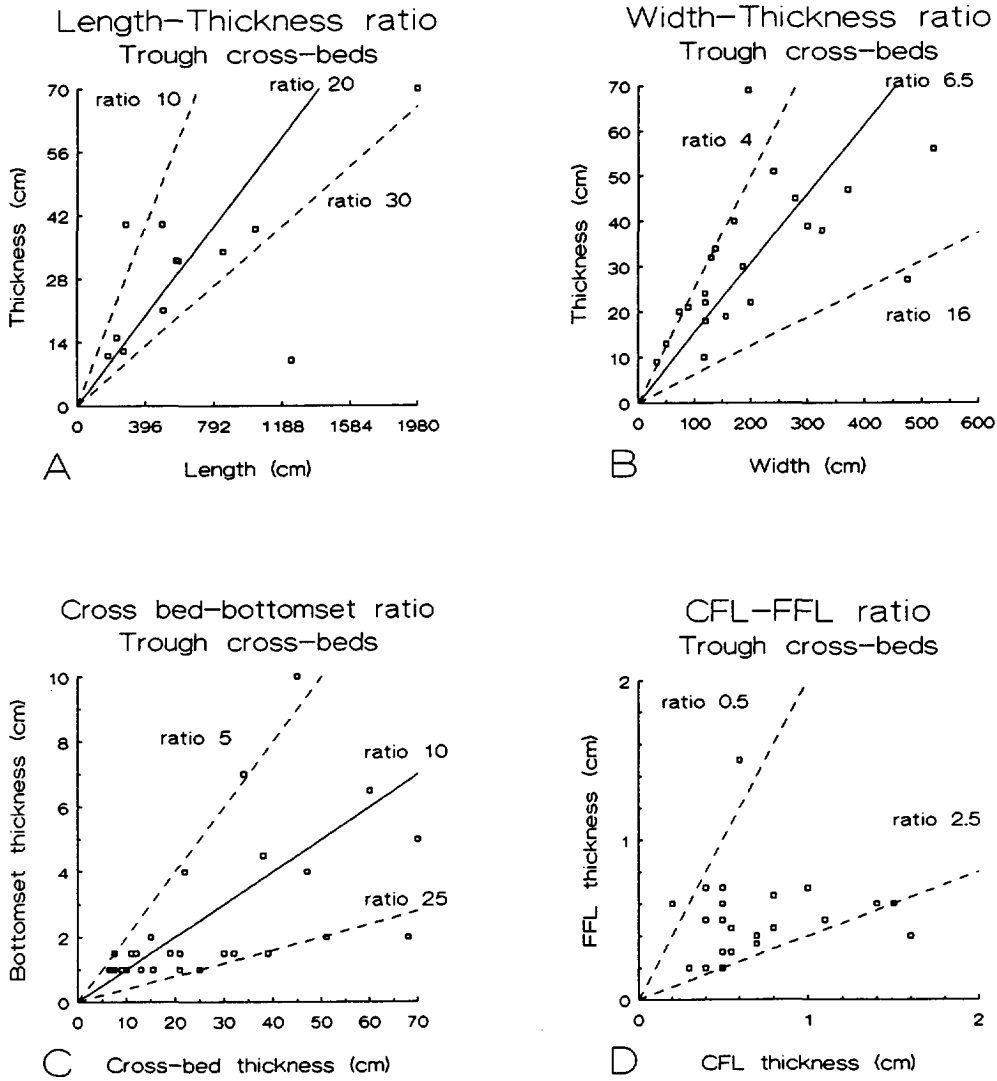

Fig. I.16 In the next plots of dimensional characteristics of trough cross-beds in the Loranca Basin, central Spain a continuous line represents the average dimensional ratio and the dashed lines indicate the approximate maximum and minimum ratios. A) Plot of length/thickness ratio; B) Plot of width/thickness ratio; C) Plot of cross-bed/bottomset thickness ratio (cross-bed thickness is measured as maximum vertical thickness in outcrop); D) Plot of CFL/FFL thickness ratio (the CFL and FFL thickness is measured as the maximum thickness perpendicular to inclined foreset laminae).

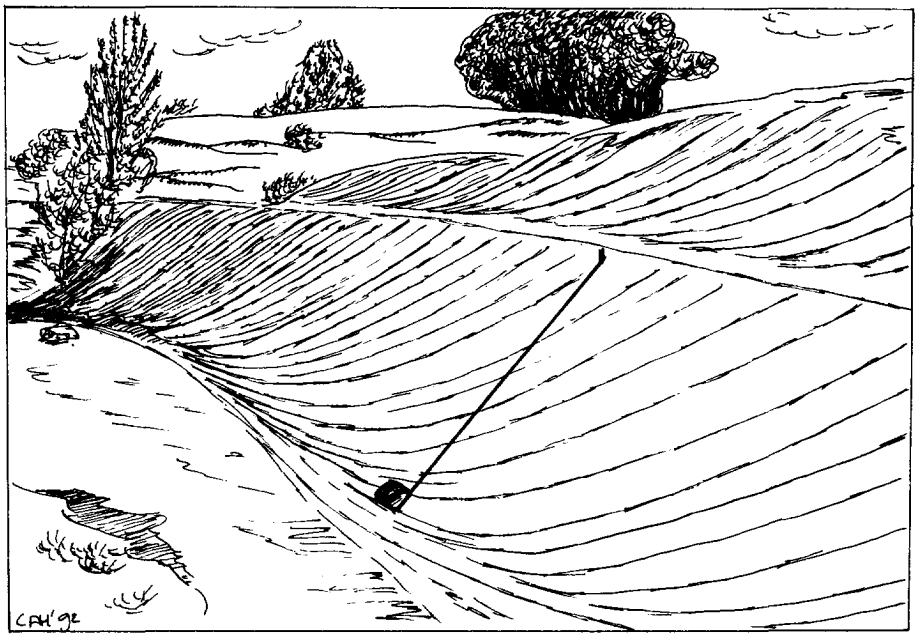

Fig. I.17 Large-scale dunes in a point-bar deposit in the proximal part of the Tórtola fan. Height of individual cross-bed sets is 80 cm. Length of stick is 1 m.

The CFL:FFL ratio varies between 0.5 and 2.5.

The heterogeneity that results from large-scale cross-bedding is determined by the contrasts in grain size between adjacent foreset laminae and between foreset laminae and bottomsets. In several cases, the range of grain sizes was found to be small and consequently, there was little difference in grain size within the bed form, which made the bed form difficult to recognize. This may be caused by seasonal or incidental variations in water and sediment supply. In several cases, in which bed forms were lacking, a homogeneous channel-fill sand was found. The lack of sedimentary structures might be caused by hydroplastic deformation, liquefaction and fluidization (Lowe 1975).

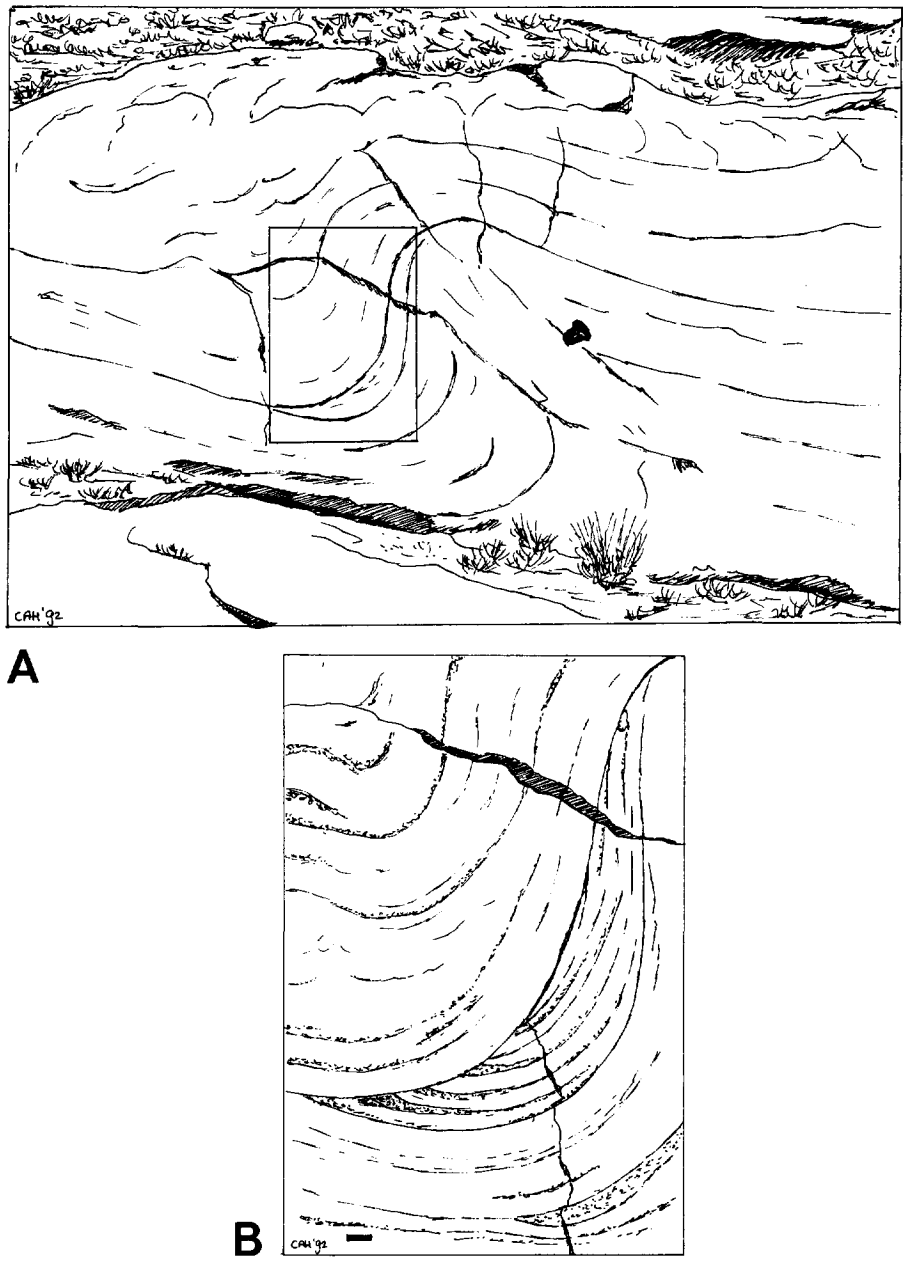

Fig. I.18 A) Soft sediment deformation of sedimentary structures in low-sinuosity channel deposit. Camera case is 20 cm. B) Detail of deformed cross-bed set, note that the internal structures are still recognizable. Scale is 5 cm.

Water escape structures

In fluvial outcrops of the Loranca Basin, water escape structures are generally found in fine- to medium-grained sand, though occasionally they also affect coarse-grained sand (Díaz Molina 1979). The sediments show deformational structures ranging from small-scale deformation of the sedimentary structures to disrupted sediment of the entire channel fills. If fluidization of the sediment was intense, the sediment may appear homogeneous. All primary sedimentary structures and ensuing internal heterogeneities have disappeared. Less intense fluidization causes disrupted sedimentary structures which often look like fold-like structures (convolute bedding). The internal heterogeneities of laminae and bottomsets are generally intact but their geometry may have changed drastically (Fig. I.18). The occurrence of bed forms resulting from plastic deformation and their complex nature may form an even more heterogeneous system within the channel fill.

I.5.2 SOLLING FORMATION, GERMANY

AN EXAMPLE OF SAND-RICH BRAID-PLAIN CHANNEL DEPOSITS

I.5.2.1 Channel types and characteristics

The Lower Triassic Solling Formation (Middle Buntsandstein) near Kassel in Germany (Fig. I.19) was deposited by a sand-rich, braided meandering river system (Olsen 1988). Within the braid plain, streams tended to meander in seasons with low water supply, whereas in seasons in which the water supply was ample the rivers formed an interweaving system of low-sinuosity channels covering the entire braid plain. The deposits form sheet-like sandstone bodies, containing internal scouring structures and small channel incisions. The outcrops were limited to several quarries in the area that seem to be concentrated in locations where the nett-to-gross ratio is high.

Fig. I.19 Location map of outcrops of the Lower Triassic Solling Formation (Middle Buntsandstein) near Kassel in Germany (modified from Olsen 1988).

I.5.2.2 Sedimentary structures and heterogeneities

The sandstones are medium- to fine-grained quartzites, with a very low porosity (approximately 5-10%) and permeability (< 0.5 mD). Several architectural elements recognised by Olsen (1988) are presented in Table I.III.

Generally, the Solling Formation shows a small variation in grain size. The homogeneity of the almost pure quartz sandstone and the small range of grain sizes may account for a low visibility and hence, low percentages of large-scale cross-bedding (between 20 - 30%). Water-escape disturbance of the sediment might have distorted the once apparent cross-bedded sedimentary structures. In some cross-stratified beds the laminae are only visible near the bottom of the layer (Fig. I.20). The large-scale troughs usually form angular to tangential sets, with little or no bottomsets developed. Cross-

Table I.III, Architectural elements in the Solling Formation, Germany (after Olsen 1988).

Facies	Frequency (%)	Grain size and structures	Interpretation
Parallel laminated sandstones	57	Vf-m sand, horizontal and low-angle ($< 16^0$) inclined parallel lamination, parting lineation.	Upper plane bed
Large-scale trough cross-bedded sandstones	19	F-m sand, sets 0.2 - 1 m thick, 1 - 5 m wide, 2,5 - 8 m long; foreset dip $< 30^0$, concave foresets.	3D large-scale dunes
Large-scale planar cross-bedded sandstones	6	F-m sand, 0.1 - 1 m thick sets, foreset dip $< 23^0$, tangential to weakly concave foresets.	2D large-scale dunes
Small-scale cross-laminated sandstones	2	Vf sand, often silty, set thickness < 1 cm.	Small-scale bedforms
Mudstones	14	Silt and mud, massive, horizontal lamination, cross-lamination.	Lower plane bed
Intraformational mudclasts	1	Granules to cobbles, usually dispersed in sand or overlying an erosion surface.	Lag deposit

bedding is found as a single set within a sequence rather than cosets of multiple stacked cross-bed sets.

Intraformational mudclasts were not only found near the bases of sandstone beds, but frequently as intraclasts within laminated or cross-stratified sand. In the abandoned quarries the mudclast-rich laminated and cross-stratified sandstone was often more weathered than the surrounding unstratified hard sandstone.

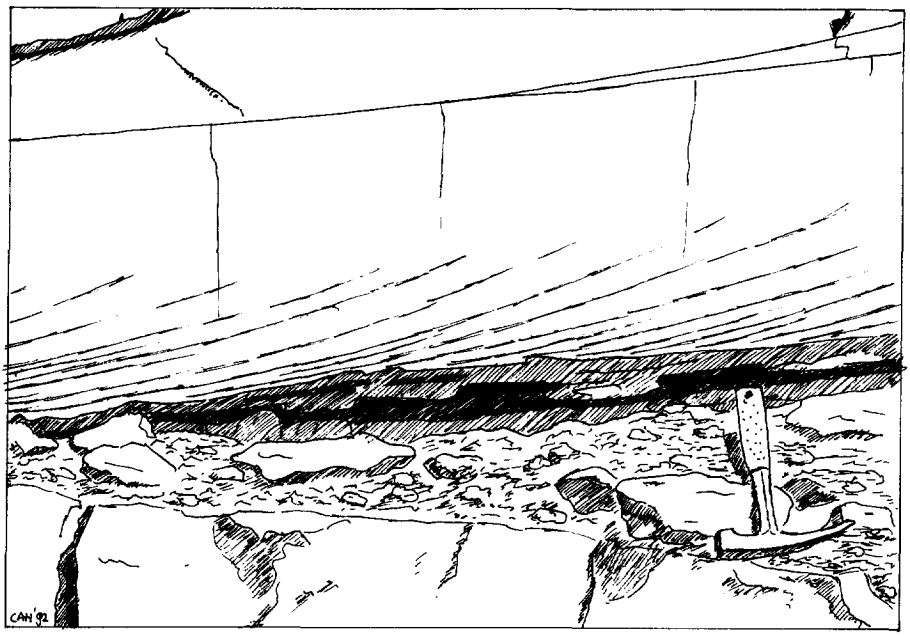

Fig. I.20 Foreset laminae only recognizable in the lower part of the bed because of limited grain size variation. Length of hammer is 28 cm.

I.5.3 CAPELLA FORMATION, PYRENEES, SPAIN

AN EXAMPLE OF TIDALLY INFLUENCED FLUVIAL CHANNEL DEPOSITS

During the Middle Eocene, a fluvio-deltaic complex occupied one of the thrust-associated foreland basins in the South-Central Pyrenees (the Tremp-Graus Basin, Fig. I.21). The fluvio-deltaic complex consists of marine deposits that are gradationally overlain by the alluvial Capella Formation (Cuevas 1989). The Capella Formation consists of sandstones, conglomerates and some gypsum levels interbedded with multicoloured

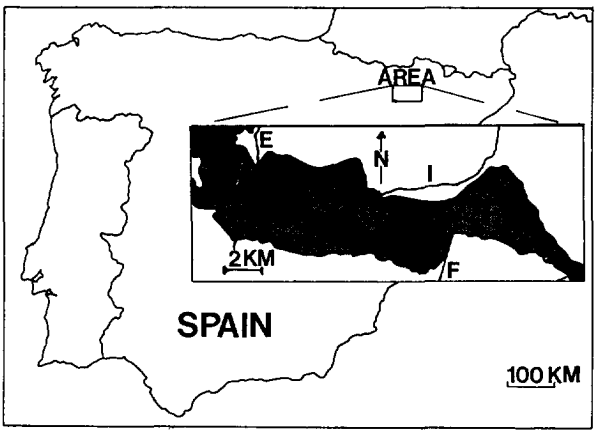

Fig. I.21 Location map of outcrops of the Tertiary Capella Formation, Southern Pyrenees, Spain. G = Graus, C = Capella, E = Esera river and I = Isabena river. F = major fault (modified from Cuevas 1989).

mudstones. The formation shows a low sand/mud ratio and consequently interconnectedness between the sand bodies is low (Cuevas 1989). Two different types of genetic units were identified by Cuevas (1989) in the Capella Formation, the infilling type (related to channel deposits) and the outbuilding type (related to depositional lobes and sheet deposits). The channel deposits consist of sand bodies formed by either lateral accretion or vertical aggradation. The association of sediment bodies suggests deposition on distal parts of alluvial fans. Influence of tides is suggested by the bipolar cross-stratification, reactivation surfaces and mud drapes occurring in some of the channel deposits or depositional lobes.

I.5.3.1 Channel types and characteristics

High-sinuosity channel deposits

The geometry and depositional characteristics of the tidally influenced fluvial deposits in the Capella Formation are similar to pure fluvial channel deposits. The point-bar sand bodies are characterized by low-angle dipping accretion surfaces. The grain size shows a fining-upward trend from medium/coarse- to fine-grained sand. Trough and planar cross-stratification is found in the lower parts of the sand bodies. The cross-strata often show long, well-developed bottomsets.

Tidal deposition is apparent from bipolar cross-stratified sandstones associated with reactivation surfaces and regularly spaced mud drapes occurring in the base of the lateral accretion units of some of the bodies (e.g. Visser 1980 De Mowbray & Visser 1984).

Straight to low-sinuosity channel deposits

In most cases, the vertical-aggradation sand bodies consist of homogeneous, well-sorted medium- or fine-grained sand. In a few cases, lag deposits with mudstone clasts or clay intercalations observed within a sand body are evidence of repeated aggradation episodes which could indicate tidal action. Typical sedimentary structures are cross-stratification, scour-and-fill structures, low-angle cross-stratification, parallel lamination and ripple lamination. The vertical-aggradation sand bodies occur as single or multi-storey ribbon bodies (Friend 1983) or as composite channel fills deposited by an anastomosing system of channels. Conglomeratic vertical-aggradation channel fills were identified as being deposited by braided channels in an alluvial fan system (Cuevas 1989). They are composed of planar cross-stratified conglomerates that are laterally associated with cross-stratified sandstones. Composite bodies containing vertical- and lateral aggradation complexes with associated internal structures occur in the area.

I.5.3.2 Sedimentary structures and heterogeneities

Sedimentation was influenced by tidal currents, especially in the distal parts of the alluvial-fan system. Sedimentary structures within the low- and high-sinuosity channel deposits and depositional lobes indicate a subordinate current direction in addition to the dominant current direction of the fluvial system. Figure I.22 shows an example of tidal

Fig. I.22 Neap-spring tide bundles in cross-bedding of a fluvial dominated deposit. Note the strong sinuous shape of the foreset laminae. The height of an individual cross-bed set is approximately 25 to 30 cm. The swiss knife is 9 cm long.

dominated cross-bedding in a fluvial sand body. In Cuevas (1989), the reversed palaeocurrent directions are described to have formed reactivation surfaces and mud drapes at regular intervals in some of the channel deposits and depositional lobes. Supratidal, intertidal and subtidal conditions locally dominated the environment of deposition.

In Shanley *et al.* (1992), field criteria to destinguish tidal processes in strata dominated by fluvial processes are carefully outlined. The following characteristics can be listed as proof of tidal influences in sedimentary structures (Fig. I.23):

a) The foreset orientation is primarily in the direction of the dominant current (fluvial

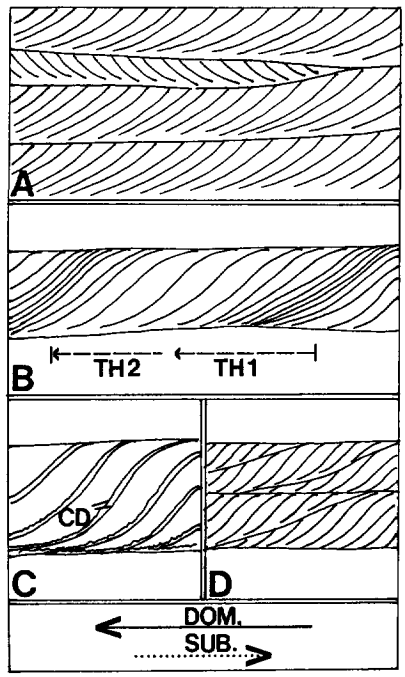

Fig. I.23 Schematic drawing of tidal features in cross-beds. The dominant current direction (fluvial current) is indicated by a black arrow and the subordinate current direction (tidal current) by a dotted arrow. A) shows stacked cross-beds of dominantly fluvial origin with one opposite oriented cross-bed set which pinches out in the subordinate current direction. B) shows sinuously shaped, foreset laminae in a thickening (TH1)/thinning (TH2) pattern, reflecting spring-neap tides. C) shows double claydrapes (CD) that cover the adjacent foreset laminae and continue into the bottomset layer. D) shows repeated discontinuity surfaces within foresets.

current), however, opposite orientations, originating from a subordinate current, occur.

b) Counter-current sets display pinching-out in the migration (subordinate) direction.

c) Trough cross-bed sets show a typical sigmoidal shape.

d) Foreset laminae show a repeated thickening and thinning pattern in the dominant current direction.

e) Mud or silt draping of foreset laminae and bottomsets occurs. Typical tidal double-mud drapes occur in the sub-tidal environment (tidal channels and river mouth bars).

f) Repeated discontinuity (reactivation) surfaces are commonly observed within foresets.

Fluvial sedimentary structures can be expected to be highly heterogeneous if they are tidally influenced. Mud or silt draping of foresets and bottomsets and reactivation surfaces within foresets cause poorly permeable to impermeable baffles. In this thesis, cross-beds of the tidally-influenced realm are excluded. The investigation focusses on adjacent laminae and bottomsets that are interconnected, but show contrasts in grain size, sorting and permeability. Poorly permeable to impermeable silt and clay draping causes disconnected foreset laminae and bottomsets and hence form a different type of heterogeneity. In the next chapter (section II.2.4), the expected effect of permeability baffles within tidally influenced cross-beds on by-passing of oil in a water flooded reservoir is briefly discussed.

I.6 CONCLUSIONS

General

1) The probability of cross-bedded sedimentary structures occurring in the active channel fill of high-sinuosity channels is significantly higher than in that of low-sinuosity channels.

Geometrical characteristics

2) Trough cross-bed sets (3D bed forms) are characterized by a maximum thickness:width:length ratio of 1:6.5:20 (W:T ratio ranges from 4 to 16, L:T ratio ranges from 10 to 30).

3) Planar cross-bed sets (2D bed forms) are characterized by a maximum thickness:width ratio of 1:20.

4) Foreset-lamina thickness varies between 0.1 and 1.5 cm. The ratio of coarse-grained-foreset-lamina thickness to fine-grained-foreset-lamina thickness varies between 0.5 and

2.5.

5) Bottomsets make up 10-30% of cross-bed sets. Cross-bed thickness:bottomset thickness ratio is approximately 10 (ranging from 5 to 25).

6) Bottomsets are laterally continuous and interconnect with bottomsets of horizontally and vertically stacked cross-beds. This results in a compartmentalization of the cross-bedded channel-fill.

Grain-size characteristics and preservation criteria

7) Large-scale bed forms show a regular and systematic variation in median grain size with respect to the successive laminae in the foreset.

8) The bottomset is characteristically finer grained than the bulk of grains of the succeeding foreset.

9) The visibility or preservation of cross-bed sets depends on A) the range of grain sizes available, B) sorting during avalanching determined by the sediment transport rate and C) homogenization of the sediment resulting from intense soft-sediment deformation (hydroplastic deformation, liquefaction and fluidization).

Characteristics of soft-sediment deformation and tidal action in cross-bed sets

10) Sedimentary structures resulting from soft-sediment deformation exhibit disrupted and folded structures. Their internal characteristics may still be intact, but their geometries have generally changed drastically, and consequently the geometrical heterogeneity is more complex.

11) Fluvial sedimentary structures deposited under the influence of tidal action may have formed poorly permeable to impermeable barriers because of silt or clay draping of the foreset laminae and bottomsets.

CHAPTER II
FLUVIAL HYDROCARBON RESERVOIRS

II.1 INTRODUCTION

Enhanced hydrocarbon recovery from reservoirs presents a challenge to the hydrocarbon industry and will be badly needed in many countries in the near future. Achieving this goal can be assisted by improving our knowledge of the three-dimensional distributions and continuities of the rocks, pore sizes, and fluids in the reservoir and aquifer system, including barriers to flow. The complexity of fluvial deposits has been of particular interest to the hydrocarbon industry since the early days of hydrocarbon production. In the last decades, many papers concerning the characterization of fluvial deposits for reservoir simulations were published (Galloway & Hobday 1983, Berg 1986, Barwis 1989). Most papers deal with the architecture and interconnectedness of the sandbodies rather than pore scale or sedimentary-structure scale heterogeneities.

Detailed knowledge of channel-fill lithology, morphology, distribution, stacking, and connectedness is essential to develop a model that accurately describes fluid flow and production characteristics within fluvial systems. The known geological detail at all scales of reservoir heterogeneity (Weber 1986) greatly exceeds the modelling capability of a simulator. Large-scale fluid flow models tend to neglect smaller-scale fluid flow characteristics and may create unrealistic models because of oversimplification of the geological data (van de Graaff & Ealey 1989). In all cases, reservoir heterogeneity needs to be assessed and quantified at a scale appropriate to the problem being analyzed. Geological data should be simplified only to the extent that the simulator can predict reservoir behaviour correctly. For this purpose it is vital to quantitatively describe the permeability characteristics of a reservoir at all relevant scales. This is especially important fot fluvial reservoirs in which even the most highly porous and permeable channel-fill deposits show very significant small-scale permeability variations because of ubiquitous cross-bedding.

Characterization of permeability heterogeneities on any scale (Weber 1986) has

interested many petroleum geologists during the past decade. The mini-permeameter (Eijpe & Weber 1972) has become an accepted tool (Appendix A) for small-scale permeability measurements at outcrops (Chandler *et al.* 1989, Dreyer *et al.* 1990, Corbett & Jensen 1993) or at cores from reservoirs (Halvorsen & Hurst 1990, Hurst & Rosvoll 1991). This tool has increased our knowledge of small-scale permeability heterogeneities occurring in reservoirs.

One of the first attempts in predicting production performance taking into account cross-bedding in a distributary channel-fill reservoir was carried out by Weber *et al.* (1972). The permeability anisotropy deduced from minipermeameter measurements at cross-bedded sections of unconsolidated channel-fill sand was compared to in-situ water-flow tests in the same sandbody. They concluded that the horizontal permeability anisotropy in unconsolidated, trough cross-bedded formations will generally be small. In addition to the former one-phase fluid flow case, Ringrose *et al.* (1992) modelled immiscible flow behaviour along layers and across layers in laminated and cross-bedded sandstones. At a typical field flow rate of 0.25 m/day, flow parallel to lamination gives a recovery 50% higher than flow perpendicular to laminae. They conclude that differences of up to a factor two in predicted ultimate recovery may be produced by differently up-scaled representations of a realistic clastic sedimentary structure. However, their study aiming at determination of correct scaling-up procedures for multiphase flow parameters is rather ambitious as long as fundamental research of the impact of sedimentary structures on water/oil displacement is neglected. This lack of fundamental understanding of two-phase fluid-flow process through stratified heterogeneous media is obvious from their descriptions of the flow behaviour under capillary- and viscous dominated force.

Kortekaas (1985) described a detailed model of water/oil displacement in trough cross-bedded reservoir zones. One-dimensional numerical models of cross-bed laminae of alternating high- and low-permeability showed that considerable amounts of movable oil are initially by-passed in the high-permeability laminae as a result of capillary pressure. In a two-dimensional model, bottomsets are taken into account, however the model is a poor representation of the trough cross-bed geometry. From chapter I in this thesis, it is concluded that bottomsets are invariably uniform and fine-grained layers that effectively compartmentalize a cross-bedded channel-fill unit. In the study by Kortekaas (1985), the

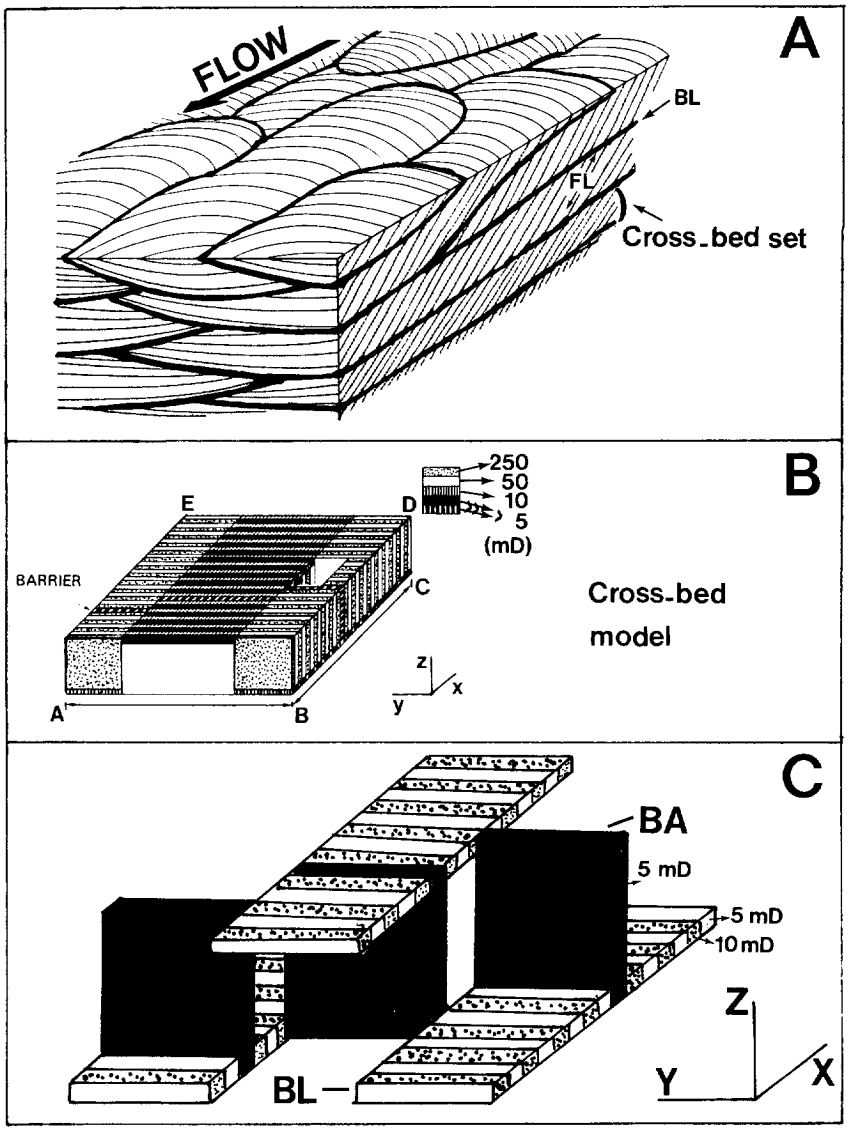

Fig. II.1 A) Features of cross-bedded sandstone with bottomsets effectively compartmentalizing the sandstone. B) The simplified model used for numerical simulations by Kortekaas (1985) (from Kortekaas 1985). C) A more detailed analysis of the model showing bottomsets (BL, alternating 5 and 10 mD) and barriers (BA, 5 mD). Note the laminated character of the bottomsets and the poor interconnection between the bottomsets in the Kortekaas model.

laminated character of the modelled bottomsets and the poor interconnection of bottomsets in the model is unrealistic (Fig. II.1). The conclusion that bottomsets only have minor effect on displacement characteristics is therefore doubtfull. For this same reason, the conclusion of a more favorable direction of flow in cross-bedded reservoir zones, based on the implementation of small-scale displacement characteristics in reservoir scale numerical simulations is questionable. This example highlights the need to study small-scale fluid flow behaviour only in geological accurate models, before any scaling-up of the fluid flow behaviour to reservoir scale is applied.

The characterization of geological heterogeneity in a reservoir based on outcrop and subsurface studies commonly preceeds the numerical and experimental modelling of fluid flow. In the previous chapter (chapter I), a geological characterization of cross-beds in fluvial channel-fills is given. This chapter comprises a literature survey and aims at establishing the possible influence of cross-beds on recovery efficiency in fluvial reservoirs in contrast with other types of heterogeneity occurring in fluvial channel-fills. In Chapter III and IV, detailed analyses are presented of permeability heterogeneity in cross-beds. Finally, in chapter V, numerical simulations and laboratory experiments are outlined that are based on well defined geological and physical models of cross-bedded reservoir zones.

II.1.1 Geological reservoir characterization

Most characterizations of reservoir heterogeneities are based on detailed outcrop studies combined with well-log and core data from subsurface reservoirs. Thus, geological models are created that focus on permeability distributions and baffles to flow. These geological models are used to study fluid flow behaviour. Little has been published about the actual production behaviour of a reservoir in comparison with the predictions that are based on these fluid flow models. Keijzer & Kortekaas (1990) investigated the history matching of fluid flow modelling, based on detailed description of the heterogeneous geology of the Statfjord reservoir, Brent Field, North Sea. They determined that a simulation model based on a probabilistic desciption of channel-sand architectures would

provide a more realistic description of displacement processes in these channel sands than a conventially constructed simulation model. Johnson & Krol (1984) incorporated results of geological modelling in the establishment of alternative development plans for the Statfjord Reservoir, Brent Field, North Sea. Many reservoir simulations are based on geological reservoir descriptions that are inadequate because wells are too far apart, too few intervals are sampled and core data are sporadic (Jones *et al.* 1984).

Reservoir characterization has also been applied for Enhanced Oil Recovery (EOR) projects (Szpakiewicz *et al.* 1987). Improvement in reservoir characterization for EOR requires an understanding of the depositional factors that affected the reservoir anatomy (internal structure and composition of the rock). Small-scale heterogeneities, not always critical in primary and secondary recovery, may affect sweep and displacement efficiencies in EOR operations significantly.

II.1.2 Comparatively low recovery factors of fluvial sandstone reservoirs

Fluvial sandstone reservoirs have been studied particularly well because large volumes of unrecovered mobile oil, almost 40% of the original mobile-oil saturations, remain to be recovered from fluvial reservoirs (Tyler 1988). Figure II.2 shows the percentages of unrecovered mobile oil as a function of depositional origin and drive mechanism. Fluvial-dominated deltas show a contrast in unrecovered mobile oil of more than 10% as a result of different drive mechanisms (strong and weak). A contrast of 20% remaining mobile oil is observed between fluvial systems and large barrier bars, both known as good potential reservoirs and both subject to a strong water drive (Tyler 1988). The difference in production behaviour between a barrier sandstone and a fluvial channel sandstone is even better shown in Fig. II.3. If a 5% oil cut (95% water cut) is assumed to be the cutoff for economic production, the channel sandstone reaches this value after approximately 35% of floodable oil has been produced. By contrast, in the barrier sandstone, oil cut is still a comfortable 20% after approximately 60% of floodable oil has been recovered (van de Graaff & Ealey 1989).

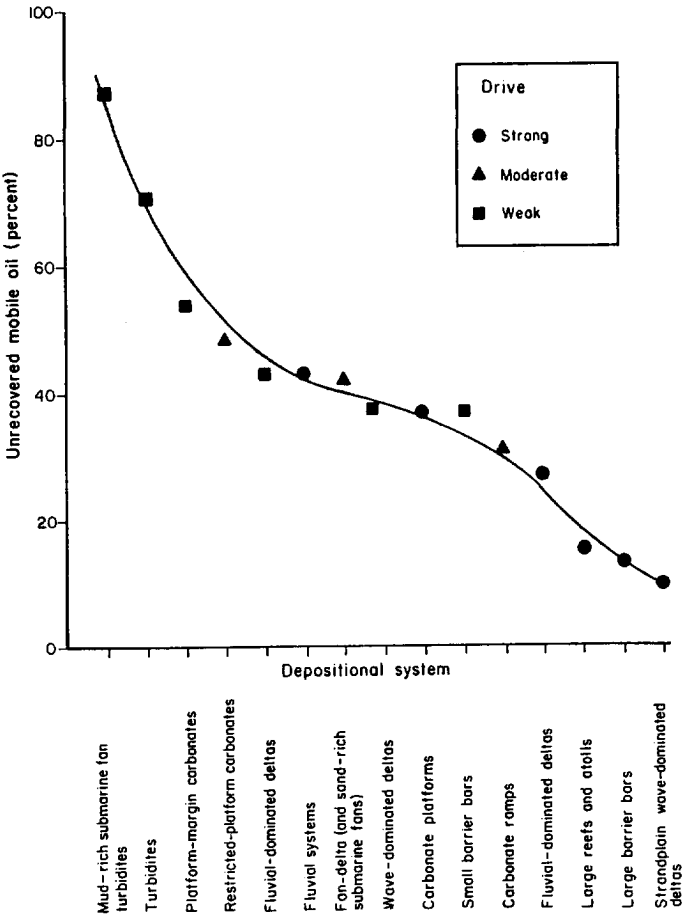

Fig. II.2 Unrecovered mobile oil is a function of depositional origin and drive mechanism. Greater volumes of mobile oil, as shown on this chart, remain in complex reservoirs with weak drive mechanisms, whereas wave reworked depositional systems with a strong water drive are efficiently flushed of mobile oil (from Tyler 1988).

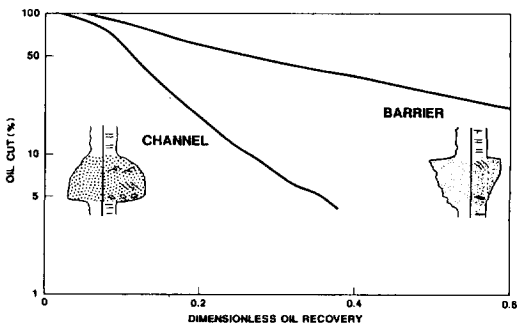

Fig. II.3 Oil cut versus oil recovery for channel sandstone and barrier sandstone reservoirs with identical absolute permeability but different permeability profiles. Channel sandstones have the highest permeability zone at base and barrier/bar sandstone at top (from van de Graaff and Ealey 1989).

II.2 CLASSIFICATION OF HETEROGENEITY SCALES

In the preceding sections several type cases were presented that illustrate the behaviour of fluvial reservoirs. The problems of fluvial reservoir performance are diverse and differ from one case to the other. Reservoir behaviour depends on heterogeneities on different scales. Weber (1986) suggested a classification of heterogeneities based on scale (Fig. II.4). The effects of different scales of heterogeneity on bypassing of movable oil is presented below and illustrated in Fig. II.5.

II.2.1 Reservoir-unit scale

The interconnectedness of sand bodies and the continuity of the reservoir units is a major factor that affects recovery in fluvial reservoirs, especially in discontinuous point-bar reservoirs (low nett-to-gross) and distributary-channel deposits on the delta plain. This

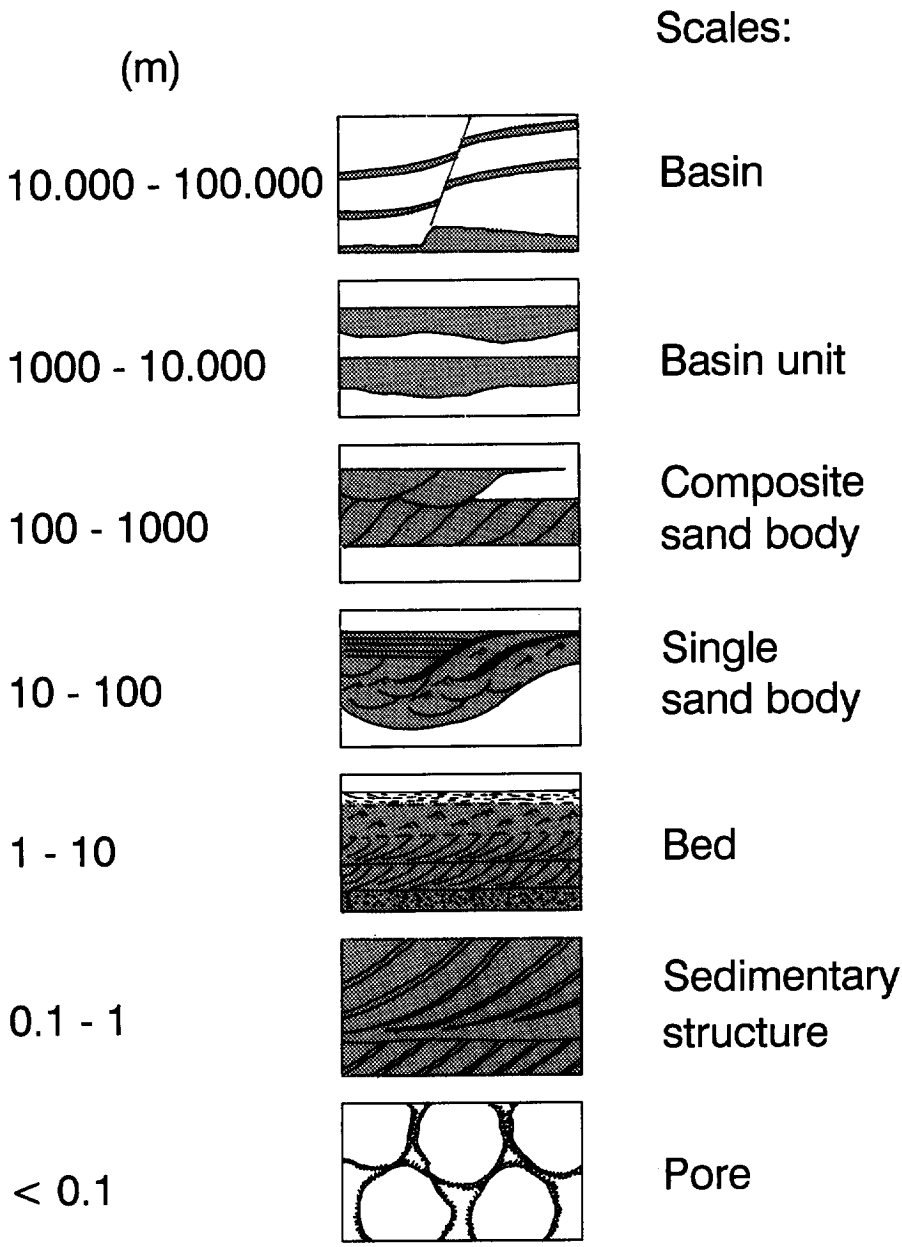

Fig. II.4 Classification of heterogeneities based on scale.

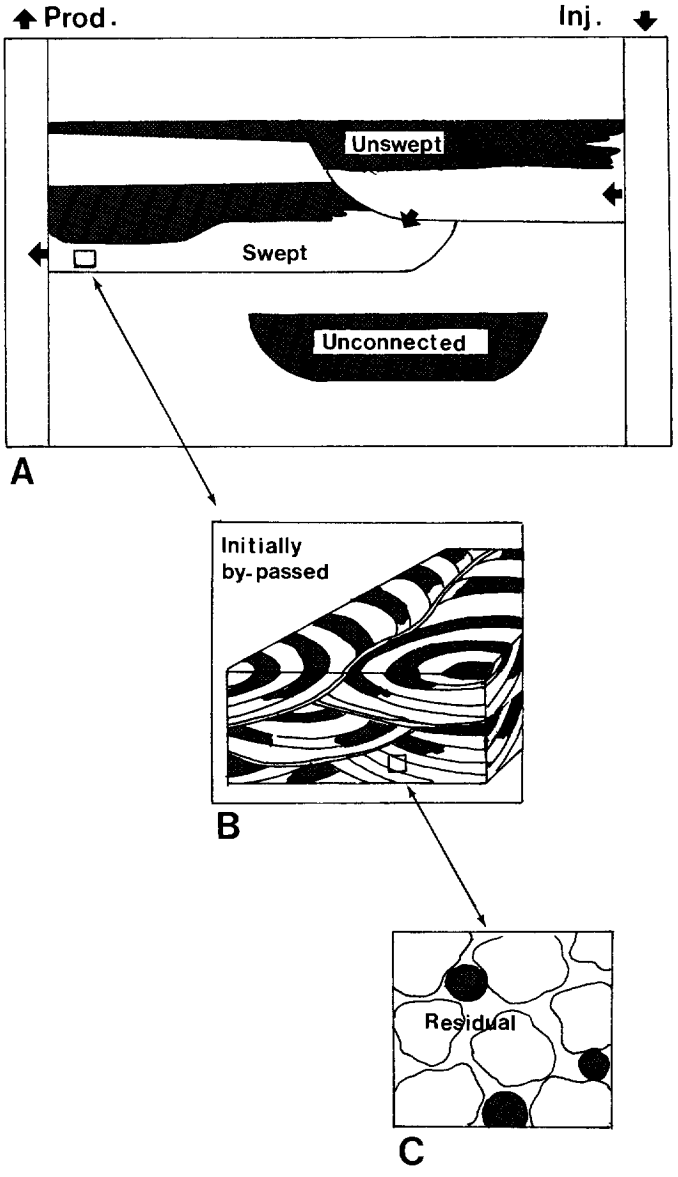

Fig. II.5 Classification of impact of different scales of heterogeneities on by-passing of oil. A) Example of by-passing on the scale of a composite sand body to single sand body (unswept and by-passed movable oil). B) Example of by-passing on the scale of sedimentary structures (initially trapped movable oil). C) Example of by-passing on the scale of pores (trapped residual oil) (modified from Weber 1986).

type of heterogeneity determines the compartmentalization of the reservoir and the areal by-passing of reservoir units after water flooding.

II.2.2 Genetic-unit scale

The internal characteristics of a distinct sand body are the main elements that affect heterogeneity on this scale. In fluvial reservoirs, typical internal characteristics of sand bodies are grain-size trends and low-permeability layers. The flow path of a waterflood and the resulting vertical by-passing of movable oil in genetic units is determined by heterogeneities on this scale.

II.2.3 Bed scale

Genetic units may consist of a stack of layers. These layers are internally characterized by a specific grain-size distribution and an accumulation of sedimentary structures. Because of the internal bedding characteristics, a waterflood preferentially follows more permeable layers and fingering occurs at the water front, resulting in bed-scale vertical by-passing of movable oil.

II.2.4 Sedimentary-structure scale

Cross-beds are laminated heterogeneous bed forms. Their internal texture and geometrical characteristics are described in section I.4. The heterogeneity of this scale is usually based on zones of contrasting grain size resulting in zones of contrasting permeability. Bottomset layers that compartmentalize the channel-fills are expected to have great influence on the flooding efficiency of a cross-bedded reservoir zone (Kortekaas 1985). This results in initial by-passing of movable oil in high-permeability foreset laminae. In tidally influenced cross-beds (see section I.5.3), impermeable barriers within

the cross-bedded sedimentary structures cause a more effective compartmentalization and may result in unswept sections in cross-beds (Fig. II.6).

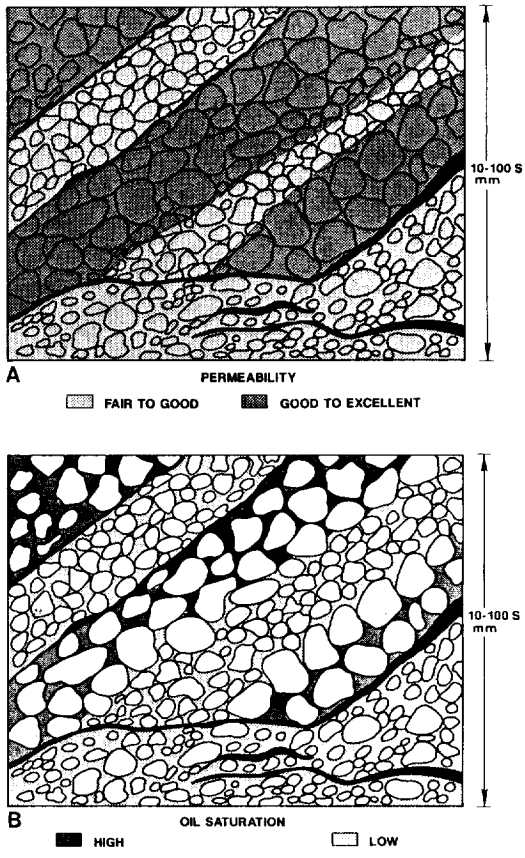

Fig. II.6 Example of sedimentary-structure-scale heterogeneity: A) Part of a cross-bed set with high and low permeability zones and clay draping of foreset laminae. B) shows the oil saturation within the same sedimentary structure (from van de Graaff and Ealey 1989).

II.2.5 Pore scale

Pore heterogeneities cause entrapment of oil in pores primarily by capillary forces. Small droplets of oil are bypassed and remain in the pores as unrecoverable (residual oil).

II.3 EXAMPLES OF HETEROGENEITIES IN FLUVIAL RESERVOIRS

II.3.1 Braided-sheet sandstone reservoirs

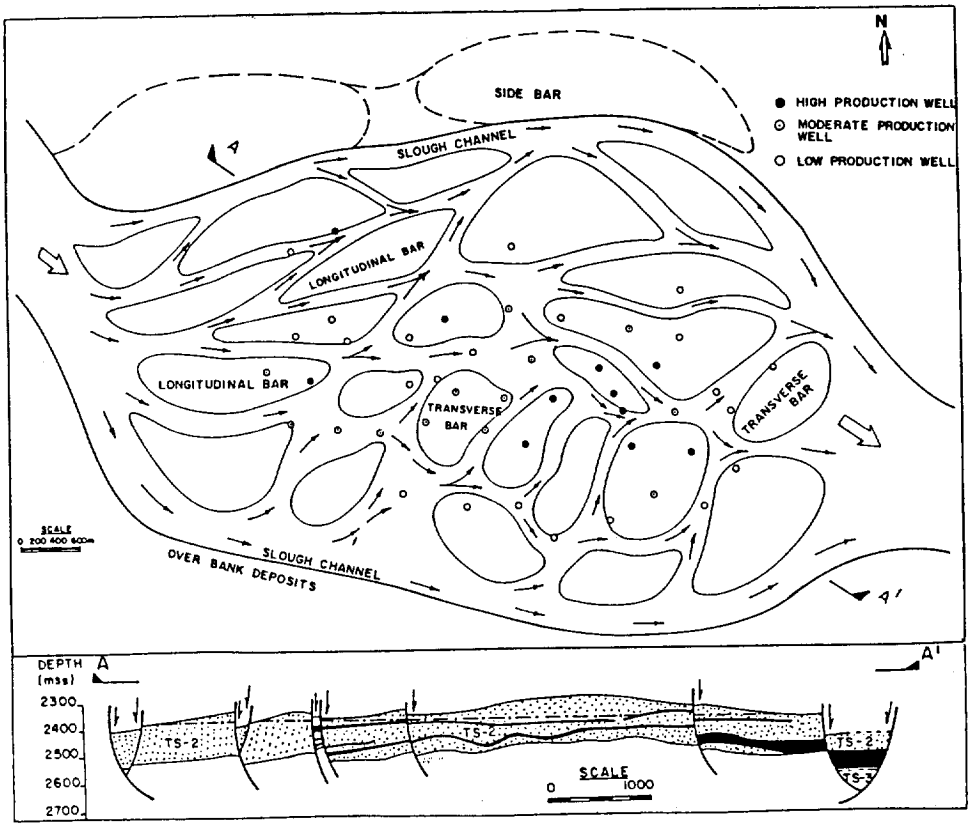

Fig. II.7 Depositional pattern of a braided channel environment of Tipam Sand-2, Lakwa Field, India and cross-section A-A' (from Singh *et al.* 1991).

Alluvial fan deposits are usually composed of sands and coarser clastic material deposited by braided streams. Braided-stream deposits exhibit a large variation in distribution and continuity determined by sediment supply, aggradation rate and basin subsidence. Some braided-stream deposits are distributed over very large areas and have extremely good lateral and vertical continuity. Composite braided sheet sandstone deposits generally contain more than 90 percent sandstone. They show repetitive incomplete (top missing) fluvial sequences, are fining upward and contain sedimentary structures. These fluvial sheet sandstones provide ideal hydrocarbon reservoirs (Le Blanc 1977).

The medium- to coarse-grained deposits of braided fluvial systems commonly have excellent reservoir characteristics. Hydrocarbon reservoirs in braided/meandering fluvial sand bodies are described from the Kern River Field by Brelih & Kodl (1990), in a braided fluvial reservoir from the Belly River Formation of the Peco Field in Alberta, Canada by Gardiner *et al.* (1990) and in the Tipam Sand-2, Lakwa Filed, India (Singh *et al.* 1991). A stacked composite braided-bar complex consists of a series of longitudinal and transverse bars which are flanked by marginal, abandoned and slough channel facies (Fig. II.7). This type of reservoir is highly heterogeneous because of multiple episodes of erosion, deposition and switching of channels, which lead to difficulties in tracing shale continuity within each sand (Singh et al. 1991). Water flooding is usually more successful in braided mid-channel bar reservoirs as a result of horizontal layering, than in other types of fluvial reservoirs (e.g. point bar reservoirs, Xue Peihua 1986).

II.3.1.1 Grain size controlled diagenesis in a braided-river reservoir

Braided river deposits usually have good reservoir quality (e.g. Singh *et al.* 1991). Fluvial hydrocarbon reservoirs typically show reasonably good porosity and permeability (ranging from 100 mD to more than 1000 mD). In contrast, an example of a severe diagenetically altered braided-river reservoir with poor porosity and permeability is given (Gardiner *et al.* 1990). This study of Gardiner *et al.* (1990) of the Belly River Formation, Peco field, Canada, shows that most diagenetic alterations of a reservoir that has undergone very severe diagenetic reservoir quality reduction are directly controlled by depositional factors, principally grain size. Three lithofacies were recognized within the

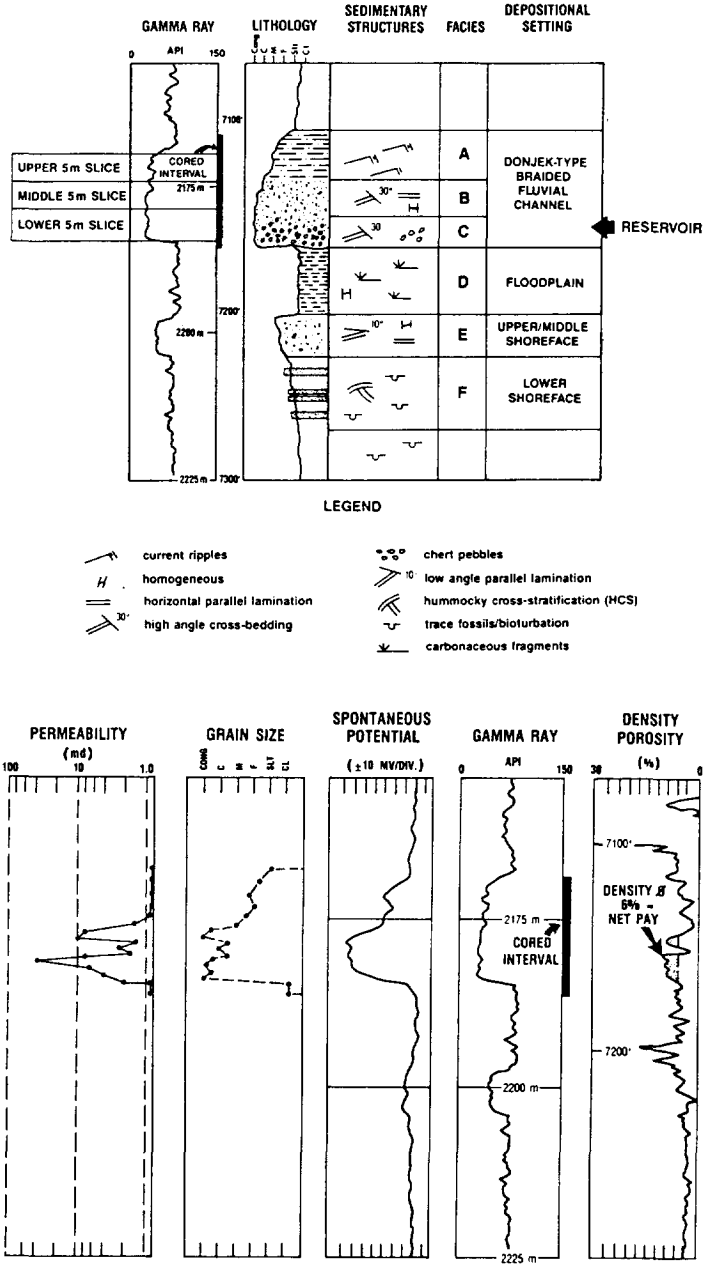

Fig. II.8 Sedimentary log and reservoir characteristics of a braided-river reservoir (from Gardiner *et al.* 1990).

braided channel sands; A) rippled, fine-grained sandstone, siltstone and shale; B) large-scale cross-bedded, fine- to medium-grained sandstone; and C) poorly sorted, large-scale cross-bedded sandy conglomerate to pebbly sandstone. The channel deposits directly overlay muddy floodplain deposits. Figure II.8 shows the sedimentary log and reservoir characteristics of the reservoir. The medium- to coarse-grained, lower part (lithofacies B+C) of the sand body is characterized by large-scale cross-bedded sedimentary structures.

The composition of the sand is related to the grain size. The percentage of chert fragments increases with increasing grain size, whereas the percentage of volcanic and argillaceous rock fragments decreases with increasing grain size. Both grain size and composition affect the reduction in total porosity resulting from compaction of the sand body; the finer-grained parts are more prone to a reduction in porosity/permeability than the coarser-grained parts.

In addition, reservoir quality has been reduced by diagenetic pore-filling clays and cements that precipitated from meteoric water. In the coarser-grained parts of the sand body some primary porosity has survived compaction, but it has been particularly affected by secondary cements and clays. Secondary leaching is common and contributes to a secondary porosity generation. Diagenetic water could more easily penetrate parts of the sand body that originally had a higher permeability and thus leach these parts to form the reservoir.

The depth of the reservoir is 2195 m, reservoir pressure varies between $12.2*10^3$ and $12.9*10^3$ kPa, reservoir temperature is not reported. Porosity averages 10% (range 6-13%) and the average permeability is 5 mD (range 1-150 mD). The drive mechanism of the reservoir is solution gas and wells have been stimulated using various types of fracturing (polyemulsion, gelled diesel). Even then, the recovery efficiency is reported to be as low as 10%.

II.3.2 Meander-belt sandstone reservoirs

Meandering streams migrate in belts that occupy 15 to 20 times the width of the

actual channel. A meandering stream produces extensive sheets consisting of coalescing point bars (Le Blanc 1977). The cross-section of a point bar is characterized by a very distinctive vertical sequence consisting of four different facieslayers: A) a poorly sorted basal section of sand and gravel, B) a zone of trough cross-bedded sand, C) a zone of horizontal and small-scale cross-bedded sand and silt and D) an upper layer of finer-grained, ripple-laminated sand and silt.

II.3.2.1 The influence of point-bar lateral-accretion surfaces on waterflooding

In China, according to incomplete statistics, hydrocarbon reserves contained in fluvial facies reservoirs are about half (53% approximately) of the recoverable reserves in currently developed major oil fields (Xue Peihua 1986). In these fields, water-flooded point-bar reservoirs often show a complex performance and poor development results. Water moves rapidly along the bottom part of the reservoir. Even when the water cut in an oil production well exceeds 90%, the water-swept thickness is only 25-50%, concentrated mostly in the lower-middle part of the sand body (Fig. II.9A). Even in this water-flushed interval, the flood efficiency is on average only about 40%. This lower-middle part of the point bar reservoir has the best porosity-permeability characteristics. In Fig. II.9B several characteristics are presented of a point-bar reservoir in the Da Qing Field. Clearly in this case is that the heterogeneity occurring in the lower-middle part of the reservoir is the result of large-scale cross-bedded sedimentary structures. The heterogeneity in the upper part is caused by the low-permeable argillaceous lateral accretion surfaces.

II.3.3 Distributary-channel sandstone reservoirs

On the delta plains, distributary channels funnel sand to the delta-front region. Most of the sand is transported as bedload and, consequently, the resulting deposits are strongly cross-bedded. Generally, most distributary-channel deposits are not completely filled with sand; only the lower portions of the deposits contain sand. Low- and high-

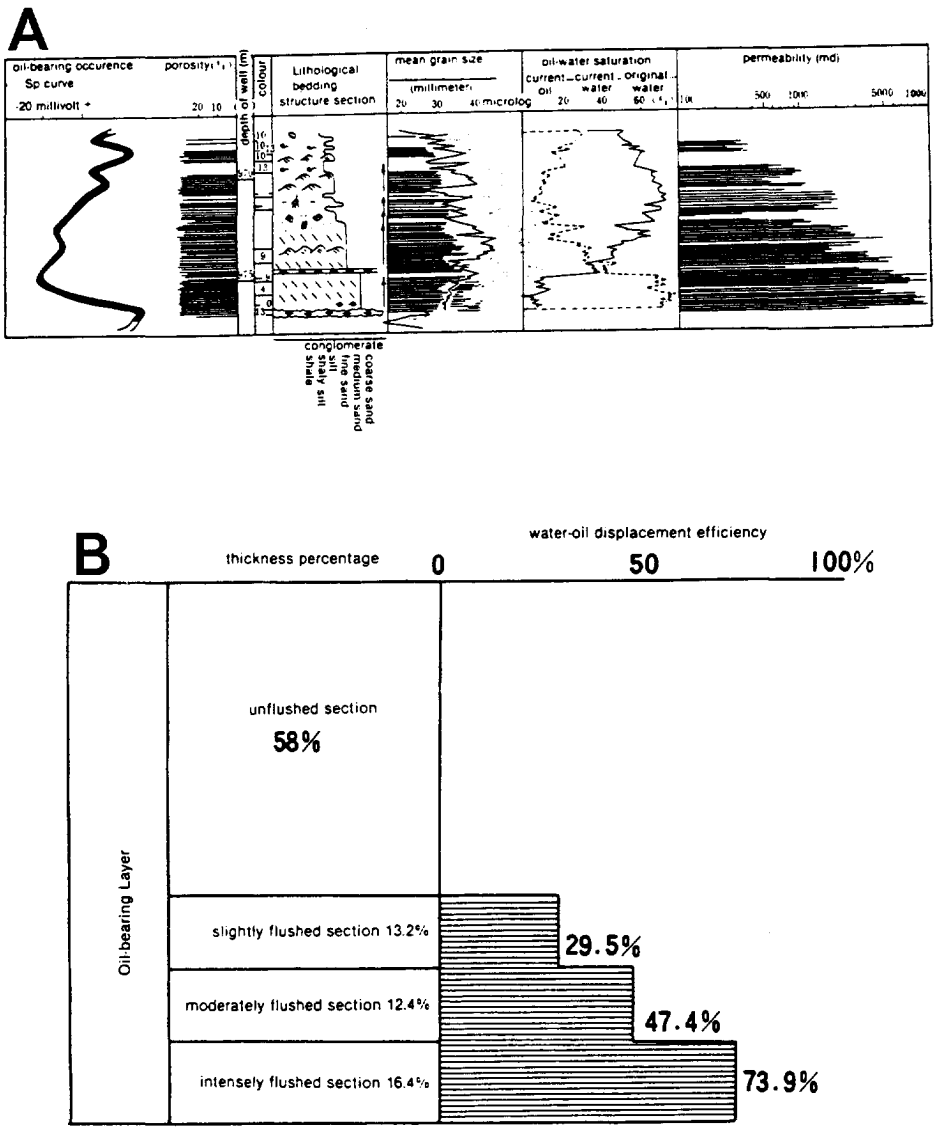

Fig. II.9 A) A columnar section of lithofacies and reservoir characteristics of a point-bar reservoir in the Da Qing Oil Field. B) Water flooding results of the oil-bearing part of the point-bar reservoir (from Xue Peihua 1986).

sinuosity channel deposits occur. Distributary-channel reservoirs are found in e.g. Venezuela (Bolivar Coast and Blocks I, III and V, Weber, personal communication), Nigeria and the U.S.A. (Weber 1971).

The reservoir heterogeneities occurring in the distributary-channel fill depend on a number of factors that control deposition of the sediment (low- or high-sinuosity channels, grain size, aggradation and subsidence rates). In the near-shore setting of these rivers, tidal influence in the river sediments can be expected, depending on the balance between tidal currents and the river's flow velocity at the time of deposition.

II.3.3.1 Permeability stratification in a delta-plain point-bar reservoir

Werren *et al.* (1990) described recovery results from reservoirs in point bars deposited on a delta plain in Mississippi, U.S.A. Despite of local heterogeneities, reservoir performance during primary production and waterflooding indicated good lateral continuity in the flooding direction. Production from these reservoirs required a thorough knowledge of a vertical permeability stratification and potential shale baffles and barriers within the point-bar sands. Average porosity and permeability are 24% and 100 mD, respectively. The recovery efficiency after primary production and waterflooding is 47%, the maximum recovery efficiency after tertiary CO_2 drive is 67%.

II.3.3.2 Stacked distributary channel fills in a fluvial-dominated delta setting

Parts of the Lower Carbonera reservoir in the Caño Limón Field in Colombia are described by Cleveland & Molina (1990) as a deltaic distributary channel sandstone. These channels show the highest reservoir quality compared with other facies, but can be very problematic as reservoirs because of their limited lateral extent and the marked variation in type of channel fill. The probability of interconnectivity between stacked channel fills increases as a result of an increasing Nett/Gross ratio. Channel fills exhibit sharp, erosional basal contacts. They consist of moderate- to poorly sorted, fining-upward sequences characterized by large-scale cross-bedded sedimentary structures. Channel-fill sequences are often obscured or incomplete as a result of channel stacking or amalgamation.

The recovery efficiency of all reservoir units in the Caño Limón Field is 54%. The major reserves occur in the distributary channel sands of the Lower Carbonera Formation, additional reserves are present in distributary and fluvial channel sands of the Upper Carbonera and in wave-dominated deltaic sands of lower units.

II.3.3.3 Permeability barriers in distributary channel fills in a wave-dominated delta

Sedimentological aspects of oil fields in a wave-dominated delta setting in the Niger Delta have been described by Weber (1971). He relied extensively on geological studies carried out in the recent Niger delta region. Samples from shallow boreholes on land as well as offshore provided the geologists with a model of the lateral and vertical geometries of the types of sand bodies present. Several genetic units were identified as barrier-bar/mouth-bar complexes and fluvial or tidal channel deposits. The delta plain behind the barrier bar comprises tidal flats and swamps alternating with tidal distributary channels and lagoons. The tidal channels are either meandering or straight. The tidal channels are characterized by a series of thin cross-bedded sequences fining upward with a clay-pebble or gravelly lag deposit at the base. The medium to fine grain sizes are similar to the fluvial deposits of the lower delta plain. Further land-inward, large sheet-like sand bodies are formed by well-developed meandering channels in a pure fluvial setting.

This model was used to interpret borehole logs from the ancient delta reservoir sand bodies. The different genetic units could be identified from the logs. The individual channel fills are characterized by clay breaks between the sequences, which give the channel fills a serrated character on the SP and gamma-ray logs. The stacked fluvial point-bar sheet sandstones usually form thick sandstone sequences with minor clayey beds between the overlapping point bars. The typical SP and gamma-ray responses show a bell or funnel shape. In particular, the width/thickness ratios of different recent channel deposits were analyzed and used in the subsurface interpretation (Fig. II.10). Information on permeability distributions in genetic units and on communication and permeability continuity between sand bodies increased the success of appraisal-well drilling in the Niger Delta reservoirs.

	Width (W) meters	Thickness (T) meters	W/T
Non-migrating distributary channel	125 - 1200	3 - 45	15 - 60
	larger ones (W > 500) tend to have W/T > 40		
Meandering channel-fills, point bars	1200 - 20000	9 - 90	100 - 800
	generally < 5000	generally 10 - 30	generally < 450
	larger ones (W > 3000) tend to have W/T > 300		
Barrier bars	1400 - 12000	8 - 30	150 - 500
	larger ones (W > 4000) tend to have W/T > 400		

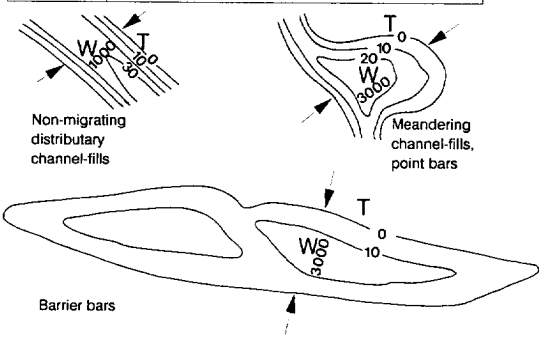

Fig. II.10 Geometry of common deltaic sandbody types and width/thickness ratios (from Weber 1986).

II.3.3.4 Braided-bar and point-bar reservoirs in a fluvio-deltaic setting

Miller *et al.* (1990) described a detailed study on the depositional setting and characteristics of the fluvio-deltaic reservoir in the Tulare Formation in the South Belridge field in California. They subdivided the depositional environments on the basis of distinctive and repeated lithofacies associations. Braided bars and point bars were distinguished within the fluvial channel sands. Point bars comprise the classical vertical fining-upward sequence of which the lower part consists of pebbly medium- to fine-grained, poorly sorted, cross-bedded sand. The braided bars are deposited as transverse

bars, which, for the major part show large-scale cross-bedding. Braided-bar deposits have the highest permeabilities and oil saturations, primarily reflecting the coarser grain size. Differences in reaction to steam drive within the reservoir can be explained by different lithofacies types and their distributions. In addition, a study by Kruit (1987) on the basis of a steam drive project in a fluvial-deltaic channel sands of East Tia Juana oil field in Venezuela shows that the success of steam injection is determined by the quality and depositional characteristics of the channel-fills. Those wells located outside a continuous channel fill produced diminished amounts of, or no, oil. The well in one of the abandoned channel fills produced only 25% as much as the well within the continuous, active channel fill.

II.3.3.5 Point-bar and vertical-accretion reservoirs in a fluvio-lacustrine deltaic setting

Qiu Yinan *et al.* (1982) discussed the results of waterflooding in braided-channel reservoirs, abandoned braided-channel reservoirs, point-bar reservoirs and distributary-channel reservoirs in a fluvio-lacustrine deltaic setting in China.

Braided-bar reservoirs that have a high horizontal and vertical permeability - 10 and 8 Darcy respectively - show a high productivity and a rapid rise in water cut in the producer wells. Gravity controlled underrunning of water is held responsible for this rapidly increasing water production. The abandoned braided-channel reservoirs are more heterogeneous because low-permeability baffles in the channel-fill complex were formed by repeated channel abandonment. The less permeable intervals are expected to restrain gravity effects and reduce the velocity of injected water which would ultimately increase the efficiency of waterflooding. The oil saturation after waterflooding in a braided-bar reservoir is still 60%, while abandoned braided bar complexes show oil saturations between 20 to 60%. Point-bar reservoirs are discussed by Xue Peihua (1986) and earlier described in this chapter (section II.3.2.1).

Distributary channels deposit sediments under low energy conditions. In general, deposited grain sizes are smaller and show better sorting than in point-bar or braided-bar deposits that were laid down under higher energy conditions. Contrary to meander-belt point bars, distributary-channel point bars form single sand bodies that have a limited

lateral extent. The distributary-channel fills often form multistorey sand bodies with a large vertical continuity. For a more detailed description see sections I.2 and I.3.

The multistorey sand bodies show a multiple rhythm of channel fills resulting from stacking of channel sands. Waterflooding takes place in the more permeable bottom parts of the multiple channel fills. Communication between the distributary channel fills increases the efficiency of waterflooding because the water-oil front will move down into a lower channel fill as a result of gravity. Figure II.9A shows the water-oil sweep efficiency in parts of a communicating channel fill. The intensely flushed section (16,4% of the oil-bearing channel-fill) is swept up to 73.9%. The moderately swept section (12,4% of the oil-bearing channel fill) is swept for 47.4%. The unflushed to slightly flushed sections (together 71,2% of the oil-bearing channel fill) is swept for less than 29.5%. It is not clear if swept zones have reached their irreducible oil saturations. However, it shows that the lower part of the channel fill, the intesively and moderately swept zones (28.8% of total oil-bearing channel fill) consist of medium-grained to fine-grained sand in which large scale cross-bedding is pervasive (Fig. II.9B).

Comparison of waterflooding in braided-bar, abandoned braided-bar, point-bar and multistorey-distributary-channel reservoirs in the China Lake Basin shows that waterflooding is most efficient in the distibutary-channel fill because of the multistorey character of these sand bodies and the good reservoir quality resulting from grain size and sorting characteristics. In addition, the study presented by van Veen (1977) of water-injection in channel-type reservoir, Lake Maracaibo, Venezuela, shows that the early identification of parallel, elongate high-permeability distributary channel-fills should help in selecting optimum points for injecting water into the reservoir.

II.4 SEDIMENTARY-STRUCTURE-SCALE RESERVOIR HETEROGENEITIES

The geological aspects of reservoirs have to be characterized on all scales for numerical studies. This includes small-scale reservoir heterogeneities.

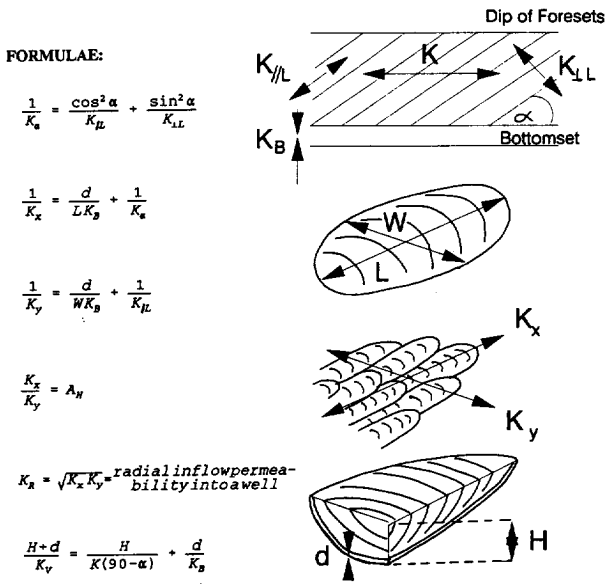

Fig. II.11 Formulae for computing directional permeability of trough cross-beds (from Weber 1986).

Several outcrop studies provided detailed descriptions and in-situ permeability measurements on a variety of scales (Chandler *et al.* 1989, Dreyer *et al.* 1990). Weber (1982) presented a paper concerning the influence of common sedimentary structures in reservoir sand bodies on fluid-flow.

Trough-cross-bedded sedimentary structures were analyzed to assess how they affected permeability in different directions (Fig. II.11). A model of a series of trough-cross-bedded sedimentary structures is displayed in a block diagram and shows the typical spoon-shaped geometry of one cross-bed set (Fig. II.12). The permeability distribution within these cross-bed sets is typical for a distributary-channel fill. Permeability is lower in the bottomset than in the foreset and in some cases bottomsets are impermeable, whereas foresets still preserve a reasonable permeability.

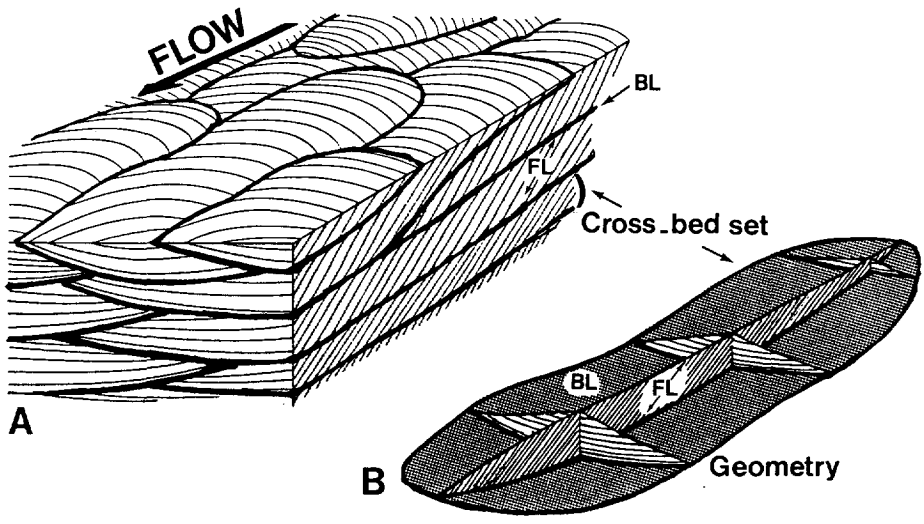

Fig. II.12 A) Three dimensional model of vertically stacked trough cross-beds with distinctive bottomset (BL) and foreset (FL) facies, note the inclined laminae (indicated by small arrows) in the foreset. Thick arrow indicates the palaeo flow direction of the river. B) Typical geometry of a trough cross-bed set (modified from Weber 1982).

In 1984 and 1987, Jones *et al.* presented a study concerning reservoir characterization for numerical simulation of a multilateral meander-belt sandstone deposit. The outcrop studied was subdivided into zones, characterized by core-plug permeability, shale-bed and clay-flake locations, stratification type and grain size. The different zones

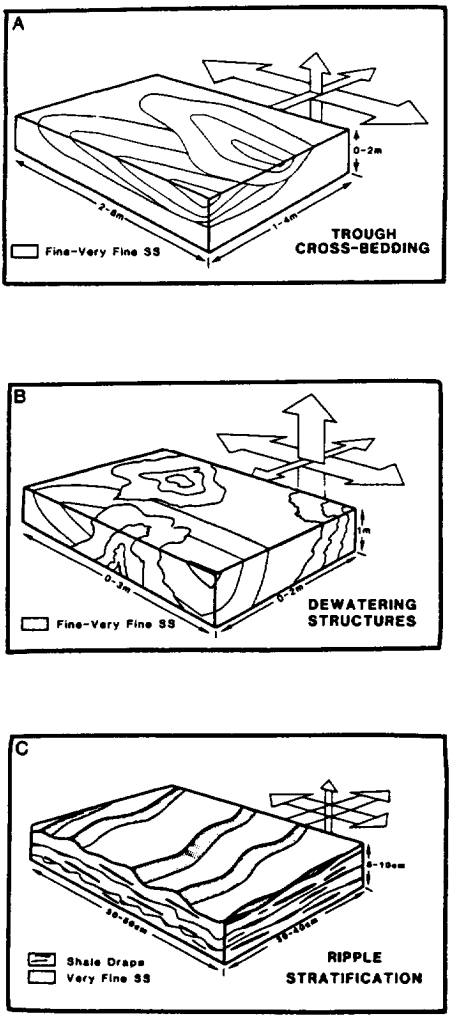

Fig. II.13 Inferred directional permeability trends for three facies types (from Jones *et al.* 1984).

recognized were: A) rippled siltstone associated with clay drapes, B) ripple stratification,

C) trough cross-bedding with clay drapes, D) trough cross-bedding and E) trough cross-bedding with dewatering structures. It was found that these five zones could be grouped into three significantly different facies on the basis of permeability measurements. Figure II.13 shows the inferred directional permeability trends for the three facies types. Trough cross-bedding exhibits maximum permeability parallel to the long axis of the trough, trough cross-bedding with dewatering structures shows enhanced vertical permeability. The facies with ripple lamination and trough cross-bed sets with clay-drapes is less permeable than the other two and its vertical permeability is greatly reduced.

Tyler *et al.* (1991) presented a study of the sand-body architecture and permeability distribution of a Gulf Coast deltaic reservoir. The Cretaceous Ferron delta system in Central Utah was selected as a suitable analog of that reservoir. The delta system was divided into different facies of which permeabilities were measured by minipermeameter. Within the delta system, distributary-channel sandstones have the highest mean permeability. Within the distributary-channel fill, trough cross-bedded deposits show the highest mean permeability. Three channel-fill types were recognized in the distributary system: A) tidally influenced channels, B) meandering channels and C) abandonment channels. The tidally influenced channel deposits are described as relatively narrow and laterally isolated channel fills. Internal structures include cross-bedding with large avalanche foresets and locally herringbone structures may be present. Palaeocurrent directions are typically bimodal. The meandering-channel fill is composed of the classical point-bar, vertical fining-up sequence. The abandoned-channel fill is characterized by a basal mudclast-rich part and an upper, intensely contorted part. Permeability measurements are presented in a frequency plot of four different lithofacies types (Fig. II.14); trough cross-bedded sets, planar cross-bedded sets, contorted bedding and bounding elements (scales of heterogeneity). Figure II.14 shows that permeabilities in trough cross-bedded sets are significantly higher than in planar cross-bedded sets. It is concluded that variation in permeability within a layer is related to grain size, sorting and mineralogy.

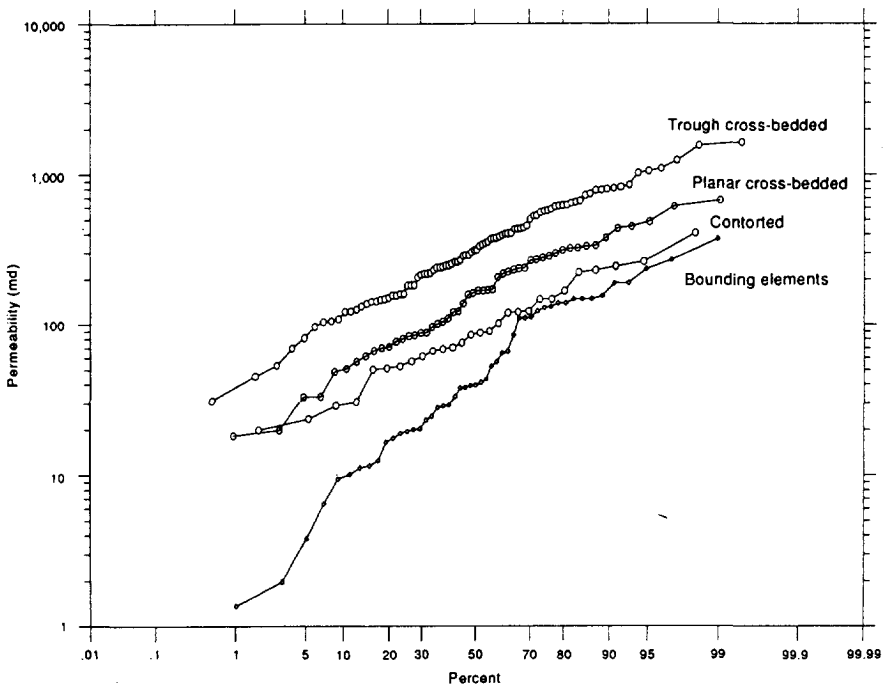

Fig. II.14 Cumulative-frequency plot of four different facies types versus permeability (from Tyler *et al.* 1991).

II.4.1 The effect of sedimentary-structure-scale heterogeneities on reservoir performance

Most lithofacies studies concerning fluvial reservoirs describe a grain size range from fine- to coarse-grained sand, showing large-scale cross-bedded sedimentary structures. The descriptions are in all cases used to identify and describe the depositional

environment of the reservoir. Only a few papers have ever been published that consider cross-bedded sedimentary structures as small-scale reservoir heterogeneities affecting fluid flow.

From the results of Xue Peihua (1986) it is obvious that the best-flooded part of a point-bar reservoir is the highly cross-bedded part. In this cross-bedded part, permeabilities are between 1 and 5 D and oil saturations after waterflooding range from 30 to 60%. Much effort is made to increase production from this reservoir by increasing the efficiency of waterflooding in the upper part of the reservoir sand body, including the "semi-connected" compartments between the low-permeable argillaceous lateral-accretion surfaces. However, there is little information about the high percentage of oil remaining in the waterflooded part. Qiu Yinan *et al.* (1982), on the other hand, recognized that cross-bedded structures are also obstacles to flow. They describe the occurrence of directional permeability as a result of foreset dip directions of cross-bedded sets in fluvial-channel sands. The waterflood migrates rapidly, preferentially in the original downstream direction. His laboratory experiments on laminated structures with alternating grain sizes showed a fingering effect of the water-oil front (Fig. II.15). It is obvious that the front shows a pronounced fingering into the laminae if waterflooding is perpendicular to the laminae. Less fingering and better flooding results were achieved in the experiment in which waterflooding was parallel to the laminae. Unfortunately, no details about the experiment or conclusions on results were presented in their paper.

Hopkins *et al.* (1991) discussed the effect of waterflooding on reservoirs in an estuarine valley fill. High water production from estuarine sediments is described to be the result of water breakthrough as a result of channelling of water parallel to shale beds. In one of the reservoir zones, shale beds and other larger-scale heterogeneities occurred less frequently, yet water production increased and was increasing long before waterflooding started. They suggest that the widespread occurrence of cross-stratification may contribute to excessive water production through low-permeable zones. Their conclusions are based on the study of Kortekaas (1985) on water/oil displacement characteristics in cross-bedded reservoirs. Although they could not actually observe or prove that increased water production occurred through low-permeable zones in cross-bedding, they could definitively exclude other causes (larger scale heterogeneities as shale

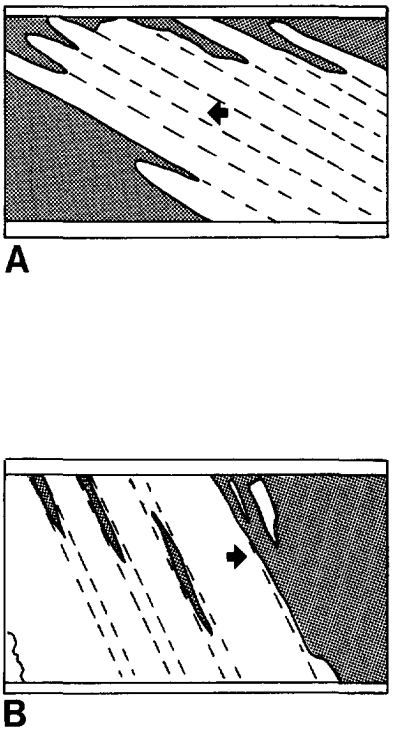

Fig. II.15 Deduced results from the laboratory experiment of water/oil displacement through a laminated model as presented by Qiu Yinan *et al.* 1982, in which in A) laminae are under a small angle to the flooding direction and B) laminae are under a large angle to flooding direction. The assumed flooding direction is indicated by black arrows. Water is white, oil is grey. A) a fingering effect of the water-oil front into a laminated sand (ultimate recovery 37.2%; Qiu Yinan *et al.* 1982) and B) less fingering (ultimate recovery 41.3%; Qiu Yinan *et al.* 1982).

layers, baffles or barriers to flow).

Their thin-section studies of the cross-stratified reservoir show contrasts in grain size and mineralogic composition between the foreset laminae that are believed to cause a significant permeability contrast of one order of magnitude between the laminae. These observations subscribed the occurrence of lower-permeable zones in the cross-stratified

sandstones.

II.5 DISCUSSION

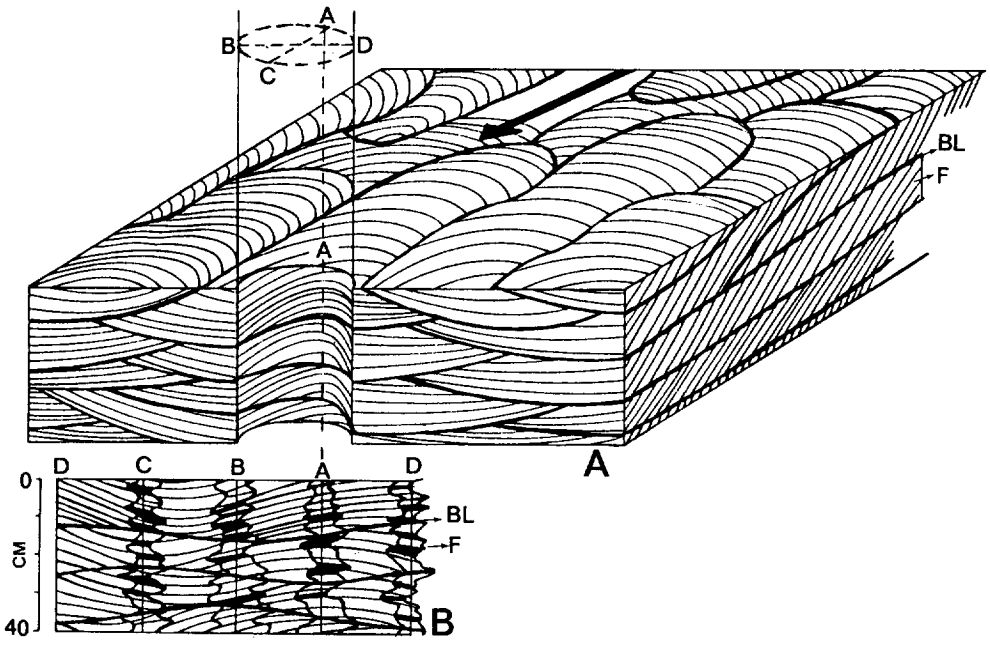

Fig. II.16 Trough cross-bedding as seen by SHDT tool. A) Cross-bedded reservoir section with bore hole indicated by A-C and B-D diameters. F is foreset, BL is bottomset. Arrow indicates the paleo depositional flow direction. B) is the bore hole wall unfolded with correlations of the vertical SHDT sections (from Höcker *et al* 1990).

Most fluid-flow modelling studies of fluvial reservoirs deal with the reservoir-unit-scale heterogeneities (e.g. Statfjord Fm., Brent field, North Sea: Johnson and Krol 1984, Brent Group, North Sea: Ravenne *et al.* 1987). So far, most large-scale reservoir fluid-

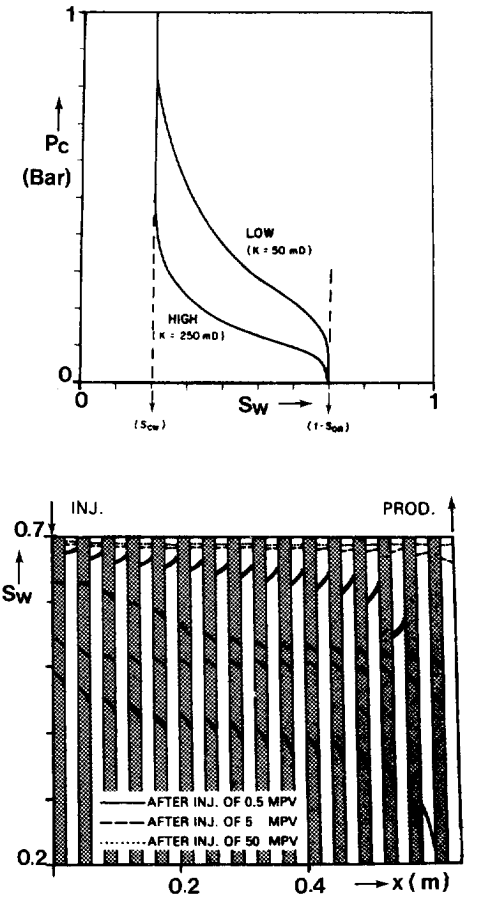

Fig. II.17 Capillary pressure curves of high- and low-permeability laminae of a one-dimensional model of a foreset and the water saturation in the high permeability (grey, 250 mD) and low permeability (white, 50 mD) laminae during a waterflood simulation (modified from Kortekaas 1985).

flow models do take pore-scale entrapment of oil into account (residual saturations) but neglect the effect of the sedimentary-structure-scale heterogeneities. Sedimentary-structure-scale entrapment of oil has not yet been identified in reservoirs, simply because tools for

detecting small local volumes of bypassed oil have not yet been developed. The identification of large-scale sedimentary structures in subsurface reservoirs is possible either from cores or by using the Stratigraphic High-Resolution Dipmeter Tool (SHDT, Höcker *et al.* 1990), the Formation Micro Scanner (FMS) and the Formation Micro Imager (FMI)[1] (Fig. II.16), the Circumferential Borehole Imaging Log (CBIL)[2] and Borehole televiewers.

The small-scale effect of cross-bedded sedimentary structures on two-phase fluid flow has been modelled by Kortekaas (1985). This model was based on assumed permeability contrasts and on contrasts in capillary-pressure characteristics between the laminae of cross-beds. One of Kortekaas computer models consists of a series of laminae with alternating permeability (contrast of a factor 5) and capillary pressure characteristics (Figs. II.17, A and B). During his modelling of water/oil displacement, water imbibition preferentially took place into the lower permeable laminae, initially bypassing the higher permeable laminae. It was this study that formed the basis of this thesis to quantify permeability contrasts between laminae and bottomsets of cross-bedded sets at outcrop and subsurface rock (CH. III A+B and CH. IV) and to improve the geological model for fluid-flow modelling (CH. V).

II.6 CONCLUSIONS

1) Cross-beds occur in the parts of fluvial sand bodies that have the best reservoir quality, that are the parts that are most easily flooded.
2) Remarkably low recovery efficiencies (40%) are reported from well-swept, good-reservoir-quality parts of fluvial reservoirs.
3) Characterization of fluvial reservoirs for fluid-flow modelling for secondary recovery or EOR projects is mostly concerned with heterogeneities on reservoir-unit scale and genetic-unit scale (sand-body geometries, interconnectedness and sand-body

[1]. Schlumberger.

[2]. Western Atlas Inc.

heterogeneities).

4) Little is known about the effect on two-phase fluid flow of sedimentary-structure-scale heterogeneities and hence their influence has essentially been ignored in large-scale models.

CHAPTER III
PERMEABILITY CHARACTERISTICS WITHIN CROSS-BEDDED LOW AND HIGH-SINUOSITY CHANNEL DEPOSITS IN CENTRAL SPAIN

III.1 FOREWORD

The contents of this chapter are presented with the permission of Blackwell Scientific Publishers. Both sub-chapters were previously published as:

III-A) HARTKAMP, C.A. AND DONSELAAR, M.E. (1993) Permeability patterns in point-bar deposits: Tertiary Loranca Basin, Central Spain. In: *The Geological Modelling of Hydrocarbon Reservoirs* (Ed. by S. Flint and I. Bryant), Spec. Publs Int. Ass. Sediment., Blackwell Scientific Publ., Oxford, **15**, 157-168.

III-B) HARTKAMP, C.A.; ARRIBAS, J. AND TORTOSA, A. (1993) Grain size, composition, porosity and permeability contrasts within cross-bedded sandstones in Tertiary fluvial deposits, Central Spain, *Sedimentology*, in press.

A few corrections were made in agreement with later findings.

The chapter aims at characterizing permeability heterogeneity in cross-bedded outcrops of Tertiary fluvial sandstones in the Loranca Basin, Central Spain. The first sub-chapter (IIIA) aims at defining permeability heterogeneity on genetic-unit scale and sedimentary-structure scale in one specific point-bar deposit. In the second sub-chapter (IIIB), permeability heterogeneity within cross-beds is related to variations in grain size, composition and porosity between adjacent foreset laminae and bottomsets. Cross-beds of several different outcrops in the same area were used for this purpose.

Permeability was measured by minipermeameter and a detailed analysis of the measurement method is given in Appendix A.

In the following sub-chapters, permeability data will be presented as arithmetic averages of data populations and sub-populations. A statistical analysis of minipermeameter sampled datasets and sub-datasets is given in Appendix B.

Finally, in appendix C, contrasts in permeability between the different sub-facies in a cross-bed as presented in sub-chapter IIIB, are evaluated.

CHAPTER IIIA
PERMEABILITY PATTERNS IN POINT BAR DEPOSITS: TERTIARY LORANCA BASIN, CENTRAL SPAIN

IIIA.1 INTRODUCTION

The low recovery efficiency of fluvial reservoirs in particular and of all heterogeneous reservoirs in general, highlights the need for better reservoir models based on detailed quantitative knowledge of the sedimentological parameters which determine the reservoir properties. Quantifiable sedimentological data include reservoir characteristics on all relevant scales, such as width-thickness ratios of sediment bodies, interconnectedness of the reservoir units, internal facies distribution, grain size and sorting, degree of bioturbation, shale length distribution, diagenesis and burial/decompaction history.

If data density is low, as is the case during the early stages of field development, probabilistic reservoir modelling can be employed and many possible realizations will be generated by the modelling exercise. Increasing the knowledge about the sedimentological parameters (the deterministic model) improves and validates the stochastic procedures and reduces the number of stochastic realizations. The upgraded stochastic models then form the basis for flow simulation studies, which help to outline the development strategy.

Research on permeability distribution on a wide range of scales and in a variety of sedimentary environments has been carried out over the last twenty years. Scales of reservoir heterogeneities based on outcrop and/or sub-surface data have been defined by Morrow (1971), Haldorsen & Lake (1984), Weber (1986) and Lewis (1988). Studies of permeability distributions in fluvial deposits are presented by Weber *et al.* (1972), Pryor (1973), Jacobsen & Rendall (1989), and Dreyer *et al.* (1990). The majority of these studies illustrate permeability characteristics on a large scale (reservoir and reservoir-unit scale, see Weber, 1986). Permeability values are generally averaged using statistical

methods (e.g. Dodge *et al.*, 1971; Pryor, 1973; Stalkup, 1986; Jacobsen & Rendall, 1989). Weber *et al.* (1972), Pryor (1973) and Chandler *et al.* (1989) focus on small-scale heterogeneities in the permeability distribution. A flow simulation study by Kortekaas (1985) has highlighted the influence of permeability anisotropy and capillary forces on fluid flow in cross-stratified sets. This study has clearly illustrated the need to incorporate small-scale (cross-set and lamina scale) permeability variations in flow simulation studies.

Fluvial hydrocarbon reservoirs with a low sand/shale ratio typically consist of a spatial arrangement of single or stacked lenticular sand bodies embedded in shale: the so-called 'labyrinth' reservoirs (Weber & van Geuns 1990). The spatial distribution of the fluvial sand bodies as well as the geometry and internal facies arrangement contribute to the complex heterogeneous nature and result in compartmentalisation of the reservoir. Oil entrapment in compartments and low-sweep efficiency through cross-bedded sedimentary structures (Kortekaas, 1985) are considered to be important causes for the low recovery efficiency typical of fluvial reservoirs. Recovery rates may be as low as 25-40% of oil in place, depending on the degree of reservoir complexity (Barwis *et al.*, 1989). Injection programs intended to enhance recovery are often unsuccessful if knowledge of the spatial arrangement, geometry and internal permeability barriers in this type of reservoir is incomplete (Van Veen, 1977).

The present study is concerned with the analysis of a detailed outcrop data set describing permeability contrasts in fluvial point bar deposits. Data acquisition was carried out in the Loranca Basin of central Spain. The object of this study is a composite point bar sandstone body which forms part of well-exposed, distal fluvial-fan deposits of late Oligocene to early Miocene age. Two types of depositional permeability heterogeneities have been studied: (a) the contact area of two stacked point bar units, and (b) the internal permeability distribution in a cross-bedded point bar. Data acquisition comprised conventional sedimentological procedures as well as on-site permeability measurements with the use of a portable permeability meter: the 'minipermeameter'.

IIIA.2 METHODS

With the portable permeability recording apparatus: the 'minipermeameter' (Fig. IIIA.1), nitrogen gas is injected into the porous rock, using a hand-held probe, with a 2 mm diameter tip-seal opening.

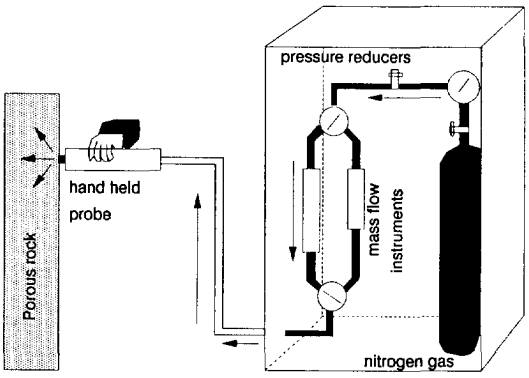

Fig. IIIA.1 Schematic drawing of the portable permeability apparatus, the 'minipermeameter'.

Both the gas-flow induced pressure differential (ΔP) and the injection pressure (P_{inj}) are recorded by a micromanometer, and recalculated to gas flow rate, using a generalized form of Darcy's law for minipermeameter experiments:

$$q_t = \frac{C\,\Delta P}{P_{inj}} \qquad (1)$$

where q_t is the flow rate in cm^3/min, C the specific calibration constant per flow tube, ΔP the pressure differential, and P_{inj} the injection pressure.

The permeability values are subsequently calculated from a series of previously established calibration curves (Fig. IIIA.2). Nitrogen gas is chosen because of its dry character and stable viscosity and flow performance in a relatively wide temperature range

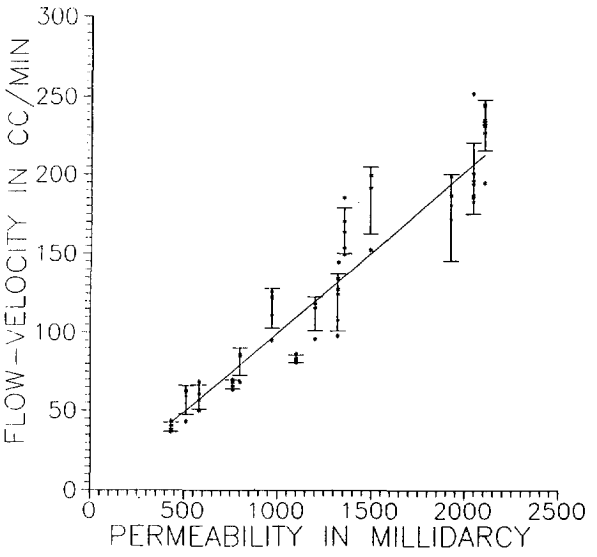

Fig. IIIA.2 Calibration curve of the relationship between flow rate and permeability, based on 65 measurements (marked with *) of 14 cores with laboratory-derived permeability values.

(Goggin, Thrasher & Lake, 1988). It should be noted however that a high temperature contrast between the nitrogen gas in the minipermeameter and the surrounding environment causes strongly varying, non-reproducible pressure readings (contrast of 10° C and higher). Measurements in highly permeable rock were expected to be problematic due to turbulent flow of the nitrogen gas (Goggin *et al.*, 1988), but during the field campaign micromanometer readings were usually stable and reproducible.

The effective penetration depth of the gas is equivalent to a core plug sample with a radius and length four times the internal tip seal radius (Goggin *et al.*,1988) (Fig. IIIA.3). In our case the minipermeameter measurements affect an area with a radius and depth of 4 mm. Eighty to ninety percent of the measurements record the permeability properties of the first few cubic millimeters of rock. Reliability of the measurements is

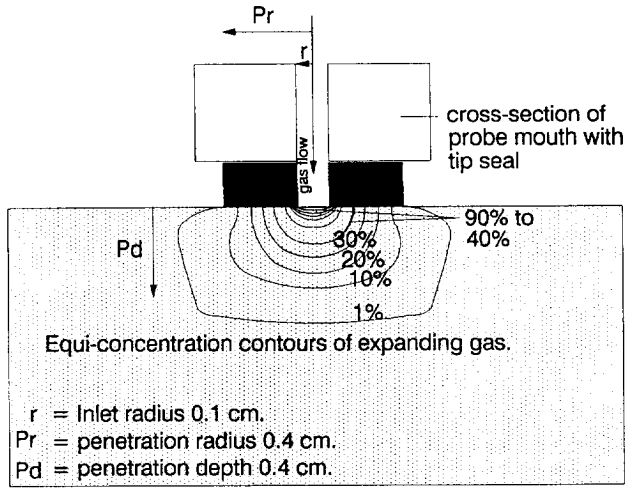

Fig. IIIA.3 Penetration radius and depth of gas invasion in a porous medium (modified from Goggin *et al.* 1988).

enhanced by removing the weathered surface of the rock. The fluvial sediments in the Loranca Basin have a low degree of cementation and hence a friable surface. Removal of the weathered surface was achieved with a steel brush. Dust was subsequently removed with a soft brush. This cleaning method enhanced the visibility of sedimentary structures on the measured surface.

The limited penetration depth (Fig. IIIA.3) and radius of the minipermeameter measurements allow the use of a closely-spaced grid without overlap of flow velocity values in successive grid points. For this study various closely-spaced grids were applied to characterize the permeability patterns of the point bar sediment body. A grid with a vertical to horizontal spacing of 2.5 cm to 5 cm respectively (number of grid points: 69) was used to measure permeability contrasts across the boundary of two stacked point bar units. A grid with a 1 cm vertical and 10 cm horizontal spacing (total number of grid points: 1096, Fig. IIIA.9) was measured to define the permeability patterns within a

single point bar unit. Additional grid points were measured on key horizons in between the grid rows. Data were processed and correlated in the field in order to have direct control on the measurements and to re-record doubtful grid point readings. Selected core samples were taken with an electrical drill. Several samples were impregnated with blue coloured araldite for microscopic analysis of the porosity distribution and petrology of the rock.

IIIA.3 GEOLOGICAL SETTING

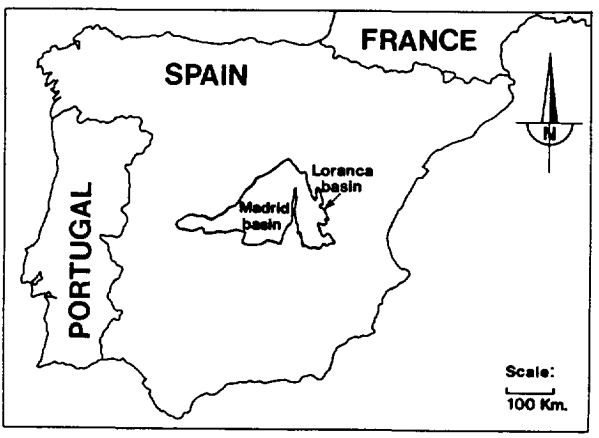

Fig. IIIA.4 Tertiary cratonic basins in central Spain. (modified from Diaz Molina *et al.* 1989).

The depositional history of the Iberian Peninsula during the Tertiary was strongly influenced by plate tectonic movements. The Iberian plate was squeezed between the northward moving African plate and the rigid Eurasian plate in a compressive period which lasted from the Late Cretaceous to the Middle Miocene (Choukroune, Le Pichon & Seguret, 1973). On the Iberian plate the compression generated a number of cratonic

depressions separated by mountain belts. The depressions were subsequently filled with molasse-type sediments.

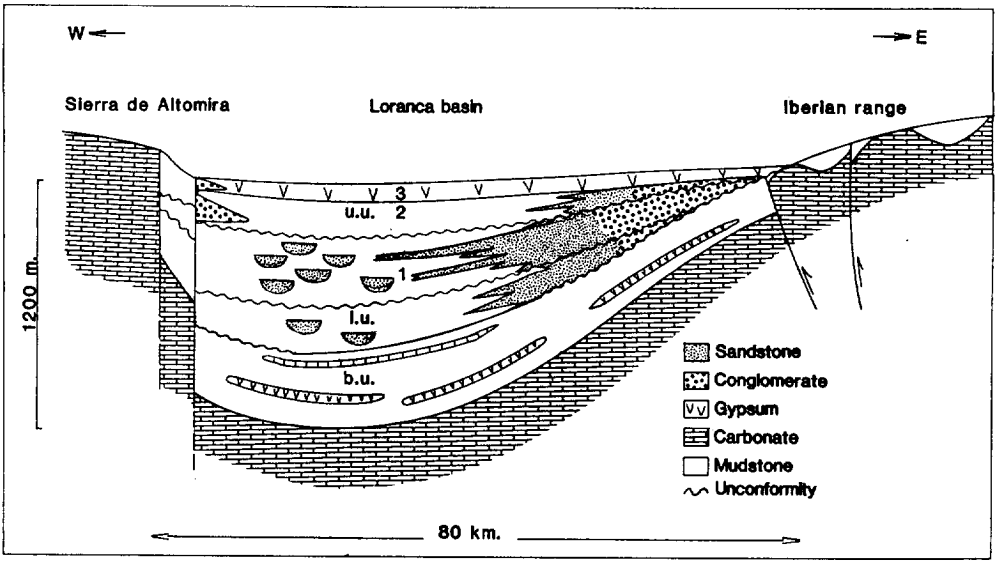

Fig. IIIA.5 Schematic cross-section through the Loranca Basin. b.u. = basal unit; l.u. = lower unit; u.u. 1-3 = upper unit with sub-units 1 to 3. Faults in the Sierra de Altomira have a sinistral strike-slip component.

The Loranca Basin of central Spain (Fig. IIIA.4) is one of these cratonic basins. The basin comprises a 100 km long and 80 km wide north-south trending depression which is limited to the east by uplifted, folded and faulted Mesozoic rocks of the Iberian Range. This mountain range acted as principal sediment source area to the Loranca Basin (Díaz Molina *et al.*, 1985). The western basin margin consists of a narrow, north-south trending thrust belt, the Sierra de Altomira. Subsidence in the Palaeogene was strongest adjacent to the Sierra de Altomira and resulted in an asymmetric basin fill (Fig. IIIA.5) with a maximum cumulative thickness in the western part of the basin of over 1200 m of Paleocene to Miocene clastic sediments (Díaz Molina *et al.*, 1985). Basin fill took place

by successive alluvial fan systems which deposited suites of fluvial fan conglomerates and sandstones and associated fine-grained clay flat, playa lake and lacustrine deposits.

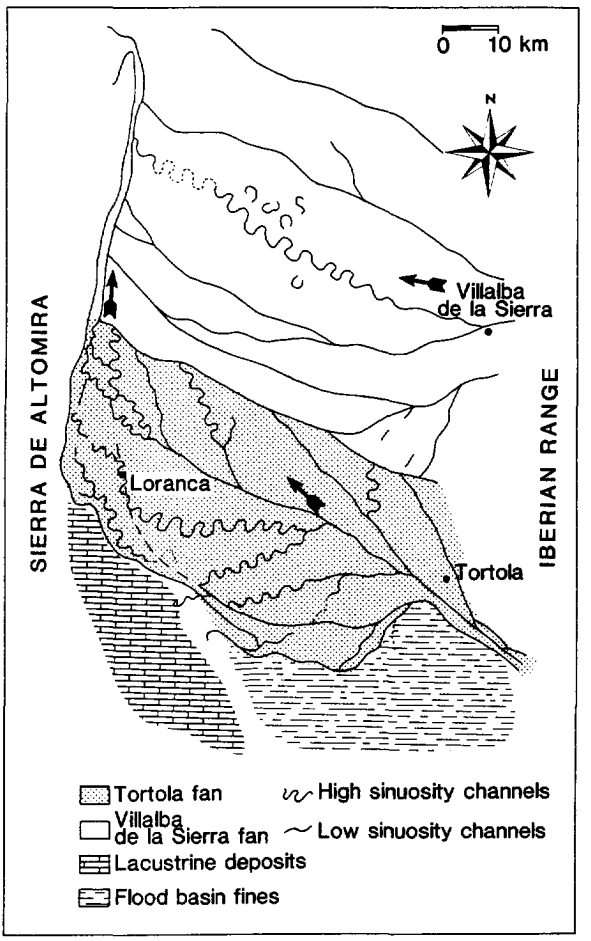

Fig. IIIA.6 Palaeogeographic reconstruction of the Tórtola and adjacent Villalba de la Sierra fan systems. Arrows indicate general flow direction of the fluvial channels (modified from Diaz Molina *et al.* (1989).

The deposits discussed in the present paper comprise the upper part of the Tórtola

fan of Late Oligocene - Early Miocene age (Díaz Molina *et al.* 1989). The Tórtola fan has its source area in the Iberian Range, its maximum length and width are 94 km and 40 km respectively, and it covers an area of 2500 km^2 (Fig. IIIA.6; Díaz Molina *et al.*, 1989). The fan is of the wet fan type (Schumm, 1977) and has a radial fluvial distributary pattern. Fan progradation in the western direction was restricted by the Sierra de Altomira thrust belt which forced the fluvial channels to flow to the north, parallel to the axis of the thrust belt. The northern part of the fan coalesced with an adjacent fan system (Fig. IIIA.6). Distal fan sedimentation produced vertically- and laterally-stacked sandstone bodies embedded in fine-grained deposits. Sandstone bodies were formed by meandering and braided fluvial channels.

IIIA.4 SEDIMENTARY FACIES DESCRIPTION

The studied fluvial sediment body (Fig. IIIB.1, location XVII) has a lenticular geometry and contains seven vertically and laterally stacked point bar units (Fig. IIIA.7). The sediment body has a length and thickness of 100 m and 6 m respectively.

Each point bar unit consists of lateral accretion deposits. During stages of channel abandonment the accretion surface was draped with mud. Partial preservation of the mud drape depends on the rate of erosion during subsequent channel reactivation, and on the orientation of the next meander loop (Díaz Molina, 1991). In the studied composite point bar complex the bounding surfaces between stacked point bar units show partially-preserved mud drapes (Fig. IIIA.7C). The drapes are restricted to the topographically higher part of the accretion slope. Downslope the mud drape is eroded and sand-on-sand contact between successive point bar units is a common feature.

The preserved abandonment layer measured in detail in this study (Fig. IIIA.8) consists of a 10-15 cm thick, 7 m long very-fine sand and silt layer. The abandonment layer is rootletted and thoroughly cemented with calcite of early-diagenetic origin. The high degree of cementation contrasts with the over- and underlying point bar sands, where calcite cementation is restricted to the grain contacts.

The lower 70-80% of the point-bar units consist of trough cross-bedded, medium-

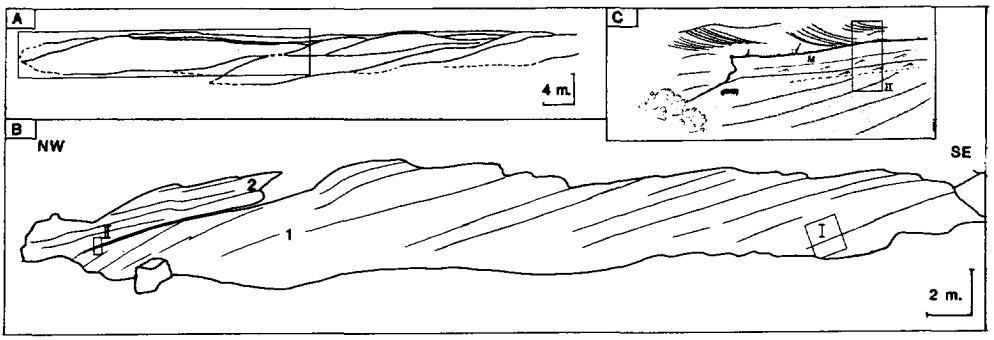

Fig. IIIA.7 A) Outcrop drawing of stacked point bar units (modified from Diaz Molina *et al.*, 1989). Box indicates the area of Fig. IIIA.7B. B) Drawing (from photo-panel) of the studied point bar units 1 and 2. Thin lines represent the lateral accretion surfaces. Thick line between units 1 and 2 is the very fine-grained, cemented horizon. Boxes I and II are the grid locations. (Box I see Fig. IIIA.9, Box II see Fig. IIIA.8). C) Drawing of the channel abandonment mud drape between two stacked point bar units. Down the accretion slope, the mud drape is eroded and a sand-on-sand contact is present. Height of box II is 30 cm.

to coarse-grained sand. The upper 20-30% is characterized by small-scale-rippled, even-laminated to non-laminated, structureless (bioturbated) fine sand. Internally each point bar unit shows lateral accretion units. These units are sandy throughout, no mud drapes are observed on the accretion surfaces. Trough cross-bed sets climb up along the lateral accretion surfaces (Fig. IIIA.9), such that bottomsets are parallel to the dip of the accretion surfaces. The foresets consist of alternating laminae of fine- and medium to coarse grain size. Lamina thickness is 1-10 mm. Individual foreset laminae are moderately to well-sorted. Bottomsets are invariably well sorted and range in grain size from very-fine to medium sand. Grain size and sorting differences typically reflect the flow conditions during sedimentation: foreset laminae are sorted by size during avalanching along the leeside of the mega-ripple, while bottomsets result from fine grained suspension fall-out. Bottomsets make up 20-30% of the total volume of the preserved part of the cross-sets.

Generally, the sandstone consists of 75% quartz, 20% carbonate and 5% feldspar and gypsum clasts, with a primary porosity of 25 - 30% and a secondary porosity of 5 -

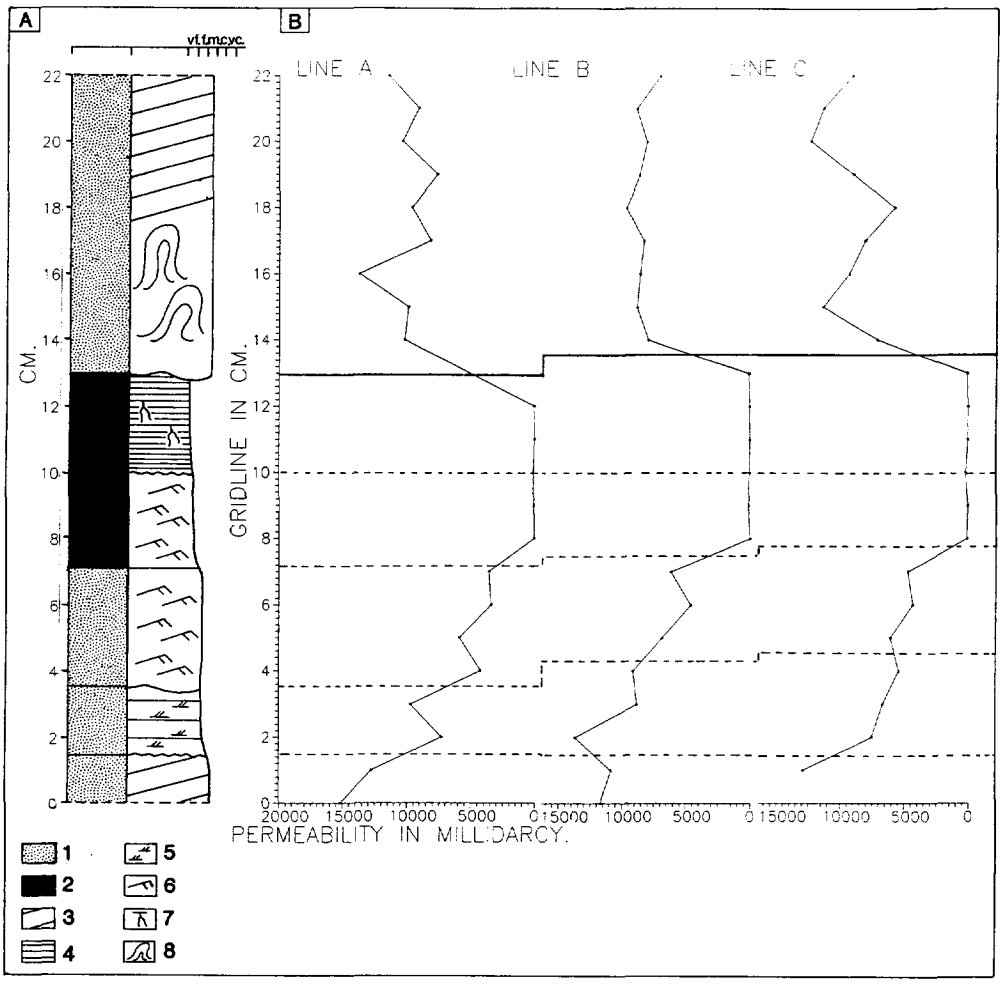

Fig. IIIA.8 A) Vertical log across the boundary of two superimposed point bar units. Legend: 1 = sand; 2 = very-fine sand and silt; 3 = lateral accretion; 4 = horizontal lamination; 5 = small-scale ripples; 6 = climbing ripples; 7 = rootlets; 8 = contorted bedding. B) Permeability pattern across the point bar transition zone. Continuous line: contact horizon between the successive point bar units. Dashed line: correlation horizons. Spacing of the grid columns is 5 cm.

10%. Detailed analysis of grain size, mineralogic composition and porosity of the

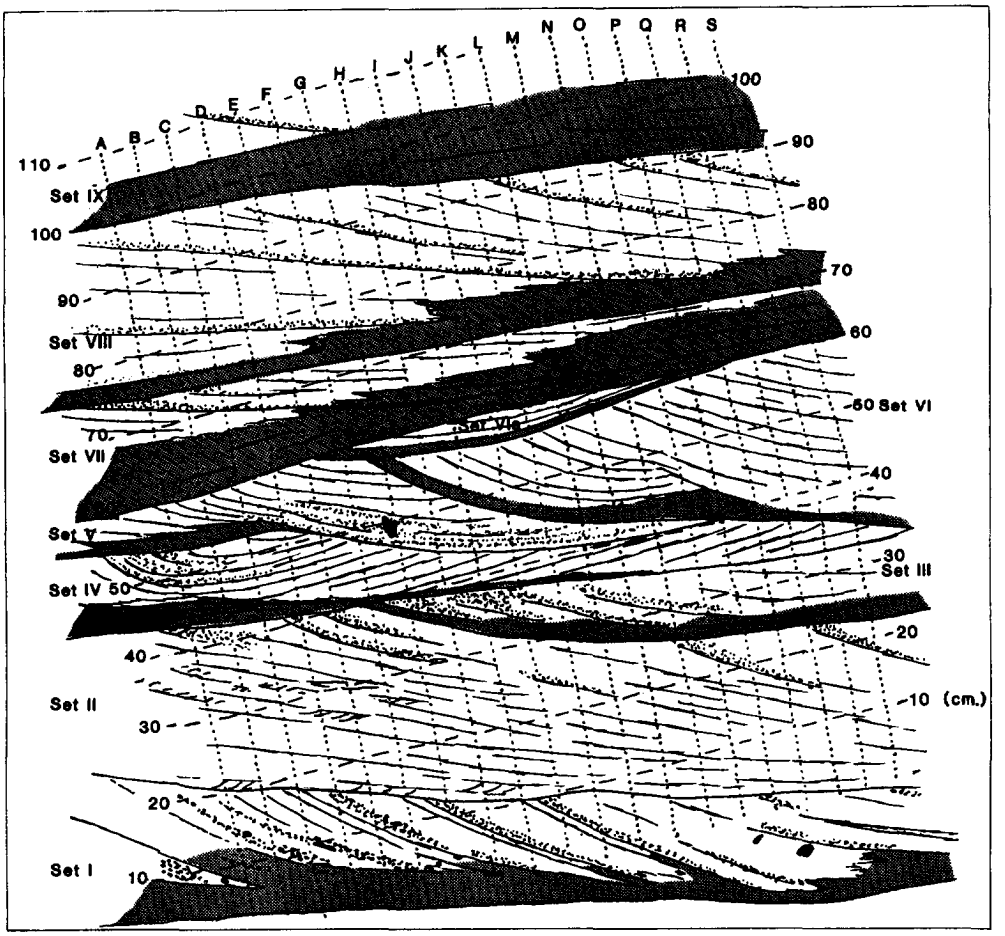

Fig. IIIA.9 Drawing (from photograph) of the measured grid over the trough cross-bed sets (set I to IX) that make up the lateral accretion units. Bottomsets are marked in grey. See Fig. IIIA.7B, box I for location of the grid. Spacing of the grid columns A-B, B-C, etc. is 5 cm, grid row points are 1 cm apart.

sandstones is presented in Chapter IIIB. The calcite cement in the very fine grained abandonment facies is probably formed as an early-diagenetic cement due to palaeosol

formation.

IIIA.5 PERMEABILITY MEASUREMENTS

IIIA.5.1 Permeability distribution over the contact area of two point bar units

The decrease of grain size and the increased degree of cementation at the transition between two stacked point bar units are reflected in the permeability pattern across the boundary (Fig. IIIA.8). A strong upward decrease in permeability (from 10 D to 0.1 D) characterizes the upper part of the lower point bar unit, and is followed by a rapid increase in permeability in the upper point bar unit to values comparable with the cross-bedded parts of the lower one. This low permeability zone between the two highly permeable units is discontinuous and extends from the adjacent flood-plain down onto the abandonment layer (the preserved part of the abandonment mudstone drape). Further downslope, stacking of the point-bar units is characterized by sand-on-sand contacts with normal, high permeable transitions (mudstone drape eroded) (Fig. IIIA.7C).

Fluvial oil reservoirs of meandering river deposits are often compartmentalized by similar low permeability abandonment layers, which result in a marked permeability anisotropy that can influence sweep efficiency.

IIIA.5.2 Small-scale permeability heterogeneities

Permeability variation in the trough cross-bedded part of a point bar is directly proportional to grain size and sorting of the cross-bed sets (Beard & Weyl, 1973). This results in a permeability contrast between bottomsets (values 0.5 - 7 D) and foresets (values 5 - 17 D) (Figs. IIIA.9, 10 and 11A). Foresets are characterized by a larger permeability variation because of the varying grain sizes of the individual laminae. The highly variable permeability values in set II (Fig. IIIA.10) are caused by the occurrence of small-scale ripples (cm-scale) on the foreset laminae. In some sets the coarse-grained

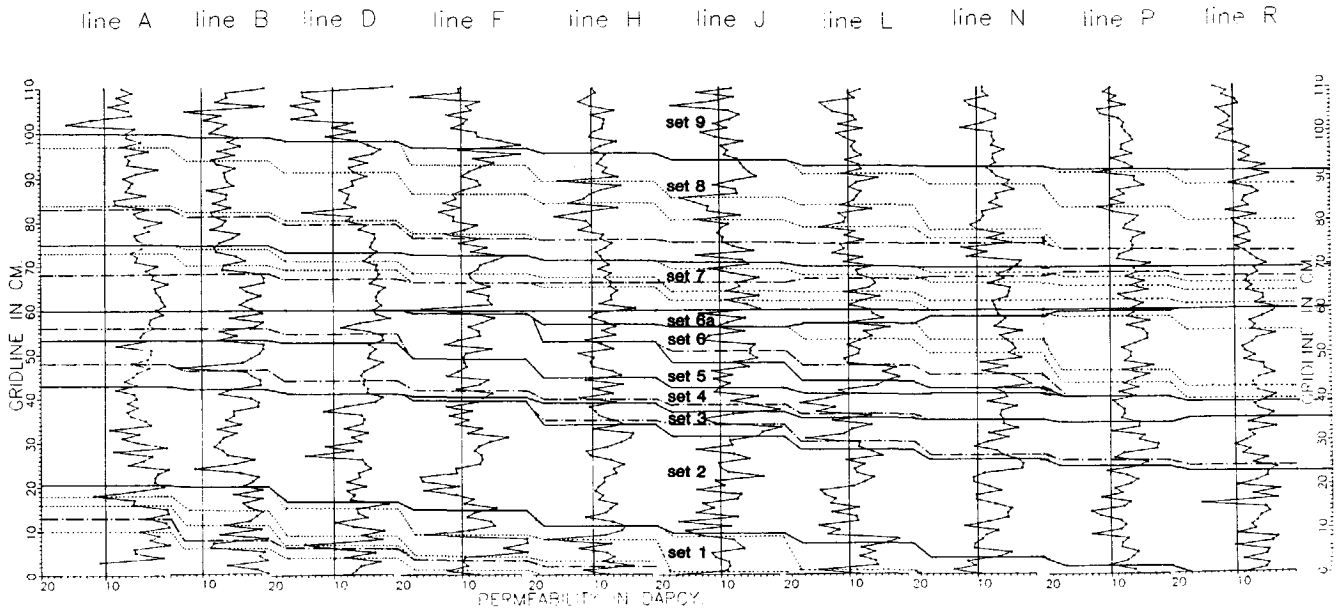

Fig. IIIA.10 Permeability pattern of trough cross-bed sets. Continuous line: base of cross-beds. Dashed-dotted line: boundary between foreset and bottomset. Dotted line: inclined foreset lamina. Spacing between vertical grid lines is 10 cm, except for lines A and B, which are 5 cm apart. Refer to Fig. IIIA.9 for exact location of grid columns.

foreset laminae grade into the bottomsets and are characterized by a vertical alternation of higher (foreset) and lower (bottomset) values.

Table IIIA.I. Average permeability, standard deviation (SD) and the number of measurements of foreset and bottomset. Refer to Figs. 9 and 10 for position of cross-bed sets 1-9.

	Foreset			Bottomset		
	Average	SD	Number	Average	SD	Number
Set 1	7.13	4.02	65	5.18	3.64	31
Set 2	7.86	3.12	176	6.61	3.4	51
Set 3	7.15	2.75	34	5.32	2.11	14
Set 4	6.83	3.99	41	5.29	2.76	26
Set 5	7.54	3.82	33	5.04	2.2	19
Set 6	6.91	2.28	79	4.9	1.94	17
Set 7	6.57	2.19	49	4.44	2.29	65
Set 8	7.84	2.77	174	6.75	2.78	62
Set 9	9.94	2.53	96	7.83	1.76	59

In order to test the statistical difference in the mean of both sets of measurements (Table IIIA.I, foreset and bottomset) the Wilcoxon test[1] was done. The total number of datapoints (1096) has been subdivided into foreset-data and bottomset-data. The data sets represent stochastically normal populations. The nine average bottomset values of the nine cross-sets were tested against the nine average foreset values. The test showed that the foreset population was characteristically more than 2 D higher than the bottomset population (confidence limit 99%) (Fig. IIIA.11). This test-case confirms the expected result of average foreset permeability values to be higher than the average bottomset values. In Table IIIA.I, average permeability values show an upward decrease and

[1] A statistical test to prove a significant difference between two distinct data populations (foreset and bottomset, Table I).

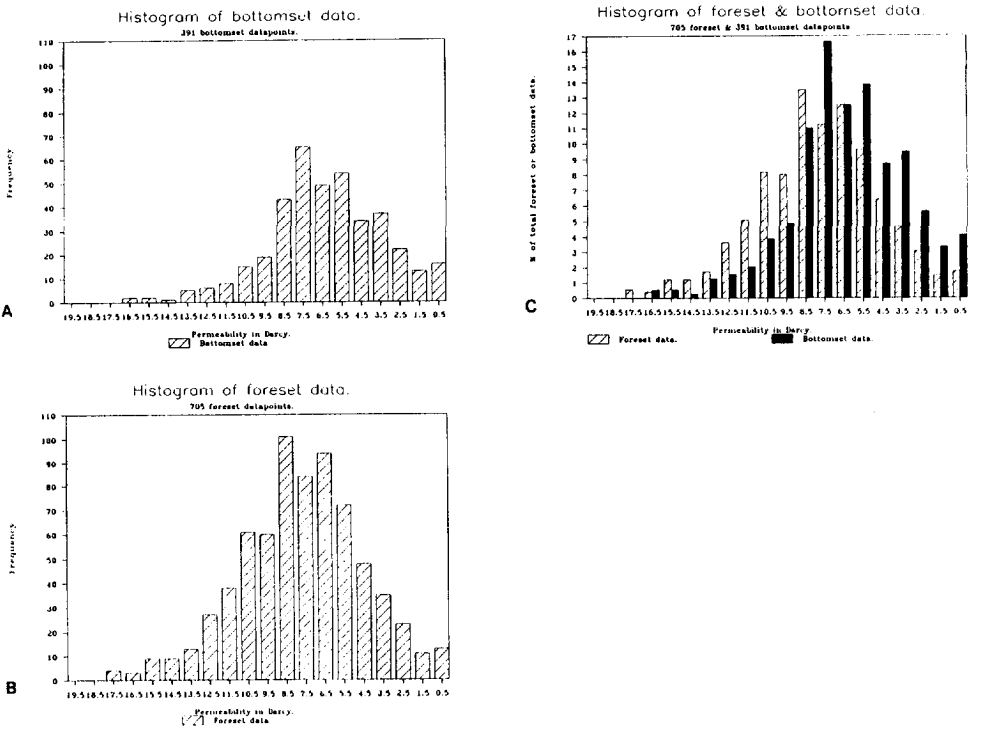

Fig. IIIA.11 A) Histogram of permeability classes of the bottomset. B) Histogram of permeability classes of the foreset. C) Histogram of normalised permeability data populations of foreset and bottomset.

subsequent increase (from set 1 to set 9). This trend is related to the average grain size trend from medium-coarse sand in set 1, to fine-medium sand in sets 4-8, and back to medium sand in set 9.

The standard deviation of permeability values is higher in the foreset than in the bottomset. This can be explained by the higher variability of foreset permeability values as compared to the bottomset.

IIIA.6 DISCUSSION

Permeability heterogeneity in cross-bedded fluvial reservoirs is principally caused by depositional grain size and sorting characteristics. The permeability contrast is often enhanced during burial and diagenesis. A study by Kortekaas (1985) indicated the likelihood of significant oil trapping in foresets as the result of the different speed of water imbibition into laminae of contrasting permeability and capillary pressure characteristics (Beard & Weyl, 1973). The permeability in the bottomsets is generally lower than in the foresets, and consequently the capillary pressure is higher in the former. Fast imbibition of water and subsequent water tonguing will occur in the bottomsets and in the lower-permeable foreset laminae. When maximum water saturation is reached a non-flow boundary is formed. Consequently, the remaining movable oil in the highly-permeable foreset laminae is initially trapped by the surrounding non-flow boundaries (Weber, 1986). The percentage of initially trapped oil is a function of the ratio of permeability of adjacent laminae and the mobility ratio of the displacing and displaced fluids. Permeability heterogeneity on the scale of cross-set laminae is likely to have a marked influence on fluid flow in oil reservoirs with a fluvial architecture similar to the studied outcrop. For this type of fluvial reservoir suitable enhanced oil recovery methods may have to be developed that decrease the interfacial tension of the driving fluid, e.g. low concentration surfactant flooding.

IIIA.7 CONCLUSIONS

Detailed permeability measurements of a composite point bar sediment body reveal a direct relationship between permeability heterogeneity and sedimentology, and allow the definition of two types of permeability heterogeneity for this group of fluvial deposits. The two types are:

(1) The bounding layer between stacked point bar units may form a low-permeable zone. The layer originates from channel abandonment and in this example is 10-15 cm thick, very-fine grained, early-cemented and rootletted. Preservation of the low-permeability

zone and lateral extent of the abandonment surface are a function of the subsequent channel reactivation. In the studied outcrop this type of low-permeability zone commonly extends from the adjacent low-permeability floodplain down onto the abandonment surface over a distance of about 7 m. Measured permeability ranges from 0.1 D (abandonment layer) to 10 D (over-and underlying point bar sand).

(2) The cross-bedded part, which makes up 70-80% of the bulk volume of the point bar sediment body, shows a marked permeability contrast between bottomsets (permeability 0.5-7.0 D) and foresets (5.0-17.0 D).

In reservoir-equivalents of the composite point bar both types of permeability heterogeneity are considered to influence fluid flow:

(a) The low-permeability channel abandonment surfaces may act as permeability baffles to fluid flow, and cause partial compartmentalisation of the reservoir;

(b) In water-flooded oil-reservoirs, permeability contrasts between adjacent foreset laminae and bottomsets may cause water fingering caused by capillary pressure effects.

CHAPTER IIIB
GRAIN SIZE, COMPOSITION, POROSITY AND PERMEABILITY CONTRASTS WITHIN CROSS-BEDDED SANDSTONES IN TERTIARY FLUVIAL DEPOSITS, CENTRAL SPAIN

IIIB.1 INTRODUCTION

Many studies have related permeability measured by a probe permeameter at outcrop face to the sampled sedimentary facies (e.g. Chandler *et al.*, 1989; Dreyer *et al.*, 1990, Hartkamp & Donselaar 1993). Most studies concentrated on permeability variations on genetic-unit scale. In a laboratory setting, probe permeameter measurements can be made on a very fine-scale grid enabling statistically valid comparisons to be made between the permeability distributions of individual laminae in cross-stratified units (grid point spacing 5 mm, Hurst & Rosvoll, 1991). However, direct correlations between detailed probe permeametry at outcrop and studies of microscopic textural and mineralogical variations are rare.

In the past decades, experimental, theoretical and semi-empirical relations have been established between pore and textural characteristics (e.g. grain size, sorting, specific surface of grains) of sands and sandstones with permeability (e.g. Kozeny, 1927; Carman, 1937; Beard & Weyl, 1973; van Baaren 1979). Textural properties are basically determined by the primary mineralogical composition and the physical processes of sedimentation, but may be affected by subsequent burial history (e.g. physical compaction, mineralogical alteration and cementation) (Pittman, 1979). Studies on reservoir sandstones have provided a more detailed insight into the dependence of permeability on porosity alteration as a result of diagenesis (e.g. Ehrenberg, 1990). Ehrenberg (1990) studied North Sea reservoir sandstones and found that both finer grain

size and higher mica content were associated with lower permeability. Differences in mineralogical composition between laminae within cross-stratified reservoir sandstones have been observed by Hopkins *et al.* (1991) to cause a significant permeability contrast of one order of magnitude between the laminae. Hurst & Rosvoll (1991) determined a permeability contrast of an order of magnitude of 1 to 3 between laminae within a cross-bed in a lightly consolidated sandstone of shallow-marine origin; they assumed that the variations in permeability reflected primary depositional characteristics.

The present study focuses on quantification of permeability variations in cross-bedded sandstones. The purpose of this paper is to discuss the depositional characteristics that affect contrasts in permeability between adjacent foreset laminae and between foreset and bottomset of cross-beds in well-exposed distal fluvial-fan deposits of Late Oligocene - Early Miocene age (Loranca Basin in Central Spain). Probe-permeameter measurements are compared with textural and compositional parameters. The studied sandbodies are lightly consolidated and have retained most of their depositional features (Díaz *et al.*, 1989).

IIIB.2 GEOLOGICAL SETTING AND FACIES DESCRIPTION

Sandstones of Mid to Late Tertiary age in the Loranca Basin, central Spain, provide the data for this study (Fig. IIIB.1). Fluvial, molasse-type, sandstones from two coalescing systems filled the Loranca depression during the Late Oligocene to Early Miocene (Díaz *et al.*, 1989). The source areas of these fluvial sediments are the Mesozoic clastic and carbonate sequences of the Iberian mountain range. Channel sandbodies were formed by low- and high-sinuosity rivers and embedded in fine-grained floodplain sediments. Large-scale trough cross-bedding is ubiquitous (Díaz *et al.*, 1985).

The trough cross-bedded sedimentary structures were formed by large-scale ripple migration over the channel floor and the depositional slope of the inner bank. The trough cross-beds have a length of up to 20 m, a thickness of 20-40 cm and a width ranging from 80 cm to 2 m. Two different facies are distinguished: the bottomset and the foreset. The bottomset layer (BL) has formed in front of migrating ripples and consists of fall-out

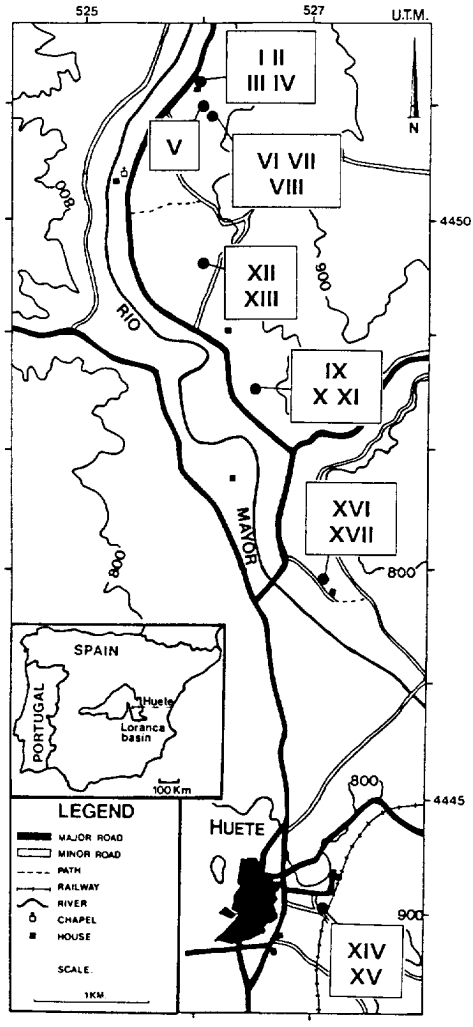

Fig. IIIB.1 Location map of the study area in the Loranca Basin, Central Spain. Studied outcrop locations are marked from I to XVII.

and suspension-load sediment. Foreset deposits consist of laminae that formed by grains

avalanching down the leeside of ripples. The inclined foreset laminae are preserved in sequence in the sandbodies and are a record of successive earlier positions of the leesides. The grains are sorted during avalanching, resulting in distinct coarse- (CFL) and fine-grained (FFL) laminae that range between 2 mm and 1.2 cm in thickness. Usually, there is a regular and systematic pattern of variation in medium grain size with respect to the successive cross-strata.

IIIB.3 METHODS

IIIB.3.1 Petrography

A total of 34 plugs of 2 inches (5.08 cm) in diameter was taken perpendicular to bedding from seventeen outcrop locations (Figs. IIIB.1, 2A, 2B and 2C). Probe permeability measurements were taken prior to coring and this technique provided us with undisturbed plugs of which the measured locations, orientations, exact sedimentological details and probe permeability data at right angle to layering were known. Thin sections of the plugs were made following impregnation with blue araldite and a qualitative evaluation was made (Figs. IIIB.2C and 2D), and nine thin sections were selected and used for optical analysis. In each thin section, the coarser-grained foreset laminae (CFL), the finer-grained foreset laminae (FFL) and the bottomset layer (BL), if present, were studied separately. The parameters studied are mineralogical composition, grain-size distribution and porosity.

The study involved a total of 3300 counted points in each plug sample. For each subfacies (CFL, FFL and BL), 400 points were counted of framework and cement type, 400 points were counted of pore type and size and another 300 points were counted of grain size. In foreset laminae the point-count parameters were counted parallel to the dip (Fig. IIIB.2D). In bottomsets the parameters were counted perpendicular to the depositional surface, to account for any anisotropy in texture that may be apparent in bottomsets (Joplin, 1965). In some samples, bottomsets display well-developed, fine- and coarse-grained laminae; in these samples point counting was done parallel to the

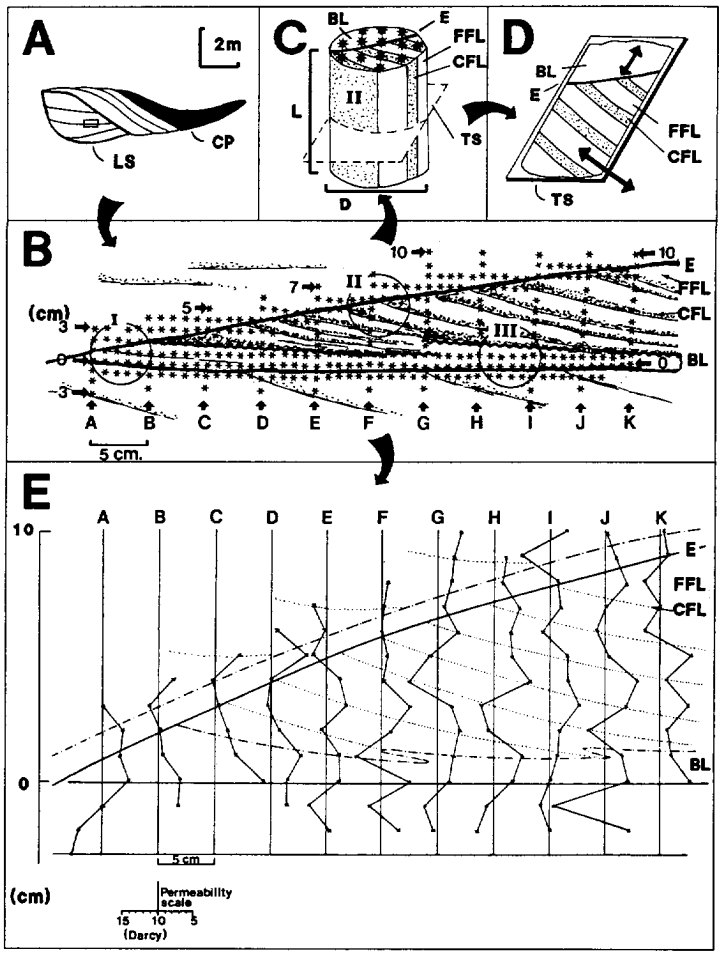

Fig. IIIB.2 A) A schematic cross-sectional view of a laterally stacked sequence of adjacent point-bar deposits (LS) and channel-abandonment deposits represented by a clay plug (CP). Outcrop sample location VI is indicated by the rectangular box. B) Drawing of the sampled cross-bed set of location VI. Coarser-grained foreset laminae (CFL) are speckled, finer-grained foreset laminae (FFL) are white, and the bottomset layer (BL) is the white zone parallel to black lined erosion surfaces (E) and the wiggly black line. Circles indicate core plug locations (I, II and III). The grid used for probe permeameter measurements is indicated as stars (vertical grid spacing is 1 cm, horizontal grid spacing between columns A to K is 5 cm, with additional gridpoints of 1 cm spacing). C) Example of core plug II with a length (L) of 6 cm and a diameter (D) of 5.08 cm. Inclined foreset laminae are presented as CFL (speckled) and FFL (white). BL is white and overlies the erosion surface (E). Stars indicate probe permeameter sample points. TS is the imaginary cross section for the thin section. D) Example of thin-section (TS) with foreset laminae CFL (speckled) and FFL (white), the erosion surface (E) and overlaying bottomset (BL). Arrows indicate the point-count directions in the foreset (CFL, FFL) and in the bottomset (BL). E) Example of permeability pattern of outcrop location VI, the dotted lines indicate inclined foreset laminae directions (CFL, FFL), the dashed line indicates the boundary between foreset and bottomset (BL), the black line indicates the erosion surface (E).

depositional surface in order to count coarse and fine grained laminae separately (BL-C and BL-F).

Maximum diameters of pore size and grain size were counted in ϕ unit intervals (-$\log_2$ of the diameter in mm, Pettijohn *et al.* 1973). Mean values of grain size or pore size were used in the correlations with permeability. Sorting (So = ϕ standard deviation) was calculated in accordance with Folk (1980). Framework composition was analyzed in petrographic groups as defined by Zuffa (1980). Porosity analysis (primary and secondary porosity) was carried out on the basis of the criteria defined by Schmidt & McDonald (1979).

IIIB.3.2 Permeability

The probe permeameter (minipermeameter) has been developed for measuring the steady-state permeability of rock and unconsolidated sand by Eijpe & Weber (1971). Sutherland *et al.* (1991) recommend codes of practice that are applicable to the variety of instruments currently available and give details of the measurement principles, apparatus, measurement procedure and quality control for probe permeametry. The apparatus and the measurement techniques used for this study are described in detail by Hartkamp & Donselaar (1993) and only summarized here. The probe permeameter consist of three units, a nitrogen gas source, a flow-meter unit and a probe. The probe is pressed against the rock surface with a controlled force (Sutherland *et al*, 1991). At a constant pressure, nitrogen is passed trough a small opening in the probe into the rock and the flow-rate is recorded when a steady-state is reached (10 sec.). Leakage between the rock and the probe is prevented by an elastic, closed-cell neoprene rubber. The inlet opening of the probe (radius of 1 mm) determines the measured rock volume (Goggin *et al.* 1988), which is estimated to have a radius and depth of 4 mm. Where the thickness of laminae is less than the measurement radius, the measured permeability is an average value defined by the unknown permeabilities of more than one lamina (Halvorsen & Hurst, 1990).

Flow rate is converted into permeability using a calibration curve (Fig. IIIB.3). This calibration curve was established in the Dietz laboratory of Delft University of Technology (The Netherlands) using a set of 99 natural and artificial homogeneous-

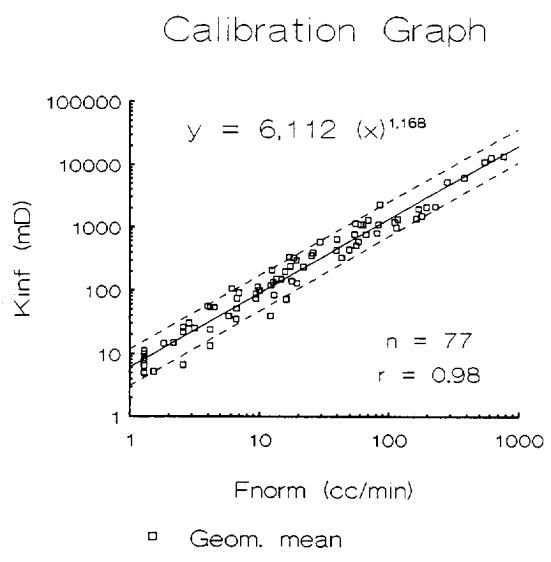

Fig. IIIB.3 Calibration graph of the normalized flow rate (Fnorm) measured by probe permeameter versus the (Kinf) infinite plug permeability (Hassler-sleeve) for the largest range in permeability (5 mD to 14000 mD). Data represent geometrical averages of four probe measurements taken at each end side of a core plug. The power regression relationship of the best-fit correlation (continuous line) is presented, together with the total number (n) of core plugs involved and the correlation coefficient (r). The 80% confidence intervals are indicated by dashed lines and show an error of calibration of a factor 1.6.

sandstone plugs, the permeabilities of which ranged from 0.1 to 14000 mD. An extensive description of the principles, calibration, response, reliability and accuracy of the equipment used for this study is presented in Appendix A.

The outcrop face was carefully prepared using a steel brush to remove the superficial weathering crust and subsequently, using a soft brush to remove the first few centimeters of the friable sandstone underneath the crust in order to remove dust and flatten the surface.

A total amount of 2600 measurements were made on cross-beds at 17 outcrop locations and statistically analysed. From this total amount of measurements, only 525

measurements from 9 locations were ultimately used for the comparative study between petrography and permeability. This limitation of data was determined by the limited amount of locations from which thin-sections could be prepared succesfully. This resulted in 25 data points as presented in Table IIIB.I, of which odd data points were eliminated from correlation graphs.

Measurements were taken on a grid with a vertical spacing of 1 cm and a horizontal spacing of 5 cm. Total column height ranged between 10 cm and 50 cm, the total number of columns ranged between 6 and 15. On key horizons (e.g. bottomsets) additional rows were measured, with a horizontal and vertical grid distance of 1 cm (Fig. IIIB.2B and 2E).

The permeability data have been grouped as CFL, FFL and BL data on the basis of sedimentological characteristics at the points of measurement (Fig. IIIB.2E). The resulting three data sets were analyzed using standard population statistical techniques. Histograms and cumulative frequency plots were used to characterize the distributions of datasets and sub-datasets, from which the optimal averaging technique was judged (an extensive description can be found in Appendix B).

IIIB.4 RESULTS

IIIB.4.1 Petrography

The cross-bedded sandstone is generally very fine- to coarse-grained and moderately well-sorted (So = 0.6-0.9) (Table IIIB.I). The grains are usually sub-angular to sub-rounded. The framework is composed of three main groups of grains; 1) the Non-Carbonate Extrabasinal grains (NCE), 2) the Carbonate Extrabasinal grains (CE) and 3) the Carbonate Intrabasinal grains (CI) (see Table IIIB.I):

1) NCE, which comprise approximately 75% of the framework, and are mainly monocrystalline and polycrystalline quartz and K-feldspar. Monocrystalline quartz grains usually show a non-undulatory extinction. The grains are typically irregularly overgrown, and in some cases, contain anhydrite inclusions. These features are indicative of

SAMPLE	TEXTURE						COMPOSITION						PERMEABILITY			
	Average grainsize (phi)	Sorting	Primary Porosity (%)	Second. Porosity (%)	P1 Pore size (phi)	P2 Pore size (phi)	Q (%)	K–Feld (%)	CEm (%)	CEsp (%)	CI (%)	Carb. cement (%)	Range (Darcy)	Average (Darcy)	Std. dev. (Darcy)	Number
CFL																
VI.2	1.42	0.80	21.2	10.8	2.26	1.10	64.3	10.0	6.3	12.6	5.6	0.9	8.20–15.45	10.72	1.77	43
IX.1	1.51	0.62	30.0	4.6	2.62	1.89	65.5	8.6	6.0	14.3	4.0	0.6	6.08–11.93	8.49	1.56	10
IX.2	1.75	0.81	24.6	7.2	2.75	1.31	59.6	10.3	9.3	14.9	5.6	0.0	6.80–10.01	8.59	1.33	7
XII.1	1.94	0.79	25.0	6.0	2.62	1.72	56.2	5.6	6.6	21.6	8.3	1.3	2.13– 6.76	4.38	1.66	4
XIII.2	2.02	0.72	23.6	4.2	2.94	2.11	48.6	7.0	9.0	24.2	10.3	0.6	4.11– 5.52	4.90	0.51	4
XIV.1	2.32	0.99	14.8	3.8	2.74	1.18	37.0	6.5	10.6	18.6	25.0	0.9	7.00–15.10	10.63	2.09	14
XV.1	1.57	0.74	19.4	10.2	2.46	0.66	57.1	5.9	4.3	11.5	16.8	4.2	3.41– 9.83	5.73	1.39	30
XV.2	2.69	0.69	16.4	3.4	3.62	2.14	65.6	3.6	4.6	11.6	13.0	4.0	8.16–11.54	9.97	1.16	8
XVII.1	2.20	0.82	19.8	5.6	2.45	1.48	67.9	5.0	4.6	6.3	13.3	2.6	6.12–18.86	12.68	3.3	28
FFL																
VI.2	2.35	0.69	18.0	7.2	3.22	2.01	68.5	3.6	9.6	10.3	6.0	1.6	4.84– 9.67	7.07	1.22	34
IX.1	2.24	0.71	24.4	4.8	3.20	2.06	69.6	3.0	6.3	13.0	4.6	3.3	3.81– 6.43	4.93	0.83	8
IX.2	2.67	0.82	17.8	3.2	3.34	2.05	59.6	6.0	10.0	10.6	10.3	3.3	4.11– 6.28	5.51	0.69	7
XII.1	2.29	0.69	22.2	5.2	3.37	2.03	62.6	4.0	12.6	12.0	8.3	1.3	2.77– 5.10	3.92	0.65	14
XIII.2	3.09	0.76	21.5	2.9	3.84	2.42	57.6	4.6	10.6	15.3	10.0	1.6	1.72– 4.31	3.39	0.72	27
XIV.1	2.54	0.92	16.6	7.0	3.30	2.40	56.2	3.6	11.6	7.0	19.0	2.3	2.70– 8.94	6.07	2.07	28
XVII.1	2.45	0.78	19.2	8.6	3.07	2.08	56.6	4.0	1.6	6.6	18.0	3.9	2.10–12.01	5.99	2.09	55
BL																
VI.2	2.14	0.67	18.1	8.7	3.10	1.79	62.5	5.6	7.6	13.6	5.3	4.9	3.01–10.60	7.28	1.42	36
IX.1	2.53	0.72	22.2	5.0	3.30	1.73	62.9	3.0	6.0	15.3	7.0	5.6	2.47– 5.93	3.74	1.04	9
XII.1	2.92	0.74	21.0	5.8	3.50	1.44	54.3	3.6	6.0	22.0	9.6	4.3	2.15– 6.89	3.95	1.14	26
XIII.2	2.97	0.71	20.8	5.4	3.60	1.83	58.9	4.6	6.3	20.0	5.6	4.3	1.62– 5.95	3.72	1.25	24
XIV.1	2.95	0.78	18.8	9.2	2.98	1.17	57.6	4.0	8.0	15.3	7.0	8.0	1.36–10.51	6.00	1.82	43
XV.1–C	2.55	0.95	16.8	3.0	3.12	1.90	52.3	5.3	5.6	11.0	23.0	1.6	2.47– 5.10	3.73	0.68	26
XV.1–F	2.36	1.05	18.2	5.4	2.54	1.43	55.6	3.6	7.6	14.6	15.3	2.3	1.72–8.03	4.77	1.91	22
XV.2–C	2.72	0.86	20.8	4.2	2.71	2.36	51.6	5.6	5.2	11.5	24.7	1.3	4.09– 7.50	6.06	1.06	8
XV.2–F	3.26	0.96	22.6	3.6	3.73	2.86	56.0	4.0	4.0	13.0	22.0	1.0	0.93–5.01	3.84	0.85	10

Table IIIB.1 Spreadsheet showing texture, composition and permeability of analyzed sandstones. Sorting is the phi standard deviation (Folk, 1980). Composition is subdivided into Quartz (Q), K-feldspar (K-Feld), micritic carbonate extrabasinal grains (CEm) and sparitic carbonate extrabasinal grains (CEsp), carbonate intrabasinal grains (CI) and carbonate cement. The range, arithmetic average and standard deviation (std. dev.) and the number of measurements (N) of permeability is presented.

provenance from a sedimentary source area (Arribas & Arribas, 1991). K-feldspar is not abundant (less than 11%), and has inherited overgrowths and filled grain fractures. Partial dissolution of K-feldspar grains is common.

2) CE, are limestone and dolostone fragments, displaying micritic (CEm) and sparitic (CEsp) textures. CE grains make up 10 to 35% of the total rock volume.

3) CI, are micritic grains and oncolite fragments. Micritic grains have a homogeneous texture and sometimes contain fragments of *characeas* and *ostracodes*. In general, they are larger than extrabasinal grains. The intrabasinal clasts were soft and unstable at the time of deposition and often have been deformed by compaction. The percentage of CI grains in the framework ranges from 5 to 25%.

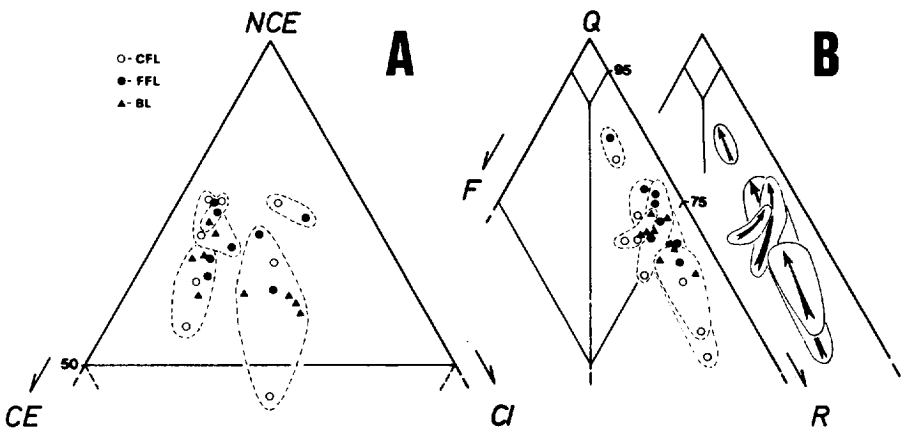

Fig. IIIB.4 Framework composition of sandstones. A) In a NCE-CE-CI diagram (after Zuffa, 1980). B) In a Q-F-R diagram (after Pettijohn *et al.*, 1973). Samples from a single outcrop are grouped. Arrows indicate a variation in composition from coarser- to finer grained subfacies in a cross-bedded set. NCE: Non-Carbonate Extrabasinal, CE: Carbonate Extrabasinal, CI: Carbonate Intrabasinal, Q: Quartz, F: Feldspar, R: Rock fragments.

The composition of the sandstones is shown in Fig. IIIB.4. All plotted points fall in the field in which extrabasinal grains dominate (Fig. IIIB.4A). The average

composition of these extrabasinal grains is lithoarenitic (Fig. IIIB.4B). In agreement with the composition of the sandstone and the sedimentary nature of the rock fragments, the deposits are defined as sedimentoclastic (c.f. Ingersoll 1983). In the NCE-CE-CI diagram (Fig. IIIB.4A) samples from each outcrop location form separate clusters indicating that each sample location has a slightly different bulk composition. In the QFR diagram (Fig. IIIB.4B) in which intrabasinal grains are not included, the separation between different outcrops is less clear. The different clusters of data vary in the ratio between quartz and rock fragments, reflecting small differences in provenance between the various outcrop locations.

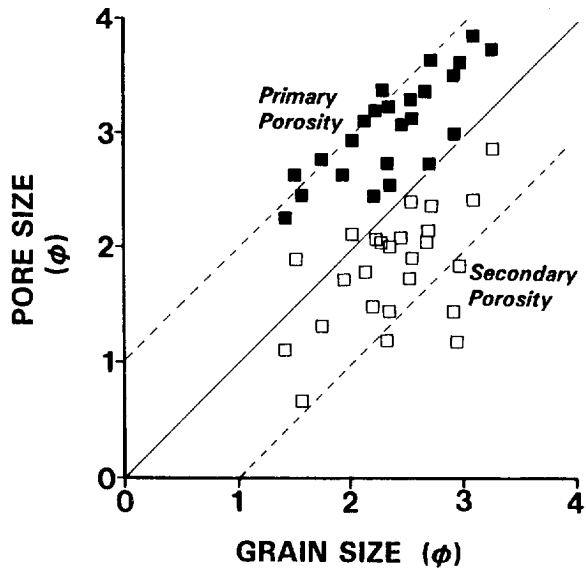

Fig. IIIB.5 Average grain size versus average pore size of primary (black squares) and secondary porosity (white squares).

Porosity is interpreted to be mainly of primary origin. Primary porosity ranges from 14.8% to 30% (Table IIIB.I). Primary porosity is characterized by interparticle

pores, with a pore-size distribution closely related to the grain size (Fig. IIIB.5). The average primary pore size is approximately 1 ϕ unit smaller than the average grain size.

IIIB.4.2 Diagenesis

Diagenesis of the sandstones includes mechanical and chemical compaction, cementation and generation of secondary porosity. Mechanical compaction mainly affected intrabasinal micritic grains and produced deformed and disintegrated grains. Chemical compaction affected hard micritic grains and some intrabasinal grains (oncolites), that often have concavo-convex contacts with siliciclastic grains, without deformation of internal textures. Cementation has generally not been intense (less than 8%) (Table IIIB.I) and cements consist mainly of calcite overgrowth around monocrystalline carbonate grains. Locally, equant calcite mosaics are present. From the textural relationship between deformed soft grains and the undeformed calcite cement, it is concluded that cementation post-dates compaction.

Secondary porosity generation is the last diagenetic process that affected the sandstones. Secondary porosity is characterized by oversized intergranular pores (Fig. IIIB.6A). Textures indicative of secondary porosity, such as inhomogeneity of packing (Schmidt & McDonald, 1979), are common. Micritic grains have very corroded edges and intragranular dissolution pores reflecting the dissolution of mainly intrabasinal, micritic grains. Secondary pore size is less well correlated with grain size than in the case of primary pore size (Fig. IIIB.5), and shows a larger scatter of data points with average pore sizes nearly 1 ϕ-unit larger than the average grain size.

Compaction is the most intense diagenetic process that has modified primary porosity by deformation of soft grains by mechanical compaction (Fig. IIIB.6B), and the interpenetration of hard grains by chemical compaction (c.f. Rittenhouse, 1971; Mitra & Beard, 1980). A clear decrease in primary porosity was found in sandstones with a high percentage of micritic grains (Fig. IIIB.7A). This relationship (correlation coefficient r = -0.555) is obscured by later diagenetic processes such as cementation and secondary porosity generation. It is assumed that secondary porosity merely resulted from

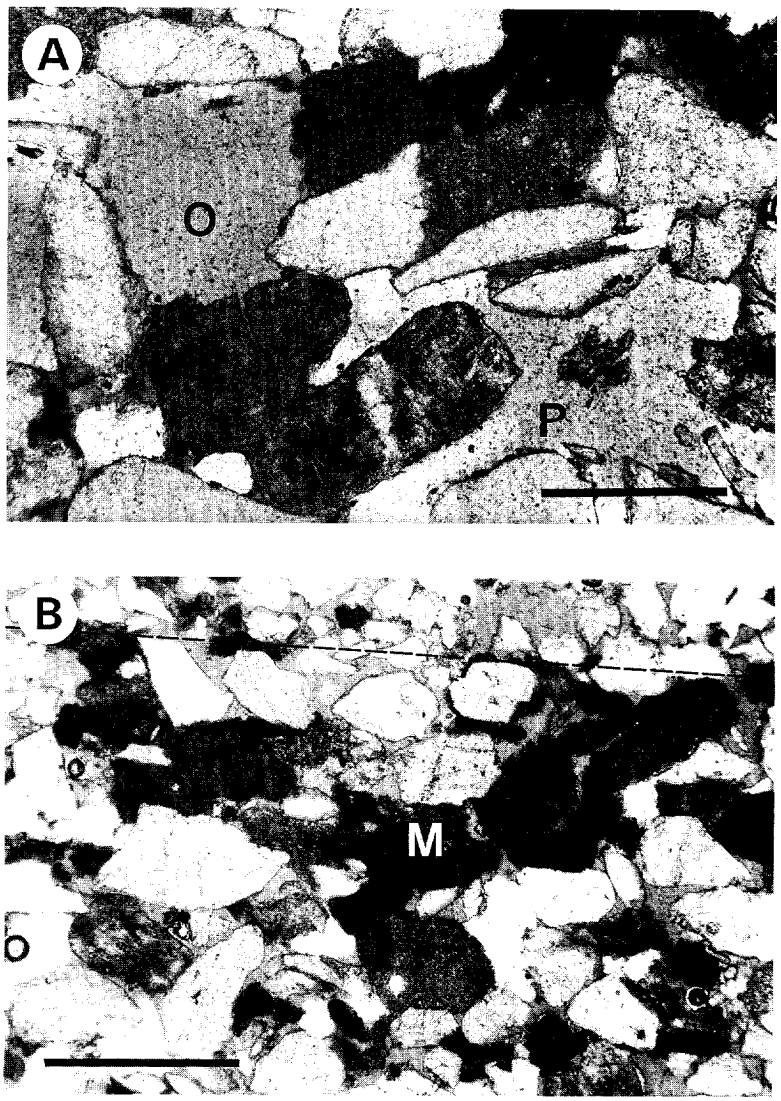

Fig. IIIB.6 A) Photomicrograph in plane-polarised light (scale bar: 0.25 mm, sample XII.1). Oversized pores of secondary origin created by complete (O) and near-complete (P) dissolution of carbonate grains. Note compaction of micritic grains (dark grey). Light-grey areas represent void space. (Sample XII.1).
B) Photomicrograph in plane-polarised light (scale bar: 0.5 mm). Reduction of primary porosity by mechanical compaction of micritic intrabasinal grains (M). Light-grey areas represent void space. Note sharp boundary between CFL (lower part) and FFL (upper part) indicated by a dashed line. (Sample XII.2).
to be continued..

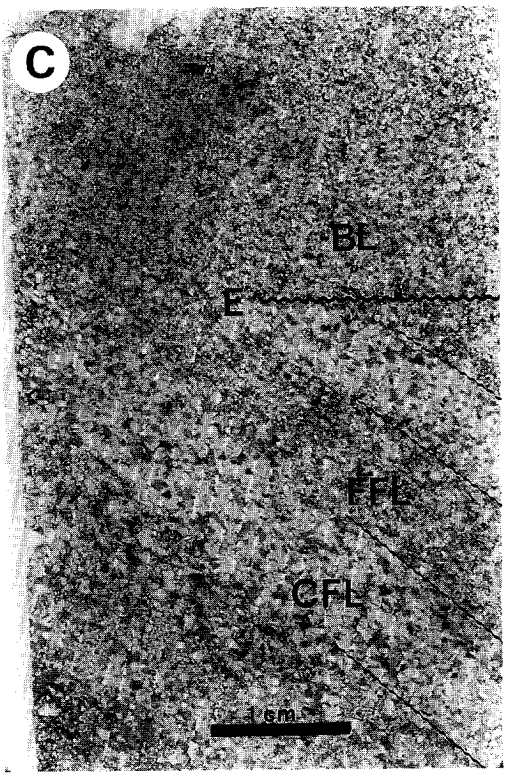

Fig. IIIB.6 C) Photomicrograph in plane-polarised light (scale bar: 1 cm) of upper part of a foreset with coarser (CFL) and finer (FFL) grained laminae, overlain by a fine-grained bottomset (BL) of the vertically stacked cross-bedded sets (sample VI.2). Sharp boundaries between the subfacies CFL and FFL are indicated by dashed lines. The erosion surface (E) that forms the boundary between the lower foreset (CFL and FFL) and the overlying BL is indicated by a continuous line.

dissolution of micritic grains. Thus, by adding the percentage of secondary porosity to the percentage of micritic grains, an estimate of the original micritic grain content is obtained. The percentage of cement, resulting in a reduction of the primary porosity, may be added to the percentage of primary porosity (horizontal axis of the graph), yielding the percentage of pre-cementation porosity (Fig. IIIB.7B). Thus, the original porosity of a sandstone with an original framework composition near the 40% carbonate micritic grains, is reduced to near 15% by compactional processes. This fact highlights the

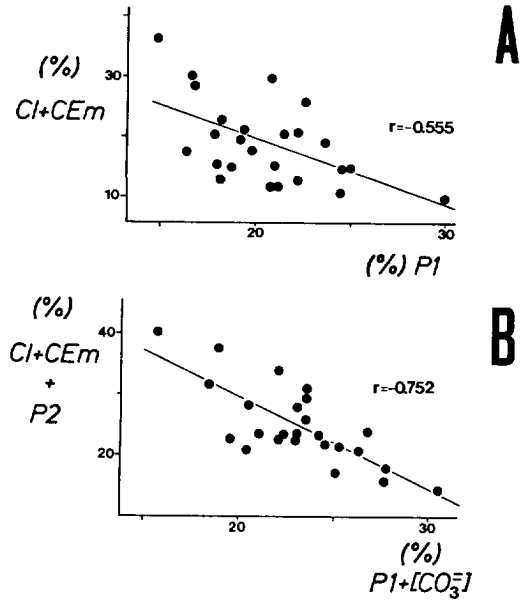

Fig. IIIB.7 A) Percentage of intrabasinal (CI) and extrabasinal carbonate micritic (CEm) grains versus percentage of primary porosity (P1). B) Percentage of secondary porosity (P2) added to (CI + CEm) versus carbonate cement percentage ($[CO_3^=]$) added to (P1).

significance of sandstone composition on primary porosity reduction.

IIIB.4.3 Contrasts in petrography

Boundaries between the different subfacies CFL, FFL and BL are often very sharp (Fig. IIIB.6C). It can be observed that the CFL is characteristically coarser grained (medium-grained sand) than the FFL and BL (fine-grained sand). Sorting of CFL has a

wider range (0.62 to 0.99, well to poorly sorted) than the FFL (0.69 to 0.92, moderately-well sorted). The bottomset sands (BL) are generally not as well-sorted as the FFL (sorting of BL ranges between the 0.67 and 1.05). In some cases, bottomsets are better sorted than the foreset laminae. The three subfacies have similar lower limits of primary porosity (16.2-16.8%, the value of 14.8% is considered anomalous), but differ in their upper limits (CFL: 30%, FFL: 24.4% and BL: 22.2%). As pore size (primary and secondary) is directly related to average grain size (see Fig. IIIB.5), the pores of CFL are larger than those in FFL and BL.

A significant difference in composition between coarser-grained (CFL) and finer-grained (FFL + BL) subfacies of individual cross-bedded sets has been observed. The QFR diagram (see Fig. IIIB.4B, direction of the arrows) shows that the percentage of quartz grains increases with decreasing grain size. Contrasts in quantity of micritic grains between the CFL, FFL and BL of individual cross-bed sets result in contrasts of primary porosity evolution and development of secondary porosity between the sub-facies (Table IIIB.I).

IIIB.4.4 Contrasts in permeability

The values of the total of 2600 outcrop-probe permeameter measurements, range between 0.5 and 20 D. In cross-bedded sets where the range in grain sizes is small, the range of permeability is also small. Population statistics prove the independence of the different sub-facies (Hartkamp & Donselaar, 1993). On the basis of histograms and cumulative frequency plots of permeability data populations and sub-populations (e.g. Fig. IIIB.8), the following observations were made: 1) Data populations show approximately normal, log-normal or bulk (frequency maxima over several permeability classes) distributions. 2) Sub-populations; i) are in general approximately normally distributed (Gaussian distributions), however, log-normal distributions also occur, ii) foreset data distributions often show two distinct frequency maxima (bi-modality according to CFL and FFL data), with a 2 to 5 Darcy difference, iii) maxima in frequency of bottomset (BL) data often fall in the same class as the lower-permeability peak (FFL) of the foreset data distribution (Appendix B). From these observations it was

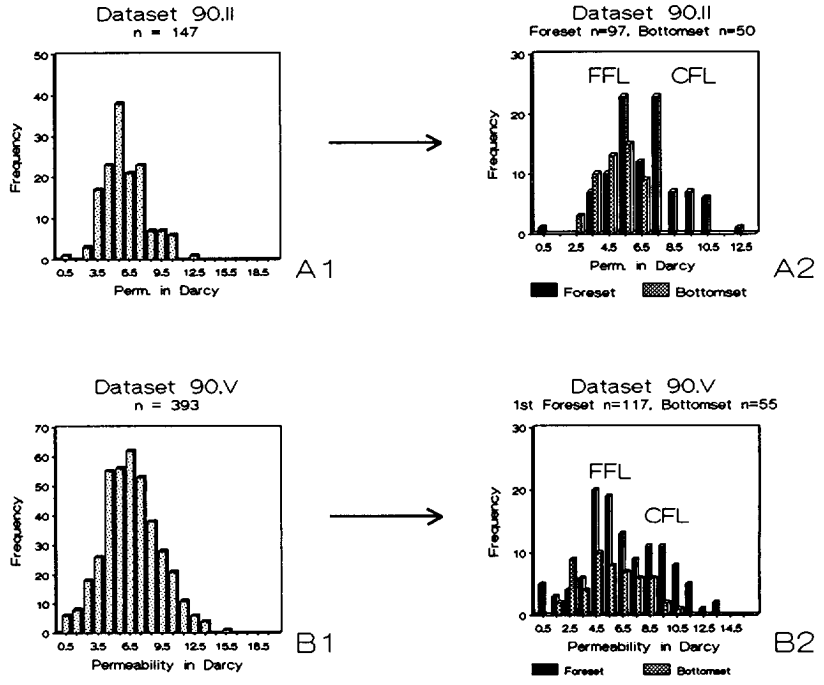

Fig. IIIB.8 Example of frequency distributions of A1) total dataset of location V and A2) sub-datasets, foreset and bottomset, of one cross-bed. Example of cumulative frequency curves of B1) total dataset of location V and B2) sub-datasets, foreset and bottomset, of one cross-bed. The number of data is indicated by n. The total dataset has an approximately normal distribution. The sub-dataset of the foreset shows a bi-modal character, according to FFL and CFL data.

concluded that the optimal procedure for calculating the mean of data sub-populations, corresponding to CFL, FFL and BL, is the arithmetic averaging method (Grindheim & Aasen 1991). The occurrence of approximately normally distributed permeability data related to 'homogeneous' strata types (bedding, sedimentary structures) is confirmed by other studies (e.g. Jensen *et al.* 1987, Gibbons *et al.* 1991, Tyler *et al.* 1991).

The frequency distributions of the arithmetic average permeability of CFL, FFL

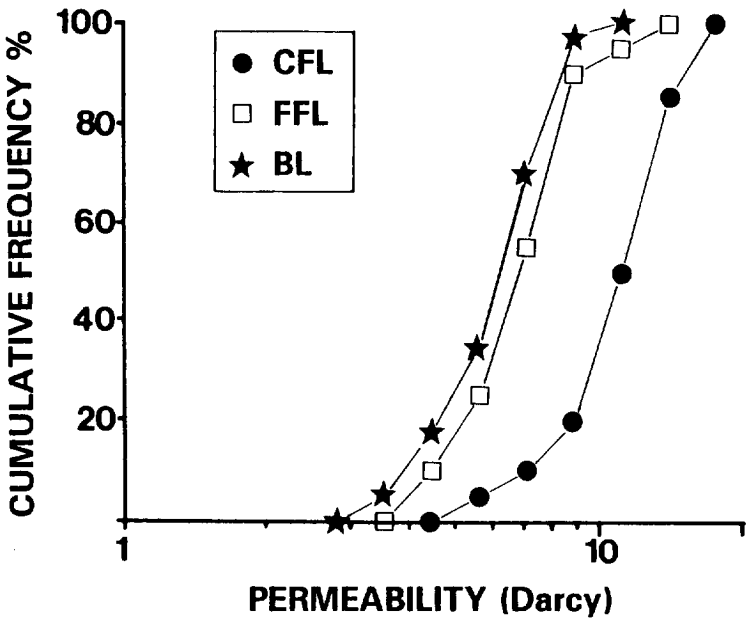

Fig. IIIB.9 Cumulative frequency distributions of arithmetic average permeability of CFL, FFL and BL data of all 17 outcrop locations (number of average permeability of CFL = 17, FFL = 17 and BL = 25). On average, contrasts are 2 : 1.25 : 1 (CFL:FFL:BL).

and BL data of all studied cross-beds (17 locations) are presented in Fig. IIIB.9. On average, contrasts between subfacies are 2 : 1.25 : 1 (CFL:FFL:BL). The specific permeability ranges, averages and standard deviations of the petrologically characterized cross-beds (525 measurements) are presented in Table IIIB.I. Standard deviations of CFL represent the largest variation in measurements, while standard deviations of FFL typify the smallest range in measured values. In Appendix C, contrasts determined by minipermeameter, and contrasts determined by the Baaren equation based on the here presented petrographical parameters are being compared.

IIIB.5 DISCUSSION

Permeability in sandstones is in general linearly related to porosity on a log-normal scale (Jensen, 1990). By contrast, Fig. IIIB.10 shows only very undistinguished trends between total porosity, primary- and secondary porosity with permeability of the studied sandstones. Data show a wide spread (correlation coefficients for best-fit lines were 0.002 of total porosity, -0.16 of primary porosity and 0.24 of secondary porosity).

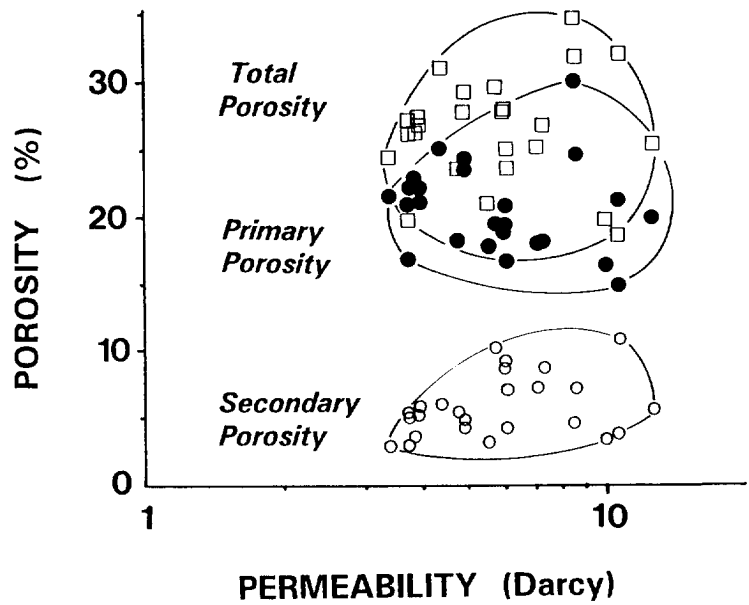

Fig. IIIB.10 Primary (black circles), secondary (white circles), and total (white squares) porosity versus permeability.

Figure IIIB.11 shows that average permeability correlates well with the average pore size of primary pores, the correlation with the average pore size of secondary pores is less clear. However, permeability clearly decreases with decreasing average pore size.

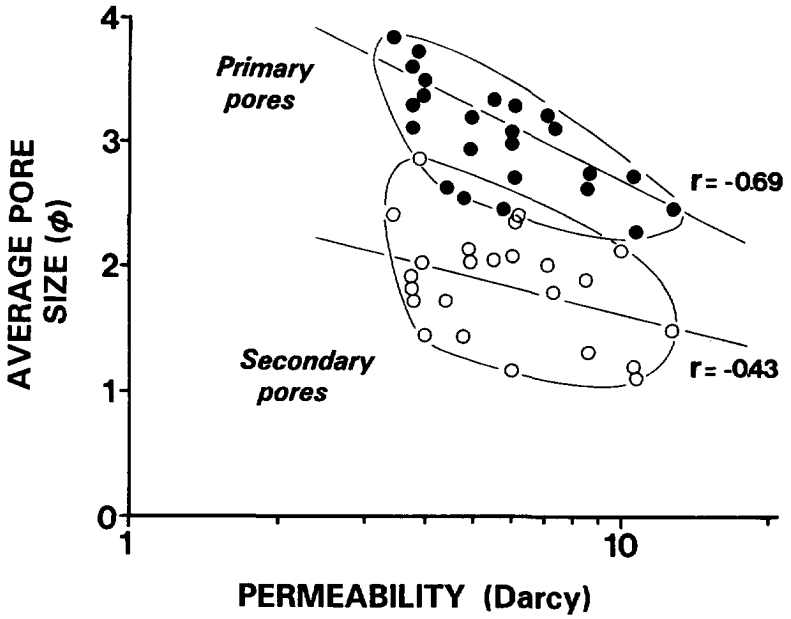

Fig. IIIB.11 Average pore size of primary (black circles) and secondary (white circles) versus permeability.

From comparison of Figs. IIIB.10 and 11 one may infer that permeability depends more on average pore size than on total porosity.

To bring out the effect of grain size and composition on permeability, a graph of permeability versus composition (ratio of carbonate to quartz grains) is presented (Fig. IIIB.12). The different grain sizes are reflected in the separation of the generally coarser grained CFL and the generally finer grained FFL and BL. For both clusters a clear correlation exists between a decreasing ratio of carbonate to quartz with increasing permeability. Figure IIIB.12 shows that permeability depends primarily on: 1) mineralogic composition and related diagenetic processes (Y-axis), and 2) the grain size.

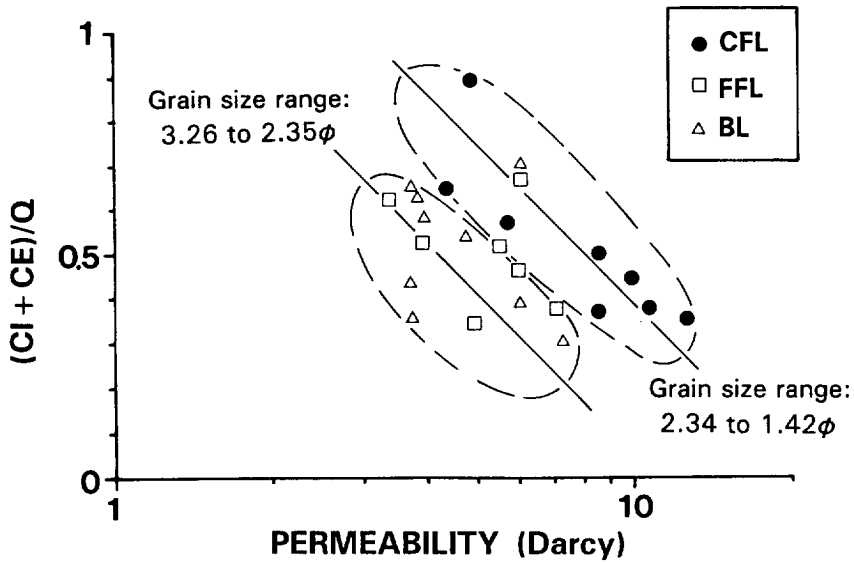

Fig. IIIB.12 Sandstone composition ((CI + CE)/Q index) versus permeability with samples grouped as a function of grain size. Note the influence of provenance (sandstone composition) and grain size on permeability. CI: Carbonate Intrabasinal, CE: Carbonate Extrabasinal, Q: Quartz)

IIIB.6 CONCLUSIONS

1) In the cross-beds, average grain sizes range from medium-grained sand in the coarser-grained foreset laminae (CFL) to fine-grained sand in the finer-grained foreset laminae (FFL) and bottomset (BL). The sand is on average moderately well-sorted (So = 0.6-0.9).

2) The average size of primary pores is approximately 1 ϕ unit smaller than the average size of the pore-forming grains. The secondary pores (oversized pores) are approximately 1 ϕ unit larger than the average grain size.

3) The differences in framework composition between the different outcrop locations are a

result of small differences in provenance. Compositional contrasts between the subfacies of a cross-bedded set are related to grain size. Coarser-grained foreset laminae (CFL) have a larger amount of carbonate intra- and extrabasinal grains than do the adjacent finer-grained laminae (FFL) and bottomsets (BL).

4) The abundance of micritic grains is decisive in the course of diagenesis, controlling the primary porosity reduction by compaction and secondary porosity generation. Contrasts in quantity of micritic grains between the CFL, FFL and BL of individual cross-bed sets result in contrasts of primary porosity evolution and development of secondary porosity between the sub-facies. A correlation exists between a decreasing ratio of carbonate to quartz and increasing permeability.

5) Outcrop probe permeameter studies showed a range in permeabilities of 0.5 to 20 D. On average, contrasts in permeability between the subfacies are 2 : 1.25 : 1 (CFL : FFL : BL).

6) Probe permeability contrasts between CFL, FFL and BL depend on pore size and mineralogic composition contrasts between the subfacies.

CHAPTER IV
SMALL-SCALE PERMEABILITY CHARACTERISTICS OF CROSS-BEDDED FLUVIAL RESERVOIR SANDSTONES

IV.1 INTRODUCTION

Fluvial gas reservoirs in the Netherlands (Fig. IV.1) have been selected for studying the small-scale permeability characteristics of cross-bed sets. Cored intervals of wells of the Upper Slochteren Formation (Lower Permian) and the Main Buntsandstein Formation (Lower Triassic) were used (Table IV.I). A total of 23 core-sections was analyzed with a total number of 1939 data points. The core-sections comprise either cross-bedded sets with identified foreset and bottomset or horizontal laminations.

IV.2 THE UPPER SLOCHTEREN SANDSTONE MEMBER AND THE TEN BOER CLAYSTONE MEMBER, UPPER ROTLIEGENDES GROUP (LOWER PERMIAN), THE NETHERLANDS

The Upper Rotliegendes Group in the subsurface of the province of Groningen (in the north-east of the Netherlands) is a mainly fluvial-aeolian deposit with a strong fluvial influence (van Wijhe *et al.* 1980). The Rotliegendes reservoirs are excellent in quality and contain large recoverable gas reserves.

From the Upper Slochteren Sandstone Member and the Ten Boer Claystone Member sandy cores were selected of a series of wells representative of a north-south cross-section through the northern part of Groningen. The minipermeameter-based study provided detailed knowledge of this part of the fluvial-dominated deposits of the Upper Rotliegendes Group. The study aimed at detailed analysis of variations in permeability as a tool for determining small-scale sandstone reservoir heterogeneity.

Table IV.I, Stratigraphic nomenclature of part of the subsurface of the Netherlands. (only representative names of the studied parts are listed).

STRATIGRAPHIC AGE	GROUP	FORMATION	MEMBER
			Hardegsen Claystone
Lower -			Hardegsen Sandstone
	Lower Germanic Triassic	Main Buntsandstein	Detfurth Claystone
			Detfurth Sandstone
Triassic			Vollpriehausen Claystone
			Vollpriehausen Sandstone
		Lower Buntsandstein -	
	Zechstein		
Permian			
			Ten Boer Claystone
			Upper Slochteren Sandstone
	Upper Rotliegendes	Upper Slochteren Sandstone	Ameland Claystone
			Lower Slochteren Sandstone

IV.2.1 Stratigraphic subdivision of the Rotliegendes

The gas reservoir sands of the Upper Rotliegendes Group of the subsurface of The Netherlands are basically found in the Upper Slochteren Formation (Table IV.I). The Upper Slochteren Formation is subdivided into: The Lower and Upper Slochteren

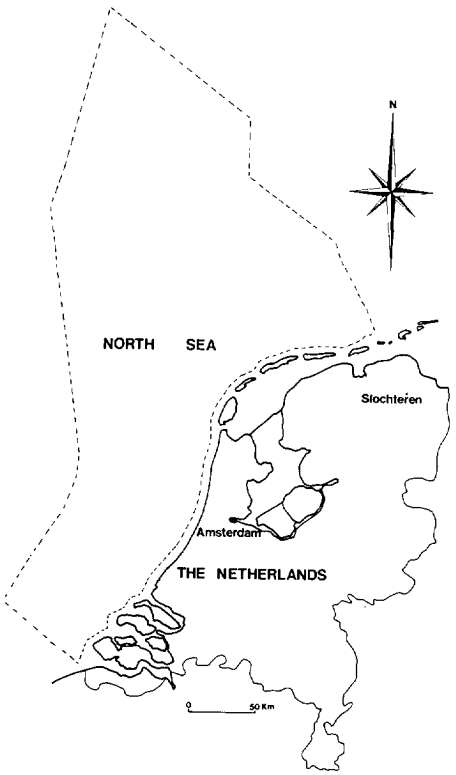

Fig. IV.1 Offshore and onshore area of the Netherlands (modified from NAM-RGD nomenclator 1980).

Sandstone Members and the Ameland and Ten Boer Claystone Members. The boundaries between the sandstone and the claystone members are defined as the transitions from one dominant lithology into the other (e.g. from >50% sandstone into >50% claystone) (van Wijhe *et al.* 1980). The alternation of sandstone and claystone members reflects changes of transport energy in the hinterland, possibly caused by climate changes or tectonic movements. Glennie (1990) presented a north-south Gamma-ray log correlation from several wells in the subsurface of North Groningen (Fig. IV.2).

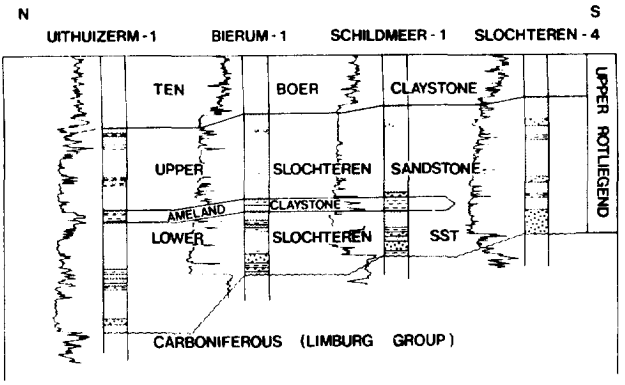

Fig. IV.2 North-south Gamma-ray log correlation panel of the Upper Rotliegendes Group for several wells in the province Groningen (modified from Glennie 1990).

The Upper Rotliegendes deposits are mainly of fluvial origin. The log shapes indicate an upward transition from high-energy Upper Slochteren Sandstone Member deposits into low-energy Ten Boer Claystone Member deposits. The Ten Boer Claystone Member is thinning in a southward direction and ultimately wedges out.

IV.2.2 Depositional model

During the Rotliegendes deposition occurred under semi-arid to arid climatic conditions (Glennie, 1990). Deposition of the Upper Slochteren Sandstone Member and Ten Boer Claystone Member took place in respectively a desert-lake environment (Fig. IV.3, wadi-sebkha environment). The deposits are coarse-grained proximal high- to low-energy wadi deposits, fine-grained distal wadi deposits, desert-lake sand and mud and aeolian reworked sand.

The Upper Slochteren Sandstone Member is characterized by a series of sandstones

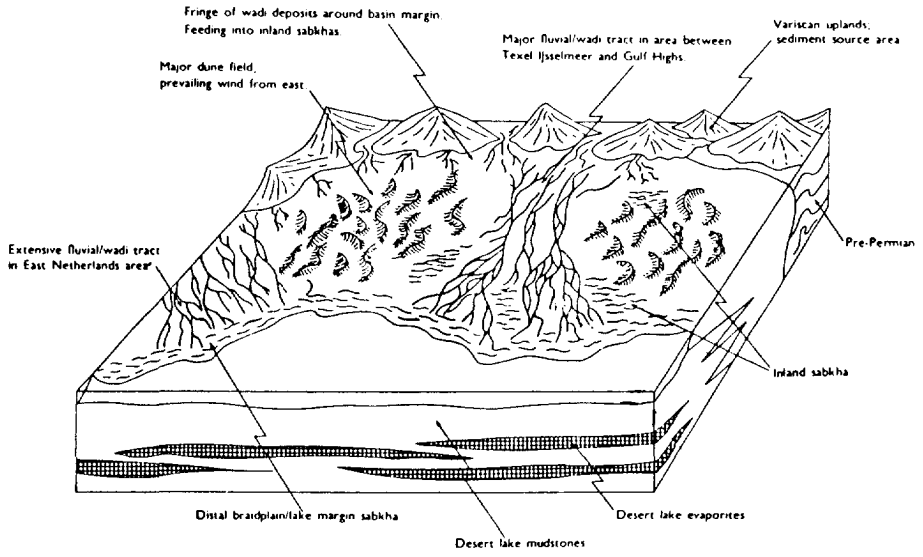

Fig. IV.3 Depositional model of the Slochteren Sandstone Formation (modified from Robertson 1985).

and conglomerates, deposited during alluvial-fan progradation. The Ten Boer Claystone Member comprises shaly-evaporite deposits and reflects the retrogradation of the alluvial-fan system. The alluvial sandstone deposits comprise large-scale ripple laminations (planar- and cross-bedding), small-scale ripple laminations and wavy, low-angle or horizontal laminations. The sediments consist of fine- to medium-grained quartz arenites and sub-litharenites.

IV.2.3 Porosity and permeability characteristics

Permeability and porosity are best in the aeolian-dune and braided-fluvial

sandstones. Primary porosity has been reduced by compaction and diagenetic grain-coating clays, which also reduced permeability, especially when re-illitisation associated with deep burial has occurred.

IV.3 THE VOLLPRIEHAUSEN SANDSTONE MEMBER, MAIN BUNTSANDSTEIN FORMATION (LOWER TRIASSIC), THE NETHERLANDS

The Main Buntsandstein Formation is the most important reservoir rock of the Lower Triassic in the North Sea Basin. The deposits comprise sandstones, siltstones and mudstones deposited in an arid/semi-arid non-marine environment. The Vollpriehausen Member is the thickest reservoir unit of the Main Buntsandstein Formation. Cores of this member from the Dutch offshore have been studied for small-scale reservoir permeability characteristics.

IV.3.1 Stratigraphic subdivision of the Main Buntsandstein Formation

The Main Buntsandstein Formation is subdivided into three depositional units, the Vollpriehausen, Detfurth and Hardegsen. Each depositional unit represents a succession of northward-prograding braided-fluvial fans. Fig. IV.4 shows that each unit include a sequence of sandstones fining upward into argillaceous-lacustrine sediments, resulting in three different fining upward sequences which represents a sequential retrogradation of the fluvial-fan system (Glennie 1990). The oldest and most widely distributed sandstone member is the Vollpriehausen Sandstone Member, followed by the Vollpriehausen Claystone Member. The middle part is represented by the Detfurth Sandstone and Claystone Members. The youngest deposits are part of the Hardegsen Member which are truncated by a major erosional event, the Hardegsen unconformity (Robertson, 1985).

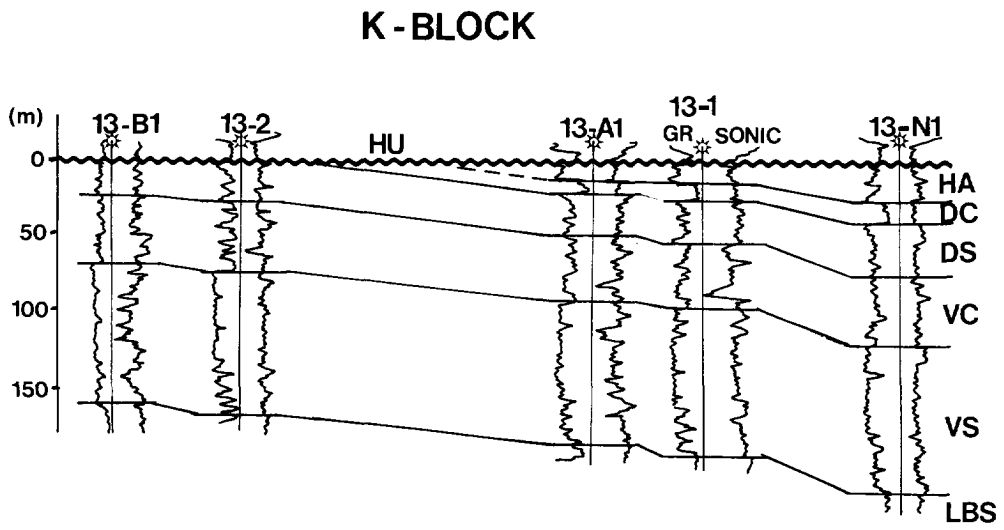

Fig. IV.4 North-south Gamma-ray/sonic log correlation panel of Members in the Main Buntsandstein Formation from several wells in the K-block offshore the Netherlands. LBS is Lower Buntsandstein, VS is Vollpriehausen Sandstone, VC is Vollpriehausen Claystone, DS is Detfurth Sandstone, DC is Detfurth Claystone, HA is Hardegsen member, The wiggly line (HU) is the Hardegsen Unconformity (modified from Roos and Smith 1983).

IV.3.2 Depositional model

In areas of rapid subsidence (e.g. Central Graben, Broad Fourteens Basin) sediments were deposited in an ephemeral river system. Local areas of slow subsidence or perhaps uplift (e.g. Cleaver Bank High, Schill Ground High and Texel-IJsselmeer High) acted as source areas. In the studied deposits of the Vollpriehausen Sandstone Member, a braided-fluvial system dominated the environment of deposition, although local aeolian reworking of the upper part of the sediments has been reported (Fig. IV.5).

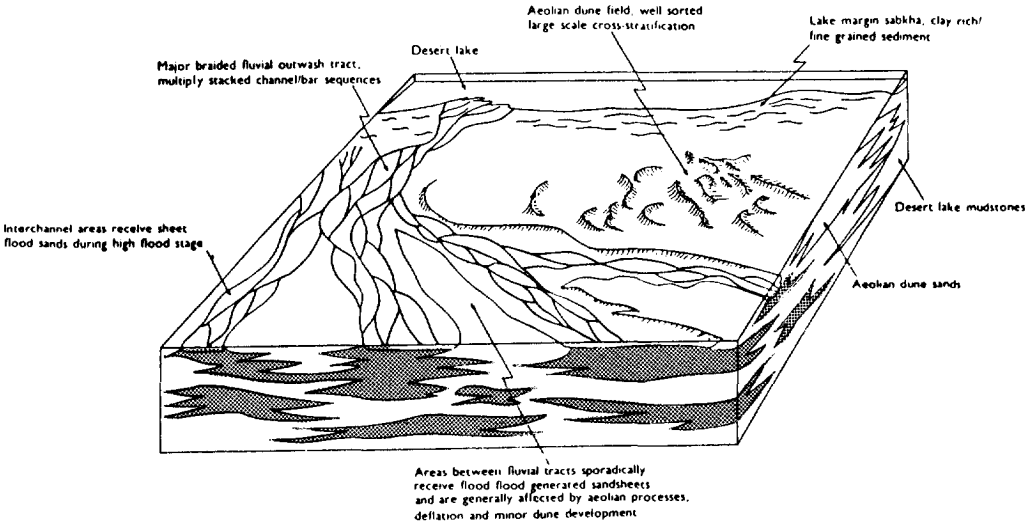

Fig. IV.5 Depositional model of the Main Buntsandstein Formation (modified from Robertsons 1985).

The fluvial deposits comprise low and high-sinuosity channel deposits. The sandstones are mostly fine-grained subarkoses in which large-scale sedimentary structures (planar and cross-bedding) are abundant. Anhydrite and authigenetic fibrous illite are found locally (Robertson 1985).

IV.3.3 Porosity and permeability characteristics

The best porosity and permeability occur in the Vollpriehausen Sandstone Member, especially in the part that shows aeolian reworking. If anhydrite and authigeneous-fibrous illite are present in the sediment, the primary porosity and permeability are reduced. Porosity and permeability have subsequently decreased as a

result of compaction and early carbonate cementation (Robertson 1985).

IV.4 METHODS

IV.4.1 Petrography

Microscopic petrological studies were carried out on five thin sections from the Vollpriehausen Sandstone Member. The thin sections consist of either a core section with well-developed foreset laminae or a core section with a bottomset and underlying foreset laminae. Coarser- and finer-grained foreset laminae and bottomsets were studied separately. Of each of these three subfacies, grain-size distribution, porosity and mineralogic composition were point counted. Grain-size distribution was analyzed in steps of one grain-size interval. Blue araldite was used to fill the pore spaces of the samples studied to analyze porosity. Each analysis included 300 points counted.

IV.4.2 Permeability

Permeability was measured with a minipermeameter (see appendix A). The measured parts of the cores were brushed and cleaned with water. Samples were dried to minimize the effect of clay swelling on the measurements.

Of the Upper Slochteren Sandstone Member and the Ten Boer Claystone Member, fifteen sandy core intervals were selected from six different wells[1]. In total, 1139 measurements were processed, 380 data points of the Ten Boer Claystone Member and 759 data points of the Upper Slochteren Sandstone Member. Measurements were performed on a grid with a vertical and horizontal spacing of 1 cm. Additional points in

[1] at the Nederlandse Aardolie Maatschappij core laboratory, Assen, The Netherlands.

the columns were measured with a spacing of 0.5 cm of very heterogeneous sections.

Of the Vollpriehausen Sandstone Member, eight cross-bedded core sections coming from three different wells were selected for minipermeameter studies[2]. 800 data points were processed. Measurements were performed on a grid with a horizontal spacing of half a centimeter and a vertical spacing of 1 centimeter.

Permeability datasets and sub-datasets were arithmetically averaged (appendix B). Average permeabilities were compared with plug-permeability values. Extreme values were excluded from processing.

IV.5 RESULTS

IV.5.1 Petrography

IV.5.1.1 Grain size

Grain-size analysis of coarser- and finer-grained foreset laminae shows an average difference between the two of at least half a grain-size interval (½ϕ unit scale interval; Pettijohn *et al.* 1973). Analysis showed that the coarser-grained foreset laminae largely consist of medium-grained sand, whereas the finer-grained d foreset laminae contained fine-grained sand. Sorting is on average moderately to well. Two bottomsets were analyzed, showing either grain sizes coarser than the foreset laminae (Fig. IV.6, L11.34) or a grain size more or less equal to the finer-grained foreset lamina, but showing a better sorting (Fig. IV.6, K10.44). The higher percentages of the finer grain sizes in all samples are a result of the fine, blocky texture of the clay mineral kaolinite that occurs between the framework grains.

IV.5.1.2 Mineralogic composition

The mineralogic composition comprises mono- and poly-crystalline quartz, rock

[2] At the Rijks Geologische Dienst core laboratory, Haarlem, The Netherlands

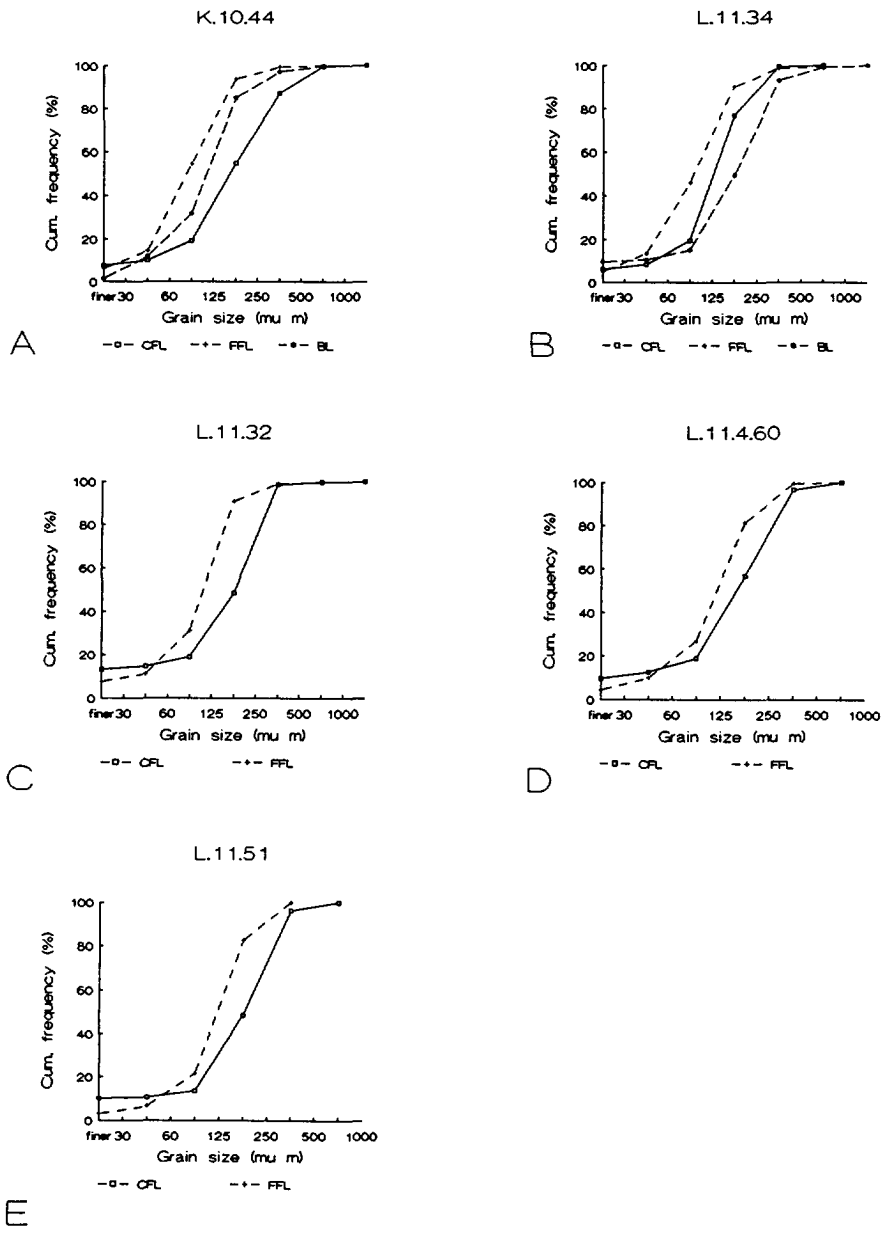

Fig. IV.6 Grain-size distribution of laminated samples (FFL = finer-grained foreset lamina, CFL is coarser-grained foreset lamina and BL = Bottomset layer).

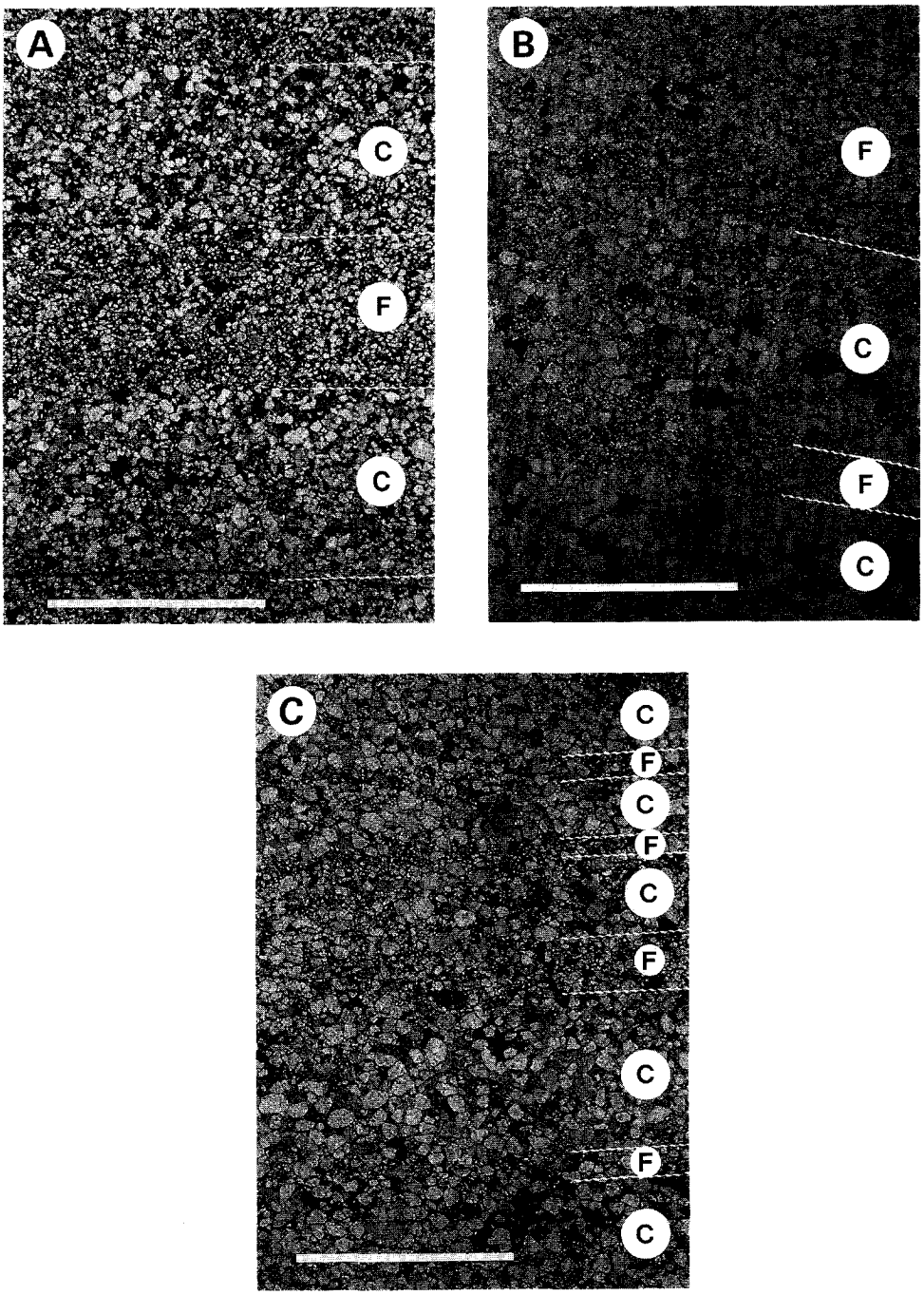
A
C
F
C
B
F
C
F
C
C
C
F
C
F
C
F
C
F
C

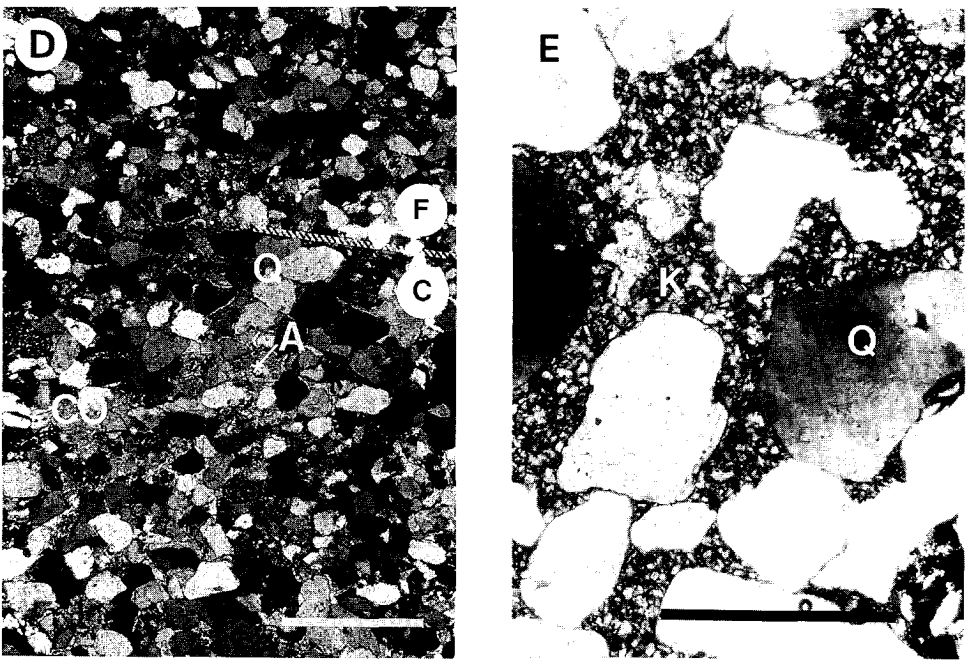

Fig. IV.7 Photomicrographs of Vollpriehausen Sandstones. A) Laminated sample (K/9-31) showing coarser-grained (C) and finer-grained (F) laminae. Fine wiggly line indicates boundary between the laminae. Scale bar is 0.5 cm. B) Laminated sample (L/11-51) showing coarser-grained (C) and finer-grained (F) laminae. Fine wiggly line indicates boundary between the laminae. Scale bar is 0.5 cm. C) Laminated sample (L/11-34) showing coarser-grained (C) and finer-grained (F) laminae. Fine wiggly line indicates boundary between the laminae. Scale bar is 0.5 cm. D) Sample (L/11-32) showing quartz grains (Q) and pores filled with Carbonate (CO, grey areas) and large-crystals of Anhydrite (A, grey areas with a very bright rim). The pore filling Anhydrite is particularly located in the coarser-grained lamina (C). The blocky line indicates the boundary between the coarser-grained lamina (C) and the finer-grained lamina (F). Scale bar is 0.1 cm.
E) Sample (L/11-34 top) showing blocky, microporous kaolinite (K) in pores between quartz grains (Q). Scale bar is 0.05 cm.

fragments and pore-filling cements (kaolinite, carbonate and anhydrite). The studied rocks can be classified as quartz-arenite, on the basis of the high content of quartz framework grains. Kaolinite cement shows a porous blocky texture. The blocky texture of kaolinite indicates a low degree of diagenesis for the studied samples. Carbonate cement is present

only as minor constituents in the pores. Anhydrite cement was found in one sample and occurs as large blocky, pore-filling crystals (Fig. IV.7).

Figures IV.8, A to E show frequency diagrams of the mineralogic components of the coarser-grained foreset laminae, finer-grained foreset laminae and bottomsets of the studied samples. The finer-grained foreset laminae usually show higher percentages of quartz and lower percentages of either rock fragments or kaolinite cement in comparison with the coarser-grained foreset laminae. In the sample with the coarser-grained bottomset (Fig. IV.8, L11.34) quartz percentages are lowest and kaolinite percentages are highest in comparison with the underlying finer-grained foreset laminae. In the sample with the well-sorted, fine-grained bottomset (K10.44), quartz percentages are highest and kaolinite percentages are lowest in comparison with the underlying foreset laminae.

IV.5.1.3 Porosity

Figures IV.8, A1 to E1 show that macroscopic porosity varies between samples and ranges between 5 and 20% (microscopic porosities in kaolinite excluded). The total porosity is determined by the percentages framework grains and pore-filling cements. The sample that contains anhydrite shows the lowest total porosities (1 and 5% respectively in finer-grained foreset laminae and coarser-grained foreset laminae). Microporosity in kaolinite showed up in the thin sections after the micropores were coloured with araldite.

IV.5.2 Discussion of petrography

Figures IV.8, A2 to E2 show all components together representing the total quantity of framework grains (Q + RF), the total amount of cement (C = Kaol. + Anh. + Carb.), and an approximation of the primary porosity (C + P), not compensated for compaction effects. The finer-grained foreset laminae generally show a higher percentage of framework grains and a lower percentage of pore-filling cements (with the exception of Sample k10.44). The coarser-grained bottomset of sample L11.34 exhibits lower percentages of framework grains and higher percentages of pore-filling cements in comparison with the underlying foreset laminae. The approximation of the

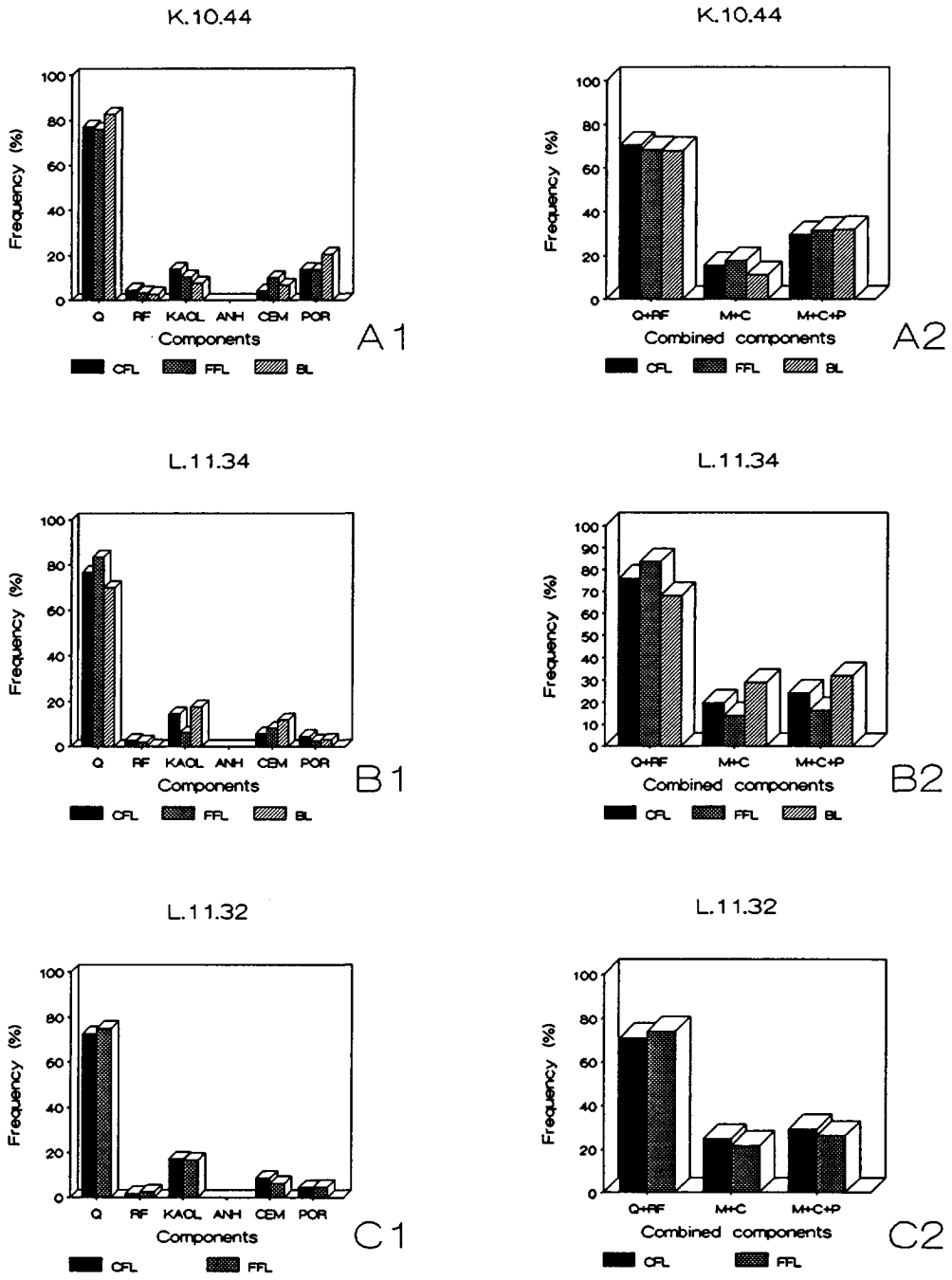
K.10.44
Frequency (%)
Q RF KAOL ANH CEM POR
Components
CFL FFL BL
A1
K.10.44
Frequency (%)
Q+RF M+C M+C+P
Combined components
CFL FFL BL
A2
L.11.34
Frequency (%)
Q RF KAOL ANH CEM POR
Components
CFL FFL BL
B1
L.11.34
Frequency (%)
Q+RF M+C M+C+P
Combined components
CFL FFL BL
B2
L.11.32
Frequency (%)
Q RF KAOL ANH CEM POR
Components
CFL FFL
C1
L.11.32
Frequency (%)
Q+RF M+C M+C+P
Combined components
CFL FFL
C2

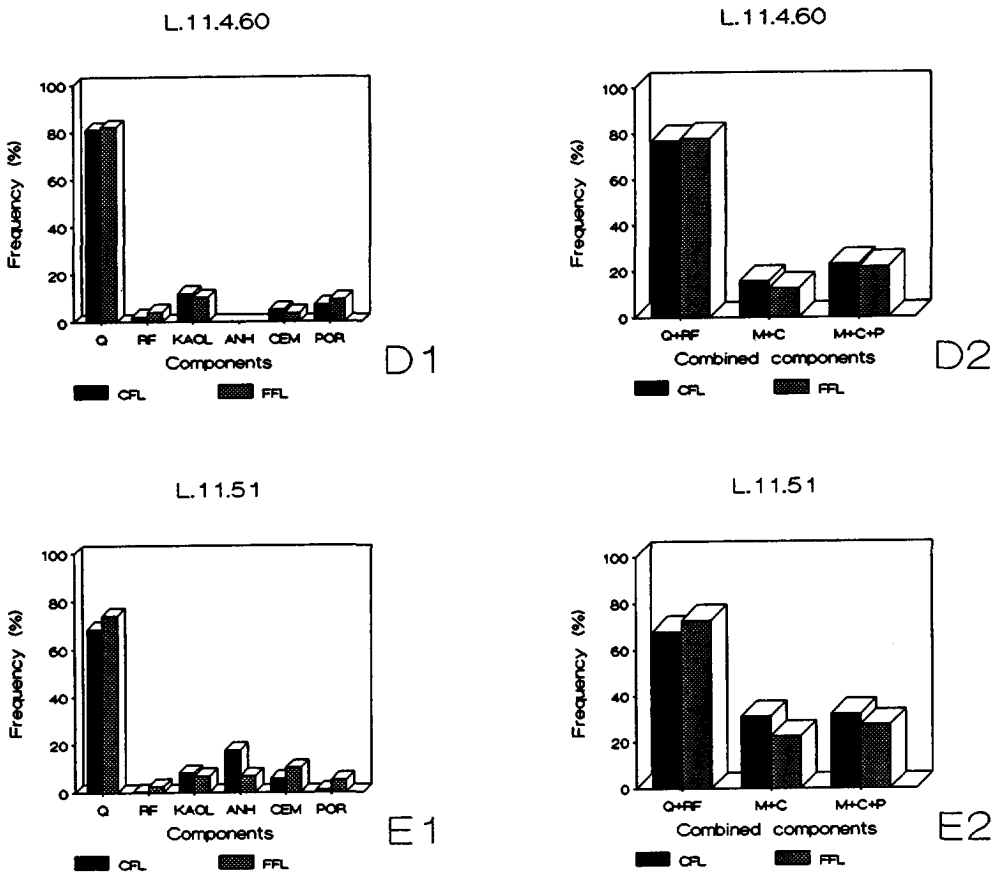

Fig. IV.8 A1 to E1) Frequency of mineralogic composition and total porosity of laminated samples (FF = finer-grained foreset lamina, CF is coarser-grained foreset lamina and B = Bottomset). A2 to E2) Frequency of combined components of laminated samples, presented are the total amount in framework grains (Q + RF), the total amount in cement (C = Kaol. + Anh. + Carb.), and an approximation of the primary porosity (C + P), not compensated for compaction effects.

primary porosity in this sample is high in comparison with the foreset laminae.

The percentages of framework grains and pore-filling cements, in particular

kaolinite, seem to reflect a grain-size trend. The occurrence of higher percentages of quartz and lower percentages of kaolinite in the finer-grained zones could reflect a depositional composition. However, no such conclusions with respect to the original depositional composition of the sediment can be drawn, because of the diagenetic character of the kaolinite.

Kaolinite may have formed out of detrital mica by recrystallization (Nadeau & Hurst 1991). Kaolinite could also have formed by chemical breakdown of feldspars (e.g. albite or K-feldspar) (Shanmugam 1985, Glasmann *et al.* 1989). Feldspar dissolution is common in other North Sea reservoirs (Bjorlykke 1984, Blackbourn 1984). No remnants of feldspars have been observed in the studied samples.

Qualitative information concerning kaolinite microporosities is given by Nadeau & Hurst (1991). They observed microporosities in blocky-kaolinite cement of approximately 15-30%. The texture and distribution of clay minerals in sandstones can have a marked effect on the permeability (Pallatt *et al.* 1984, Waal *et al.* 1988).

IV.5.3 Permeability

In Fig. IV.9, an example is presented of minipermeameter measurements over a section of a core from the Upper Slochteren Sandstone Member. The permeability patterns over the measured columns show a comparable pattern, related to the grain-size characteristics of the core.

Average permeabilities measured by minipermeameter were correlated with the core-plug permeabilities in order to verify the accuracy of the measurements (see also appendix C, in which measurement were further compared to estimated permeability). Figure IV.10 shows the correlation of minipermeameter versus core-plug permeabilities of several core-sections of the Upper Slochteren Sandstone Member and Ten Boer Claystone Member. In general, correlation is good with the exception of a few data points. Correlations of minipermeameter measurements with plug permeabilities and Baaren estimated permeabilities are further discussed in Appendix C.

The average permeabilities measured on sandstone core sections of the Ten Boer

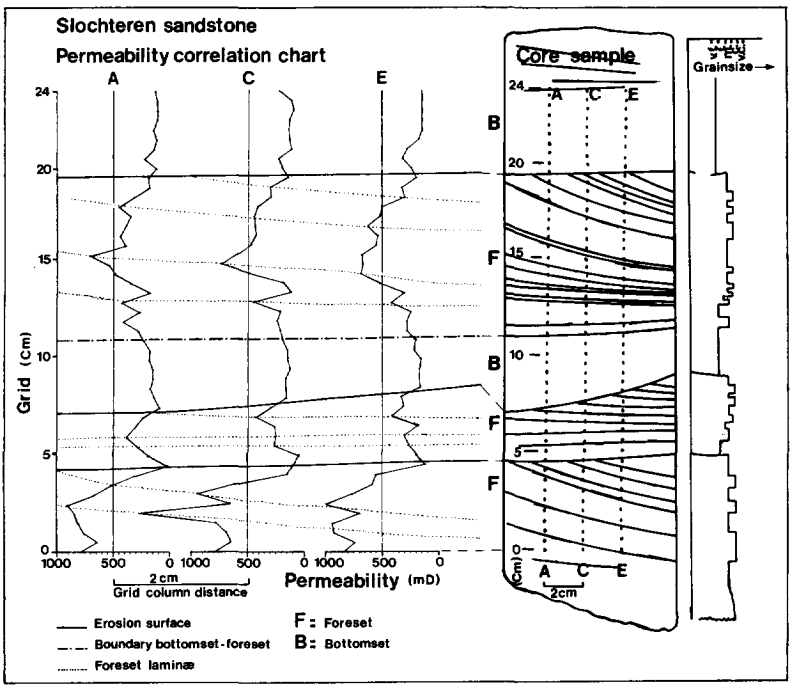

Fig. IV.9 Core-section of the Slochteren Sandstone Member showing the measured grid, the permeability graphs and sedimentological interpretations and a grain size log.

Claystone Member, the Upper Slochteren Sandstone Member and the Vollpriehausen Sandstone Member are presented in Table IV.II. For obvious reasons, names of cored sections of the Slochteren and Ten Boer sections were changed. Average permeabilities of coarser-grained foreset laminae and finer-grained foreset laminae were calculated whenever present. The permeability contrasts between bottomset layer (BL), finer-grained foreset laminae (FFL), and coarser-grained foreset laminae (CFL) are presented. Average contrasts vary between 1.7 : 1.1 : 1 (CFL:FFL:BL) and 27.9 : 9.6 : 1 (CFL:FFL:BL). Contrasts between finer-grained foreset laminae and coarser-grained foreset laminae vary

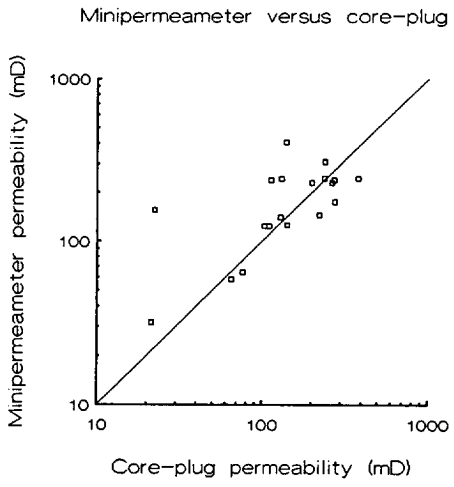

Fig. IV.10 Correlation between minipermeameter average permeabilities versus core-plug permeabilities.

between 1.3 : 1 (CFL:FFL) and 5.4 : 1 (CFL:FFL). High permeability contrasts between subfacies are probably determined by subfacies-related diagenetic mineral growth that locally reduces porosity. The diagenical variations may reflect the initial compositional contrasts between the subfacies.

Standard deviations of permeability values over the measured range were generally 15 to 20%, some extreme standard deviations (50 to 80%) are measured in some core sections of Ten Boer and Slochteren core-sections.

IV.6 DISCUSSION

The quantity of core samples available for thin-section studies (only from the Vollpriehausen Sandstone Member) was too small to draw conclusions about the influence

Table IV.II, Average permeability (in mD), standard deviation (in %) and permeability contrasts of cored sections of the Upper Slochteren Sandstone Member and the Vollpriehausen Sandstone Member.

Core-section	Foreset (F)	Coarser-grained foreset laminae (CFL)	Finer-grained foreset laminae (FFL)	Bottomset (BL)	Contrasts *=CFL/FFL @=CFL/FFL/BL
Ten Boer CH-1	390 mD (±43.3%)	544 mD (±22.4%)	339 mD (±44.5%)		* 1.6 : 1
Ten Boer CH-1	307 mD (±75.6%)	498 mD (±20.5%)	340 mD (±20%)		* 1.5 : 1
Slochteren CH-3	403 mD (±39.7%)	509 mD (±12.2%)	370 mD (±15.7%)		* 1.4 : 1
Ten Boer CH-4	146 mD (±46.6%)	186 mD (±39.2%)	119 mD (±46.2%)	106 mD (±26%)	* 1.6 : 1 @ 1.75 : 1.1 : 1
Ten Boer CH-5	347 mD (±98%)	950 mD (±13.7%)	328 mD (±77.7%)	34 mD (±89.1%)	* 2.9 : 1 @ 27.9 : 9.6 : 1
Slochteren CH-8	246 mD (±147.9%)	463 mD (±34.3%)	190 mD (±59.2%)		* 2.4 : 1
Slochteren CH-9	49 mD (±132.6%)	157 mD (±50.9%)	30 mD (±73.3%)		* 5.2 : 1
Ten Boer CH-11	44 mD (±54.5%)	75 mD (±14.6%)	30 mD (±20%)		* 2.5 : 1
Ten Boer CH-11	44 mD (±54.5%)	55 mD (±16.2%)	28 mD (±21.4%)		* 2 : 1
Slochteren CH-12-2	42 mD (±66.6%)	64 mD (±51.5%)	29 mD (±34.4%)		* 2.2 : 1
Slochteren CH-12-3	229 mD (±55.4%)	329 mD (±36.7%)	156 mD (±42.9%)		* 2.1 : 1
Vollpriehausen K/13-12	129 mD (±25.3%)	145 mD (±16.2%)	94 mD (±19.1%)	74.5 mD (±29.5%)	* 1.5 : 1 @ 1.9 : 1.3 : 1
Vollpriehausen K/13-12	181 mD (±36.7%)				
Vollpriehausen K/10-44	466 mD (±36.9%)	680 mD (±21.4%)	371 mD (±16.4%)	242 mD (±25.2%)	* 1.8 : 1 @ 2.8 : 1.5 : 1
Vollpriehausen L/11-34	128 mD (±23.4%)	145 mD (±17.2%)	105 mD (±17.5%)	39 mD (±51.3%)	* 1.3 : 1 @ 3.7 : 2.6 : 1
Vollpriehausen L/11-51	60 mD (±40.5%)	79 mD (±14.8%)	35 mD (±39.6%)		* 2.3 : 1
Vollpriehausen L/11-51	50 mD (±56.1%)	79 mD (±13.6%)	30 mD (±57%)		* 2.6 : 1
Vollpriehausen K/10-44	414 mD (±62.1%)	451 mD (±32.4%)	222 mD (±44.1%)	165 mD (±36.6%)	* 2 : 1 @ 2.7 : 1.4 : 1
Vollpriehausen K/13-12a	83 mD (±20.4%)	94 mD (±16.3%)	73 mD (±16.4%)	85 mD (±20.9%)	* 1.3 : 1 @ 1.1 : 0.8 : 1
Vollpriehausen K/10-24	410 mD (±21.7%)			308 mD (±23%)	(F:BL) 1.3 : 1
Vollpriehausen K/10-24	516 mD (±28.7%)	632 mD (±17.5%)	400 mD (±16.4%)		* 1.6 : 1

of grain size or porosity on the measured permeability values. Apart from the grain size and total porosity, the microporosity in the kaolinite is expected to have affected the permeability values of the examined samples. The differences in the percentages kaolinite (microporosity) between the coarser-grained foreset laminae, finer-grained foreset laminae and the bottomset in the studied samples resulted in a permeability contrast, partly

determined by microporosity.

The average contrasts in permeability between the studied subjects are listed in Table IV.II. The standard deviations from the mean indicate the variations in permeability between all data points. Specific contrasts between one foreset lamina and the other and between the foreset laminae and the bottomset vary from place to place. The minipermeameter studies and thin section studies clearly show that no general rule for the grain-size contrasts, compositional contrasts and permeability contrasts in cross-bedded sets can be formulated. The original sedimentary conditions under which cross-bed sets are formed are unique and so are the diagenetic changes that act on the sediments to form the host rock for reservoirs. Generally, the presence of cross-bedded sedimentary structures in a reservoir, causes a pronounced permeability contrast.

IV.7 CONCLUSIONS

1) Thin-section studies showed an average difference of half a grain-size interval between coarser-grained and finer-grained foreset laminae. Bottomsets may show coarser or finer grain sizes than the underlying foreset laminae, but always a better sorting than the individual foreset laminae.

2) Kaolinite cement shows a recrystallized texture and a microporosity of 15 to 30%.

3) The percentages of framework grains and pore-filling cements, especially kaolinite, indicate that the composition is determined by the grain size. The finer-grained zones show higher percentages of quartz and lower percentages of kaolinite.

4) In the examined samples, contrasts in permeability values are determined by contrasts in grain size and total porosity as well as by microporosity in the kaolinite.

5) Average permeability contrasts between bottomset layers (BL), finer-grained foreset laminae (FFL), and coarser-grained foreset laminae (CFL) vary between 1.7 : 1.1 : 1 (CFL:FFL:BL) and 27.9 : 9.6 : 1 (CFL:FFL:BL). Contrasts between finer-grained foreset laminae and coarser-grained foreset laminae vary between 1.3 : 1 (CFL:FFL) and 5.4 : 1 CFL:FFL).

6) The original sedimentary conditions under which each cross-bed set formed are unique and so are the diagenetic changes that act on the sediments to form the host rock for reservoirs. If cross-bedded sedimentary structures occur in a reservoir, a pronounced permeability contrast can be expected.

CHAPTER V
EFFECT OF CROSS-BEDS ON ULTIMATE RECOVERY

V.1 INTRODUCTION

The petrophysical parameter, permeability, is the capacity of a porous medium for transmitting a gas or liquid; it is a measure of the relative ease of flow. In the first few chapters, the heterogeneity of cross-bedded sets with respect to permeability has been demonstrated.

The performance of an oil/water flow in a heterogeneous reservoir has been a major concern of many reservoir engineers. In many presentations, heterogeneity is described only on the reservoir-unit and genetic-unit scale (horizontal stratification; Berruin & Morse (1979), Brett Fischbuch & Wattenbarger (1991), shale-distributions; Haldorsen & Lake (1984), Haldorsen & Chang (1986)) or the pore-scale (pore-structure heterogeneities, Wardlaw & Cassan (1978 & 1979), Yadav *et al.* (1987), Mohanty *et al.* (1987)). The influence of common sedimentary structures on fluid flow in reservoirs has been outlined by Weber (1982).

Experimental investigations of capillary-pressure effects on immiscible displacement in lensed and layered porous media is documented by Dawe *et al.* (1992). Water flooding of oil-saturated models with a lens of high permeability surrounded by a region of low permeability shows that water initially bypasses the lens. In each experiment, a large portion of oil was left in the lens after the displacement front had passed. Experiments on movement through a cross-bedded system have been visualized by Qui Yinan *et al.* (1982). These experiments show pronounced fingering of the water-oil front into foreset laminae when the flooding direction is perpendicular to the laminae.

Simulation studies on two-phase fluid flow through a cross-bedded heterogeneous system have been presented by Kortekaas (1985). He showed imbibition of the water-oil front into finer-grained laminae. The paper of Kortekaas is the first to present the effect of

grain-size-determined capillary-pressure characteristics in laminae of a cross-bed set on the imbibition of the water front. Kocberber & Collins (1990) described the impact of reservoir heterogeneity on the initial distribution of hydrocarbons, on the basis of the same principle of capillary-pressure heterogeneities in cross-bedding.

In this thesis the study of Kortekaas is expanded, the problem of two-phase fluid flow through cross-bedded sets in a water-wet reservoir was evaluated numerically[1] and experimentally[1] and results are discussed. To begin with, an overview is given of different parameters that influence ultimate recovery in a "homogeneous" and in a "cross-stratified heterogeneous" system.

V.2 FACTORS THAT INFLUENCE TWO-PHASE FLUID FLOW IN A POROUS MEDIUM

Figure V.1 shows a flow chart of all factors that influence two-phase fluid flow and ultimate recovery.

V.2.1 The homogeneous porous system

V.2.1.1 Reservoir rock properties

In chapter 3 the influence of grain size, sorting, pore-size distribution and framework composition on permeability was demonstrated. The temperature/pressure conditions during burial of the sand body determine the degree of compaction or diagenesis affecting the sediments. The framework composition of the sediment in combination with the grain-size and sorting characteristics are important factors that control the compaction and mineralogical changes in the sediment. These factors ultimately determine the porosity and permeability of the sand body before hydrocarbon migration. Early hydrocarbon migration may have a retarding effect on compactional and

[1] By Reservoir Engineers, Dietz Laboratory, Delft University of Technology.

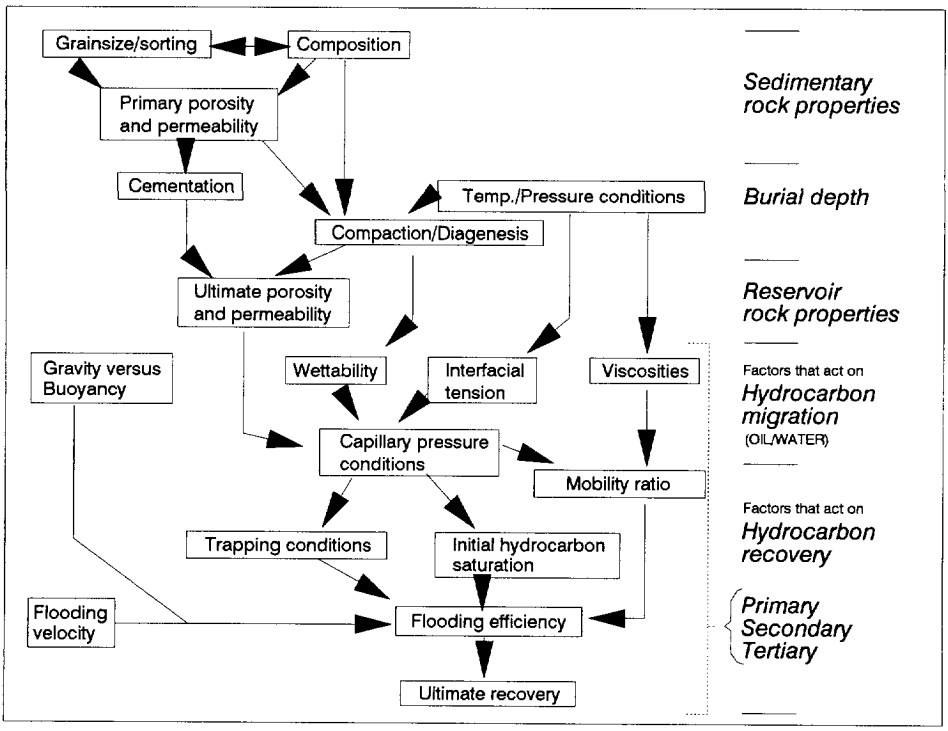

Fig. V.1 Flowchart of factors influencing ultimate recovery.

diagenetic changes in the sediment and favour preservation of primary porosity and permeability characteristics (Nagtegaal 1980).

V.2.1.2 Forces that act on hydrocarbon migration

The mechanics of secondary hydrocarbon migration and entrapment are determined by the equilibrium of gravity, buoyancy and capillary forces (Schowalter 1979). The main driving force is the buoyant force, which is related to the densities of the hydrocarbon phase and water phase. A force that resists migration is the capillary force. The factors

that determine the magnitude of the capillary force (P_c) are the radii of the pore throats (r) of the rock, the hydrocarbon/water interfacial tension (σ), and a function of the wettability ($f(\theta)$). Thus, the capillary force is given by:

$$P_c = \frac{f(\theta) . \sigma}{r} \qquad (1)$$

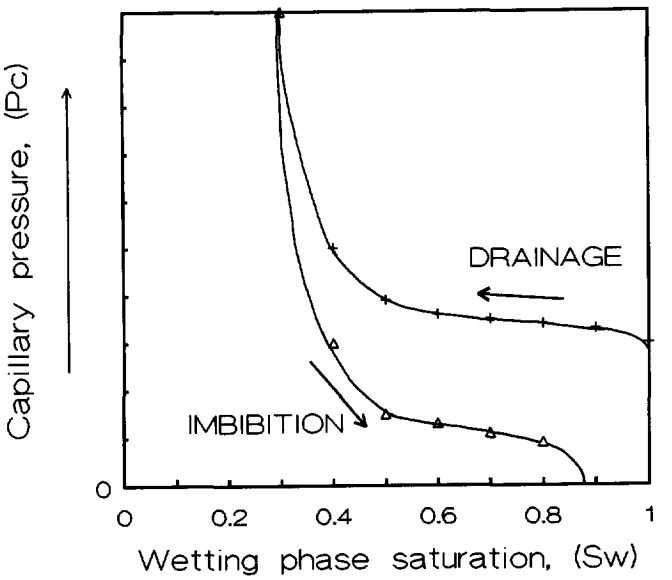

Fig. V.2 Hysteresis between drainage and imbibition capillary pressure curves (modified from Melrose *et al.* 1974).

Wettability

The adhesive force or attraction of the wetting fluid to the solid in any oil/water/rock system is the result of the combined interfacial energy of the oil/water, oil/rock, and water/rock surfaces. Sedimentary rocks that were deposited in water are

generally considered to be preferentially water-wet because of the strong attraction of water to rock surfaces and the initial exposure, during sedimentation and early diagenesis, of pore surfaces to water rather than hydrocarbons (Schowalter 1979).

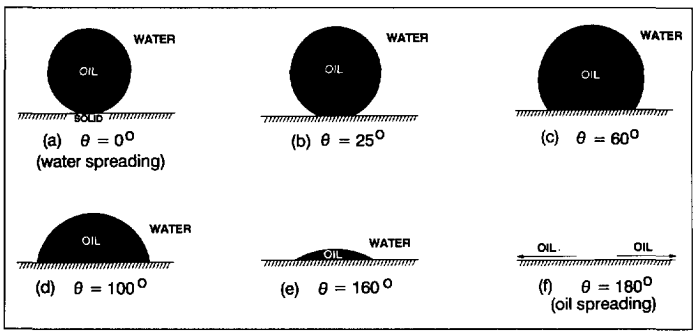

Fig. V.3 Contact angles at different wettability (from Morrow 1990). θ = 0° is water wet, θ = 180° is oil wet.

The wettability of subsurface rocks is still a matter of debate (Morrow 1989) and it is widely believed that hydrocarbon-reservoir rocks are seldom completely water or oil-wet. They show a fractional wettability to oil and water. Grain surfaces that are exposed to surface-active molecules in the oil phase may be partially oil-wet (Salathiel 1972). Organic material or iron minerals in sediments attract the hydrocarbon phase rather than the water phase. This means that the wettability of a reservoir rock depends, as a result of diagenetic changes, on the original framework composition of the sediment. However, large quantities of organic material or iron minerals are needed in clastic sedimentary rocks to produce a significant effect on the overall wettability of these rocks (Schowalter 1979). Generally, clastic fluvial reservoir sandstones are considered to be preferentially water-wet.

The migration of oil in a water-wet rock is characterized by a decrease of the wetting phase, this situation is called drainage. The opposite situation, in which the

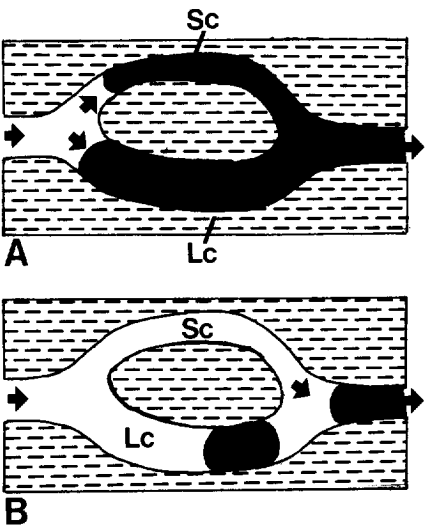

Fig. V.4 Pore-scale capillary trapping. Sc is small capillary, Lc is large capillary. Arrows indicate direction of fluid movement. Water is white, oil is grey. A) initiation phase of competition of the water/oil movement in the two separate capillaries. B) Termination of this competition, the front moved faster through the small capillary as a result of faster imbibition of water and movable oil is bypassed in the large capillary (drawing based on Abrams 1975).

wetting phase increases is called imbibition. The difference between drainage and imbibition capillary-pressure curves is called hysteresis (Fig. V.2), it is partly determined by the difference in the wettability function between the two situations. Wettability is traditionally expressed as the contact angle between the wetting and non-wetting phases (Fig. V.3). This idealized expression is difficult to apply to a crude-oil/water/rock system, in which contact angles are random as a result of e.g. grain-surface roughness, variations in composition. Relations between wettability and capillary-displacement pressures are complicated by the complex pore structure and mineralogy of reservoir rocks and the effect of organic components that are adsorbed from the crude oil (Morrow 1989). This is the reason that the capillary-pressure function for a oil/water/rock system is

determined by a function of wettability ($f(\theta)$) rather than the traditionally expressed contact angle (θ).

Interfacial tension

The interfacial tension of the oil/water interface varies as a function of the chemical composition of the oil, the amounts and types of surface-active agents, the types and quantities of gas in solution, the pH of the water and the temperature conditions of a reservoir (Schowalter 1979). A decrease in interfacial tension results in a reduction of the capillary force. This can be achieved by the addition of surfactant to the flooding water or by increasing the temperature conditions of the reservoir. At an increase in temperature, the oil/water interfacial tension generally decreases (Hjelmeland & Larrondo 1986).

Initial hydrocarbon saturation and residual hydrocarbon saturation.

The initial hydrocarbon saturation is primarily dependent on capillary-pressure characteristics. These characteristics also determine the pore-scale capillary trapping conditions (residual-hydrocarbon saturation) in the porous system (Fig. V.4).

V.2.1.3 Factors that act on hydrocarbon recovery

Flooding efficiency and ultimate recovery

Ultimate recovery is that volume of oil that can be produced by whatever means until the economic limit is reached. In a natural water-wet porous system, displacement of oil by water is governed by fluid viscosity, interfacial tension and flow velocity, in other words: the combined effect of viscous and capillary forces (Abrams 1975). The pores and pore throats of a natural porous system consist of a three-dimensional network in which the capillaries vary in length, size and shape. The difference in capillary pressure between two pore throats is the main factor controlling relative velocities and making the oil/water front move more rapidly through the smaller capillary. Blobs of oil are trapped in the larger pores (Abrams 1975). Pore-throat bypassing is considered to result in macroscopic entrapment. The tendency to trap oil in the larger pores becomes less as the ratio of

viscous force and capillary force increases.

Secondary and tertiary recovery techniques have been developed to increase recovery by decreasing the ratio of viscous force and capillary force. This could be achieved by adding chemicals to the flooding water in order to increase the water viscosity and decrease the water-oil interfacial tension.

V.2.2 The cross-bedded heterogeneous porous system

If a porous system consists of zones that have different grain-size, sorting and composition characteristics, the combination of all zones determines the ultimate recovery of the entire system. The foreset laminae and bottomsets of cross-bed sets form such a system of zones with different capillary-pressure characteristics. The principles of capillary trapping on a pore-throat scale (Abrams 1975) are expected to play a major role in the entrapment of pockets of oil in a laminated system under the combined influence of viscous and capillary forces.

Zones that have higher capillary-pressure characteristics will show a higher initial water saturation than zones that have lower capillary-pressure characteristics as a consequence of the capillary/gravity equilibrium (Fig. V.5). Kocberber & Collins (1990) demonstrated the effects of the capillary/gravity equilibrium in cross-bedded sets on initial distributions of oil, water and gas in sandstone reservoirs and provided a preliminary assessment of the effect of these structures on primary recovery. They demonstrated that severe discontinuities in initial saturation and effective permeability occur in adjacent foreset laminae and between the foreset and bottomset of a cross-bed set. These effects are most dramatic in water-wet systems; the higher capillary-pressure characteristics in the low-permeability zones of a cross-bed set cause a high degree of water retention, with correspondingly low hydrocarbon permeabilities, over the entire range of average saturations. These zones literally become permeability barriers to hydrocarbon flow and cause very irregular reservoir-drainage patterns; extensive pockets of trapped hydrocarbons may result. The effective permeabilities in an imbibition process (recovery) would be further reduced, especially in the low-permeable zones, making these zones an

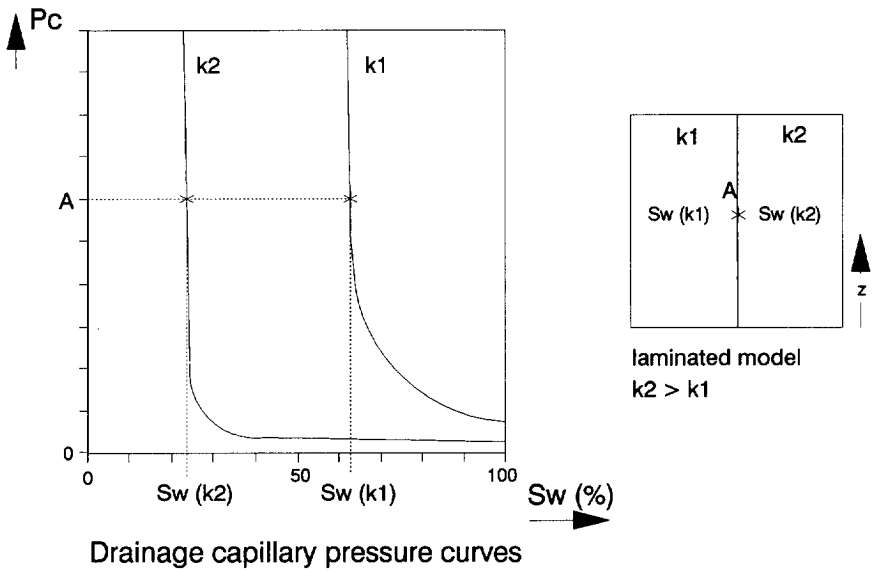

Fig. V.5 Drainage capillary pressure curves determined initial hydrocarbon saturations of zones with different capillary pressure characteristics (modified from Kocberber and Collins 1990).

even larger barrier to flow. Results from Kocberber & Collins (1990), combined with results from Kortekaas (1985) indicate that the macroscopic pockets of trapped hydrocarbons in the highly permeable laminae of a cross-bedded water-wet reservoir zone may have a significant effect on ultimate recovery.

V.3 CAPILLARY-PRESSURE CHARACTERISTICS IN CROSS-BEDDED RESERVOIRS

V.3.1 Capillary-pressure curves

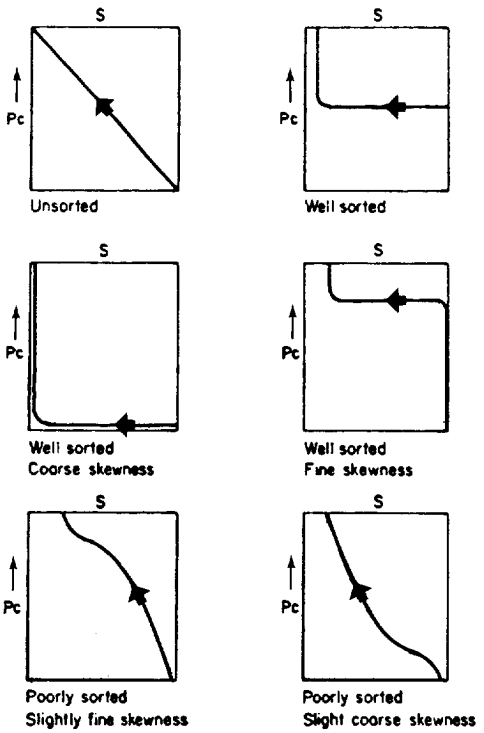

Fig. V.6 Porosity and pore-size distribution determined shapes of capillary-pressure curves (modified from Archer and Wall 1986). S is saturation, Pc is capillary pressure.

The pore-size distribution (sorting of pore sizes) determines the shape of the

capillary-pressure curve (Leverett 1941, Thomeer 1960, Stout 1964, Neasham 1977). Figure V.6 shows extreme shapes of drainage capillary-pressure curves from rocks with different grain size and sorting characteristics.

The relation between water saturation and capillary pressure is usually obtained from measurements on cm-scale cores. Although these measurements are affected by factors on pore level, such as radius of curvature, they are usually strictly macroscopic, empiric relations. New techniques are being developed (Ampex capillary-pressure curve measurements) that measure very detailed pressure-saturation increments such that pore-size distribution can be accurately obtained.

As shown by Chatzis *et al.* (1988) and Lake (1989), the microscopic distribution of oil in each pore is absolutely uncertain. The first drainage and imbibition capillary-pressure curves show a hysteresis between the two curves (Fig. V.2). The first drainage curve is formed, starting with a rock sample saturated with a wetting phase (water) and replacing this wetting phase by a non-wetting phase (oil) under increasing pressure, upto a pressure where the wetting phase becomes irreducible. The first imbibition curve is formed, starting from the end-point situation of the drainage experiment, with the sample maximally saturated by a non-wetting phase (oil) and replacing this non-wetting phase by a wetting phase (water) under depressuring. The end point of the imbibition curve shows the percentage of macroscopic residual oil trapped when capillary pressure is zero (only water is flowing) (Wardlaw & Taylor 1976). This percentage of macroscopically trapped residual oil is determined by the capillary-pressure characteristics of the rock sample. Rocks that have higher capillary-pressure characteristics show higher residual oil saturations than rocks that have lower capillary-pressure characteristics (see the different 1-Sor values at zero pressure of each of the imbibition capillary-pressure curves, Fig. V.7A).

V.3.2 Theoretical models

V.3.2.1 The ideal cross-bed model

If we consider a heterogeneous water-wet system consisting of three zones of

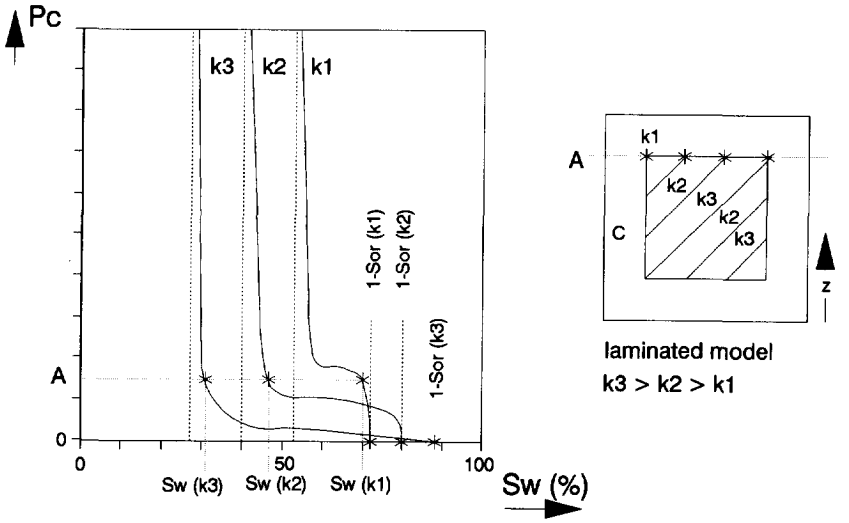

A Imbibition capillary pressure curves

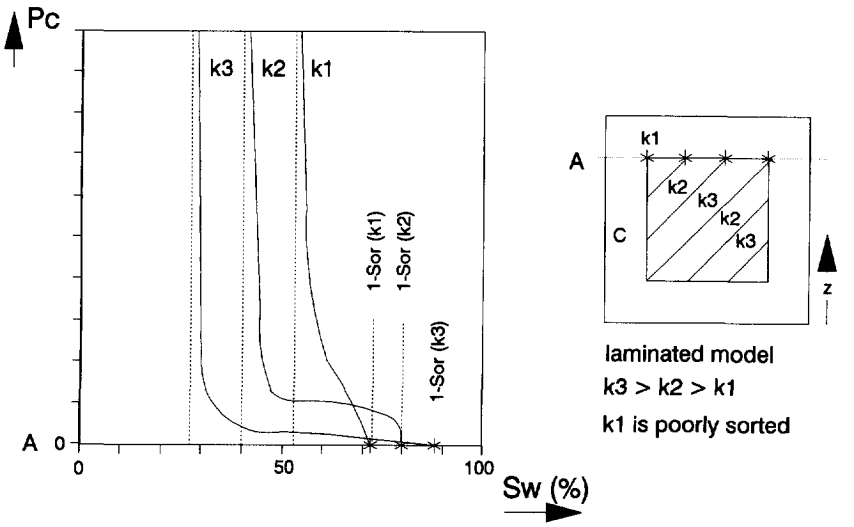

B Imbibition capillary pressure curves

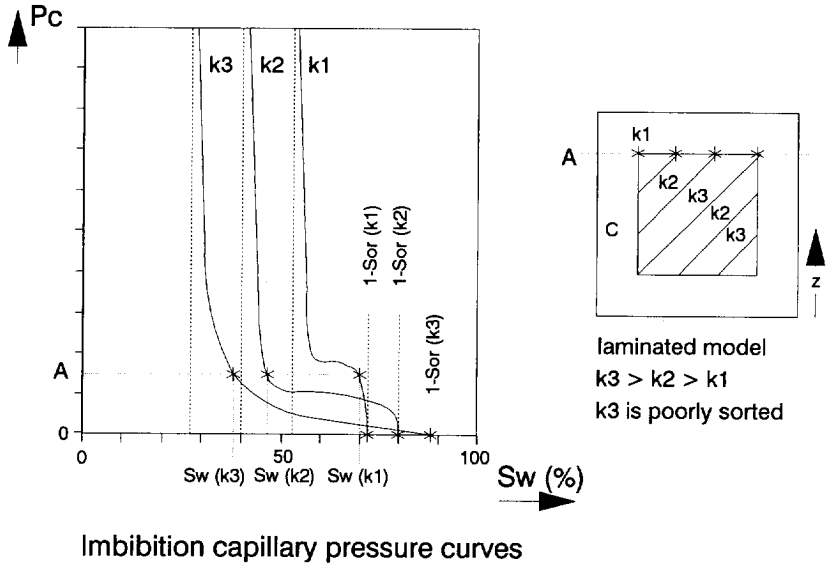

Fig. V.7 A) Imbibition capillary pressure curves of three zones with contrasting permeabilities as drawn in the model (k1, k2 and k3). The curves show contrasts in saturation between the zones at pressure point A (curves after Stout 1964, Pickell *et al.* 1966, Diaz *et al.* 1987 and Kocberber and Collins 1990). B) Imbibition capillary pressure curves of the same model as presented in Fig. V.7A except for the assumption that zone k3 is poorly sorted. C) Imbibition capillary pressure curves of the same model as presented in Fig. V.7A, except for the assumption that zone k1 is poorly sorted.

different porosities, permeabilities and pore-size distributions, these zones will show distinct capillary-pressure characteristics (Fig. V.7A, curves based on; Stout 1964, Pickell *et al.* 1966, Diaz *et al.* 1987 and Kocberber & Collins 1990). The three zones represent three sub-facies that occur in natural cross-bedded sediments, i.e. k1) bottomsets, k2) finer-grained foreset laminae and k3) coarser-grained foreset laminae. The individual capillary-pressure characteristics of the zones determine differences in initial hydrocarbon saturations between the three zones, under the assumption of capillary-pressure equilibrium, as is shown by Kocberber & Collins (1990) and in Figure V.5. After water

drive or water flooding, differences in residual-oil saturation at zero pressure between the three zones are to be expected as a result of the same principle, as is shown by the imbibition capillary-pressure curves (Fig. V.7A). During flooding, however, the zone with higher capillary-pressure characteristics (k1) will almost reach maximum water saturation when the zones with lower capillary-pressure characteristics (k2 and k3) still contain large amounts of movable oil (pressure point A). At this point, the high capillary-pressure zone (k1) is only capable of transporting very small percentages of oil. The movable oil in zones k2 and k3 is literally trapped, although it is expected that eventually zero-pressure residual-oil saturation may be reached in all zones. Is the time needed to reach this greatly exceeding the economic life of the reservoir?

V.3.2.2 Two alternatives to the cross-bed model

In the first alternative model (Fig. V.7B), the foreset laminae are assumed to be well-sorted, whereas the bottomset is poorly sorted, according to Weber (1982) and Weber (1986). The capillary-pressure curve for the poorly sorted bottomset lacks a well-developed plateau shape (Fig. V.7B). As a consequence, during the imbibition process, water saturation in the bottomset will increase very uniformly and only reach its maximum at almost zero capillary pressure. From this model it may be concluded that poor sorting of the bottomset (zone K3) decreases the trapping capacity of the cross-bed model.

The second alternative model (Fig. V.7C), is based on the sorting characteristics of cross-bed laminae and bottomsets presented in chapter IIIB. The bottomset and the finer-grained foreset laminae are characteristically well sorted and the coarser-grained foreset laminae show poorer sorting. This is in agreement with grain-size characteristics of experimentally obtained cross-beds as described by Joplin (1965, 1967) and Allen (1970). Because finer grain sizes are deposited in coarser-grained foreset laminae as well as in finer-grained foreset laminae and bottomset layers (see grain-size distributions, sections IIIB.4 and IV.5.1), fine pore sizes are present in all three sub-facies. It may therefore be concluded that imbibition will start in the fine capillaries in all sub-facies at approximately the same capillary pressure. Consequently, in the coarser-grained foreset laminae, water-saturations increase before entrapment occurs resulting in lower oil

saturations at the moment of initially trapping.

The models explain that the sedimentologically determined rock properties of the different sub-facies in the cross-bed sets determine the capillary trapping conditions and the amount of movable oil that may be trapped. In addition, the cross-bed geometry is an important factor, because it determines the compartmentalization of the cross-bedded reservoir by low-permeability bottomsets (see chapter I) and actually defines the natural trapping conditions. The contrast in dominant pore size, which is also reflected in contrasts of permeability, that occur between adjacent sub-facies in cross-beds defines the contrast in pressure/saturation between the sub-facies. Contrasts in sorting of the pores between adjacent sub-facies determine the actual oil/water saturations at the moment initial capillary entrapment occurs. The contrasts in dominant pore sizes again determine the end-point saturations (initial water and residual-oil saturation).

V.3.3 Capillary-pressure experiments

V.3.3.1 Methods

In order to describe the capillary discontinuity in laminated samples, air-mercury drainage and imbibition capillary-pressure curves were determined of ten subsurface core and outcrop samples, with the technique as described by Purcell (1949). The samples used in the experiments[2] were 1.5 cm in diameter and 1 to 1.5 cm long. They were either homogeneous or laminated containing a few laminae with specific grain-size and pore-size characteristics. Helium porosity of each sample was determined prior to mercury injection. Injection was achieved by increasing the pressure until a maximum injection pressure of 2000 Psi was reached. The imbibition curve was determined by decreasing the pressure stepwise. Pore-size distributions were calculated using the La Place equation assuming cylindrical pores.

[2] GAPS Nederland B.V., Warmond, The Netherlands.

V.3.3.2 Results

Total porosity versus average permeability

The helium porosities of the ten samples are plotted in Fig. V.8 against the average permeabilities over the core section measured by mini-permeameter. The relation between the log permeability and porosity is linear. This is in agreement with Jensen (1990) who stated that porosity and log permeability are linearly related.

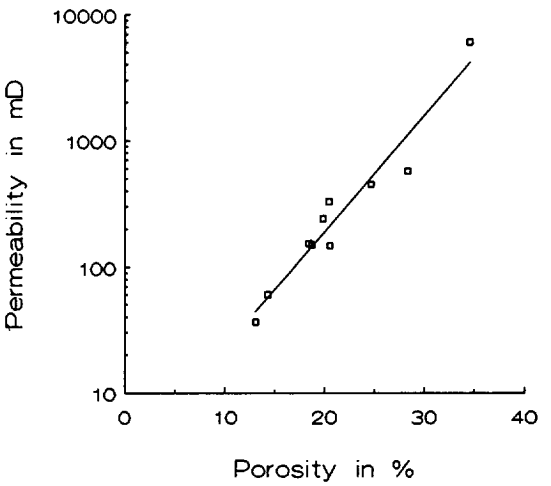

Fig. V.8 Total porosity versus permeability of ten subsurface and outcrop samples.

Capillary-pressure curve characteristics

In Figs. V.9, A to J, drainage and imbibition capillary-pressure curves and related pore size distributions are presented of the ten samples that have different porosity and permeability characteristics. In addition, average porosity and permeability are presented in the graphs. Figs. V.9, B and C show errors as a result of earlier filling of the pores by

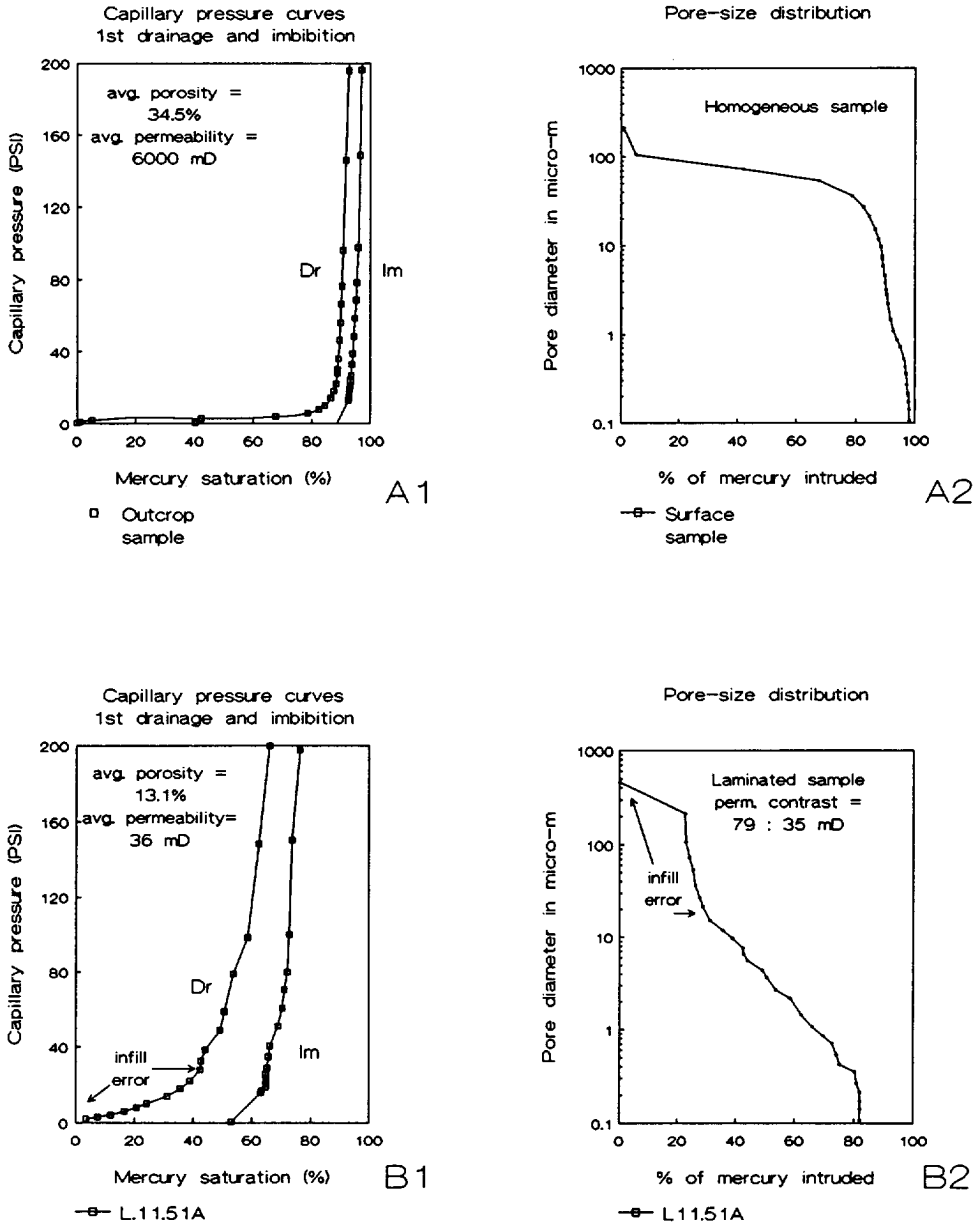

Fig. V.9 to be continued

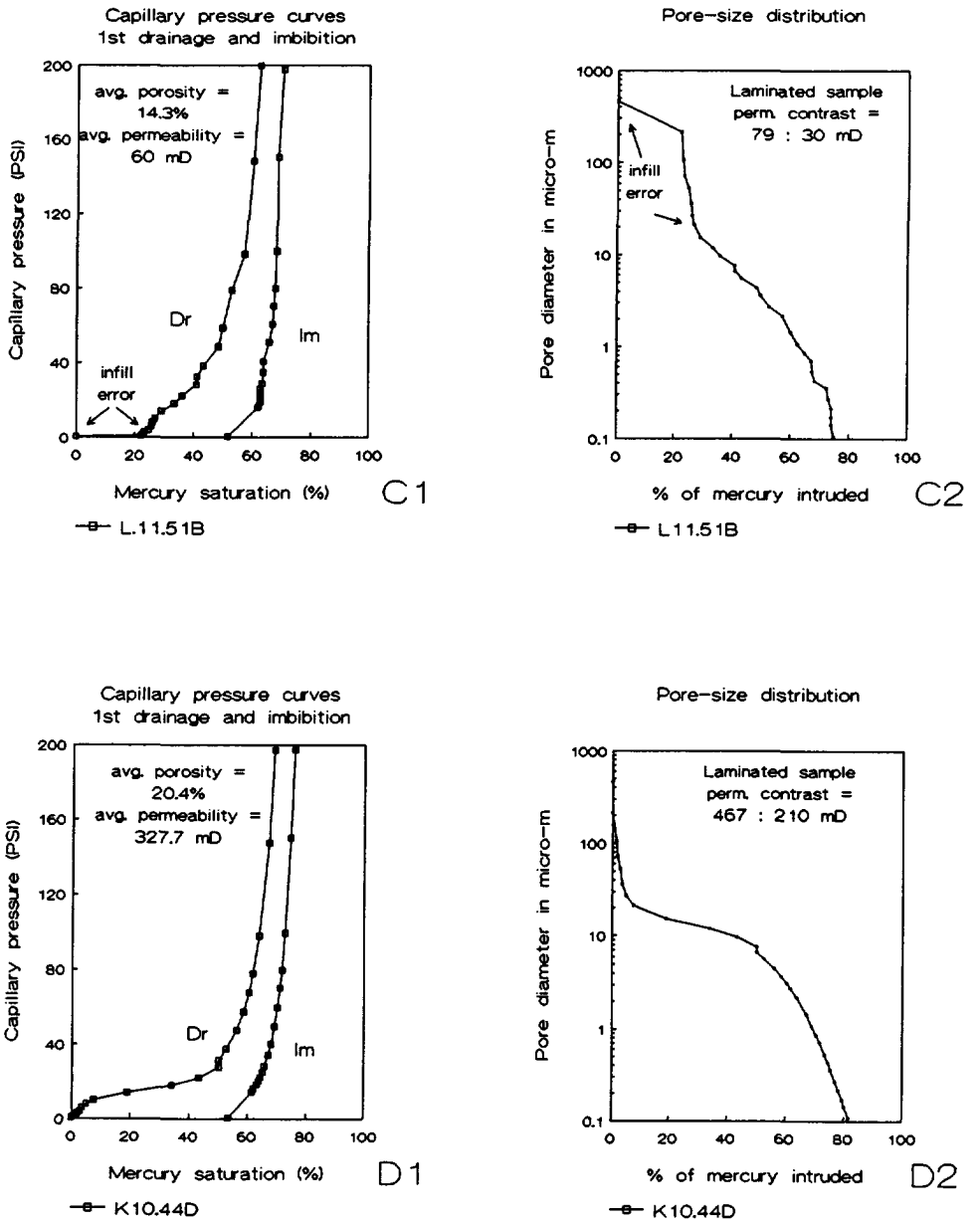

Fig. V.9 to be continued

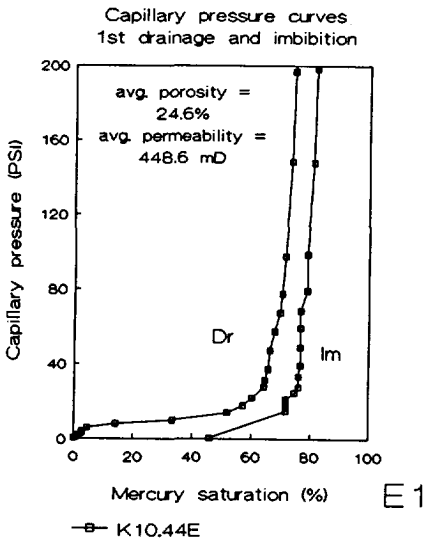

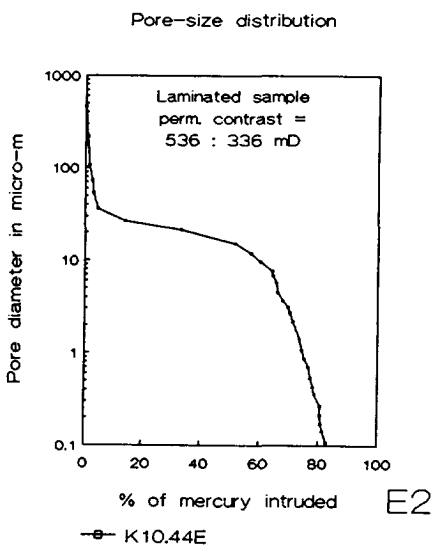

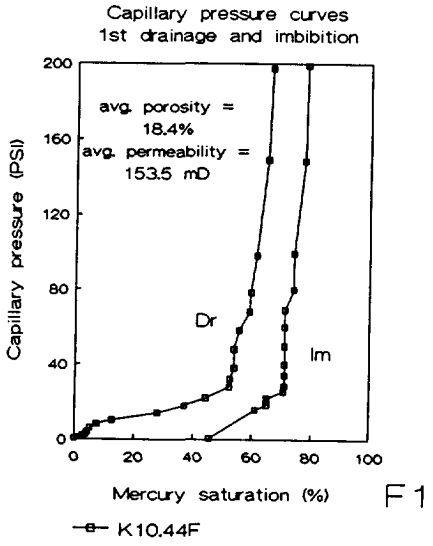

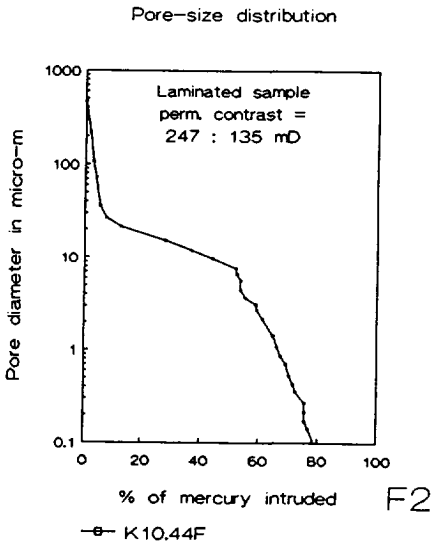

Fig. V.9 to be continued

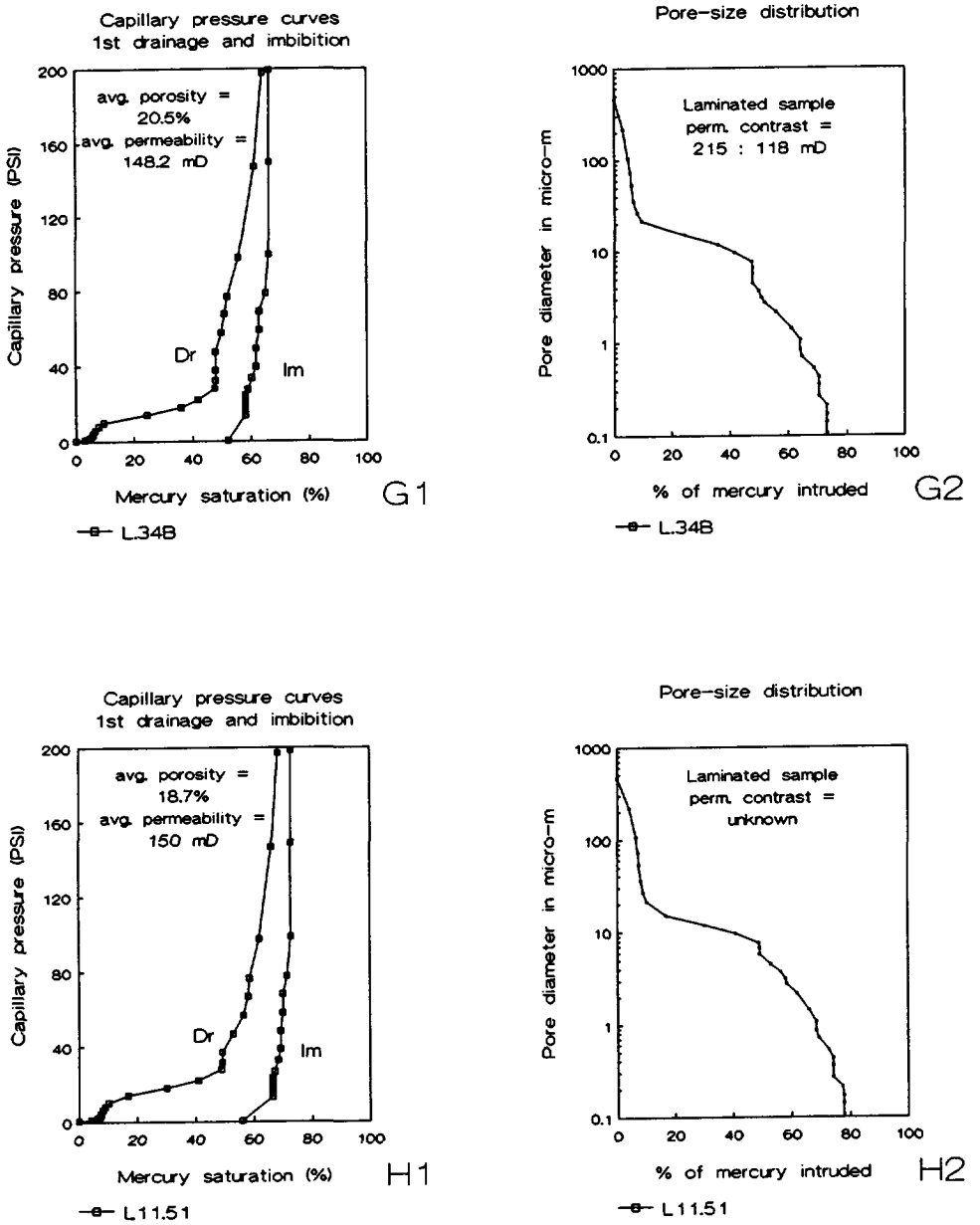

Fig. V.9 to be continued

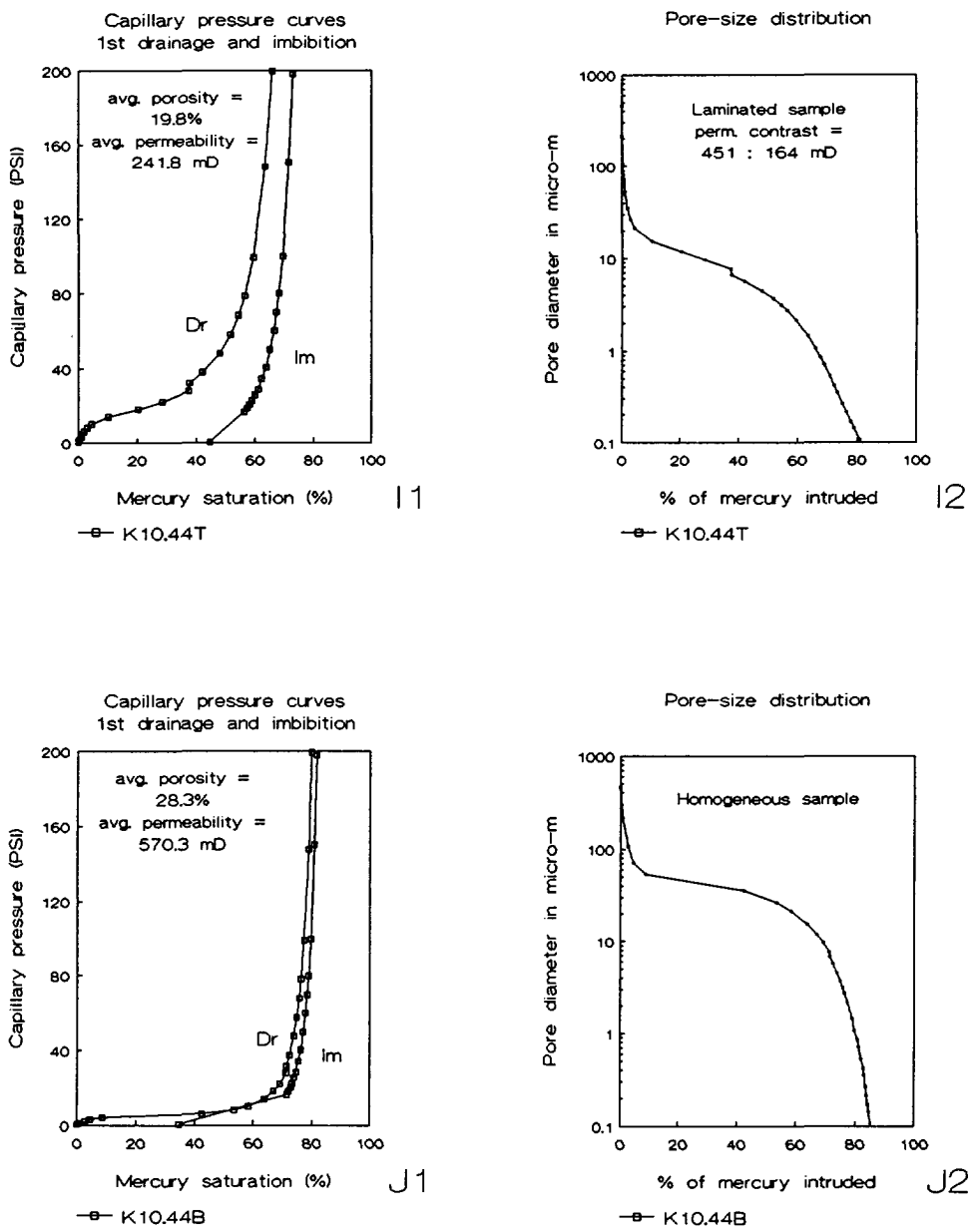

Fig. V.9 A1 to J1) Experimentally determined capillary-pressure curves of samples with different average porosity and permeability. A2 to J2) Pore-size distribution curves. Sedimentary characteristics are reported as well as the average permeability contrast of coarser-grained laminae to finer-grained laminae.

mercury. Figs. V.9, A, D, E, I and J show curves for relatively homogeneous samples, although some samples show a minor irregularity in the pore size distribution curve as a result of lamination (Fig. V.9 D, E and I). The curves are invariably very smooth. Their maximum mercury saturations differ as a result of differences in porosity and permeability between the samples. After depressurisation, the end points of the imbibition residual mercury saturation vary as well. Figs. V.9, B, C, F, G and H show curves of laminated samples that have different porosity and permeability. The capillary pressure curves are shaped irregularly, although parts may be characterized as smooth. It is obvious that the irregular shape of the capillary pressure curves reflects a bimodal or multimodal pore-space distribution. Again, maximum mercury saturations and, after depressurisation, end point residual mercury saturations differ as a result of different porosity and permeability.

Pore-size distribution characteristics

In Figs. V.9, A2 to J2 pore-size distributions are presented of the ten samples. The shape of the curve reflects the pore size distribution. The step-wise filling of specific pore diameters demonstrates the presence of different groups of pore sizes in a number of the samples. These specific groups of pore sizes reflect the laminae in the sample. This shows that each lamina has its own specific capillary-pressure behaviour and may be considered as an independent zone with specific capillary-pressure characteristics. In chapter IV, thin-sections are shown of several samples here presented. From these thin-sections it is obvious that adjacent laminae are independent zones with a specific grain size/pore size characteristic, separated by a very sharp interface.

In addition, the permeability contrasts of measurements taken at the sampled section are presented in the pore-size distribution graphs. It is obvious that the maximum pore diameter that was filled with mercury is larger for higher average permeability than for lower average permeability. However, no direct relationship was found between permeability contrast and pore size distribution. The volume percentage ratio of finer-grained laminae to coarser-grained laminae in the sample and the specific pore-size distribution in each lamina determines the percentage of mercury intruding a specific pore diameter.

V.4 NUMERICAL SIMULATIONS

Two-dimensional numerical simulations were performed using a conventional black-oil simulator (MULTIFLOOD) (van Rhijn 1990), a probabilistic simulator (Bakken 1991, Bakken *et al.* 1991 and Batenburg *et al.* 1991). All simulations were based on the numerical simulation of two-phase fluid flow through a foreset laminated system including capillary forces as presented by Kortekaas (1985). The Kortekaas model was expanded to include bottomsets and several variables (permeability contrasts, capillary number (N'_{ce})) were tested for their influence on trapping conditions. Additionally, flooding experiments, described in the next section V.5, were performed to investigate the fluid flow behaviour through a cross-bedded heterogeneity. Figure V.10 shows the three-dimensional representation of cross-beds together with the simplified geological model on which models of numerical simulations and flooding experiments were based. In Table V.I, the basic analogies and differences between simulations and experiments are outlined.

Table V.I, Analogies and differences between numerical simulations and flooding experiments.

	NUMERICAL SIMULATIONS		FLOODING EXPERIMENTS
	MULTIFLOOD (section V.4.2)	STREAMLINES (section V.4.3)	(section V.5)
Solution method:	Implicit in pressure and explicit in saturation and concentration of phases	Probabilistic	
Parameters based on:	Kortekaas (1985)	Kortekaas (1985)	Kortekaas (1985) Dawe *et al.* (1992)
Model:	2-D	2-D	2-D
Gravity:	Gravity included	Gravity excluded	Gravity excluded
Heterogeneity versus flow direction	Laminae 30° inclined to flow direction One-directional flow	Laminae parallel to flow direction One-directional flow	Laminae 30° inclined to flow direction Two-directional flow

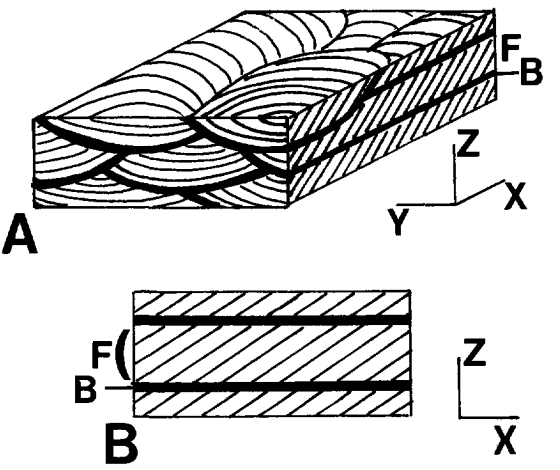

Fig. V.10 A) Three-dimensional representation of a trough cross-bedded reservoir section, with foresets (F) and bottomsets (B). B) Two-dimensional cross-section (X-Z) of trough cross-beds with foresets (F) and bottomsets (B).

V.4.1 Conditions for numerical simulations

V.4.1.1 The Leverett-J function

In 1941 Leverett defined a dimensionless capillary-pressure function dependent on water saturation ($J(S_w)$) as a function of capillary pressure (P_c), interfacial tension (σ), porosity (Φ) and permeability (k) assuming water-wet reservoir conditions as follows:

$$J(S_w) = \frac{P_c(S_w)}{\sigma} \cdot \sqrt{\frac{k}{\Phi}} \qquad (2)$$

Since the Leverett-J function depends on rock properties, it is used in numerical simulations to describe the capillary-pressure characteristics of zones that have different

absolute permeabilities (Fig. V.11).

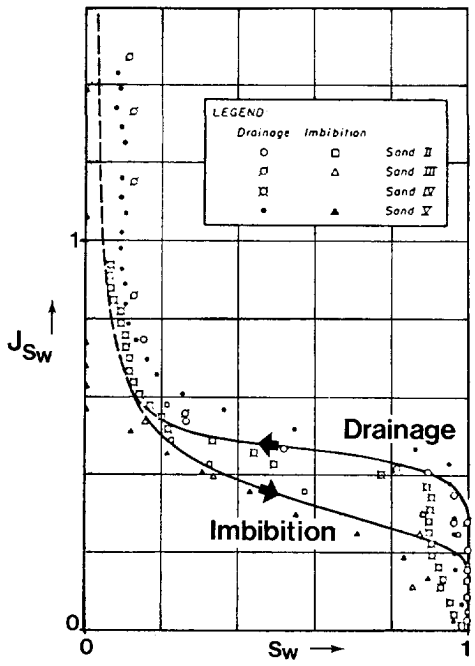

Fig. V.11 Leverett-J drainage and imbibition curves as function of water saturation (S_w) (modified from Leverett 1941).

V.4.1.2 Two-phase fluid-flow relative permeabilities

Simultaneous flow of two immiscible fluids in a porous medium is far more complex than the equivalent one-phase case described by Darcy's law for permeability. The rock's ability to transport each phase is defined as the effective permeability for that phase. According to Dullien (1988) relative permeability is exclusively a function of fluid saturation. The relative permeability curves of oil and water to saturation were calculated in accordance with Corey & Rathjens (1956) in Kortekaas (1985) and Rhijn (1990) or in

accordance with Dullien (1988) in Bakken (1991). In Fig. V.12 an example of oil and water relative permeabilities in correlation with the saturation distribution is presented.

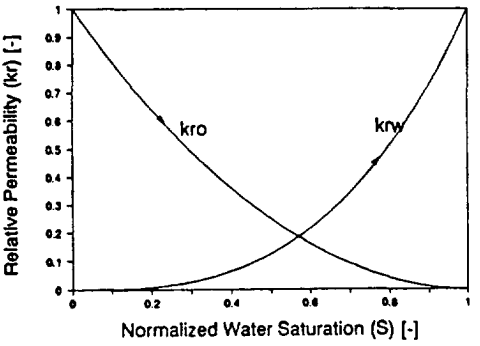

Fig. V.12 Oil-water relative permeabilities (from Bakken 1991).

V.4.1.3 Reduced water saturations

Profiles of reduced water saturation distributions represent the outcomes of the numerical simulations at different pore-volumes (PV) water injected (= different time steps (Td)). The reduced water saturation (S_{wr}) is defined as:

$$S_{wr} = \frac{S_w - S_{wc}}{1 - S_{wc} - S_{or}} \qquad (3)$$

In which S_w is the water saturation, S_{wc} is the connate water saturation and S_{or} is the residual oil saturation.

V.4.2 The MULTIFLOOD Simulator

V.4.2.1 The system

The MULTIFLOOD reservoir simulator[3] was developed for simulating incompressible, isothermal, immiscible two-phase displacement. The solution method is implicit in pressure and explicit in saturation and concentration of the phases (IMPES). The MULTIFLOOD simulator is a conventional black-oil simulator. Further descriptions can be found in the TDC User's Manual for the MULTIFLOOD Simulator.

V.4.2.2 The model

Modelling of fluid-flow behaviour in a cross-bedded system was studied in several steps (a one-dimensional homogeneous model, a one-dimensional laminated model and a two-dimensional laminated model, simulating foreset laminae in the absence of bottomsets (van Rhijn 1990).

The final and most realistic model used to describe fluvial cross-bedding is presented in Fig. V.13. It is a two-dimensional representation of dipping foreset laminae over- and underlain by bottomset layers. The model consists of 48 gridblocks in the horizontal direction and 22 gridblocks in the vertical direction. The dipping foreset laminae and the bottomsets are defined by a width of three gridblocks. Water injection takes place along the entire left side of the model, production of oil and water along the entire right side. The top and bottom sides of the model are defined as no-flow boundaries.

The porosities of the three rock types were assumed to be identical. The absolute permeability of the alternating higher- and lower-permeable foreset laminae were 50 and 250 mD, the absolute permeability of the bottomset was defined as 10 mD.
The simulation was carried out under capillary-gravity equilibrium.

V.4.2.3 Results

Figs. V.14, A and B, shows the contours of the reduced water saturation at increasing time-steps. Water imbibition preferentially occurs through the two bottomsets. Water break-through is likely to occur first in these two layers. The bottomsets initially reach maximum water saturation. This causes a no-flow boundary for the oil remaining in

[3] Developed by TDC, Inc.

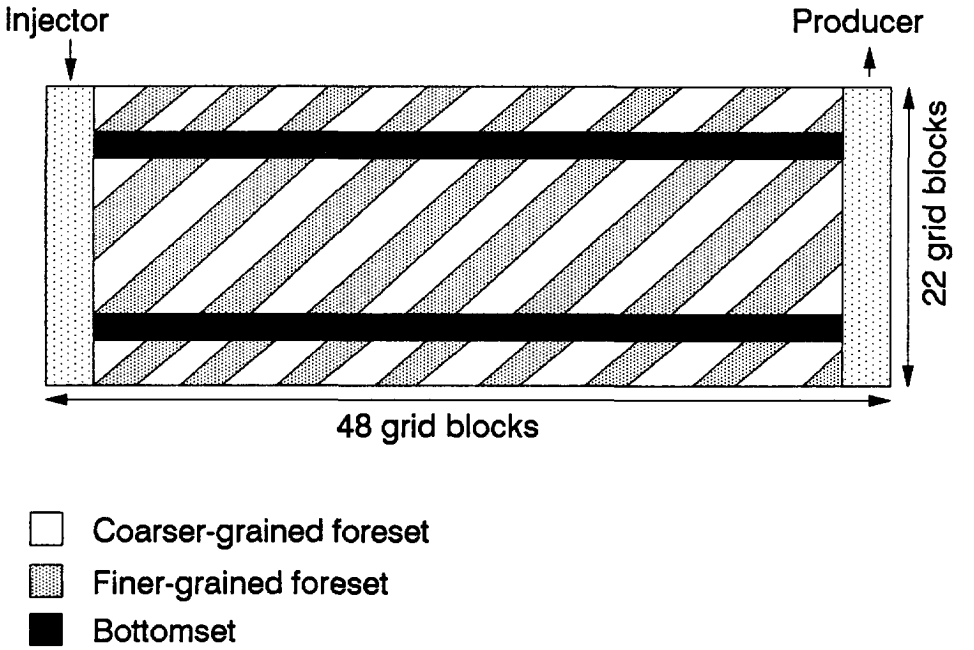

Fig. V.13 *Model for MULTIFLOOD simulation of two-phase fluid flow through a cross-bedded* heterogeneous system (from van Rhijn 1990). Injection/production occured from left to right, top and bottom are no-flow boundaries. The permeability of the bottomset is 10 mD, the finer grained foreset laminae are 50 mD and the coarser grained foreset laminae are 250 mD.

the foreset laminae, located mainly in the higher-permeable foreset laminae.

V.4.2.4 Discussion of MULTIFLOOD results

The results generally agree with the results of Kortekaas (1985). The bottomsets are characterized by the lowest permeability and hence imbibition of the water-oil front is strongest in these layers. The effect of gravity is visible in the difference in distance between the water-oil front in the two bottomsets. A shortcoming of the black-oil

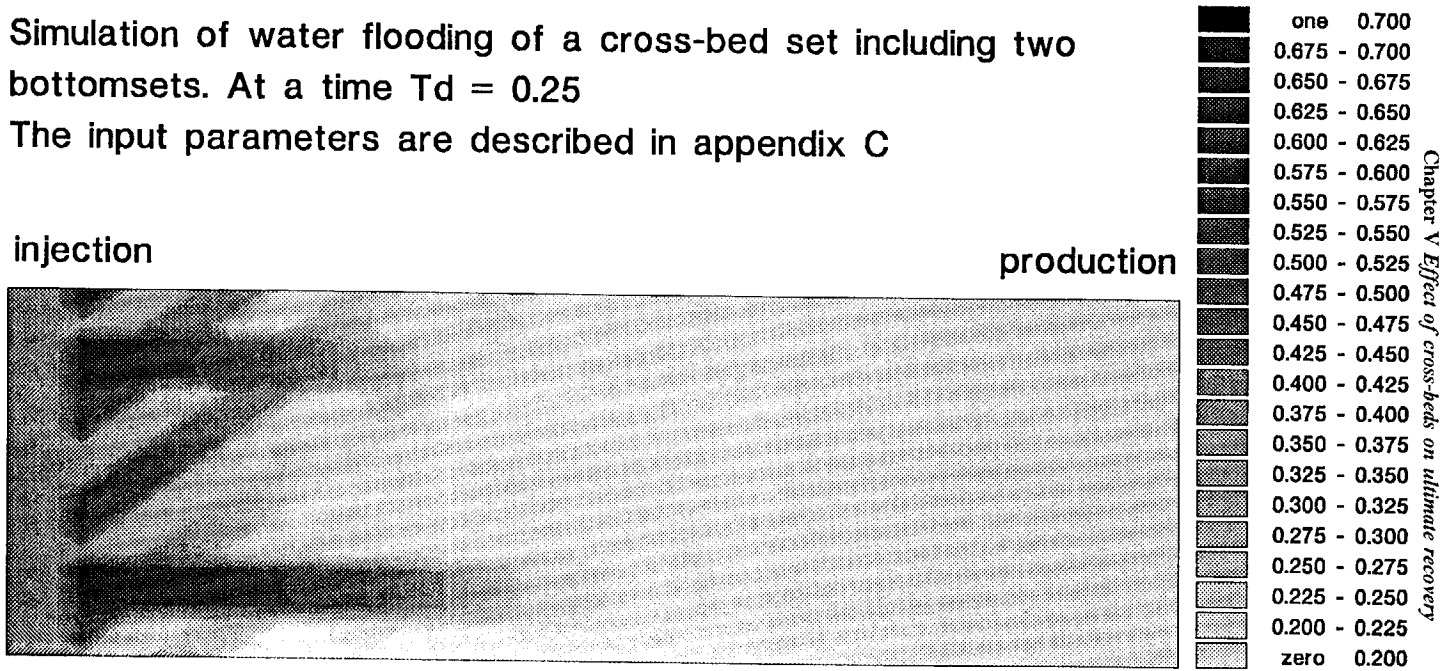

Fig. V.14 A) to be continued

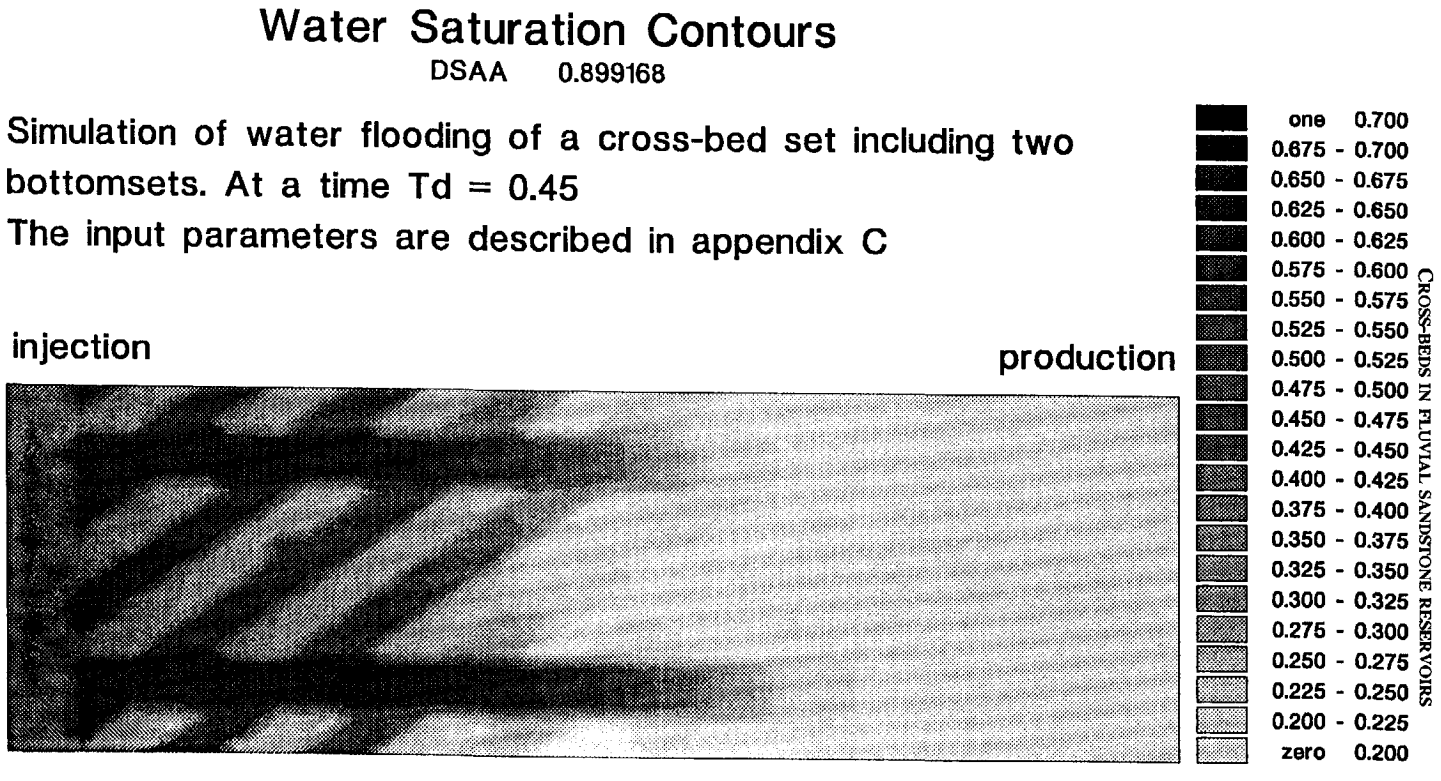

Fig. V.14 A and B) Contours of the reduced water saturation at increasing time steps (from van Rhijn 1990).

simulator is that boundary conditions between the gridblocks are physically poorly defined. It is likely that the front moves fastest in the direction in which few obstacles exist (changes in gridblock definitions). The question arises why the first coarse-grained foreset lamina is not fully saturated with water, whereas the injector is connected to its lower entrance.

A shortcoming of the simulation model is the large size that was necessary to describe the geology in great detail. The time needed to run this model exceeded the economically feasible limits (24 hours)[4]. The final result (Fig. V.14B) shows trapping in the first foreset lamina that has a higher permeability and might not be representative to draw conclusions.

V.4.3 The probabilistic simulator

V.4.3.1 The system

The two-dimensional probabilistic simulator is based on the work of King & Scher (1985) and King (1987) and differs from the traditional simulators because it includes fluctuations that are inherent to fluid flow in porous media. The saturation changes are probabilistically placed into the model. A description and validation of the simulator has been presented by Bakken (1991) and Batenburg *et al.* (1991).

V.4.3.2 The model

Simple one-dimensional homogeneous and heterogeneous models and simple two-dimensional heterogeneous models (Bakken 1991) were used to study the effect of capillary forces on oil recovery. This model was extended to a simplified cross-bed heterogeneous model (Fig. V.15). The sizes of the model were defined by 45 gridblocks in the horizontal and vertical directions (l1 and w1). Each lamina was defined by 15 gridblocks in the horizontal direction and 5 gridblocks in the vertical direction (resp. 12

[4]. at the faculty of Mining and Petroleum Engineering, Delft University of Technology, The Netherlands.

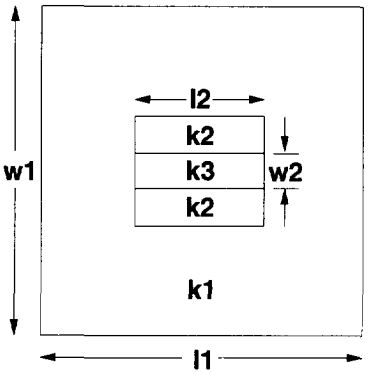

Fig. V.15 Model for probabilistic simulation of two-phase fluid flow through a cross-bedded heterogeneous system (from Bakken 1991). Injection/production occured from left to right, top and bottom are no-flow boundaries. The sizes of the model in gridblocks (gb) are; l1 = 45 gb., l2 = 15 gb., w1 = 45 gb., w2 = 5 gb., k1 = 5 mD., k2 = 25 mD, k3 = 125 mD.

and w2). Porosity was assumed to be constant for the three zones. Permeability contrasts were defined as alternating 25 mD (k2) and 125 mD (k3) in the foreset laminae and 5 mD (k1) in the bottomset. The input parameters for the cross-bed model are defined in Table V.II.

Table V.II, Input parameters for the cross-bed model.

Parameter	Symbols	Value
Flow velocity	v	$4.7*10^{-6}$ m/s
Surface tension	σ	$3.0*10^{-2}$ N/m
Porosity	ϕ	0.3
Viscosity of oil	μo	$10.0*10^{-3}$ Pa.s
Viscosity of water	μw	$0.5*10^{-3}$ Pa.s

Generalized dimensionless numbers were introduced to understand and discuss the physics of the flow process (dimensional analysis is described in Bakken 1991). A

relevant dimensionless number is the capillary number (N'_{cv}), which expresses the macroscopic ratio of viscous to capillary forces for a defined flow situation as follows:

$$N'_{cv} = \frac{\sigma}{\mu_o v} \qquad (4)$$

Where μ_o is the viscosity of the oil phase, v is the velocity and σ is the interfacial tension.

V.4.3.3 Results

Figure V.16 shows that the water-oil front is extremely affected by the permeability heterogeneity. Initially most of the flux (streamline density) flows through the more permeable foreset laminae (Figs. V.16, A and B). As the front reaches the heterogeneity, the flux pattern changes completely. The front moves more or less independently around the heterogeneity. Figure V.16C is an exellent example of the extreme "disturbance" of the streamlines at the front, where capillary forces are strongest. Behind the front, capillary forces decrease and water saturation increases, which is visible in the pattern of the streamlines approaching the initial situation. In the final Figure V.16D, the heterogeneity is not yet bypassed completely. However, the computer run was terminated at this point, when 0.79 pore volumes of water had been injected. The lamina (k3) that has the highest permeability shows a lower water-saturation at the lower boundary with respect to its surroundings as a result of the permeability contrast in all directions.

V.4.3.4 Discussion of results of the probabilistic simulator

The results obtained by probabilistic simulations show that capillary forces affect oil-water displacement in these heterogeneity models. This depends largely on the permeability contrast but is independent of capillary number (Bakken 1991). The simulations make use of the reduced water saturation, which implies that all oil left is definitely macroscopic remaining oil as defined by Lake (1989). Chatzis *et al.* (1984) and Garnes *et al.* (1990) assumed that microscopic residual oil can be mobilized by decreasing the capillary number. This may imply that the residual oil saturation could simply be the

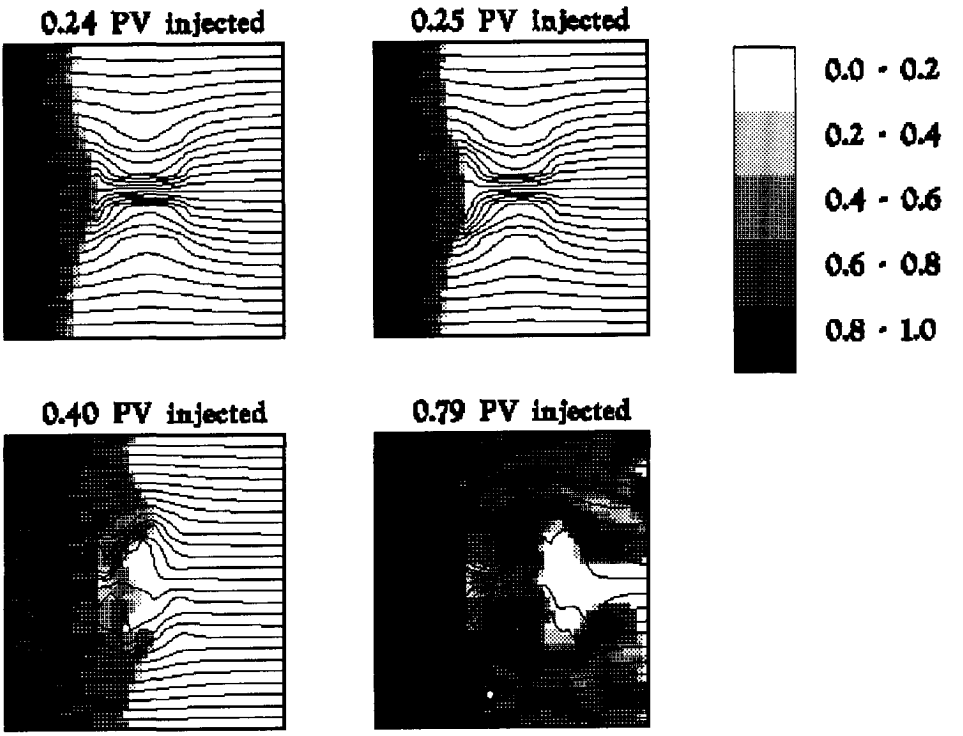

Fig. V.16 Contours of the reduced water saturation and flow line representation of direction of flow at four different time intervals during the imbibition process (from Bakken 1991).

remaining oil saturation on a scale smaller than the scale under consideration (Bakken 1991).

An increase in permeability contrast affects oil-water displacement in two ways. The difference in front velocity between the regions increases and the saturation jump over the heterogeneity increases. Both effects decrease the recovery of oil at breakthrough (Bakken 1991).

A limitation of the model is the very simple representation of the laminated

heterogeneity, where laminae are parallel to the direction of fluid flow. An advantage of the simplicity of the model is that the physical behaviour of the fluid flow could be observed in great detail.

V.5 FLOODING EXPERIMENTS

Dawe *et al.* (1992) described an experimental set-up for studying capillary effects on immiscible displacement in lensed and layered heterogeneous models. They report on extensive experimental studies of drainage and imbibition displacements, with and without initial residual fluid saturation, at a variety of flow rates. Two-dimensional glass-bead models were used, matching the size of a typical large core test (85 * 10 * 0.6 cm).

In immiscible multi-phase flow, saturation effects are reflected in relative permeability and capillary pressure. Capillary-pressure effects occur at saturation discontinuities, where capillary forces (interfacial curvatures) can change over a few grain diameters giving rise to large pressure gradients. In homogeneous media, such discontinuities may occur at displacement fronts and at the ends of the porous media (end effects). In heterogeneous media, capillary-pressure effects may arise also at boundaries between media that have different properties, such as permeability, pore-size, porosity or wettability changes (Dawe *et al.* 1992).

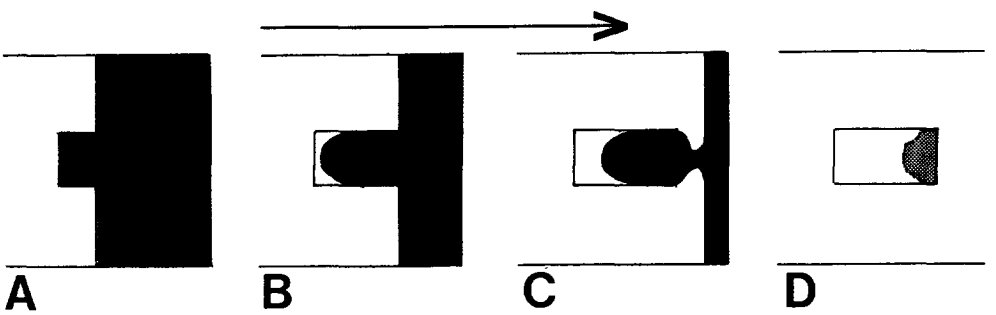

Fig. V.17 Water/oil flooding experiment with lens of higher-permeability than that of surrounding media at different time steps (A to D) during the flooding experiment. Experiment was done with an initial residual water saturation (modified from Dawe *et al.* 1992).

The results of the water-flooding experiments through a lensed system with a

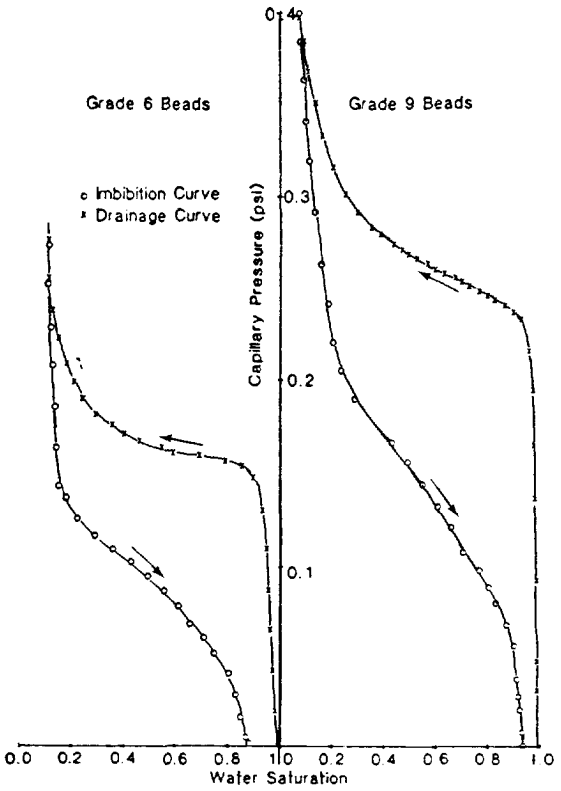

Fig. V.18 Water/oil capillary-pressure curves for higher and lower-permeable zones in the "Dawe" experiment (modified from Dawe *et al.* 1992).

higher-permeability zone (360 D) surrounded by a lower-permeability zone (144 D) carried out by Dawe *et al.* (1992) are discussed here. Figure V.17 shows schematically their results from water-flooding experiments, with a water saturation initially irreducible. Figure V.18 shows the experimentally determined capillary-pressure curves for the two permeability zones. In the experiment, the water initially bypassed the lens, however, the flood water began to enter the lens before the displacement front reached the end of the

model. A large portion of oil was left in the lens after the displacement of the front had passed; this was then gradually displaced from the lens. Dawe *et al.* (1992) conclude that the more rapidly advancing water/oil front in the lower-permeability zones is caused by stronger imbibition forces. Increasing water-flood rates (viscous forces) will reduce the effects of capillary forces. The general conclusion is that direct scaling of immiscible displacements from physical models or cores to reservoirs may not be valid because capillary forces depend on flow rate, especially in heterogeneous media. Therefore, care should be taken with the data assumed to represent the fluid transmissibilities from block to block in a reservoir simulator.

In the Dietz laboratory of the Delft University of Technology (Ledeboer 1992), a two-dimensional experimental set up was designed to study the effects of laminated heterogeneous porous media on immiscible displacement. In Table V.I, a comparison is made between the numerical simulations, described in the previous sections, and the flooding experiments. In the next sections, the model and results of the two-phase fluid-flow experiments through the cross-bedded heterogeneous model will be discussed.

V.5.1 Cross-bed model experiments

V.5.1.1 The model

The model is made of transparent perspex and is 50 cm long, 16 cm wide and 2 mm thick. Glass beads are inserted between the perspex panes in distinct layers. Several layers of different bead sizes can be inserted such that many different heterogeneity shapes can be investigated. When the packing is completed, the model is covered by a plastic foil which is sealed on the top of the beads by vacuum. Finally, the model is connected via a system of valves and plastic tubes to a pump and fluid storage tanks (Ledeboer 1992).

Three different sieve fractions of glass beads (95 μm, 250 μm and 460 μm) were used to build a cross-bed model as presented in Fig. V.19 (Ledeboer 1992). Again, this model was based on the geological cross-bed model as presented in Fig. V.10.

Table V.III, average size of glass beads and calculated Kozeny-Carman and van Baaren permeability at constant porosity (37%).

Zones in model	Average size glass beads (μm)	Permeability in Darcy Kozeny-Carman	van Baaren
k1	95	8.00	1.56
k2	205	37.25	7.25
k3	460	187.53	36.51
Permeability Contrasts:		k2/k1: 4.66	
		k3/k2: 5.04	
		k3/k1: 23.44	

Permeabilities were calculated in accordance with the Kozeny (1927) - Carman (1937) equation, being:

$$k = \frac{1}{72\theta} \frac{\phi^3 D^2}{(1-\phi)^2} \qquad (5)$$

in which the permeability (k) is determined from the porosity (ϕ) and the average grain size (D). The porosity for all bead sizes was assumed to be constant (37%). The calculated permeabilities are 187 D for the coarsest-grained zones (k3), 37 D for the medium-grained zones (k2) and 8 D for the finest-grained zone (k1). The permeability contrast is nearly a factor 5 (k1 and k2, k2 and k3) and a factor 25 (k1 and k3). Table V.III shows average grain sizes of glass beads, permeability according to Kozeny-Carman and van Baaren (1979, Appendix C: eq. 1), and the permeability contrasts.

Experiments were based on displacement of oil by water under irreducible water-saturation conditions (conditions for model is listed in Table V.IV) . The viscosity of the oil (n-Decane, $\mu = 0.92.10^{-3}$ Ns/m^2 at 20°C) is very close to that of water ($\mu = 1.0\ 10^{-3}$ Ns/m^2 at 20°C). This results in a small Mobility ratio (less than 1) and hence, a stable oil displacement at the water front (Dake 1978). The equation for the mobility ratio, in which μ_o is the viscosity of oil, μ_w is the viscosity of water, k_{ro} is the end-point relative

Table V.IV, Parameters, symbols and units of prototype (North Sea reservoir) values scaled to model values.

Parameter and symbol	Prototype	Model	Unit
Interfacial tension (σ)	$30 * 10^{-3}$	$30 * 10^{-3}$	N/m
Viscosity oil (μ_o)	$0.92 * 10^{-3}$	$0.92 * 10^{-3}$	Ns/m^2
Viscosity water (μ_w)	$1 * 10^{-3}$	$1 * 10^{-3}$	Ns/m^2
Flow velocity (u)	$4.6 * 10^{-6}$	$2.6 * 10^{-4}$	m/s
Time (t)	4.7 days	1 hour	
Porosity (ϕ)	37	37	%
Pore-volume model		59.2	ml

permeability of oil and k_{rw} is the end point relative permeability of water, is:

$$M = \frac{k_{rw}\,\mu_o}{k_{ro}\,\mu_w} \qquad (6)$$

A flow velocity of $4.6\ 10^{-6}$ m/s was chosen as being representative of a reservoir, resulting in an average flow velocity of $2.6\ 10^{-4}$ m/s in the model. The experiments were performed during 24 hours. A model experiment lasting 1 day represents 112,8 days in a reservoir (Table V.IV, time equivalent). As total field life can easily be as long as 20 years, the phenomena seen in the experiment will occur in a reservoir, provided conditions are similar.

Non-gravity conditions were imitated by placing the model horizontally. The model was initially filled with water under vacuum and then oil-flooded to residual water saturation, assuming water-wet reservoir conditions. During the experiment, oil was displaced by water horizontally from left to right, parallel to the length of the model (Fig. V.19). Water was injected along the entire left side of the model to obtain a straight flood front. Blue powder was added to the oil in order to obtain sufficient color difference between oil and water. Displacement experiments were recorded photographically. Figures V.20, A to F, are based on pictures taken from the experiment at several phases of the flooding process as presented by Ledeboer (1992).

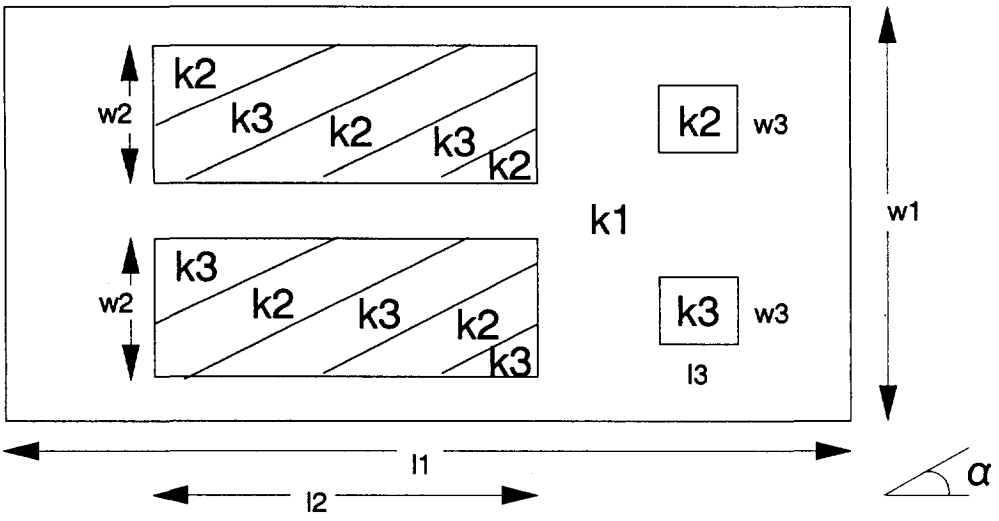

Fig. V.19 Model for experimental set up of cross-bedded heterogeneities, representative glass beads sizes and permeabilities are; zone K1: 95 μm and 8 D, zone k2: 250 μm and 37 D and zone k3: 450 μm and 187 D. Total length of the model (l1) is 50 cm, the width of the model (w1) is 16 cm. The length of the cross-bed heterogeneity (l2) is 12 cm and the width (w2) is 4 cm. The length (l3) and width (w3) of the squared heterogeneities is 2cm. The angle of cross-bedding (α) is 30°. Injection of water occurred along the entire left side of the model, oil and water were produced along the entire right side of the model (from Ledeboer 1992).

V.5.1.2 Results

The water front enters over the complete width of the model and is quite stable, nicely sweeping the region of low permeability (k1) (Fig. V.20A). The water front is disrupted as soon as it encounters the two cross-bed heterogeneities and the water tries to flow around the heterogeneities. Figure V.20B shows that water actually flows around the cross-bedded lenses by creating three separate fronts in the low-permeability region. It is also visible that first imbibition of water takes place in the intermeadiate permeability zones (cross-bed laminae: k2). Water first stops at the boundary between k1 and k2 but subsequently enters the heterogeneity, flowing in between the neighbouring high-

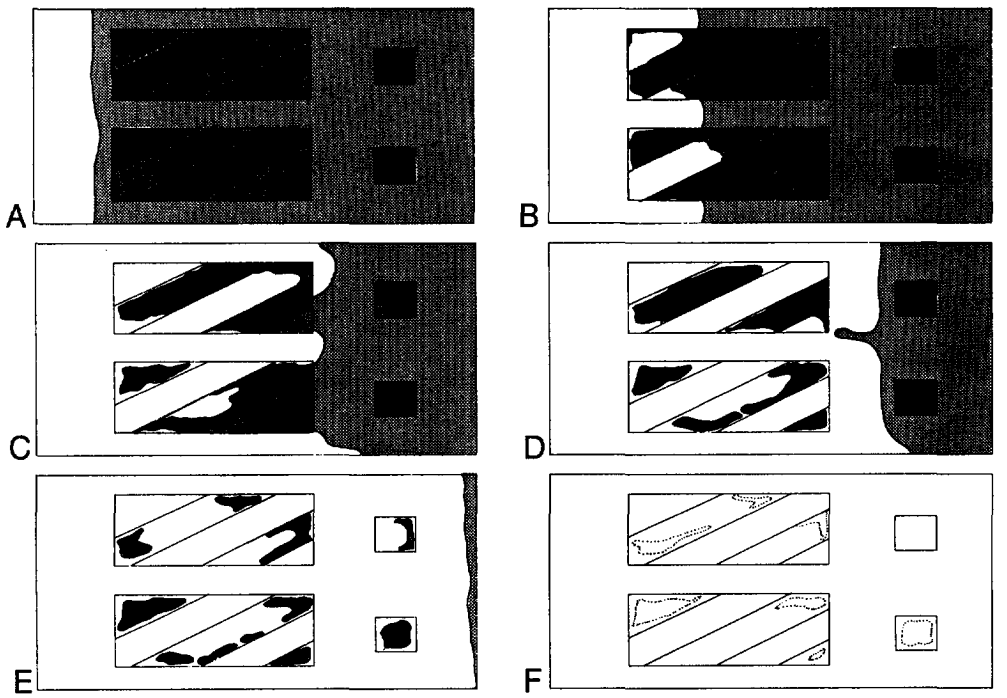

Fig. V.20 A to F) Results of flooding experiment of cross-bed model (from Ledeboer 1992) at different phases in the flooding process. A) oil/water front is approaching the cross-bed heterogeneities. B) oil/water front is surrounding the cross-bed heterogeneities, inmibition occurs in the k2 regions. C) oil/water front has almost passed the cross-bed heterogeneities, k2 regions are flooded, imbibition starts in the k3 regions. D) oil/water front has passed the cross-bed heterogeneities and is recombined, moving as one front towards the squared heterogeneities, k3 regions filled with movable oil lost contact with the main oil bank and oil is initially trapped. E) One movable pore volume of water has flooded the model, K3 regions are continuously produced, The squared heterogeneities show a same trapping mechanism as is visible in the cross-bed heterogeneity. F) Final result after 7 pore volumes of water has flooded the model, all regions are flooded leaving no extra oil in the model above residual saturations.

permeability regions (cross-bed laminae: k3). The oil is easily pushed out of the k2 regions and consequently the regions are swept properly.

The water has a lot more difficulty entering the high-permeability regions (k3).

The water easily flows around the heterogeneity (Fig. V.20C). Once the main water front passed the two cross-bed heterogeneities (Fig. V.20D), oil that is still present in the k3 regions has almost certainly lost contact with the main oil bank.

The recombined water front advances to the right and encounters the two small square heterogeneities of intermediate (k2) and high (k3) permeability. Although water could flow around these regions, it enters and sweeps the region of intermediate permeability (Fig. V.20E). The water has much more difficulty in entering the high-permeability block and leaves quite some oil behind. Water breakthrough at the right side of the model (producer) occurs after 1 hour and 13 minutes after injecting 0.77 pore volumes of water.

At this moment unswept oil is still present in the high-permeability regions. This oil can be considered as by-passed and is not continuous across the model. Oil is continuously produced and consequently, oil saturation in the high-permeability regions is still lowered after pumping an extra 4.3 pore volumes of water through the model. Finally, the pumping rate is increased from 1 to 3.46 ml/min until a total of 7.15 pore volumes has been injected. Fig. V.20F shows the ultimate results. Oil is still being produced and intensity of the colour of the high-permeability regions has decreased. Ledeboer (1992) determined the final oil saturation in the high-permeability regions and concluded that it has finally become almost residual (S_{or}).

V.5.1.3 General remarks on the process of entrapment

1) Injection of 5 to 7 extra pore volumes of water will produce the oil from the high-permeability regions which was initially left behind. This oil was removed as individual blobs. The removal of blobs of oil takes a lot more time and effort compared with the sweeping of the lower-permeability regions (1 hour and 13 minutes versus 24 hours or more).

2) The injection rate clearly effected the sweeping process. The lower the injection rate, the slower the by-passed oil was produced.

3) After the model had been swept by 7 pore volumes of water, the different regions still showed a colour difference, which resulted of differences in residual-oil saturations (S_{or}) determined by the capillary force characteristics of each region in the model.

4) If the scaling is applied correctly, all water-flooding experiments have taken place at a higher capillary number than assumed for field conditions (N_{cv} = 1.3). This means that the experiments are dominated more by the capillary force than under natural conditions. The effect of oil trapping will therefore in reality be less strong.

V.5.1.4 Discussion of flooding experiments

The permeability contrast between bottomset layers (k1), foreset fine-grained laminae (k2) and coarse-grained laminae (k3) is large. Chapter 4, Table IV.II showed that the maximum average permeability contrast in reservoir rock observed during research for this thesis was 27.9 : 9.6 : 1 (CFL:FFL:BL). However, most of the average contrasts are much smaller and are approximately 4 : 2 : 1. This does not imply that a contrast of 25 : 5 : 1 (model) is unusual in cross-beds. It stresses the need to sample the permeability contrasts in cross-beds of a specific reservoir, before any conclusion is made with respect to capillary entrapment. The lower the permeability contrasts, the less probable it is that entrapment occurs.

The calculated permeability contrasts as presented in Table V.II are overestimated. In Appendix C it is concluded that the calculated permeability at constant porosity generates a much larger contrast than measured liquid permeabilities of different artificial sandstone samples. It is likely that the calculated contrasts are a factor 2 or 3 higher than in reality. The observed flow performance might have taken place under a much lower contrast in real liquid permeabilities (e.g. varying between 12.5 : 2.5 : 1 and 8.3 : 1.6 : 1).

Ledeboer (1992) outlined conditions for water flooding, according to the conditions in the model, for a cross-bedded section somewhere in a reservoir. He concluded that depending on the position of the cross-beds in the reservoir, 5 to 7 model pore volumes of water could easily sweep the section. The specific cross-bedded section thus will be swept to residual oil saturation leaving no extra oil trapped as a result of capillary forces.

V.6 DISCUSSION

The laboratory experiments and computer simulations of fluid flow through a laminated heterogeneous system shows clearly that initial trapping of movable oil occurs under the controlled conditions. In reality, conditions are not always as constant. The following variables generally determine the trapping conditions in cross-bedded reservoirs:

V.6.1 Permeability contrast

The simulations and experiments are based on a contrast of a factor five between bottomset, fine-grained foreset and coarse-grained foreset laminae. This contrast was varied to study the effect on capillary pressure and fluid flow behaviour. A larger contrast results in a stronger bypassing effect of the coarser-grained foreset laminae and hence leads to a higher percentage of initially trapped movable oil. A lower contrast leads to a weaker bypassing effect. Chapter IV, Table IV.II shows that average permeability contrasts between bottomsets (BL), finer-grained foreset values (FFL), and coarser-grained foreset values (CFL) vary between 1.7 : 1.1 : 1 (CFL:FFL:BL) and 27.9 : 9.6 : 1 (CFL:FFL:BL). Contrasts between finer-grained foreset laminae and coarser-grained foreset laminae vary between 1.3 : 1 (CFL:FFL) and 5.4 : 1 (CFL:FFL). In reality, the absolute contrast measured from one lamina to another and from the foreset laminae to the bottomset varies from place to place, owing to natural variations in grain size, sorting, composition and diagenesis. Initial bypassing of oil in the coarser-grained foreset laminae therefore depends on the specific permeability contrasts of surrounding foreset laminae and bottomset.

V.6.2 Wettability

Fluvial sandstone reservoirs are considered to be preferentially water-wet. However, on a sedimentary-structure scale the fractional wettability may vary between the

adjacent foreset laminae and between the foreset and bottomset as a result of variations in framework composition (Chapter IIIB). Diagenetical alterations and cementation create differences in percentages cement and/or secondary porosity (Chapter IV). In the CFL, large blocky crystals may have filled the pore spaces (Chapter IV, anhydrite). However, the effect of variations in composition on wettability have not been investigated. Small variations in fractional wettability between the zones will affect the capillary-pressure characteristics and mobility of the two-phases.

V.6.3 Capillary-pressure characteristics

The Leverett-J functions describe the capillary-pressure curves of zones between which a certain permeability contrast exists (porosity is assumed constant). They are defined as depending solely on the lithology of the rock. Capillary pressure is determined by events taking place on a pore scale, in which the factors porosity and permeability are more important than pore-size distribution. On a sedimentary-structure scale, the pore-size distribution is an important factor determining the characteristic shape of the capillary-pressure curve.

As visible in Figs. V.9, A to J rock imbibition capillary-pressure curves show endpoint residual oil saturation, that increase with increasing porosity. The imbibition curves cross-over at a certain pressure and initial water saturations decrease as the porosity of the sample increases as is best visualized in Fig. V.7A. The Leverett-J functions used in the simulations, have a same initial- and residual oil saturation for all heterogeneity zones. This is in disagreement with the real-rock capillary-pressure curves in which the irreducible-water saturations and residual-oil saturations differ between samples of different porosity. The endpoint behaviour (a same residual-oil saturation) and the shape of the curves determine the final result of a simulation. The basic concepts described in section V.3 and shown in Figs. V.7, A to C, control the bypassing of oil and the amount of trapped movable oil on sedimentary-structure scale in actual reservoir rocks. It is obvious that movable oil is not actually trapped and that entrapment is primarily determined by the shape of the curves (pore-size distribution) for the different

zones, in addition to permeability contrast.

V.6.4 Rate of waterflood

The rate of the water flood influences the effect of capillary forces. From eq 4 (capillary number) it is clear that higher flooding rates decrease the capillary number and hence capillary forces have less influence on the flooding process.

V.6.5 Mobility ratio

The viscosity of the oil is another important factor on water/oil displacement and is best represented by the mobility ratio (eq 6). If the mobility ratio increases (meaning a decreasing oil mobility), the probability of oil entrapment through by-passing increases.

V.6.6 Gravity

Gravity/Buoyancy as a result of the difference in specific gravity of oil and water, determine the vertical distribution of the two phases in a reservoir. The specific gravity of oil is commonly lower than that of the formation water. The nett result is that oil is commonly forced to move upward. In cross-beds, this means that the initially trapped volumes of oil in the CFL are located in the top of cross-beds. Hence, the geometry of a cross-bed specifies the volumetric conditions for initial entrapment of movable oil (outlined in Chapter VI).

The bouyancy force may increase the generation of oil blobs and hence decrease the probability of long-lasting entrapment of movable oil. Gravity will affect the distribution and shape of the flood front. The effect of gravity on the whole process of entrapment has not been investigated.

V.7 CONCLUSIONS

1) On a sedimentary-structure scale, ultimate oil-recovery from a porous system is mainly determined by capillary pressure.

2) Contrasting capillary-pressure characteristics determine the differences in initial oil saturation and residual oil saturation between zones of contrasting permeability.

3) If a low-permeability zone almost reaches maximum water saturation, under the assumption of capillary-pressure equilibrium, the higher-permeability zones will still contain large quantities of movable oil. Volumes of movable oil are literally cut-off and trapped in higher-permeability zones, if these are enclosed by lower-permeability zones. However, the oil does not remain permanently trapped and can still be produced by continual flooding. This process takes much more time and many more pore volumes of water than achieving initial breakthrough. Eventually zero-pressure residual-oil saturation may be reached in all zones.

4) The amount of movable oil that initially will be trapped depends on the difference in shape and height between the capillary-pressure curves. The distance between the curves is determined by the permeability contrasts between zones of contrasting permeability and the shape of the curves is determined by the pore-size distribution (sorting of pore sizes).

5) Experiments and different computer simulations show that the geometry, size and shape, of the high-permeability zones have no effect on the sweeping efficiency, if gravity effects are ignored. At very slow flooding speed, capillary forces dominate the flow behaviour and as these forces act on pore scale, geometry of the heterogeneity on a larger scale is not important. If gravity effects are included, the geometry influences the shape and distribution of the flood front around the heterogeneity.

6) In a reservoir, the mechanism resulting in initial oil entrapment might lead to permanent entrapment under certain conditions. These conditions are:

A) rock property determined conditions as the specific permeability contrasts, capillary-pressure characteristics and wettability of surrounding foreset laminae and overlying bottomsets. These conditions are governed by natural variations in grain size, sorting, composition and diagenesis.

B) physical conditions as the rate of water flooding, the mobility ratio, and gravity.

C) time related conditions as the economic life of a reservoir.

CHAPTER VI
CAPILLARY OIL ENTRAPMENT IN CROSS-BEDS OF FLUVIAL SANDSTONE RESERVOIRS

VI.1 FOREWORD

The contents of this chapter are presented with permission of the Society of Petroleum Engineers and were earlier published by Hartkamp (1991) In: *Proceedings of the Soc. of Petrol. Engineers Annual Technical Conference and Exhibitions, Dallas, U.S.A.* **SPE 22761**, October 6-9, 959-968. A few modifications have been made in accordance with later findings.

This chapter aims at combining results from all previous chapters in order to estimate the likely percentages of movable oil initially trapped in cross-beds of fluvial sandstone reservoirs under assumed conditions. The validation of the minipermeameter measurements is outlined in Appendix A. Statistical analysis of permeability data is presented in Appendix B.

VI.2 INTRODUCTION

Many oilfields produce from fluvial reservoir sands. These include major accumulations of more than 10 billion barrels such as fields in Venezuela, Colombia, Nigeria, Alaska and the North Sea. The variability of fluvial sand-body architecture and reservoir quality is large and as a consequence, reservoir performance is difficult to predict accurately even if the recovery mechanism such as water drive is well known. Water drive is an important recovery mechanism for hydrocarbon reservoirs and is applied as a secondary recovery technique (waterflooding) (Thomas *et al.* 1987). Oil recovery percentages up to 25-35% have been reported in water flooded fluvial reservoirs (Barwis

et al. 1990). This means that at least 65% of the original oil in place is still left in the reservoir upon abandonment. Reservoir heterogeneity is one of the major reasons for disappointing enhanced oil recovery results (Weber 1986). Intra reservoir heterogeneities include genetic unit boundaries, permeability zonations, permeability baffles, cross-bed laminations and microscopical textural or mineralogical features.

The effect of small-scale heterogeneities on overall reservoir performance can be incorporated by averaging properties (Kasap and Lake 1990[1], Kasap and Lake 1990[2], Hewett and Behrens 1990). An important type of small-scale heterogeneity is trough cross-bedding. Trough cross-bedding is one of the most common sedimentary structures in fluvial deposits and is uniquely heterogeneous in grain size and sorting on a small-scale. In Weber (1986), methods to derive average permeabilities for a cross-bedded heterogeneous system are presented that are valid for single phase flow. However, the use of average properties for two-phase fluid flow modelling procedures is questionable. If, on a small-scale contrasting permeability regions are present, capillary forces have a marked influence on small-scale displacement of oil (Kortekaas 1985, Lasseter *et al.* 1986). This means that it is essential to characterize these small-scale permeability variations and to measure foreset and bottomset separately as suggested by Weber (1982 and 1986) and Weber & Geuns (1990). They further suggested to investigate the 3D configuration of cross-bed sets. From the results of such detailed measurements one can infer whether the measured contrast would lead to a significant anisotropy controlling two-phase fluid flow. This is best evaluated through small-scale fluid-flow simulation studies, which help to increase the understanding of the recovery process in a reservoir and may ultimately lead to improved enhanced oil recovery methods based on lowering the interfacial tension (Garnes *et al.* 1990), e.g. the possible use of surfactants (Keijzer & de Vries 1990).

This study focuses on the quantification of sedimentological and physical properties of trough cross-bedded sets of fluvial origin. The acquired data consists of minipermeameter permeabilities of cross-bedded fluvial deposits from two regions. Namely, the well-exposed Tertiary Loranca Basin of Central Spain (Chapter III) and the Permian Slochteren Formation and the Triassic Buntsandstein Formation in the offshore and onshore subsurface of the Netherlands (Chapter IV). Additional research focuses on

grain size, sorting, porosity (Chapters III and IV), pore-size distribution and capillary pressure (Chapter V). Results are used in probabilistic computer simulations to study the effect of capillary forces on water-oil displacement in cross-bed set models (Chapter V). Finally, likely percentages of movable oil that are initially trapped in a cross-bedded reservoir are estimated.

VI.3 GEOLOGICAL DESCRIPTION OF OUTCROP AND SUBSURFACE FLUVIAL FORMATIONS

VI.3.1 Outcrop: Fluvial Fans, Central Spain

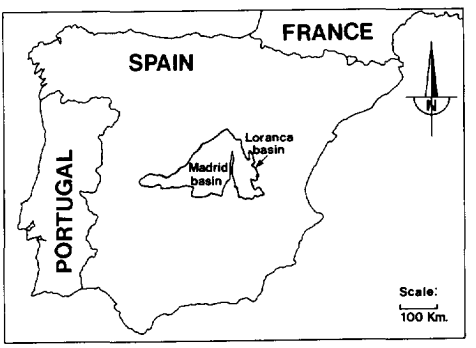

Fig. VI.1 Tertiary cratonic basins of central Spain.

The outcrop area is situated in the Loranca Basin of Central Spain (Fig. VI.1). The Loranca basin is part of a number of intracratonic depressions formed during a compressive period which lasted from the Late Cretaceous to the Middle Miocene. From the Late Oligocene to Early Miocene, the Loranca Basin was filled with two coalescing

fluvial systems (Fig. VI.2) (Díaz Molina *et al.* 1989). The fluvial fans were wet-fluvial fan systems (Schumm 1977) in a usually dry, subtropical climate alternating with humid periods (Daams & van der Meulen 1984, Álvarez Sierra *et al.* 1987).

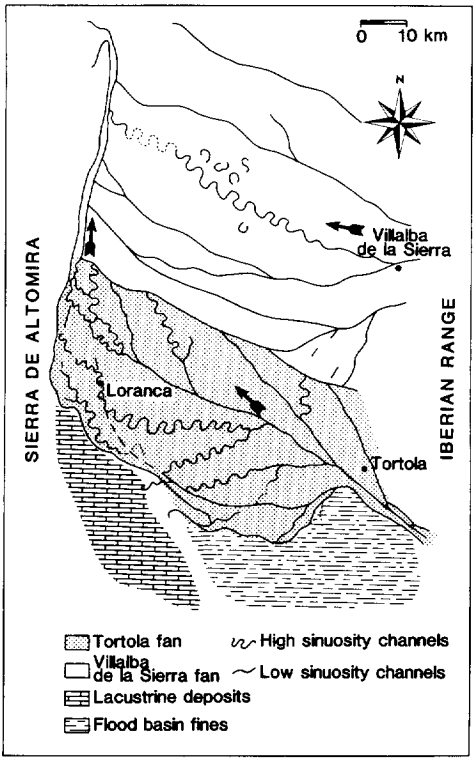

Fig. VI.2 Palaeogeographic reconstruction of the fluvial fan systems of the Loranca Basin. Arrows indicate general flow direction of the channels (modified from Diaz Molina *et al.* 1989).

The provenance area of the fluvial sediments was situated in the east, in the Mesozoic clastic- and carbonate rocks of the Iberian Mountain Range. The deposits are characterized by individual meandering- and straight channel sands embedded in floodplain fines (Fig. VI.3) and associated with thin-bedded lake evaporites and root-letted palaeosols (Díaz Molina *et al.* 1989).

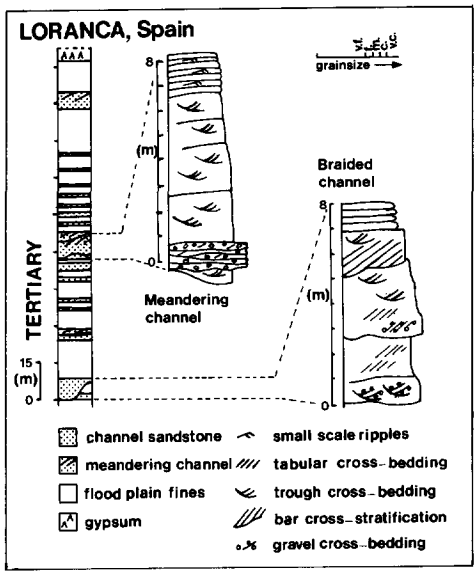

Fig. VI.3 Schematic sedimentary log through the Loranca Basin; detailed schematic sedimentary logs of a meandering- and a braided channel (modified from Diaz Molina *et al.* 1989).

The channel sandbodies consist of fine-coarse sized quartz-arenites and are of a very friable nature due to the partly dissolved calcite cement. Total porosity of the sandstone is 30-35%, of which some 7%-8% is secondary porosity. Low- and high sinuosity channel sandbodies consist for 70-80% of trough cross-bedded sedimentary structures. The upper 20% of the sandbodies comprise small-rippled, horizontally laminated or homogeneous fine sand and silt.

VI.3.2 Subsurface: The Slochteren Sandstone Member, The Netherlands

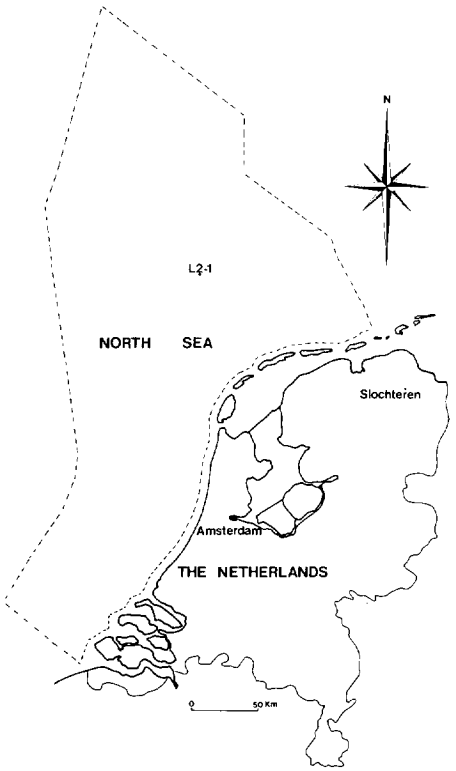

Fig. VI.4 The onschore and offshore area of the Netherlands with locations of schematic log sections.

In the subsurface of the Netherlands (Fig. VI.4), the Permian Upper Rotliegendes Group (NAM & RGD 1980) can be subdivided into: The Lower- and Upper Slochteren Sandstone Members and the Ameland- and Ten Boer Claystone Members (Fig. VI.5A). The two Slochteren Sandstone Members are the most important gas-productive units of the Dutch subsurface. The depositional environment of the Upper Slochteren Sandstone

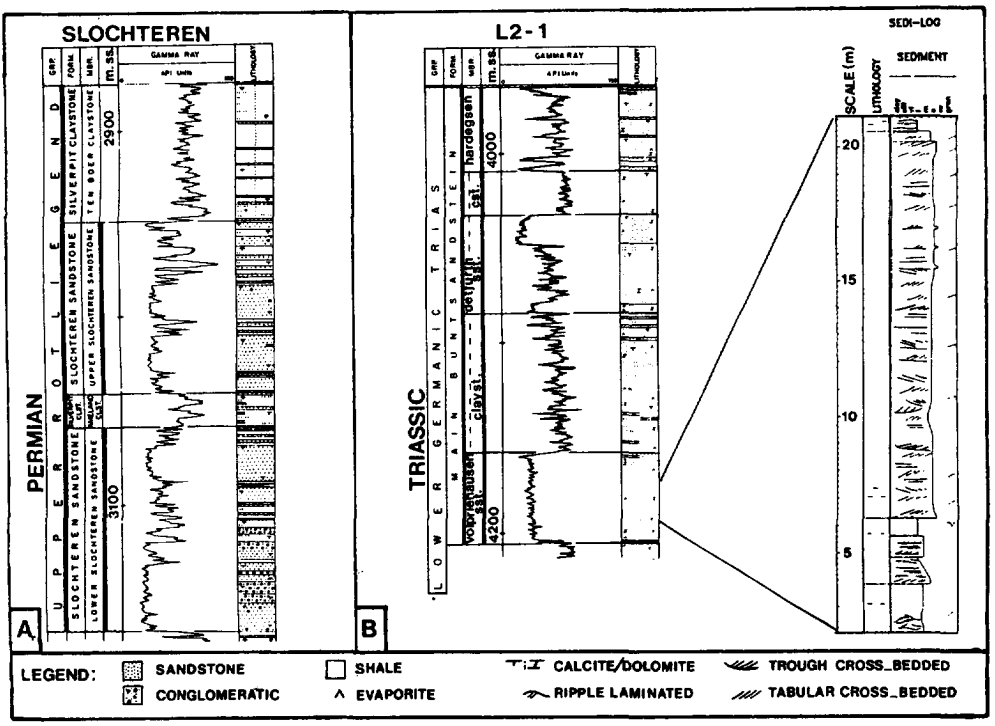

Fig. VI.5 A) Schematic sedimentary log of the Permian Upper Rotliegendes Group of the Dutch subsurface. B) Schematic sedimentary log of the Triassic Main Buntsandstein Formation of the Dutch subsurface with a detailed sedimentary log of a part of the Volpriehausen sandstone member (modified from NAM/RGD Nomenclature 1980).

Member and Ten Boer Claystone Member corresponds to a fluvial fan system in a desert environment (wadi-sebkha environment) (Wijhe *et al.* 1980). The deposits are coarse-grained high- to low energy proximal wadi deposits, fine-grained distal wadi deposits, desert lake sand and mud and aeolian reworked sand. The sandstone deposits comprise large scale ripple laminations (planar- and cross-bedding), small ripple laminations and wavy-, low-angle or horizontal laminations. The sandstone consists of fine- to medium quartz arenites and sublitharenites. Primary porosity has been reduced by compaction and diagenetic grain coating clays, which also reduces permeability. The porosity of the sandstones ranges from 10% to 25%.

VI.3.3 Subsurface: The Vollpriehausen Sandstone Member, The Netherlands

The Volpriehausen Sandstone Member (Fig. VI.5B) is part of the Triassic Main Buntsandstein Formation. Three sandstone to mudstone members (fining-upward cycli) represent braided-fluvial and braidplain facies, interbedded by desert lake facies. The Volpriehausen Sandstone Member is the lower, well defined sandstone unit, and represents the first phase of braided river deposition and remains the most attractive gas-reservoir target of the Triassic deposits. The sandstone deposits comprise large-scale trough cross-bedding, ripple laminations and horizontal laminations. The upper part of the Volpriehausen sandstone has partly been reworked by aeolian influences.

The Volpriehausen sandstone Member consists of fine-medium grained subarkoses. Primary porosity has been reduced by compaction and early carbonate cement. Authigenetic fibrous illite and anhydrite are locally present and reduce permeability. Porosity ranges from 10% to 30%.

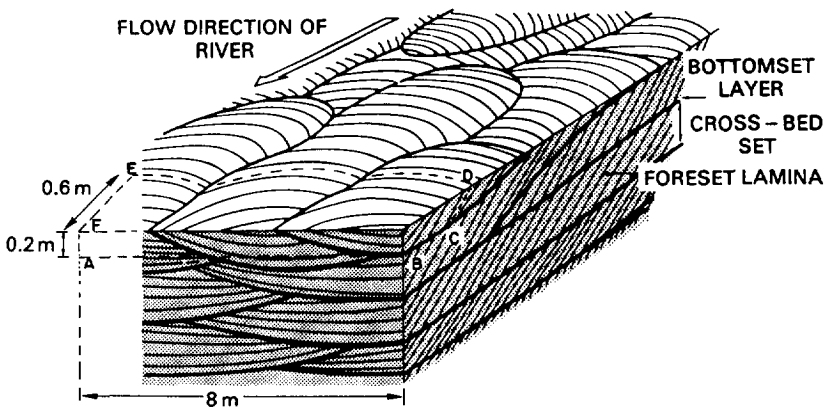

Fig. VI.6 Features of trough cross-bed sets (modified from Kortekaas 1985).

VI.3.4 Cross-bed set Sedimentology and Petrography

The thickness of the preserved part of the cross-bed sets ranges between 20 and 40 cm.

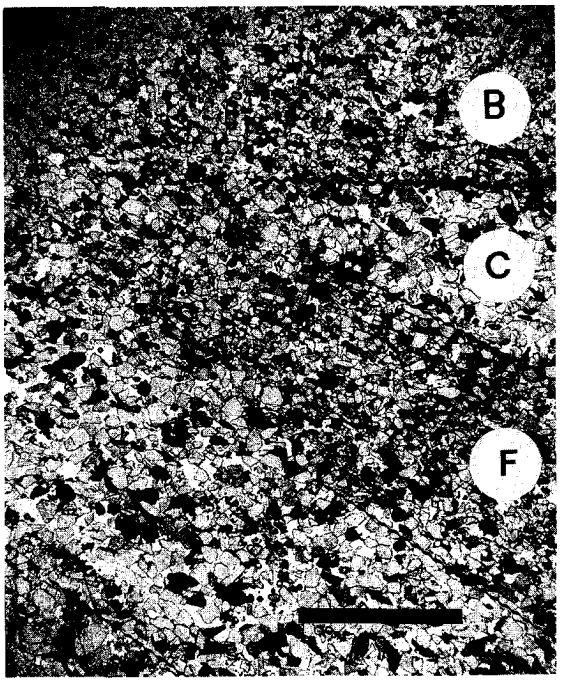

Fig. VI.7 Microscopic vieuw of the top part of a cross-bed set with the overlying bottomset: F.L. = foreset lamina, B. = bottomset. dashed lines indicate direction.

Bottomsets make up 10-30% of the total volume of the preserved part of the cross-bed set. The lower surfaces of trough cross-bed sets are spoon shaped (Fig. VI.6).

Individual foreset laminae are moderately to well-sorted, bottomsets are invariably well sorted. Sorting differences typically reflect the flow conditions during sedimentation:

foreset laminae are sorted to size during avalanching along the leeside of the ripple, while bottomsets result from fine grained suspension fall-out. Cross-bed set laminae are defined by sharp interfaces over which grain size changes instantaneously (Fig. VI.7). Tops of the ripple foreset-laminae are cut-off by a later erosional event and hence, sharp boundaries between the top of the foreset and the overlying bottomset are often observed (Fig. VI.7). Average foreset laminae thickness ranges from 0.1 to 1 cm. The alternation and thickness of the foreset laminae depends on the availability of several grain size classes in the transported sediment or micro-fluctuations in water energy.

Irrespective of the degree of authigenic mineralization, those sands with better initial porosity at the time of deposition (avalanche rather than bottomset) (Glennie 1990) retain better porosity and permeability. Diagenetic processes usually enhance the permeability contrasts between the foreset laminae and also between foreset and bottomset.

VI.4 METHODS

VI.4.1 Outcrop

Seventeen outcrop locations were selected to study grain size and sorting characteristics of trough cross-bedded sets. The studied deposits comprise low- and high sinuosity channel sandbodies. Permeability was measured on-site with a portable minipermeameter (Hartkamp & Donselaar 1993). The individual outcrop locations were prepared for measurements by removing the weathering surface of the outcrop (Goggin *et al.* 1988). An area grid was marked on the outcrops. Data was collected at several sampling intervals (Hartkamp & Donselaar 1993, Hartkamp *et al.* 1993). Individual grid-spacings were; 1) a column spacing of 1 cm. and a row spacing of 10 cm. over a total column height of 110 cm. and width of 85 cm.; 2) a column spacing of 1 cm. and a row spacing of 5 cm. over a range in height of 10-50 cm. and a range in width of 25-65 cm. Over specific key-horizons (e.g. bottomsets) additional rows and columns were measured.

A total of 3800 measurements was processed. For petrological research and laboratory experiments, several cores were drilled.

VI.4.2 Subsurface

Eighteen core intervals of cross-bedded or laminated sandstone deposits were selected to measure permeability with a minipermeameter. The slabbed core-sections were brushed and cleaned with water and dried for several days, in order to limit the influence of clay-swell by the water. Measurements were performed on a grid with a column spacing of 0.5 cm. and a row spacing of 1 or 2 cm., over a range in column height of 10-70 cm. and a range in width of 1-5 cm. In very heterogeneous cores, additional datapoints were measured in the columns, with a vertical spacing of 0.5 cm. A total number of 1939 datapoints were processed. Rock samples of measured core-sections were used for petrological studies and laboratory experiments.

VI.4.3 Permeability data processing

The permeability data has been interpreted and correlated with the sedimentary structures of the locations. This led to a subdivision into three groups, based on sedimentological criteria; a group of bottomset measurements, a group of fine-grained laminae measurements and a group of coarse grained laminae measurements. The groups of measurements were analyzed with basic population statistics, including average values and standard deviation. The average values of the different populations were tested with classical statistics (Appendix B).

VI.4.4 Capillary pressure measurements

Air-Mercury drainage and imbibition capillary pressure curves were determined of

ten subsurface core- and the outcrop samples, in laboratory settings (Purcell 1949). Samples of 1.5 cm diameter were drilled for these measurements with Helium Porosity of the samples determined prior to their injection. The maximum injection pressure used was 2000 Psi. Pore-size distributions of the samples were calculated using the La Place equation assuming cylindrical pores.

VI.4.5 Simulation of fluid-flow

A two dimensional probabilistic simulator was applied to study capillary effects in presence of heterogeneities on a centimetre-scale (Bakken 1991).

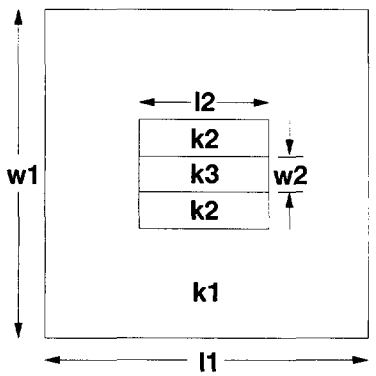

Fig. VI.8 Cross-bed heterogeneity model. The values of the variables are indicated in table 1.

The simulator is based on the work of King & Scher (1985) and King (1987), and differs from the traditional simulators by its implementation of fluctuations, that are inherent to fluid flow in porous media. A description and validation of the simulator has been

presented by van Batenburg et al.(1991). The model used in the simulations is presented in Figure VI.8. The horizontal model comprises three high permeability beds surrounded by a low permeability region. Water is injected into the low permeability region along the entire left side of the model, while oil and water are produced along the right side. The upper and lower margins are considered no-flow boundaries. Athough the geometry is simplified with respect to the model of Kortekaas (1985), it preserves the essential features of crossbed sets. The rock is assumed water-wet. Permeability dependent capillary pressure curves were used for the different regions in the model. Relevant parameters used in the simulations are presented in Table VI.I and in Table V.II in the previous chapter.

Table VI.I, Parameters characterizing the cross-bed model.

Model	Parameter	Value
Total length	l_1	0.075 m
Length of lamina	l_2	0.025 m
Total width	w_1	0.08 m
Width of lamina	w_2	0.015 m
Permeability of bottomset region	k_1	5 mD
Permeability of lamina	k_2	25 mD
Permeability of lamina	k_3	125 mD

VI.5 RESULTS

VI.5.1 Permeability and porosity

Outcrop minipermeameter studies showed a significant difference in average permeabilities of foresets and bottomsets (permeability ranges from 0.5-20 Darcy). Measurements of coarser and finer avalanche laminae could be correlated and the foreset-data subdivided into these two groups (Hartkamp *et al.* 1993). The porosity and permeability contrasts in cross-bed sets of reservoir sandstone reflect the initial depositional characteristics of grain size and sorting (Fig. VI.9). In Figure VI.10 a linear

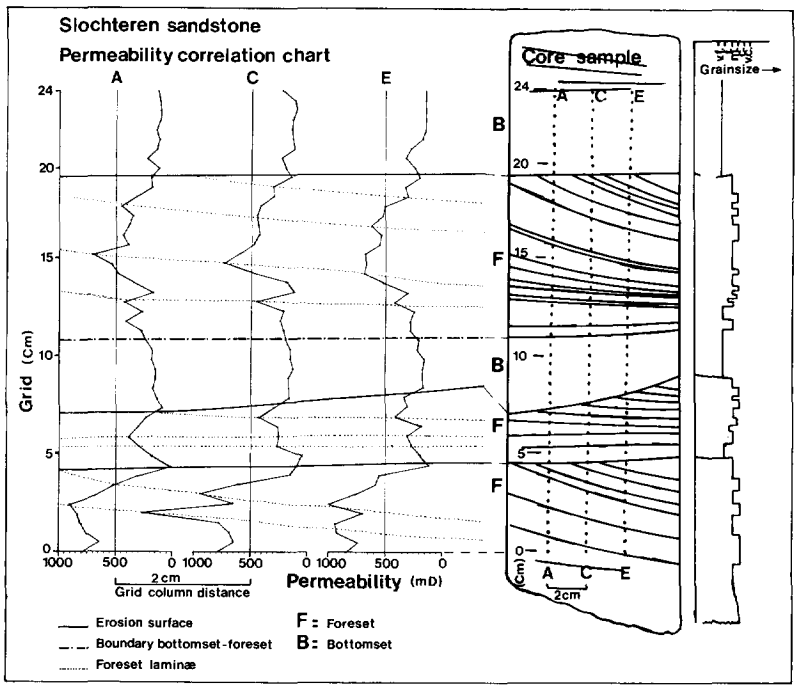

Fig. VI.9 Example of a measured cross-bedded core section, with grain sizes and correlated permeability patterns.

relationship of porosity versus log-permeability is shown of outcrop and subsurface minipermeameter data. This is described by Jensen (1990) as a common relationship for the two parameters. The datasets of core-sections of the subsurface Slochteren and Vollpriehausen Sandstone Members show characteristic ranges in permeability anisotropy. Permeability of tightly cemented, fine grained sandstone cores show a measured range from 0 to 100 mD. Fine-medium grained sandstone cores, with a well developed porosity have permeabilities from 100-1000 mD. The deviation in permeability data-populations of foreset and bottomset increases with decreasing average porosity (Fig. VI.11). In the low

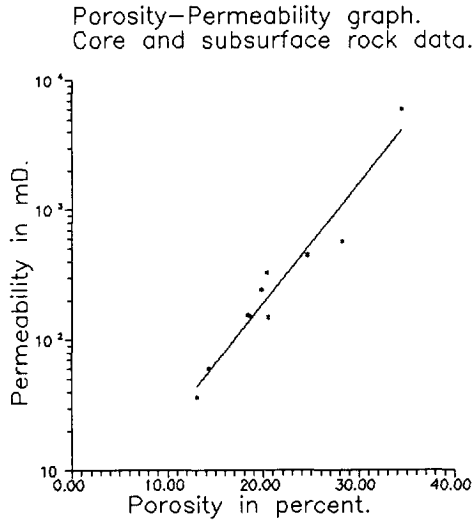

Fig. VI.10 Porosity versus log-permeability.

permeability samples this trend of increasing contrast in average permeabilities reverses. The average permeability contrast measured in outcrop samples is 2 : 1.3 : 1 (coarser grained foreset : finer grained foreset : bottomset). The core samples ranging from 100-1000 mD have an average contrast of 10 : 6.3 : 1. The low permeability core samples ranging from 1-100 mD have an average contrast of 2.5 : 2 : 1.

VI.5.2 Capillary pressure curves

The measured capillary pressure curves were either very smooth or irregular in shape. The irregularities were defined by heterogeneities in the sample (Stout 1964, Pickell *et al.* 1966). In Figure VI.12 (A,B and C) three capillary pressure curves are presented. The first curve (Fig. VI.12A) represents a homogeneous outcrop sample

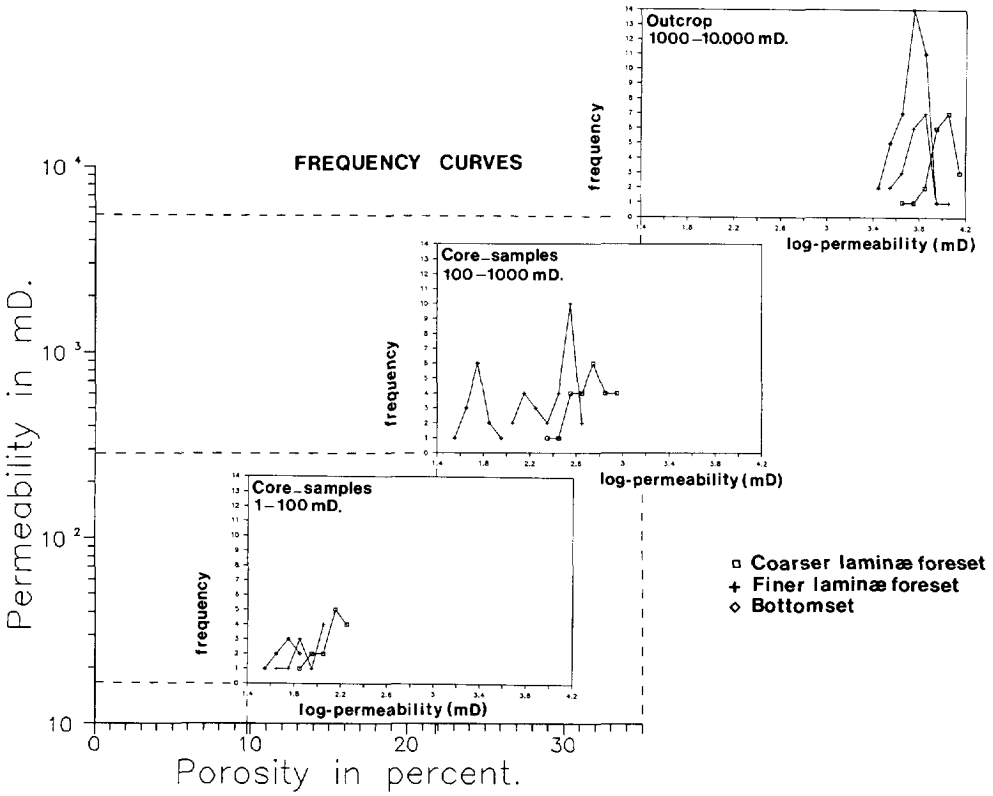

Fig. VI.11 Frequency curves of average coarser- and finer foreset and bottomset permeabilities with decreasing average porosity.

(sample 10, porosity 28.3%). Figure VI.12B represents a laminated, heterogeneous sample of subsurface reservoir rock of intermediate porosity (sample 7, average porosity 20.5%). The third curve (Fig. VI.12C) shows a curve shape of a heterogeneous subsurface sample of low porosity (sample 2, porosity 13.1%). The stepwise increase in capillary pressure of the laminated core reflects the different pore sizes occurring in the laminations of the sample. The horizontal 'plateau' parts in the curve represent the infill

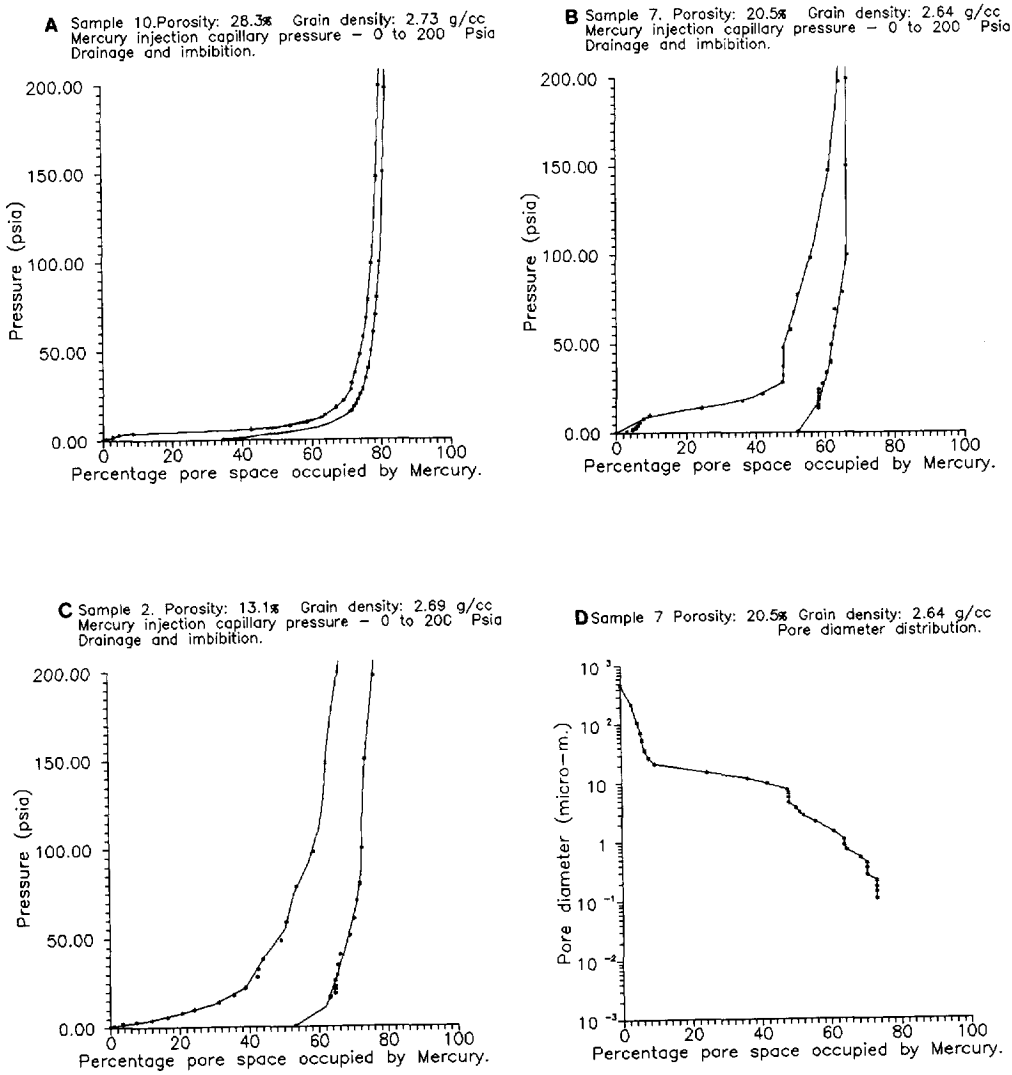

Fig. VI.12 A) Capillary pressure curve of a highly porous sample (28.3%). B) Capillary pressure curve of a heterogeneous sample of intermediate porosity (20.5%). C) Capillary pressure curve of a sample of low porosity (13.1%). D) Pore diameter distribution of the same sample as curve B.

of the individually homogeneous laminae. In Figure VI.12D, the pore diameter distribution of sample 7 is displayed. The stepwise infill of pore-space by Mercury demonstrates the presence of different groups of pore-sizes. The curve shape can be subdivided into different parts corresponding to the different laminae (individual homogeneous groups of pore-sizes) occurring in the sample. The sorting of the sand is reflected in the dip of the "plateau" of the curve. The endpoint theoretical residual oil saturations decrease with increasing sample porosity.

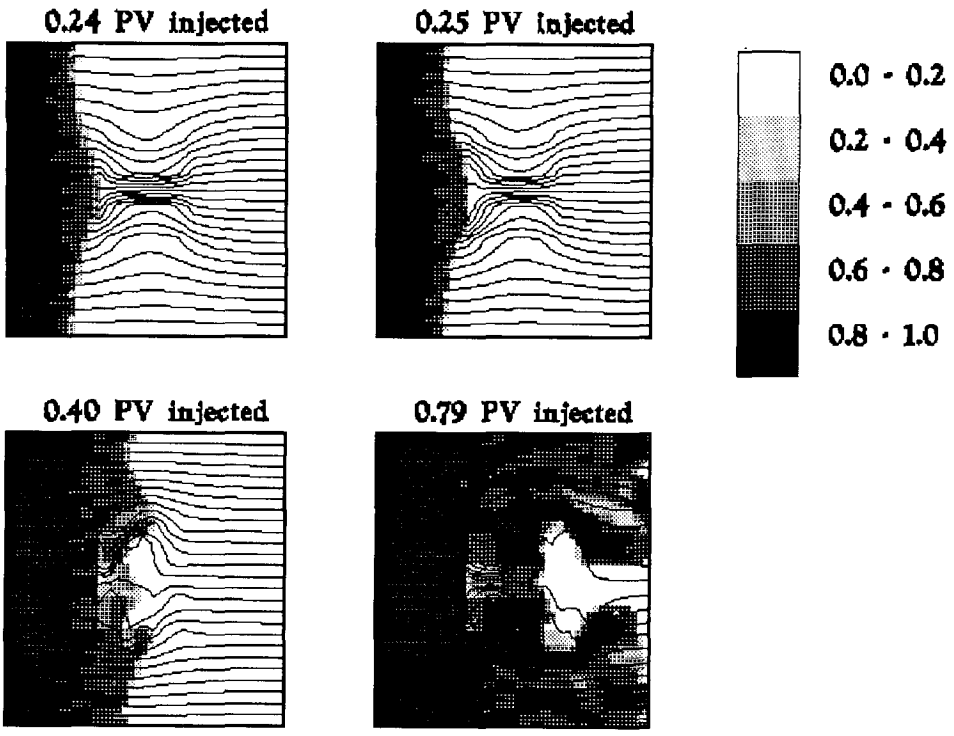

Fig. VI.13 Reduced water saturation distribution in % and streamlines for the heterogeneous model at 0.24, 0.25, 0.40 and 0.79 pore volumes of water injected.

VI.5.3 Simulation of fluid-flow

In Figure VI.13 streamlines and reduced water saturation distributions are shown at different pore volumes (PV) injected. The reduced water saturation is defined as the ratio of the actual water saturation and the endpoint water saturation.
At 0.24 PV and 0.25 PV the high permeability regions can be identified because of the concentration of streamlines in these regions. Further examination of streamline-distribution at 0.24 PV and 0.25 PV shows that the streamline pattern changes as soon as the front reaches the boundary of the heterogeneity and as a consequence, flow is enveloping the high.permeability region. At 0.4 PV injected, The front continues to surround the higher permeability regions and front velocity is higher in the low permeability region compared to the higher permeability regions. Finally, this results in bypassing of the high permeability regions as suggested in Figure VI.13 at 0.79 PV injected. In general, it is observed that streamlines are concentrated in the low permeability region at the water/oil front, where capillary forces are strongest (Fig. VI.13). Behind the front the capillary pressure decreases and the streamline pattern approaches the initial situation (concentrated in the high permeability region).

VI.6 DISCUSSION

Fluvial channel sandbodies of similar architecture to the studied outcrop and subsurface deposits, typically consist for 70-80% of fine-medium grained, trough cross-bedded sands. The sets consist for 80-90% of foreset avalanche deposits. Water energy fluctuations and the grain sizes in the transported sediment determine the alternation of coarse and fine laminae in the foreset. Generally, half of a foreset consists of coarser grained laminae. The amount of movable oil initially trapped in the heterogeneities depends on the mobility ratio of the two fluids involved, the permeability contrast between foreset laminae and bottomsets as well as the shape of the cross-bed set and the extend of individual laminae of contrasting permeability within a set.

The three dimensional shape of the cross-bed sets determines the proportion of a set in which oil will be initially trapped. Assuming that in the upper third of the coarse grained laminae oil will initially remain during water flooding. The relative proportion of initially capillary by-passed oil within different types of cross-sets is easily estimated. Spoon shaped trough cross-bed sets show small volumes near the top of the sets, in which the remaining oil will be initially trapped (20% of the total volume). Tabular cross-bed sets, straight crested, have a much larger possible volume in which oil may be initially trapped (33.3% of the total volume). As a proportion of movable oil these figures are respectively 12% in tabular sets and 7.2% in trough cross-bedded sets.

VI.7 CONCLUSIONS

1. Contrasts in permeability of adjacent foreset laminae and bottomsets are primarily determined by grain size and sorting contrasts in the cross-bed sets.
2. Contrasts in average permeability between the laminae increase with increasing cementation and diagenesis and hence decreasing average porosity. In low permeability cores, however, the contrast in average permeability of foreset and bottomset decreases again.
3. Capillary-pressure curves can be used to identify the heterogeneous character of the sample. The stepwise shape of the curve corresponds to the different laminae (groups of different pore-sizes) occurring in the sample.
4. Capillary forces lead to the initial entrapment of mobile oil in high permeability regions of small-scale heterogeneities. The entrapment behaviour depends on the mobility ratio of water/oil and the permeability contrast of the hetergeneous medium.
5. It is conceivable that between the 7-12% of movable oil may initially be trapped by the effect of capillary forces in the coarser grained laminae of cross-bed sets.
6. The three dimensional shape of the cross-bed sets defines the volume of the sets and hence specifies the possible volume of oil to be initially trapped.

SI METRIC CONVERSION FACTORS

bbl * 1.589873 E-01 = m^3

psi * 6.894757 E+00 = kPa

CONCLUSIONS

1) Characteristics of cross-beds

- The probability of cross-bedded sedimentary structures occurring in the active channel fill of high-sinuosity channels is significantly higher than in that of low-sinuosity channels.
- Trough cross-bed sets (3D bed forms) are characterized by a maximum thickness:width:length ratio of 1:6.5:20 (W:T ratio ranges from 4 to 16, L:T ratio ranges from 10 to 30).
- Planar cross-bed sets (2D bed forms) are characterized by a maximum thickness:width ratio of 1:20.
- Foreset-lamina thickness varies between 0.1 and 1.5 cm. The ratio of coarse-grained-foreset-lamina thickness to fine-grained-foreset-lamina thickness varies between 0.5 and 2.5.
- Bottomsets make up 10-30% of cross-bed sets. The ratio of cross-bed thickness to bottomset thickness is approximately 10 (ranging from 5 to 25).
- The three-dimensional shape of trough cross-beds results in bottomsets being connected in a stacked system of multiple sets. The resulting compartmentalization of the cross-bedded channel fill controls the volume of movable oil that is trapped initially.
- Experimental and numerical models show that, excluding the effect of gravity, initial capillary entrapment is not influenced by flooding direction or by geometrical characteristics such as size and shape of the cross-bedded region.

2) Textural and compositional characteristics that determine permeability and capillary-pressure conditions

- Differences in grain size, sorting, composition and porosity between the sub facies of cross-beds in fluvial sandstone reservoirs (coarser-grained foreset laminae, CFL; finer-grained foreset laminae, FFL; and bottomset layers, BL) determine contrasts in permeability and capillary-pressure characteristics.

- In the BL dominant grain sizes vary between very fine-grained sand and fine-grained sand. In the foreset, CFL and FFL alternate in dominant grain size between resp. medium-grained sand and fine-grained sand. On average, the difference is half a phi unit ($-\frac{1}{2}\log_2$ interval of grain size in mm) between CFL and FFL. The grain sizes in the BL are equal to or a fraction finer than in the FFL.
- Good sorting occurs in the FFL and BL, whereas moderate sorting characterizes the CFL. The moderate sorting of the CFL is a result of mixing of the dominantly coarser-grained avalanche deposits with finer grain sizes in the sediment (either bed-load or suspension load material).
- In outcrop samples and reservoir cores, differences in framework composition (quartz/non-quartz ratio) occur between CFL, FFL and BL. A differential pore-space reduction between CFL, FFL and BL has been observed in samples of the studied reservoir cores. In these samples, differences in percentages pore-filling clay minerals (kaolinite) and cement (anhydrite) have been identified between CFL, FFL and BL.

3) Permeability contrasts in fluvial reservoirs and the probability of capillary entrapment

- Permeability contrasts between BL and CFL measured at almost unconsolidated outcrops of fluvial deposits in Central Spain are on average a factor 2 (lowest permeability in BL). In the studied cores of fluvial reservoirs permeability contrast between BL and CFL ranged from a factor 2 to a factor 30.
- The capillary-pressure curves of the CFL, FFL and BL differ in the sense that the moderately sorted CFL show a more gradual decrease of capillary pressure with increasing water saturation, whereas the better sorted FFL and BL yield a more plateau shaped curve. One can therefore expect a gradual increase in water saturation during imbibition in the CFL. In the FFL and BL saturations will change more suddenly at specific capillary-pressure levels.
- Oil/water saturation in the different sub-facies, at the moment entrapment occurs, is defined by microscopic distribution of pore sizes. Imbibition of water in the CFL will start in the finer pore sizes, which result from finer sediment deposited

in the CFL. It is therefore expected that water saturations increase in all three sub-facies before entrapment occurs and result in non-maximum oil saturations in the CFL as soon as oil is initially trapped.

- Computer simulations and laboratory experiments show that movable oil is initially trapped in CFL when surrounding finer-grained laminae and bottomsets have almost reached their maximum water saturations (non-zero capillary-pressure condition).

4) The likelihood of initially trapped movable oil being flooded before the economic limits of a reservoir

- Laboratory experiments demonstrated that initial trapping of light oil under model conditions occurs after injection of 0.77 pore volumes of water at a permeability contrast of 25 between BL and CFL. The movable oil that was initially trapped in the CFL was ultimately flooded to zero-pressure residual oil saturations. Five to seven pore volumes of water were needed to reach this ultimate situation.
- The permeability measurements on natural cross-bed set laminae show that a contrast of 25 between BL and CFL is generally not reached. For highly permeable reservoirs the contrast is more likely to be in the range of 2 to 3. Thus the trapping effect is probably limited in good quality fluvial rock especially after a prolonged water drive period. The observed lower oil recoveries from fluvial reservoirs, in comparison to, for example, barrier bars are probably due to other types of heterogeneity.

5) Possibility to quantify amounts of movable oil initially trapped in cross-bedding

- Theoretically, some capillary trapping can be expected in CFL, especially in diagenetically altered rock with high permeability contrasts between CFL, FFL and BL. The computer simulations and flooding experiments indicate that longer flooding periods with several pore volumes of water significantly reduce the trapped volumes. Thus, it is not possible to present general conclusions on the recovery efficiency as a function of the permeability of foreset laminae. However,

the effect is unlikely to be strong enough to make recovery by surfactant flooding economically attractive even at considerably higher oil prices.

RECOMMENDATIONS

The geological framework of cross-beds in fluvial sandstone reservoirs and the basic principles of the impact of cross-beds on water/oil displacement have been descibed in this thesis. To extend this basis to real field situations, more numerical and experimental research is needed. It is therefore recommended to:

* Incorporate capillary-pressure curves that depend on pore-size distribution in the cross-bed models.

* Establish the critical permeability contrasts at which entrapment is initiated for various mobility ratios and capillary numbers.

* Define the ratio of the pore volumes (model) of flooded water required for the initial occurrence of entrapment and for ultimate flooding under various permeability contrasts, mobility ratios and flooding speed.

* Determine the influence of gravity on capillary entrapment behaviour.

* Establish the effect of the three-dimensional geometry of cross-beds on the capillary entrapment behaviour under gravity conditions.

* Ideally one would like to carry out 3-D flow experiments with realistic models of cross-beds. Models of cross-beds can be produced in flumes. Such experiments should be compared with computer simulations to arrive at truly calibrated conditions.

* The introduction of techniques like sponge coring and high-resolution resistivity logging may provide direct evidence of the remaining oil distribution after a water flood. It is recommended to select a suitable case, preferably for a case with a relatively high CFL/BL permeability contrast.

These points will physically define the effect of cross-beds on water/oil displacement. Only then, it will be possible to relate scaled down experiments with the behaviour of cross-beds during water flooding in actual field situations.

APPENDIX A
"THE MINIPERMEAMETER" - VALIDATION OF THE MEASUREMENT METHOD

A.1 INTRODUCTION

A minipermeameter is an instrument capable of measuring fluid flow into porous media via a probe, the tip of which is sealed against a sample surface (Sutherland *et al.* 1991). The minipermeameter has been proven a successful tool for the qualitative and quantitative description of the permeability distribution on a small scale. Numerous studies (e.g. Chandler *et al.* 1989, Dreyer *et al.* 1990, Halvorsen & Hurst 1990) have shown that the minipermeameter can give realistic and reliable information on the permeability and permeability variations of outcrop and reservoir rocks. In 1950, Dykstra and Parsons described a tool for detailed in-situ permeability measurements, the "micropermeameter". Later, Morineau *et al.* (1965) used a modified version of this "micropermeameter" to prove the existence of permeability heterogeneities in laminated rock. Eype & Weber (1971) were the first to publish a paper on the description, the principles and the calibration technique of the "minipermeameter". Since the first International Meeting on Minipermeametry in Edinbugh, U.K. the term probe permeameter was introduced by Sutherland *et al.* (1991). The "micropermeameter", "minipermeameter" and "probe permeameter" are based on the same principles and are used to make rapid, non-destructive and spatially precise permeability measurements. In the framework of this thesis, the term "minipermeameter" is preferred.

In the next sections, the principles of the apparatus, the calibration method and results and the accuracy of the calibration method and minipermeameter response will be discussed. In the last section a theoretical model will be presented of minipermeameter response in laminated heterogeneous media.

A.2 THE APPARATUS

For the minipermeameter measurements that were taken for the studies presented in this thesis, an Electronic Field Minipermeameter (EFMP) was used, developed at the Imperial College of Science, London (U.K.). The EFMP is a steady-state minipermeameter. It was bought in 1989 from Imperial College when the apparatus was not yet marketed commercially. The initial calibration was carried out in Delft using a set of 39 core plugs, the permeabilities of which ranged from 1.5 mD to 2100 mD. Calibration was found to be satisfactory, although a more extensive calibration would be needed to analyze the accuracy of the apparatus. This was done by van Rijn (1992), who used a set of 94 reservoir-sandstone plugs, the permeabilities of which ranged from 0 to 2200 mD. This range was expanded by five artificially constructed sandstone plugs, the permeabilities of which ranged from 5000 to 14000 mD.

A.3 THE PRINCIPLES

A steady-state minipermeameter consists of three units (Fig. A.1), i.e.: 1) a gas source, 2) a flow-meter unit and 3) a probe. The probe is pressed against the rock surface with a controlled force. At a constant pressure, gas is forced through the probe into the rock. Both flow rate and pressure at the probe tip are measured under steady-state conditions. To satisfy these conditions it is necessary to allow the gas flow to stabilize. The pressure measured at the probe tip is used to correct the flow rate for variations in pressure drop that result from variations in permeability of the sampled rock volume. The flow-rate response is proportional to the permeability of the sampled rock volume.

The EFMP is constructed in such a way that it can use a bottle of nitrogen gas under high pressure. The flow-meter unit consists of four Laminar Flow Elements (2 cc, 20 cc, 200 cc and 2000 cc LFEs) to cover a wide range of permeabilities. Essentially, the pressure drop is measured along a LFE and is proportional to the gas-flow rate. The probe has a spring-loaded head introduced by Morineau *et al.* (1965). Elastic, closed-cell neoprene is used to obtain a perfect seal between the probe and the rock.

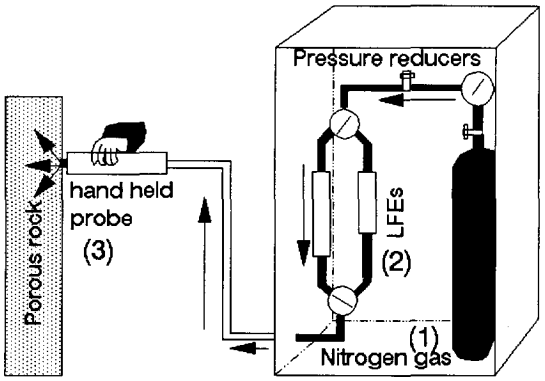

Fig. A.1 A minipermeameter device with the three basic units: 1) a gas source, 2) a flow- meter unit and 3) a probe.

The EFMP was used in its "original" configuration (van Rijn 1992) in the research for this thesis. In this configuration, bypassing could occur as a result of communication between the LFE elements through the manometer-pressure line (Fig. A.2). The gas could flow over more than one LFE element and consequently, an average pressure drop over several elements was measured instead of a pressure drop over a single element. This yields calibration graphs (Figs. A.3, A to D) showing no distinctive minimum or maximum. The accuracy of the calibration was not affected by an erroneously installed flow-meter system (van Rijn 1992).

A.4 THE CALIBRATION

Calibration was performed by comparing the minipermeameter measured flow rates with the permeabilities of a set of 115 homogeneous core plugs.

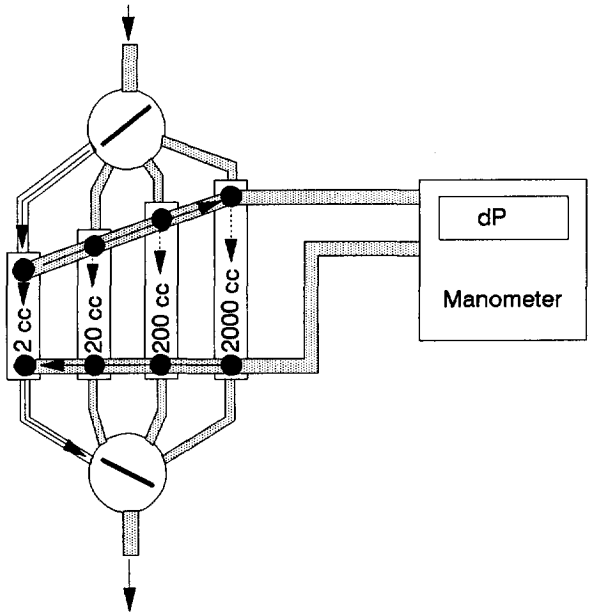

Fig. A.2 The flow-meter unit of the "original" configuration of the minipermeameter. The gas flow direction is indicated by arrows. Four laminar flow elements (2cc, 20cc, 200cc, 2000cc LFEs) can be selected by the two valves (upstream and downstream). The LFEs are connected through manometer-pressure lines with an electronic manometer. Through this pressure line, bypassing could occur through all LFE's as indicated by the arrows.

A.4.1 Standard plug permeability

As a standard permeability of the core plugs, a one-directional total plug permeability was obtained by an unsteady-state CMS-300™ (Automated Core Measurement System[1]). The plug is placed in a plug-holder, the reservoir is filled with helium up to a standard pressure. Closure of the upstream valve and opening of the

[1] Western Atlas International, former CORE LABORATORIES, Rijswijk, The Netherlands.

downstream valve result in gas flow through the plug volume. The pressure declines during the measurement and is monitored by a pressure transducer. Each sampled permeability has a characteristical pressure decay versus time. An algorithm, based on the unsteady-state formula as described by Jones (1972), calculates the corresponding infinite permeability (K_{inf}). This is also known as the Klinkenberg (1941) correction method for gas slippage. For obvious reasons, the algorithm used to calculate the infinite permeability is kept confidential.

Of five artificial sandstone samples, standard permeabilities were obtained by a Liquid Permeability Meter[2] (Kok 1982). The plug is placed in a holder and the reservoir is filled with liquid (H_2O). Opening of a downstream valve allows the liquid to flow through the sample as a result of the difference in height between the reservoir and the datumn level. During the measurement four parameters are recorded, namely the volume of liquid that flows through the plug, the time needed for this volume to flow through the plug, the pressure drop over the plug and the temperature of the liquid.
From these parameters, the permeability can be calculated using Darcy's formula:

$$K = \frac{Q dp A}{\mu L} \qquad (1)$$

in which:

K = permeability (mD)
Q = volumetric velocity (cc/min)
dp = pressure difference (atm)
μ = viscosity (cP)
L = Length (cm)
A = surface area (cm^2)

A.4.2 Minipermeameter flow rate

The EFMP gives a read-out of the injection pressure at the probe tip in psi units

[2] Dietz Laboratory, Mining and Petroleum Engineering, University of Technology, Delft, The Netherlands.

and of the pressure drop over a LFE in mmH_2O units. These values are used in the calculation of a normalized flow (normalized with respect to a standard pressure drop of 3 psi). The calculation is carried out as follows:

$$F_{norm} = dP \left(\frac{LFE}{P_{cali}}\right) \left(\frac{3}{P_{inj}}\right) \quad (2)$$

In which:

- dP = the pressure drop (mmH_2O)
- LFE = the maximum flow rate of the selected LFE (cc/min)
- P_{cali} = calibrated pressure drop corresponding to the maximum flow rate of the LFE selected (mmH_2O)
- P_{inj} = the measured injection pressure at the probe tip (psi)
- F_{norm} = the normalized flow rate (cc/min) with respect to a standard injection pressure of 3 psi.

The term LFE over P_{cali} is a calibation constant for each LFE and the terms are:

$$\left(\frac{LFE}{P_{cali}}\right)_{(2000\ cc)} = \left(\frac{2000}{10.33}\right) \quad (3)$$

$$\left(\frac{LFE}{P_{cali}}\right)_{(200\ cc)} = \left(\frac{200}{9.74}\right) \quad (4)$$

$$\left(\frac{LFE}{P_{cali}}\right)_{(20\ cc)} = \left(\frac{20}{5.00}\right) \quad (5)$$

$$\left(\frac{LFE}{P_{cali}}\right)_{(2\ cc)} = \left(\frac{2}{9.89}\right) \quad (6)$$

Four measurements are taken of each plug holding the minipermeameter probe in the central area of both end faces (Halvorsen & Hurst 1990, van Rijn 1992). The four measurements are geometrically averaged.

In order to investigate the repeatability of a measurement, twenty measurements were taken at exactly the same position of several cores. The experiments were performed

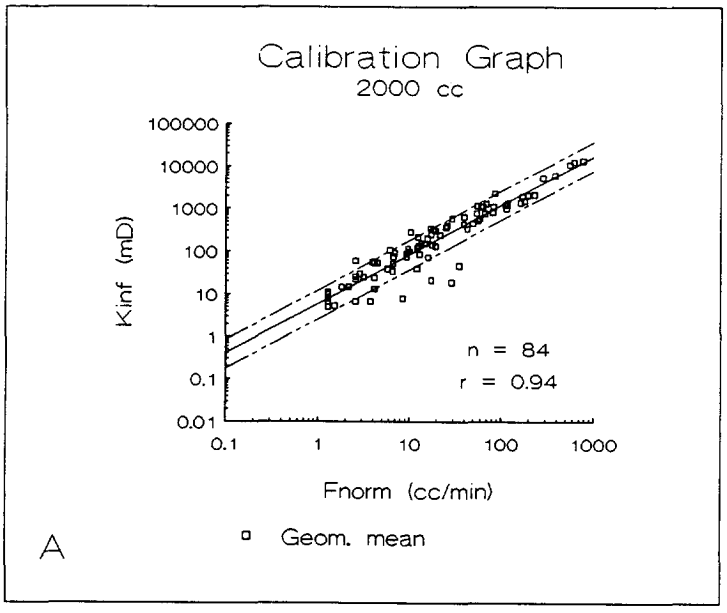

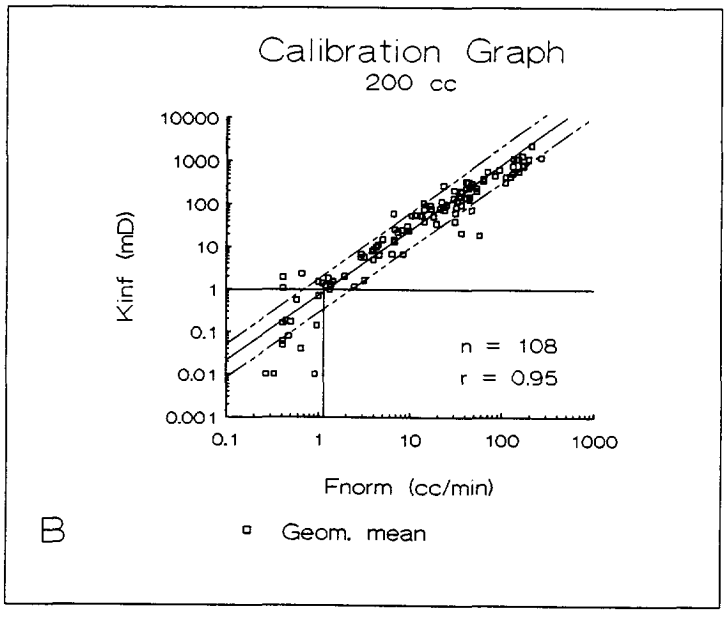

Fig. A.3 to be continued

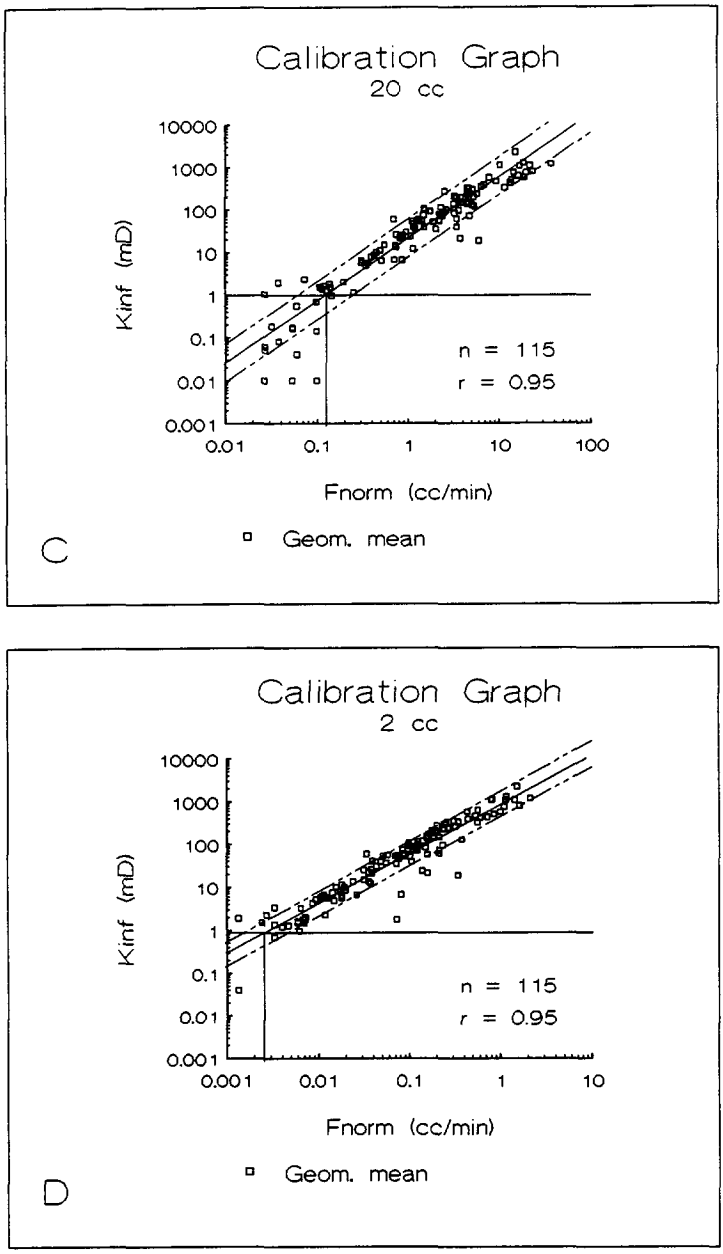

Fig. A.3 A to D) Calibration graphs showing the infinite plug permeability (Kinf) versus minipermeameter normalised flow rate (Fnorm) of unprocessed data. The graphs represent: A) the 2000cc LFE, B) the 200cc LFE, C) the 20cc LFE and D) the 2cc LFE in which n is the number of plugs involved in the calibration and r is the correlation coefficient. The solid lines indicate the lower limit of reliable correlations between plug permeability and minipermeameter response.

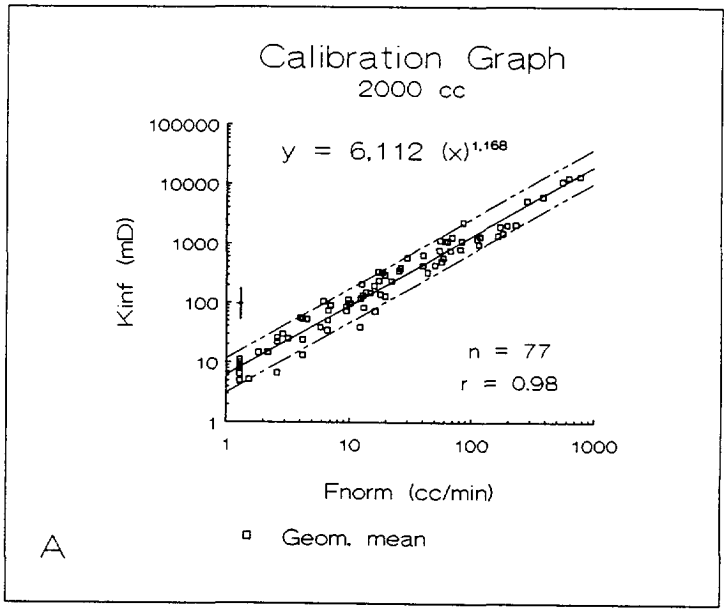

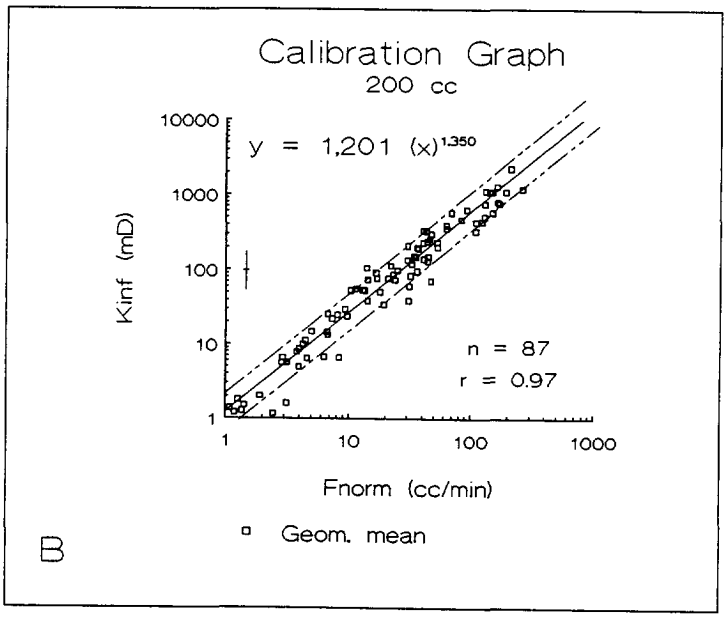

Fig. A.4 to be continued

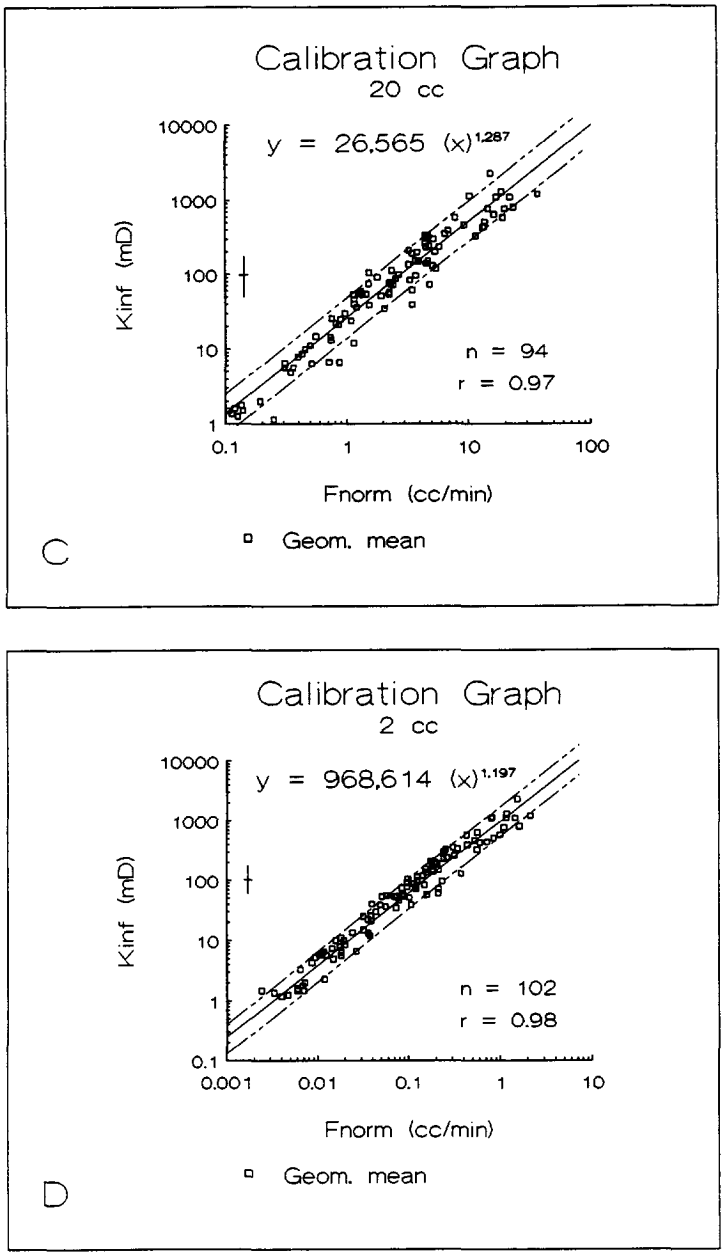

Fig. A.4 A to D) Calibration graphs showing the infinite plug permeability (Kinf) versus minipermeameter normalised flow rate (Fnorm) corrected for outlying datapoints and data below 1 mD. The graphs represent: A) the 2000cc LFE, B) the 200cc LFE, C) the 20cc LFE and D) the 2cc LFE in which n is the number of plugs involved and r is the correlaton coefficient. The dashed lines indicate the 80% confidence interval. An error bar illustrates the error of calibration.

over two days, taking five measurements at the beginning and at the end of each day. This resulted in an error of repeatability of less than 4% (van Rijn 1992).

A.4.3 Calibration results

Calibration curves illustrate the relationship between the geometrical average of normalized flow rate (ccmin) versus the standard permeability (mD) of the core plugs (Figs. A.3, A to D). These graphs show three significant matters: 1) There are outlying datapoints of specific plug samples, 2) No correlation exist below the 1 mD and 3) The correlation is linear throughout (no gas-slippage (Klinkenberg) effects or high velocity flow (turbulence) effects). The eighty per cent confidence interval shows the limits of error around the best-fit line. The error is a factor 2.5 for the 2000 cc tube, a factor 3.5 for the 200 cc tube, a factor 2.5 for the 20 cc tube and a factor 2 for the 2 cc tube. Correlation coefficients for best-fit lines vary between the 0.94 and 0.96.

These initial results were used to enhance the dataset to derive a more accurate calibration. Outlying data reflecting general errors in the calibration (van Rijn 1992) were taken out and data below the 1 mD were eliminated. The final calibration graphs are shown in Figs. A.4, A to D. The enhancement of calibration is visible in the correlation coefficients, which vary between the 0.97 and 0.98. The eighty per cent confidence limits show a measurement error of a factor 1.7 for the 2000 cc tube, a factor 1.8 for the 200 cc tube, a factor 1.8 for the 20 cc tube and a factor 1.6 for the 2 cc tube. The relation between normalized flow rate (F_{norm}) and permeability (K) can be obtained by power regression (van Rijn 1992). The equations are:

$$K_{(2000\,cc)} = 6.112\,(F_{norm})^{1.168} \qquad (7)$$

$$K_{(200\,cc)} = 1.201\,(F_{norm})^{1.350} \qquad (8)$$

$$K_{(20\,cc)} = 26.565\,(F_{norm})^{1.287} \qquad (9)$$

$$K_{(2\,cc)} = 968.614\,(F_{norm})^{1.197} \qquad (10)$$

It is obvious that the normalised flow derived from the combination of equation (2) with the calibration constants of equations (3),(4),(5) and (6) can be added to the equations (7),(8),(9) and (10). This leads to a direct calculation of permeability in mD. For future research, it is highly recommended to connect a programmable pocket calculator or notebook computer to the manometers of the minipermeameter device to obtain the measured permeability immediately.

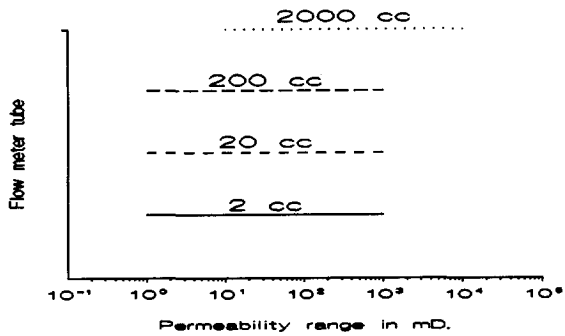

Fig. A.5 Ranges of permeability that are covered by the LFEs of the minipermeameter in the "original" configuration.

The by-passing of gas through more than one LFE has been advantageous for the total range of permeability in which the calibration of each LFE could be performed. It is obvious from the calibration graphs that there are no real limits in the range of each LFE. Figure A.5 shows that there is a large overlap in the range of permeabilities between the LFE's.

A.5 MINIPERMEAMETER RESPONSE "INTERNAL" FACTORS

A.5.1 Specific errors in the calibration

scale errors - The comparison of whole-rock measurements (core plug) with surface measurements (minipermeameter).

method errors - The comparison of one-directional whole-rock measurements (core plug) with the uni-directional surface measurements (minipermeameter).

Method and scale discrepancies have no effect if perfectly homogeneous plugs are used. Since completely homogeneous rocks are almost never encountered, a certain degree of heterogeneity is allowed in the calibration procedure, which ultimately affects the quality of the calibration. A large number of plugs over a wide range of permeabilities will enlarge the accuracy of the determined best-fit line. A simple method for testing sample homogeneity is presented by Halvorsen & Hurst (1990), and is based on comparison of the arithmetic, harmonic and geometric mean of plug measurements. Similarity between the three averaging methods is an objective indicator of sample homogeneity with respect to minipermeameter measurements. The degree of similarity between the averages to decide wether a sample is homogeneous enough to be used for the calibration procedure is unknown. Another method is CT-scanning of plugs (Halvorsen & Hurst 1990, van Rijn 1992). A disadvantage of this technique is that the homogeneity of plugs is judged by observation (subjective method).

A.5.2 Errors in minipermeameter measurements

Accidental and random errors, technical errors and systematic errors

Accidental errors are data out-liers, outside the general permeability interval. They have to be disregarded. Random errors are general errors of repeatability and are less than

4%. Technical errors are errors of the system units (i.e. flowmeters, amplifiers, manometers), usually defined in the technical specifications of the system units. Systematic errors are errors caused by improper installation of the system during the measurement campaign. This error affects all measurements but is not significant if the data are only used for determination of permeability contrasts.

A.6 MINIPERMEAMETER RESPONSE "EXTERNAL" FACTORS

The response of the minipermeameter is also affected by external factors. Most of these factors are related to climate, outcrop face and operation of the device and can be divided as follows:

1) Gas source -	the viscosity of the gas at injection pressure and temperature
3) Electronic manometers -	temperature
2) LFE -	gas-slippage effects
	turbulence effects
4) Probe vs. rock -	rock-surface
	gas leakage
	flow geometry

In order to optimize the permeability measurement, the factors listed above have to be kept constant or have to be corrected for.

The viscosity of nitrogen gas is assumed to be constant for the duration of the operation. During outcrop studies, temperatures in the shade ranged between the 18 and 30 degrees Celcius. The electronic manometers were found to be sensitive to large changes in temperature and produced very irregular readings as soon as the apparatus was placed in full sunlight. These two factors were reasons to work under controlled temperature conditions.

Non-Darcy flow effects cause a deviation from a linear relation between the measured gas flow rate and the permeability in a calibration curve. Gas-slippage effects

(Klinkenberg effects) result in measured flow rates that are higher than expected for low gas flow velocities. Turbulence effects cause measured flow rates that are lower than expected for high gas flow velocities. The reason for not having identified the gas-slippage and high velocity flow effects in the calibration graphs may be a result of the bypassing that could occur through the LFEs.

Alteration of the sampled rock surface resulting from e.g. weathering or stress reduction could produce non-representative permeability measurements. Gas leakage may occur between the probe and the rock if the probe is not placed over a smooth rock surface. Careful preparation of the rock surface before a measurement campaign is therefore essential to reduce rock-surface contamination and gas-leakage effects. A second reason for gas leakage might be an extreme injection pressure. The injection pressure should be kept constant (4.5 psi) and regularly controlled during a measurement campaign.

The gas-flow geometry of gas entering the rock is directly connected to the size of the tip seal and the dimensions of the rock sample. A geometrical factor, introduced by Goggin *et al.* (1988), may correct for differences in flow geometry between probe tips and core plugs of homogeneous rocks if these have different diameters. The theory of the geometry of gas flow entering laminated heterogeneous rock and its effect on the measurement will be outlined in the next section.

A.7 FLOW GEOMETRY IN HOMOGENEOUS AND HETEROGENEOUS MEDIA

Goggin *et al.* (1988) presented the flow geometry of expanding gas as it enters a homogeneous rock sample during a measurement by minipermeameter (Fig. A.6). In an half-infinitive rock sample (outcrop), the penetration depth and radius is equal to four times the inlet radius of the tip seal. The expanding gas occupies a more or less three-dimensional ellipsoid (Fig. A.6). Although measurements are affected by the entire volume of expanding gas, measurements are primarily affected by the first few cubic

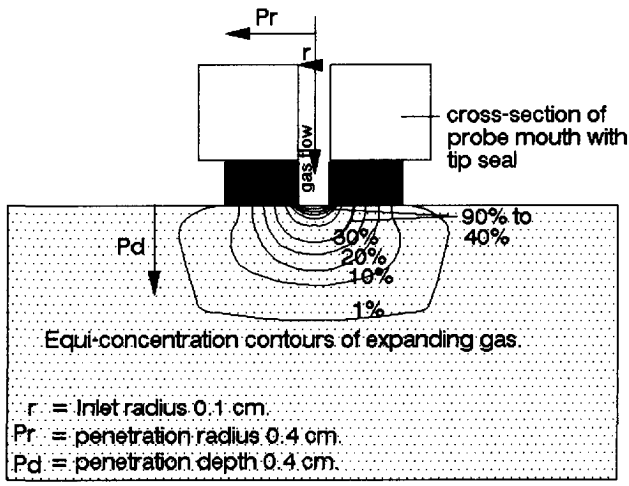

Fig. A.6 Cross-sectional model of gas-flow geometry during a minipermeameter measurement in a homogeneous rock sample (modified from Goggin *et al.* 1988).

millimeters of rock injected by the gas. This is illustrated by the clustering of equi-concentration contours below the inlet opening of the tip seal (Fig. A.6).

The flow geometry changes drastically as soon as the sampled rock volume is heterogeneous. In case of a laminated heterogeneous sample, the flow geometry depends on the permeability contrast between the laminae and on the thickness of the laminae. Figures A7 and 8 show modified versions of the illustration presented by Goggin *et al.* (1988). Figure A.7A shows a cross-sectional view of the flow geometry of the gas entering a less-permeable lamina (finer-grained lamina). As soon as the expanding gas reaches the neighbouring more-permeable laminae it will preferentially flow into these laminae. The surface view is illustrated in Fig. A.7B, in which this preferred flow into the more-permeable laminae is clearly visible. The opposite is shown in Figs. A.8A and 8B, the gas is entering a more-permeable lamina. The gas-flow geometry is elongated in the direction of the lamina and little or no gas will flow into the less-permeable laminae.

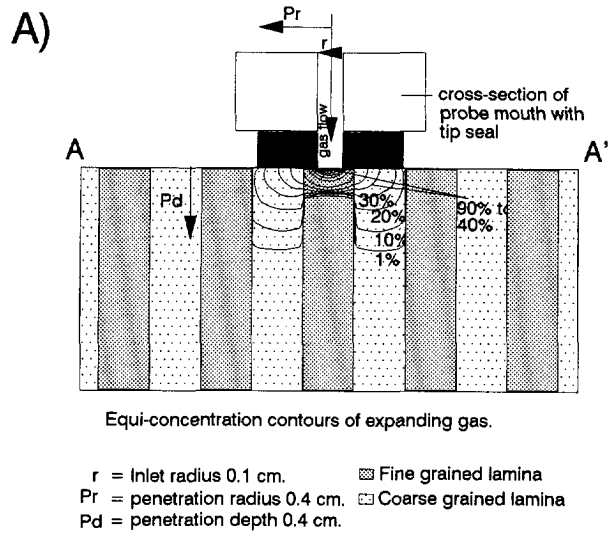

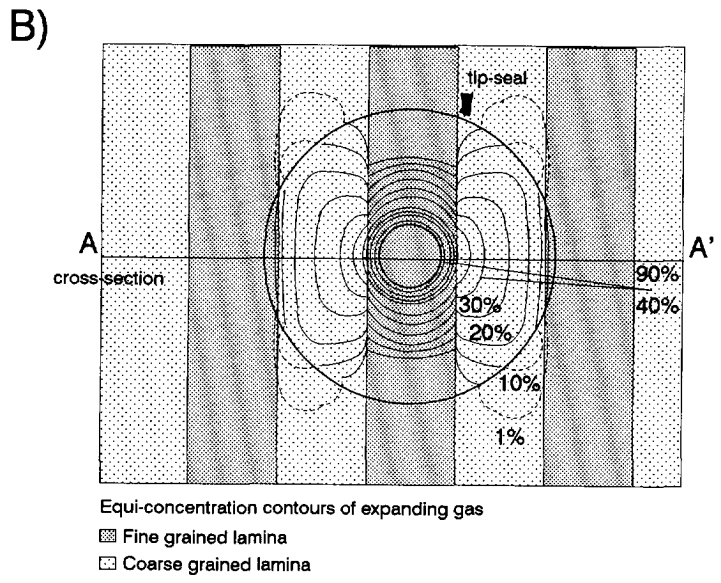

Fig. A.7 A and B) Model of gas-flow geometry during a minipermeameter measurement in a low-permeability lamina of a laminated heterogeneous rock sample in A) cross-sectional view A-A' and B) surfacial view (modified from Goggin *et al.* 1988).

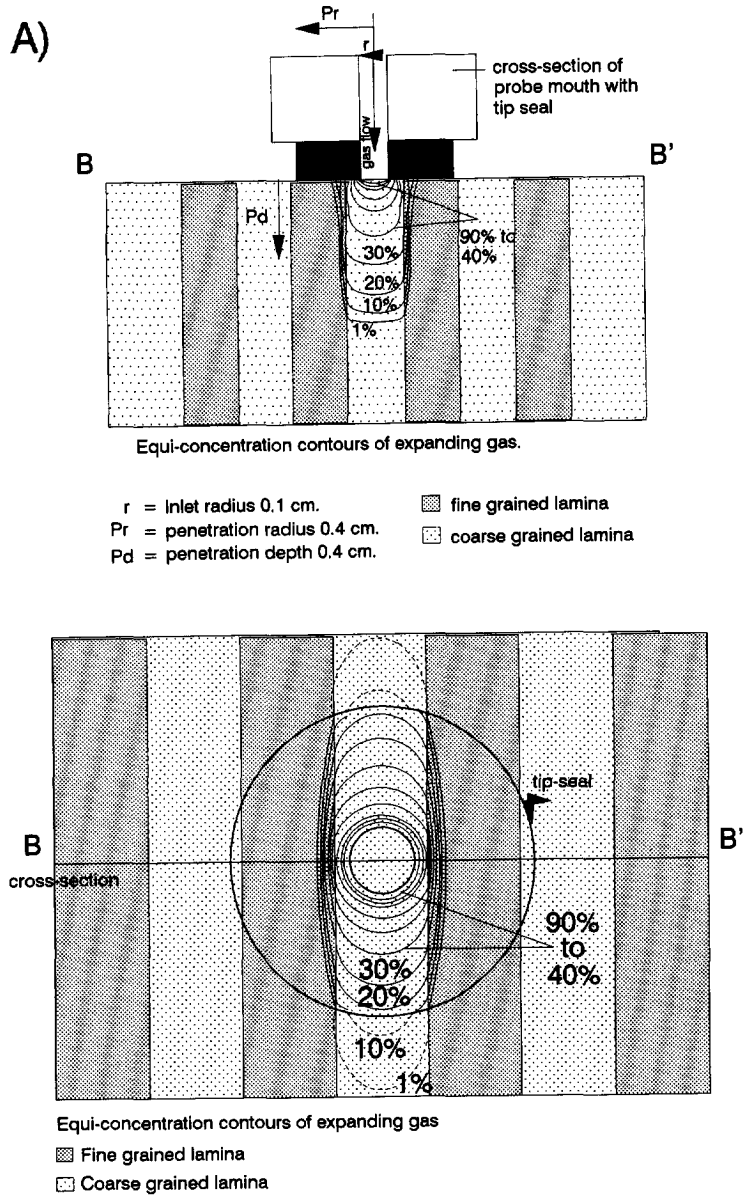

Fig. A.8 A and B) Model of gas-flow geometry during a minipermeameter measurement in a high-permeability lamina of a laminated heterogeneous rock sample in A) Cross-sectional view B-B' and B) surfacial view (modified from Goggin *et al.* 1988).

In the first example, the measured permeability will be an average value affected by the less-permeable laminae as well as the more-permeable laminae. In the second example, the measurement is mostly affected by the permeability of the more-permeable lamina.

The illustrations are based on two end members of a theoretical model which assumes that the inlet opening is placed entirely over one single lamina. In reality, the location of the inlet opening cannot be controlled entirely and width of laminae will show variations with respect to the inlet opening and tip-seal diameter. In laminated heterogeneous rock, the values measured by the minipermeameter will always reflect an average permeability of the sampled heterogeneity. This average value may reflect an arithmetic, geometric or harmonic mean, depending on way the heterogeneity is sampled.

In Chapters III and IV, measurements are averaged for the purpose of contrast characterization. It should be realized though that the individual measurements are already average values of the sampled heterogeneity. The presented contrasts between laminae of higher and lower permeability and between foresets and bottomsets are evidence of heterogeneity. The absolute contrasts in the cross-bed sets are probably larger than the contrasts measured by minipermeameter.

A.8 CONCLUSIONS

1) The minipermeameter is an accurate and reliable device for detailed permeability measurements. Repeatability of the measurements is within a 4% error.
2) Calibration from measured flow rates to standard permeability for the different LFE's (2cc, 20cc, 200cc and 2000cc) is determined by best-fit power regression correlations (correlation coefficients vary between 0.97 and 0.98). The correlation dependent errors are defined by 80% confidence intervals and vary between a factor 1.6 to 1.8.
3) The erroneously installed flow meter system (by-passing of gas through more than one LFE) of the "original" configuration of the minipermeameter have been advantageous for the accuracy of calibration, especially in the high permeability range.
4) The response of the minipermeameter depend on "internal" and "external" factors. The "internal" factors are basically errors in the calibration and measurement related errors

(e.g. errors in repeatability, data out-liers). The "external" factors are climate (gas viscosity and manometer response), operation of the device (wrongly chosen LFE: Turbulence effects or gas-slippage effects) and outcrop face (gas leakage, weathered rock surface, flow geometry of gas).

5) The flow geometry in a laminated heterogeneous sample depends on the permeability contrast between the laminae, the thickness of the laminae and the location and diameter of the tip-seal and inlet opening of the probe. In the case that the probe is placed over a high permeable lamina, the measured permeability will reflect the permeability of the lamina. In the case that the probe is placed over a low permeable lamina, the gas will tend to stream into the neighbouring high permeable laminae, and the measured permeability is reflecting an average permeability of the low- and high permeable laminae.

APPENDIX B
STATISTICAL ANALYSIS
OF PERMEABILITY DATA

B.1 INTRODUCTION

Reservoir modelling requires estimates of reservoir properties that adequately describe fluid flow. For instance, permeabilities sampled by means of a minipermeameter, yield a number of measurements which have to be analyzed. Usually, the dataset obtained is large and difficult to evaluate unless it is ordered in some fashion. Histograms and cumulative frequency plots are consistent and unbiased methods to characterize the distribution of a dataset from which the optimal averaging technique is judged.

The distribution of permeability data is still controversial. Semi-empirical studies (Kozeny 1927, Carman 1937, Berg 1970, van Baaren 1979) show that permeability is an exponential function of porosity and grain size. From the facts that grain sizes often show a log-normal distribution and porosity is usually normally distributed, Desbarats (1988) concludes that permeability must be log-normally distributed. However, the number of examples of non-log-normal-distributed permeabilities is on the increase (Jensen *et al.* 1987, Tyler *et al.* 1991, Gibbons *et al.* 1991, Jacquin *et al.* 1991).

Tyler *et al.* (1991) examined permeability distributions on different heterogeneity scales. Aggregate data populations (unit and facies scale) often lie inbetween a normal and log-normal distribution. Populations (unit scale) may approach log-normal distributions, while subpopulations (bed scale) may approach normal distributions.

Jensen *et al.* (1987) conclude that permeability is not necessarily log-normally distributed. However, a strictly normally distributed variable has a probability of obtaining a negative value. Hence, the permeability population distribution is defined as approximately normal.

Gibbons *et al.* (1991) have studied variograms on different scales, i.e. from the reservoir to the bed and bedform scale. They transformed permeability data

logarithmically to fit a normal distribution. Although they used the same transformation for all scales, they conclude that the optimal transformation may differ from facies to facies. They recognized that for some facies, permeability data approach a normal rather than a log-normal distribution.

Two parameters defined by the distribution of permeability are important (Corbett & Jensen, 1992);

- the value of the centre of the range around which observations tend to cluster, which is estimated by an averaging technique, and
- the spread around this centre, specified by the standard deviation.

This appendix focuses on the theoretical description of distributions and averaging methods. The distributions of minipermeameter datasets from outcrops in the Loranca Basin, Central Spain, and from cored sections of the Upper Rotliegendes Sandstone Member and the Vollpriehausen Sandstone Member of the Dutch subsurface are analyzed. Several of these data populations are divided into sub-populations corresponding to the sub-facies in cross bedding (coarse-grained foreset laminae, fine-grained foreset laminae and bottomsets). These data sub-populations are also analyzed for their distributions and a corresponding averaging method is chosen.

B.2 THE DISTRIBUTIONS

B.2.1 The normal distribution

A normal probability density distribution or Gaussian distribution is characterized by two parameters, the mean and the variance (Fig. B.1). In this case, the mean, mode and median coincide. The probability density function is symmetrical and allows the occurrence of negative variables (Aitchison & Brown, 1957). The function is given by:

$$f_x = \frac{1}{\sigma\sqrt{2\pi}} \exp\left[-\frac{1}{2}\left(\frac{x-m}{\sigma}\right)^2\right] \qquad (1)$$

in which: σ = the standard deviation

m = the mean

x = the variable

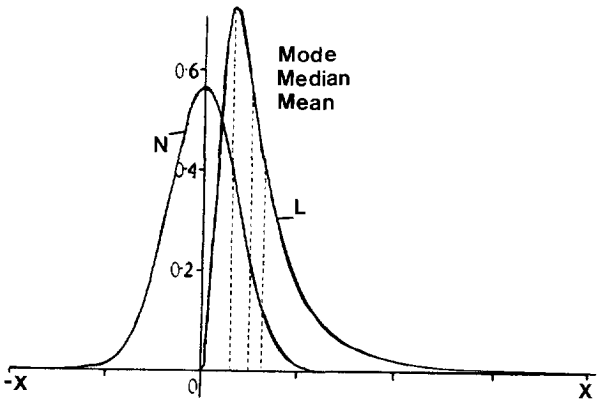

Fig. B.1 A normal (N) and log-normal (L) probability density function (modified from Aitchison and Brown 1957).

B.2.2 The log-normal distribution

The shape of a log-normally distributed probability density curve is skewed to the right (Fig. B.1). The function allows no negative variables. In this case, the mean is different from the median and the mode. A positive random variable ($Y > 0$) is log-normally distributed if its $\ln X = \ln Y$ is normally distributed (standard normal density function) and plots as a straight line (Isaaks & Shivastava 1989). The log-normal probability density function is:

$$f_y = \frac{1}{\sigma'} g_0 \left(\frac{\ln(y) - m'}{\sigma'} \right) \quad (2)$$

in which:

g_0 = the standard normal density function

m' = the logarithmic mean

σ' = the logarithmic variance

y = the variable

B.3 AVERAGING TECHNIQUES

B.3.1 The arithmetic average

The arithmetic average (m_a) is:

$$\overline{m}_a = \frac{1}{n} \Sigma x_i \quad (3)$$

in which:

n = the total number of data

x_i = the ith sample value.

For the simple case of a heterogeneous formation consisting of parallel beds of uniform permeability, the effective permeability parallel to the bedding can be derived from the arithmetic mean of the permeabilities (Weber 1972, Desbarats 1988) (Fig. B.2). Grindheim & Aasen (1991) conclude that the arithmetic average severely overestimates the effective permeability in most cases. This is only true for log-normally distributed data. If data populations are distributed approximately normally, the arithmetic mean is the best averaging technique for deriving the effective permeability.

B.3.2 The harmonic average

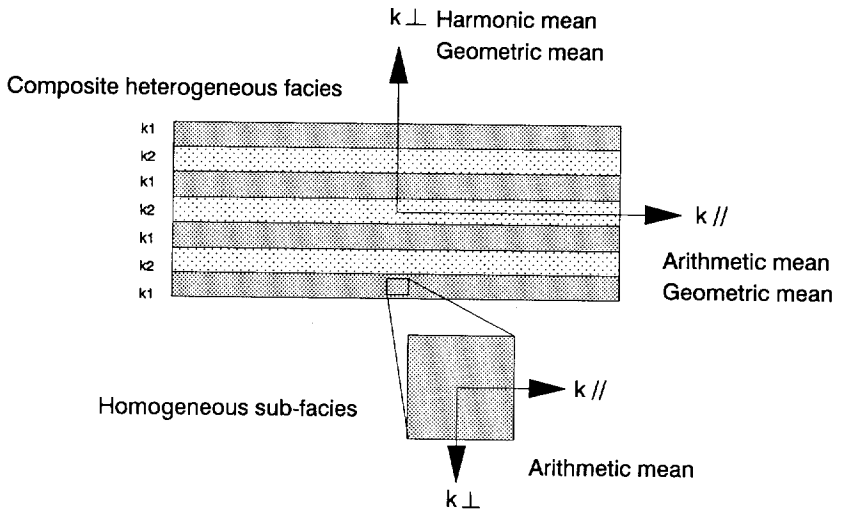

Fig. B.2 Effective permeability perpendicular ($k_\perp$) and parallel ($k_{//}$) to a laminated (composite) heterogeneous facies. Calculation of $k_\perp$ by the Harmonic- or geometric averaging method and of $k_{//}$ by the arithmetic or geometric averaging method depend on the distribution of permeability data. If in a sub-facies, the distribution of permeability data is approximately normal, the arithmetic averaging method is applied to calculate $k_\perp$ and $k_{//}$.

The harmonic average (m_h) is:

$$\overline{m}_h = \frac{n}{\Sigma \frac{1}{x_i}} \qquad (4)$$

in which: n = the total number of data

x_i = the ith sample value.

For a heterogeneous formation consisting of parallel beds of uniform permeability, the effective permeability perpendicular to the bedding is the harmonic mean of the permeabilities (Weber 1972, Debarats 1988) (Fig. B.2). The harmonic average underestimates the effective permeability according to Grindheim & Aasen (1991).

B.3.3 The geometric average

The technique is well suited for a log-normally distributed permeability population (Grindheim & Aasen 1991). The conditional distribution of ln x, given the sample values x_1, x_2, x_3,...., x_n, is a normal distribution, with mean (Rendu 1979):

$$E[\ln x(x_1, x_2, x_3, \ldots . x_n)] = C + \Sigma b_i \ln x_i \qquad (5)$$

in which: C = a constant

x_i = the ith sample value

b_i = the weight given to the ith sample value x_i.

If the logarithmic parameters of equation 5 [lnx (x_1, x_2,..., x_n)] are transformed to normal parameters, the mean of the population becomes:

$$E[x(x_1, x_2, x_3, \ldots, x_n)] = C' + \exp(\Sigma b_i \ln x_i) \qquad (6)$$

in which: C' = a constant

x_i = the ith sample value

b_i = the weight given to the ith sample value x_i.

The last term can also be written as:

$$\exp[b_1 \ln x_1, b_2 \ln x_2, \ldots, b_n \ln x_n] = \prod_i (x_i)^{b_i} \qquad (7)$$

in which: x_i = the ith sample value

b_i = the weight given to the ith sample value x_i.

The equation for the geometric average is:

$$\overline{x_g} = \prod_i (x_i)^{\frac{1}{n}} \qquad (8)$$

in which: n = the total number of data

x_i = the ith sample value.

The equation for the geometric average (8) is similar to the equation for the mean of a log-normally distributed population (7).

The geometric mean is therefore the best technique for calculating the effective permeability of a log-normally distributed population of permeabilities. In a formation consisting of parallel beds of uniform permeability, the geometric average over- or underestimates the effective permeability, depending on the direction of averaging to bedding. This averaging technique is used traditionally for estimating the vertical effective permeability of a horizontally layered system (Fig. B.2).

B.4 APPLICATIONS OF AVERAGING TECHNIQUES TO MINIPERMEAMETER DATA

A set of very detailed permeability data, such as those sampled over a grid with a minipermeameter, comprises so much information that it is difficult to apply these data in a reservoir characterization study. A minipermeameter dataset can be used in various ways. It may be applied to identify the permeability variations present in sedimentary structures (Hurst & Rossvoll 1991, Hartkamp & Donselaar 1993). Alternatively, it may also be applied to characterize permeability contrasts between individual subfacies in sedimentary structures (Hartkamp *et al.* 1993). The datasets may also be used in larger-scale reservoir characterization studies (Dreyer *et al.* 1990, Martinius *et al.* 1993). Each scale of interest involves a specific sampling density.

Hurst & Rossvoll (1991) claim that a sampling density of 5 to 10 mm is required to detect the variation of permeability on lamina scale in cross-bedded cores within a 5% error. This is correct for determining a specific permeability contrast between a few laminae. However, for the purpose of characterizing a permeability heterogeneity in e.g. cross-beds, averaging of permeability data is a routine procedure and therefore, less dense grids may be used to find the characteristic permeability contrast between laminae over larger areas. The optimal grid spacing must still be within the scale of the sampled heterogeneity.

Statistical analysis of data allows unevenly distributed grids. In case of

characterization of permeability contrast between laminae in foresets and between foresets and bottomsets of cross-beds, the optimal grid spacing may be 0.5 to 1 cm in vertical columns while the horizontal spacing between the columns may increase to 5 to 10 cm.

Up-scaling of minipermeameter data for the purpose of reservoir-unit scale permeability characterization often requires sub-grid sampling (Martinius *et al.* 1993). For up-scaling procedures, a geostatistical averaging method, such as Kriging, is used to derive a linear estimate of point values. Geostatistical analysis requires evenly squared grids so that the heterogeneity is sampled optimally (Soeters 1992).

B.5 DATA POPULATION ANALYSIS

Minipermeameter datasets of cross-bedded outcrops in the Loranca basin, Spain, and cored sections of the Upper Slochteren Sandstone Member and the Vollpriehausen Sandstone Member of the Dutch subsurface were analyzed for their distributions, to determine the optimal averaging procedure. This was also done for sub-populations of data, corresponding to subfacies in the sedimentological units.

B.5.1 Outcrop datasets, Huete, Spain.

Figure IIIA.11, Chapter III shows a histogram of dataset 89-1 (Hartkamp & Donselaar 1993). This dataset was used for a detailed statistical analysis. The dataset shows an approximately normal distribution. Figure B.3, 90.I to 90.XVII show histograms of additional outcrop permeability data populations and their sub-populations. Data populations of I, III, VI, XV, XVII and the combined histogram of datasets IX, X and XI are log-normally distributed. Datasets II, IV, V, VII and VIII are approximately normally distributed. There are several datasets that show a number of distinct peaks, others show a mass of data spread over several classes. Some histograms clearly present a population of permeability data composed of sub-populations.

Sub-populations were created by dividing the permeability data populations into sub-populations corresponding to foreset and bottomset and, if possible, to the sub-facies

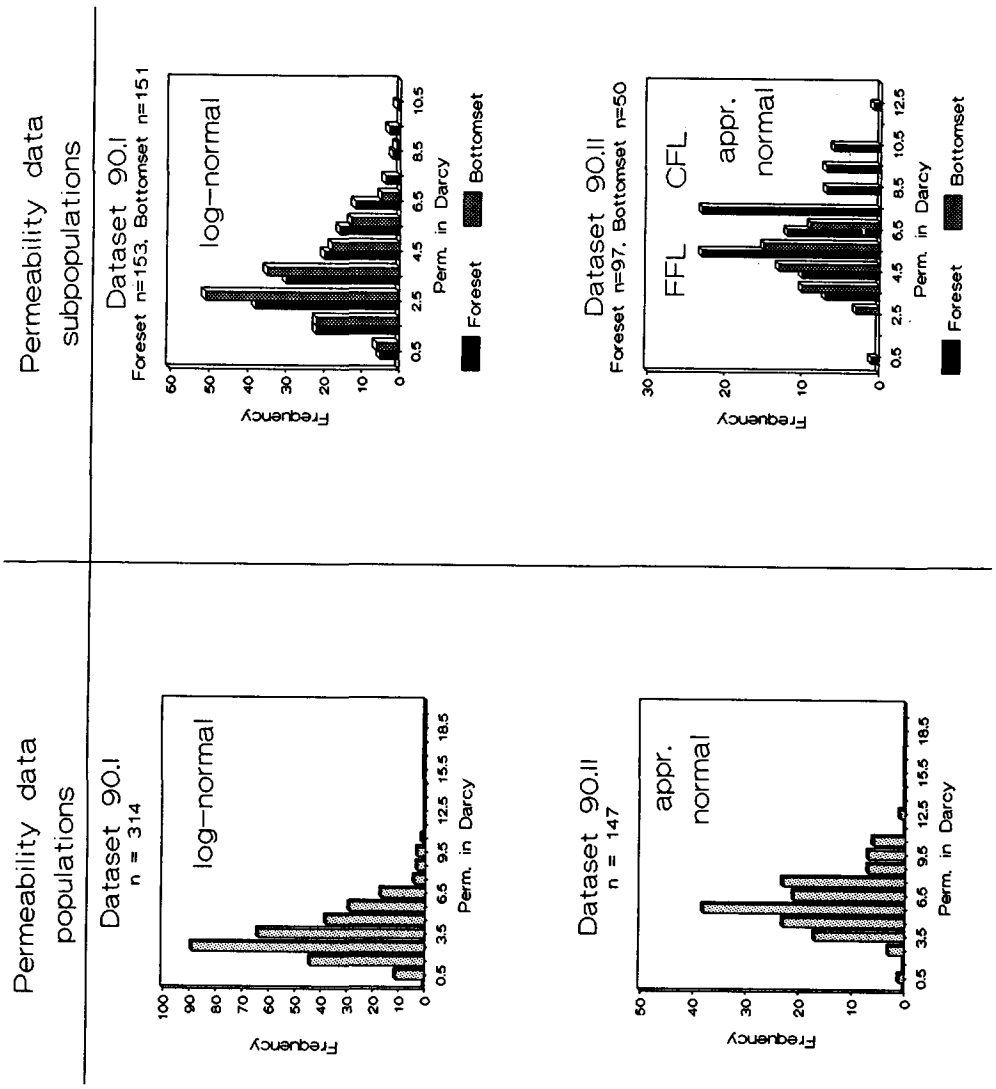

Fig. B.3 to be continued

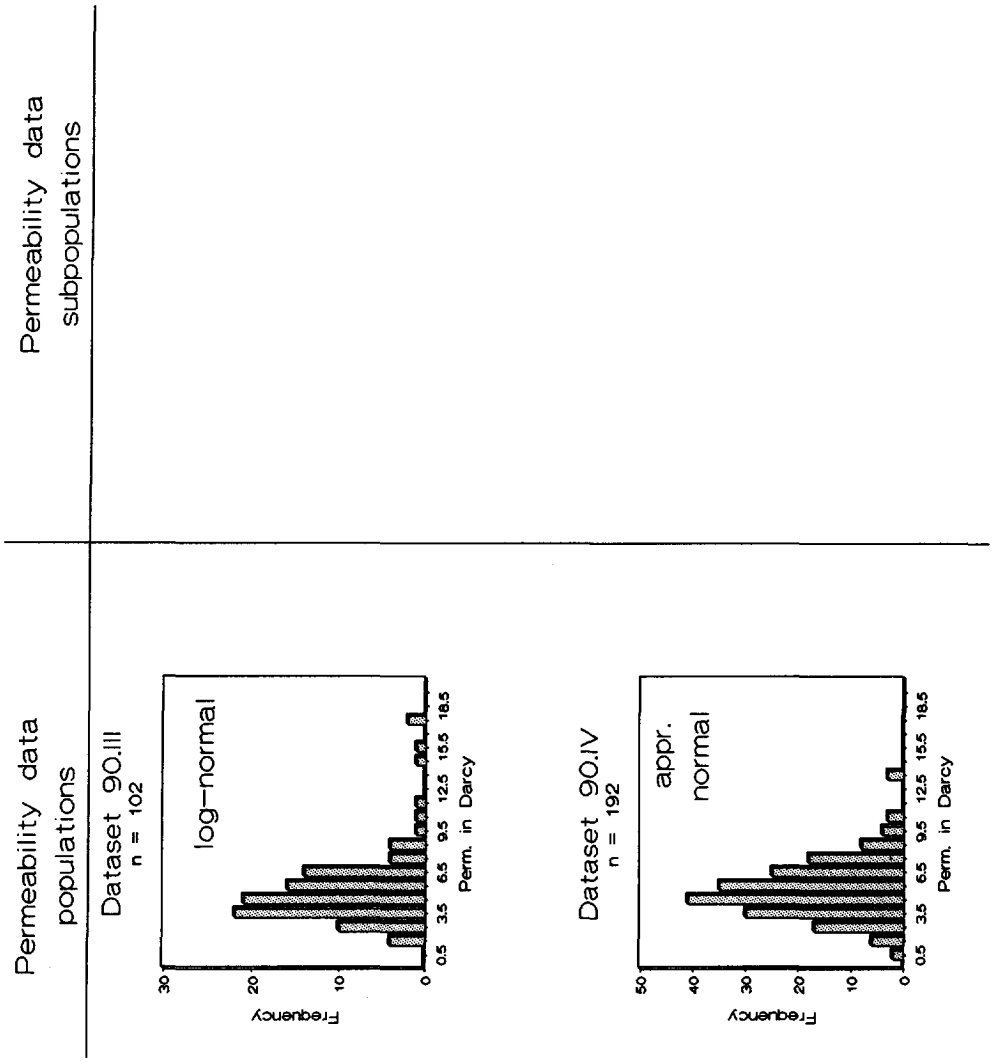

Fig. B.3 to be continued

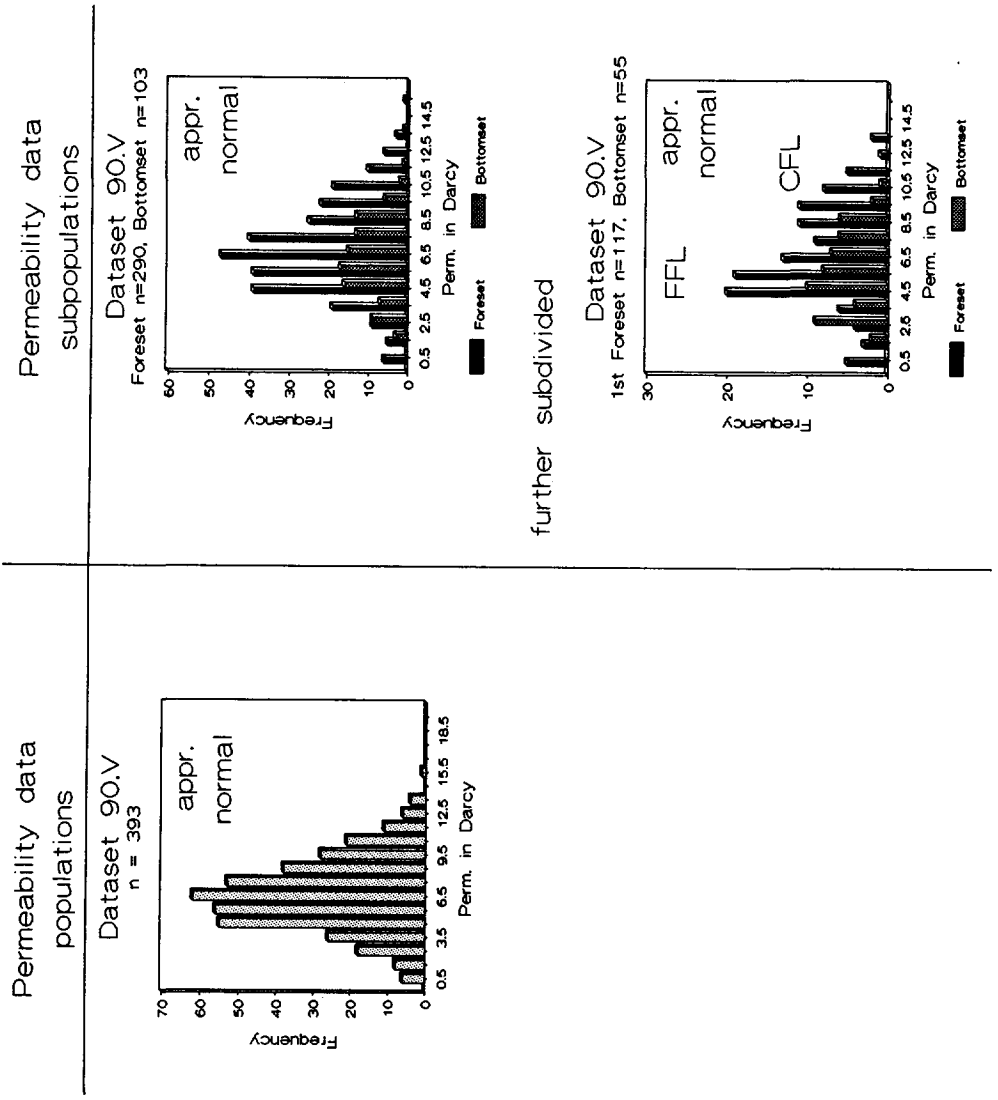

Fig. B.3 to be continued

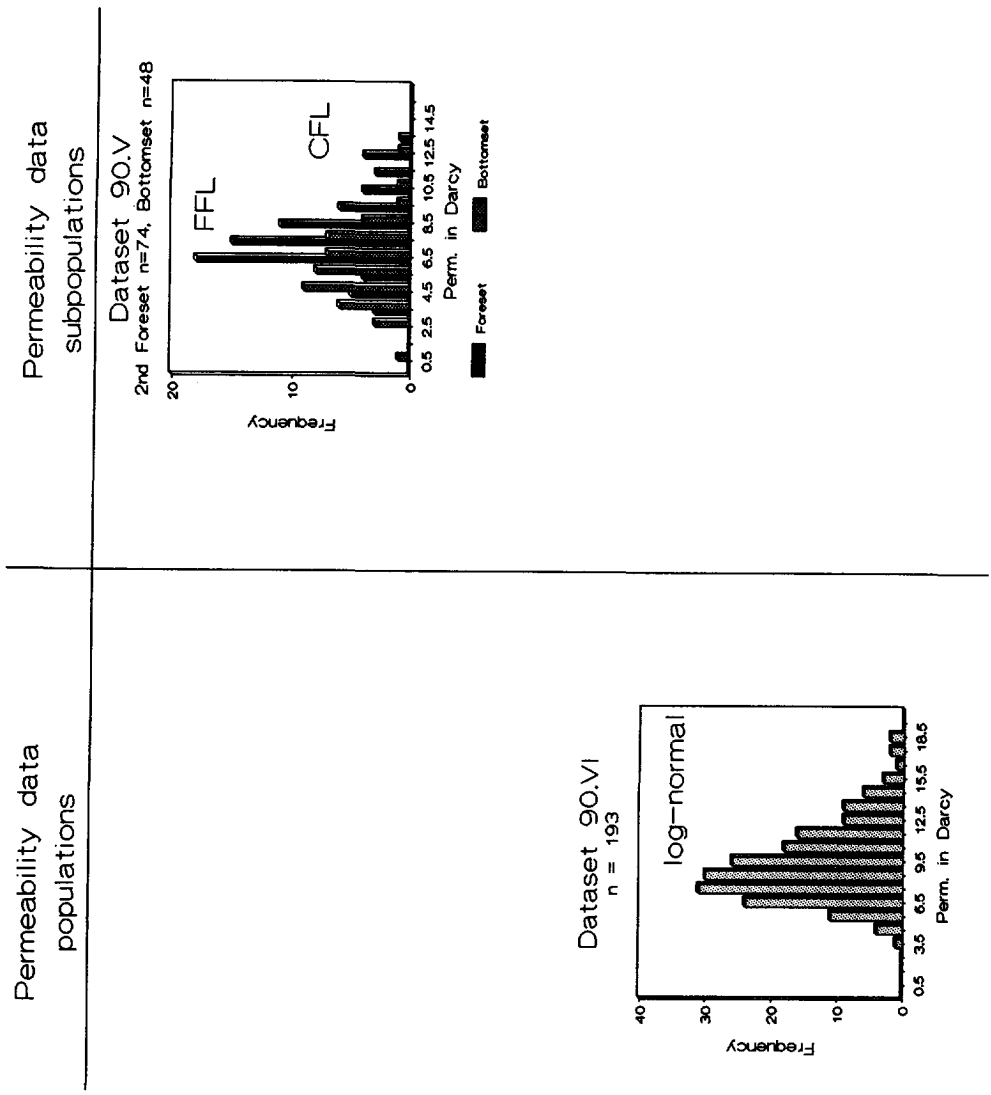

Fig. B.3 to be continued

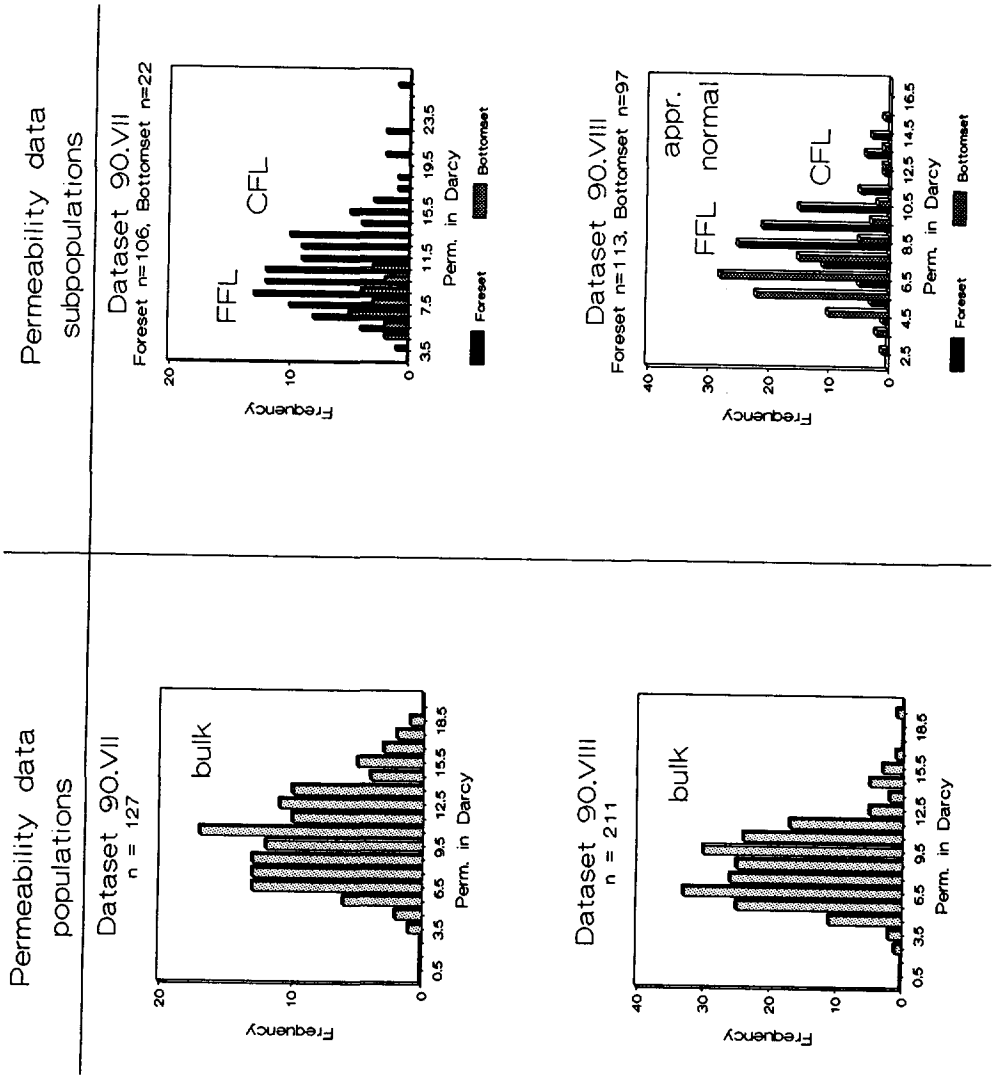

Fig. B.3 to be continued

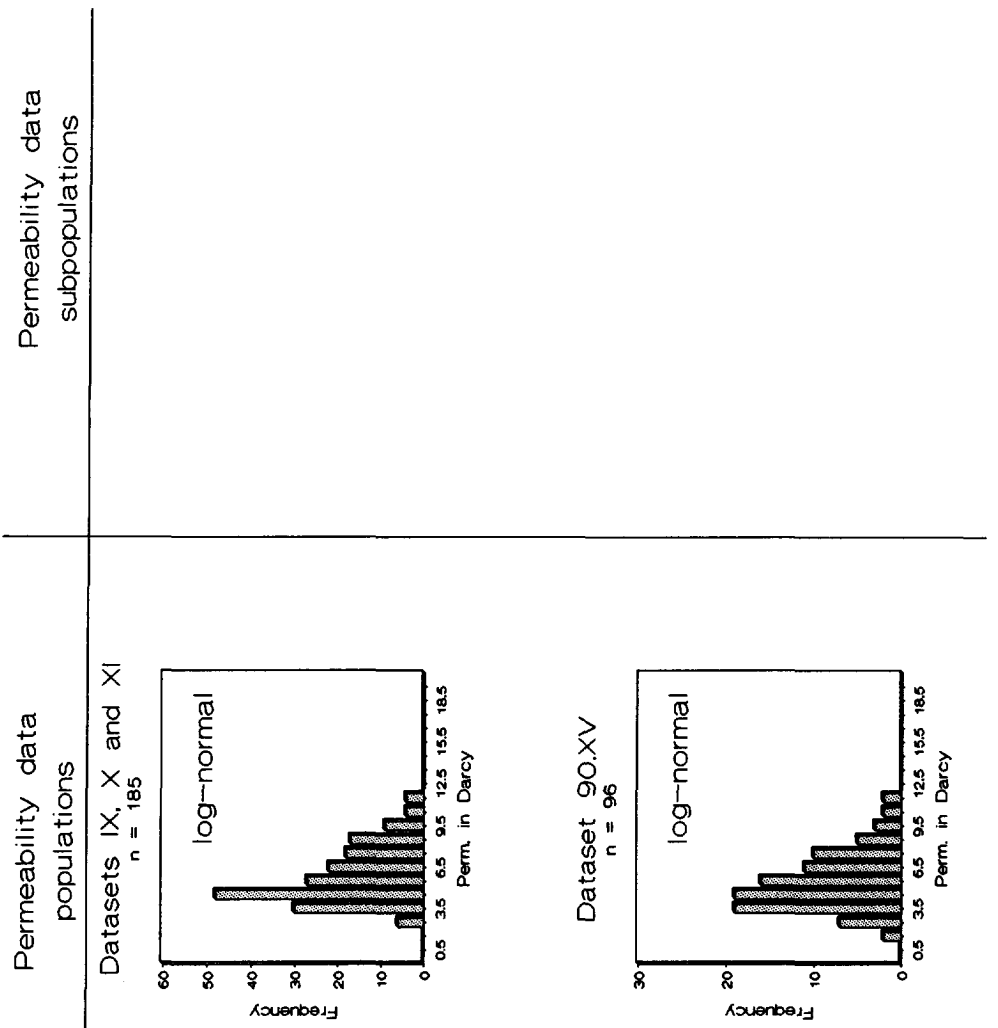

Fig. B.3 to be continued

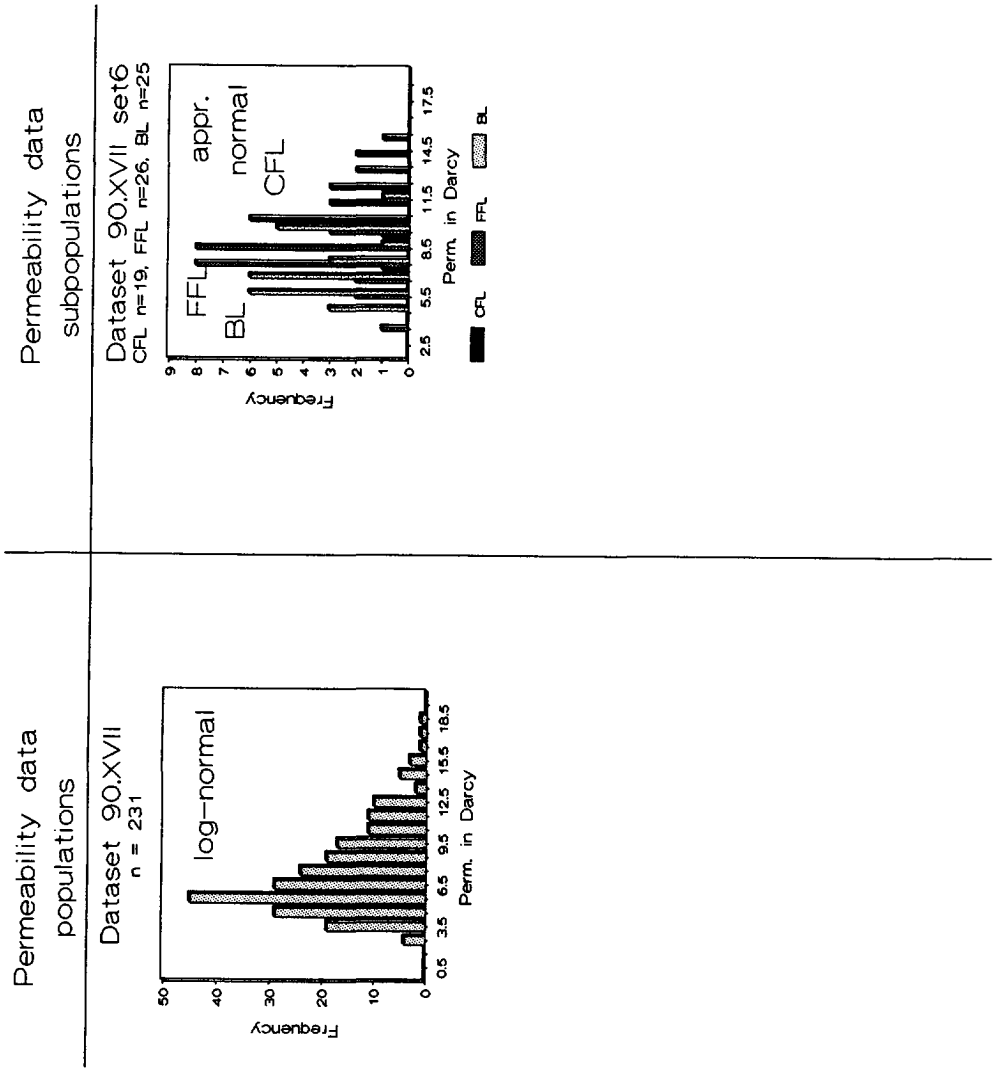

Fig. B.3 Frequency distributions of permeability datasets of composite heterogeneous facies; cross-bedded sandstones, Loranca Basin, Central Spain (90.I to 90.XVII) and additional frequency distributions of sub-datasets, corresponding to relatively homogeneous sub-facies. The number (n) of the datasets are presented on top of each graph. Approximately normal, log-normal or bulky distributions are indicated. Coarser-grained foreset laminae (CFL), finer-grained foreset laminae (FFL) and bottomset (BL) frequency peaks, if detectable, are marked.

in the foreset (CFL and FFL sets of data). Histograms were made if the number of data was sufficient (Fig. B.3, 90.I to 90.XVII). These sub-populations were tested for their distributions. The following observations can be made on the basis of these graphs: 1) Sub-populations are generally approximately normally distributed, however, log-normal distributions also occur. 2) Foreset data distributions often show two distinct frequency maxima with a 2 to 5 Darcy difference. 3) Maxima in frequency of bottomset data often fall in the same class as the lower-permeability peak of the foreset distribution.

B.5.2 Datasets of cored sections of the Vollpriehausen Sandstone Member and the Upper Slochteren Sandstone Member, The Netherlands

Permeability datasets of cored sections of laminated Vollpriehausen Sandstone Member and Upper Slochteren Sandstone Member reservoir rock were tested. Examples are presented in histograms of entire datasets and additional sub-populations in Fig. B.4. The sub-populations are based on parts of the cored sections with identical sedimentological characteristics. A subdivision in foreset-bottomset was impossible as a result of the small number of data in the cored part of one cross-bed.

In the histograms of datapopulations and sub-populations (Fig. B.4) the following characteristics can be observed: 1) The distribution is often log-normal, and 2) Most histograms show a number of frequency maxima. Histograms of sub-populations show that: 1) Sub-populations have an approximately normal distribution and 2) Only one frequency maximum is apparent.

B.6 DISCUSSION

The fact that permeability datasets occasionally are approximately normally distributed was already mentioned in the introduction of this appendix (Jensen *et al.* 1987, Tyler *et al.* 1991, Gibbons *et al.* 1991, Jacquin *et al.* 1991). When the sampled facies is homogeneous with respect to grain size, sorting and porosity, the probability density

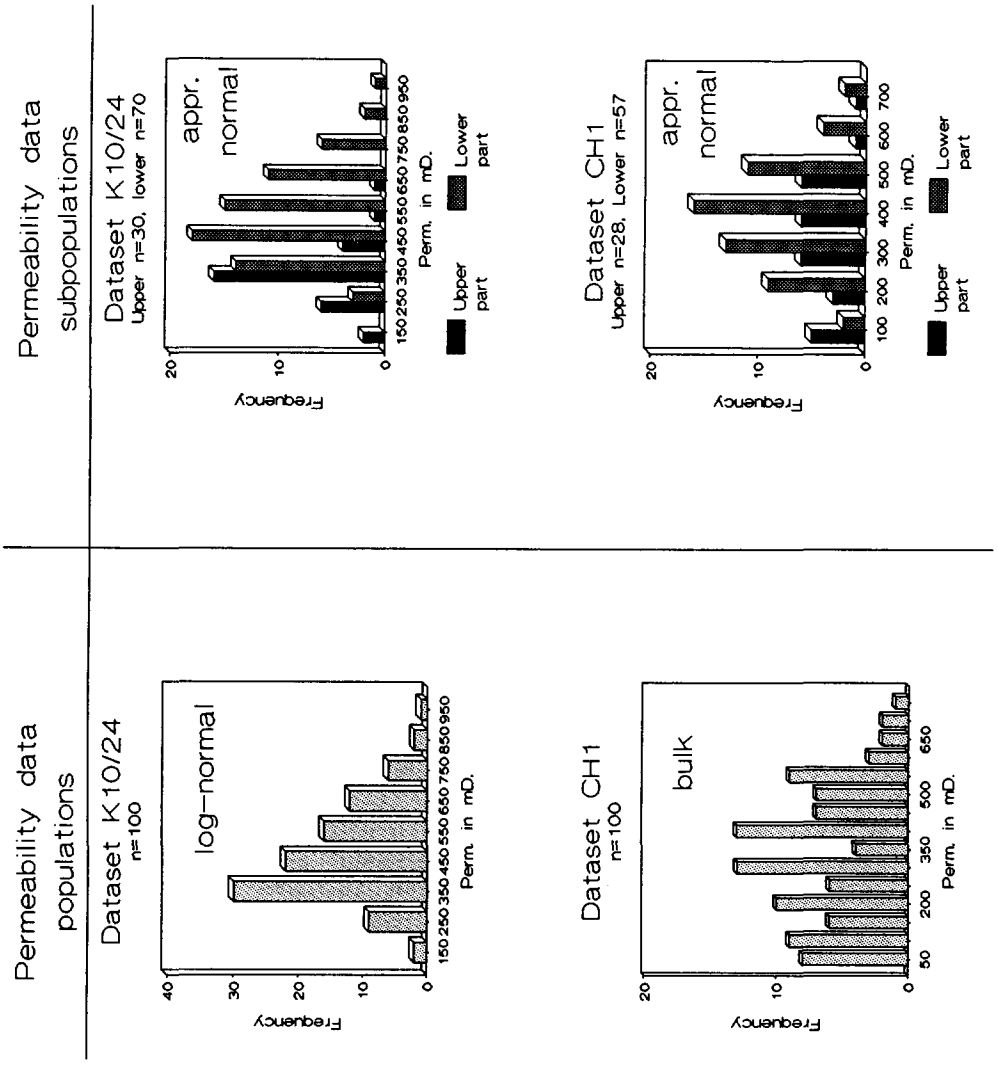

Fig. B.4 to be continued

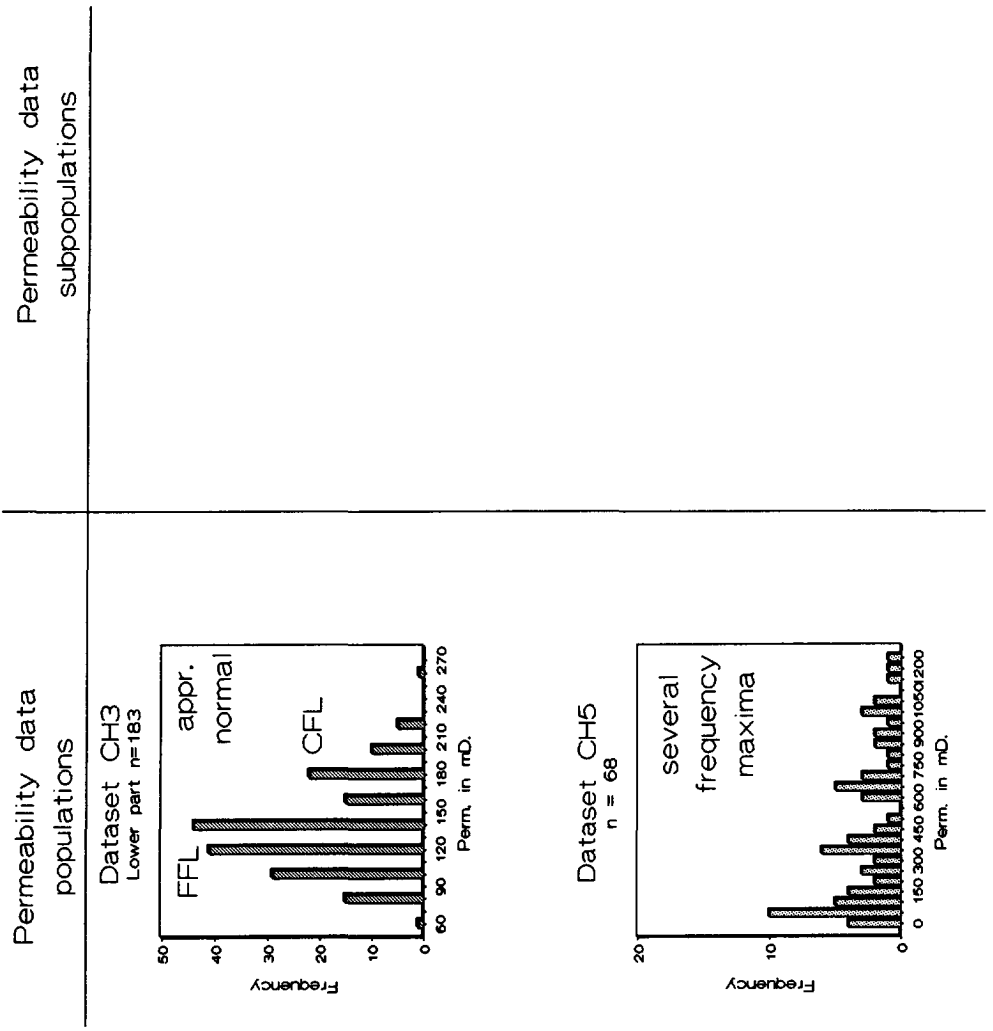

Fig. B.4 to be continued

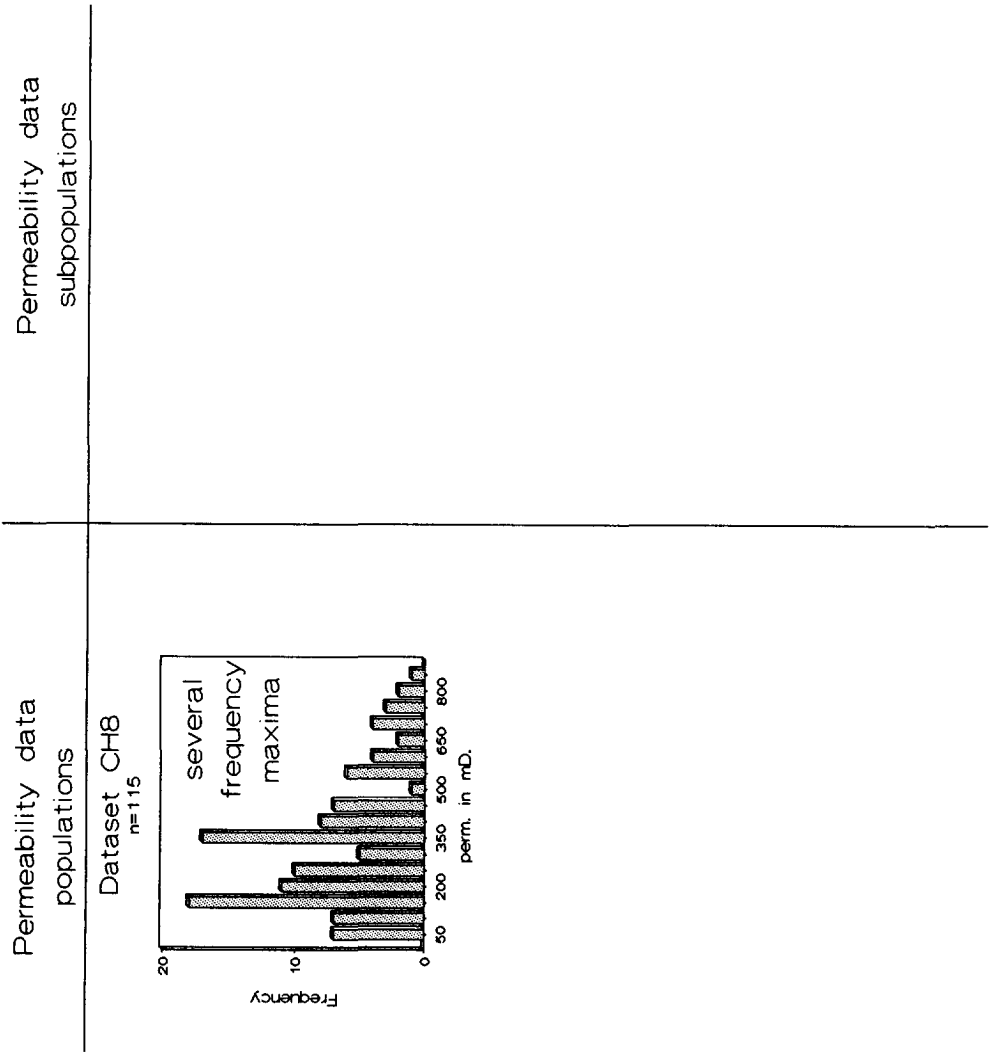

Fig. B.4 Frequency distribution of composite permeability datasets of cored sections of laminated reservoir sandstones of the Dutch subsurface and additional frequency distributions of sub-datasets, corresponding to relatively homogeneous sub-facies. The number (n) of the datasets are presented on top of each graph. Approximately normal, log-normal or bulky distributions are indicated. Coarser-grained foreset laminae (CFL), finer-grained foreset laminae (FFL) and bottomset (BL) frequency peaks, if detectable, are marked.

function of a permeability dataset approaches a normal distribution. In case of a heterogeneous facies, i.e. assorted grain sizes, sorting and porosity, the probability density function of a permeability dataset approaches a log-normal distribution. When a heterogeneous facies consists of distinct homogeneous sub-facies, the probability density function may be between a normal and log-normal distribution.

The permeability data populations, presented in this thesis, are collected at cross-bedded or laminated sandstones. Permeability data populations show either approximately normal or log-normal distributions. Foreset datasets often show two distinct frequency maxima with a 2 to 5 Darcy difference according to the occurrence of two distinct sub-facies, the coarser-grained foreset laminae (CFL) and finer-grained foreset laminae (FFL). The sub-facies are characterized by nearly homogeneous sedimentological facies (grain size, sorting and porosity). Their distributions are approximately normal. The optimal method for calculating the mean of data subpopulations is the arithmetic averaging technique.

B.7 CONCLUSIONS

1) The probability density function of a permeability dataset sampled over a heterogeneous facies composed of assorted grain sizes, sorting and porosity approaches a log-normal distribution.

2) The probability density function of a composite permeability dataset sampled over a heterogeneous facies composed of distinct homogeneous sub-facies (homogeneous grain size, sorting and porosity characteristics), is between a normal and a log-normal distribution.

3) The number of frequency maxima in composite population histograms reflects the occurrence of a number of distinct sedimentological facies.

4) Data sub-populations corresponding to facies with sedimentological homogeneous characteristics (homogeneous in terms of grain size, sorting and porosity) have an approximately-normal distribution.

5) The mean of data sub-populations corresponding to a homogeneous sub-facies is best

characterized by the arithmetic averaging method.

APPENDIX C
ANALYSIS AND APPLICATION OF ESTIMATED PERMEABILITY "THE VAN BAAREN EQUATION"

C.1 INTRODUCTION

Many attempts have been made to derive a general expression that relates fluid flow to the properties of reservoir rock. One of the earliest was by Slichter (1899) who derived a theoretical relationship based on the uniform packing of spheres. He concluded that the rate of fluid flow should be proportional to the square of the grain diameter and to a factor that was based on packing of grains. These basic elements have later been implemented in experimental and theoretical equations (Kozeny 1927; Carman 1937; Krumbein & Monk 1942; Berg 1970; van Baaren 1979).

Van Baaren (1979) presented a semi-empirically determined relationship between permeability and grain size, sorting, porosity and the degree of cementation. This equation was developed for quickly deriving a general estimate (with a 20% confidence) of permeability from sidewall samples and core plugs of clean (low interstitial clay content) sandstones.

The question whether the van Baaren equation (1979) is adequate for permeability calculations and contrast determination on laminae scale is tested and resolved in the next sections. First, five artificial sandstones (from the minipermeameter calibration set) with controlled grain sizes, sorting, porosity and liquid permeabilities will be used for permeability determination with the van Baaren equation. The sensitivity of the estimate is tested for the different variables in the equation. Subsequently, the equation is used to estimate the permeabilities of core plugs from reservoir rocks of which minipermeameter measurements were available. These estimates are compared to the plug (gas) permeabilities and average minipermeameter permeabilities.

C.2 THE VAN BAAREN EQUATION

A semi-empirical expression of permeability (k in mD) was obtained by van Baaren (1979) and resulted in:

$$k = 10\, D^{2}_{dom}\, C^{-3.64}\, \phi^{(m+3.64)} \qquad (1)$$

in which:

D_{dom} = dominant grain size (μm)

C = a constant derived from the sorting (Table C.I).

ϕ = porosity (fraction of bulk volume)

m = cementation factor (Table C.II).

Table C.I Constant of sorting (C) and its relation to the spread in dominant grain size.

Sorting	C	$D_{dom.}max/D_{dom.}min$
extremely well to very well	0.70	2.5
very well to well	0.77	
well	0.84	3.5
well to moderately	0.87	
moderately	0.91	8.0
moderately to poorly	0.95	
poorly	1.00	

The equation was developed for quickly deriving a general estimate of permeability from log derived porosity and dominant grain size and sorting characteristics. Permeability, calculated with porosity-log information corresponded, on average within 50% confidence, with subsequently measured core permeabilities. Application of the equation to core plugs using measured porosities increased the accuracy of the estimates to

Table C.II, Relation of cementation factor (m) and sand consolidation.

Consolidation	Cementation factor, m	
	atmospheric	in-situ
unconsolidated	1.4	1.6
unconsolidated-friable	1.5	1.7
friable	1.6	1.8
friable-hard	1.7	1.9
hard	1.8	2.0
very hard	2.0	2.2

about 20% in clean sandstones (van Baaren 1979).

C.3 SENSITIVITY OF THE EQUATION

C.3.1 Method

To test the sensitivity of the equation, five artificially constructed sandstones were used for quick-look estimates of permeability. The five sandstones were constructed such that grain size, sorting, cementation and porosity were fully controlled. The permeability of the sandstones was determined by means of a liquid permeameter (see section "Calibration" in Appendix A). Since this method is based on the Darcy principles (1856), the outcomes are considered as a standard and hence, liquid permeabilities were used for calibrating the minipermeameter. Porosity was measured by means of a Boyle's law porosimeter (van Rijn 1992).

C.3.2 Results

In Table C.III, grain sizes, porosities, liquid permeabilities and calculated permeabilities are listed according to different variables. The van Baaren estimated permeability is of the same magnitude as the measured liquid permeability.

Table C.III, Liquid and van Baaren-calculated permeabilities of artificial sandstones (C is sorting constant, m is cementation factor).

				A	B	C	D
Grain size	Porosity		Liquid	van Baaren C = 0.7 m = 1.6 Real porosity	van Baaren C = 0.77 m = 1.4 Real porosity	van Baaren C = 0.77 m = 1.6 Real Porosity	van Baaren C = 0.7 m = 1.6 Porosity 39.2%
(μm)	(%)		(mD)	(mD)	(mD)	(mD)	(mD)
110	41.74	------	5227	4552	3832	3218	3280
160	37.52	------	6092	5513	4741	3897	6940
226	40.03	------	10945	15436	13104	10911	13847
275	39.03	------	12640	20009	17072	14143	20502
320	37.72	------	13398	22677	19480	16029	27760

Figure C.1 shows the measured liquid permeability and the estimated permeability according to different variables for sorting and cementation. Curve A (liquid) is very smooth except for the stepward increase between the second and third sample. All van Baaren calculated permeability curves are steeper but show a similar trend as the liquid curve. The curve that fits best with the known sorting and cementation of the artificial sands is curve B. In this curve sorting is extremely good (C = 0.7) and the sandstone is of a friable character (m = 1.6). Curves C and D are illustrative for the way the estimated permeability changes if one or both variables are changed. The stepwise trend in the curves is caused by the difference in porosity of the samples. The porosity versus grain-size graph (Fig. C.2) illustrates this trend well.

In Fig. C.3 curves A and B are resp. the liquid curve and the van Baaren curve (Table C.III, column C; C = 0.77 and m = 1.6). Curve C, however, shows the

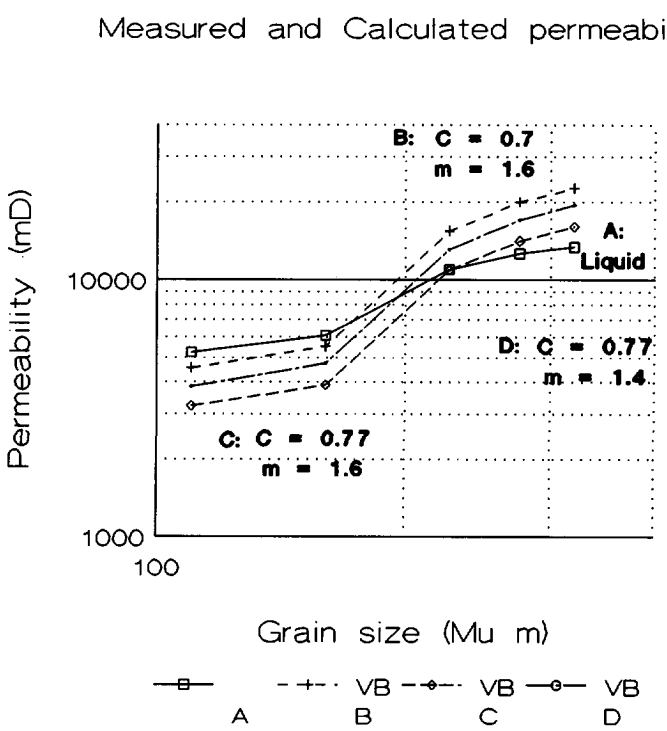

Fig. C.1 Crossplot of measured and calculated permeabilities versus grain size of artificial sandstone samples. Curve A represents the measured liquid curve. Curves B, C and D represent Baaren estimated permeabilities with different constant parameters for C (constant of Sorting) and m (cementation factor).

outcomes of the van Baaren equation given a constant average porosity of 39.2% (Table C.III, column D). In this last curve, the results are fully dominated by grain size, since all other factors are constant.

The difference between the liquid and estimated curves as shown in Fig. C.3, is characterised by the contrast in permeability over the given grain-size range. The liquid curve shows a contrast (High/Low = Permeability at 320 μm and at 110 μm) of 2.56, the van Baaren curve B, shows a contrast of 5.08 and the van Baaren curve C (constant

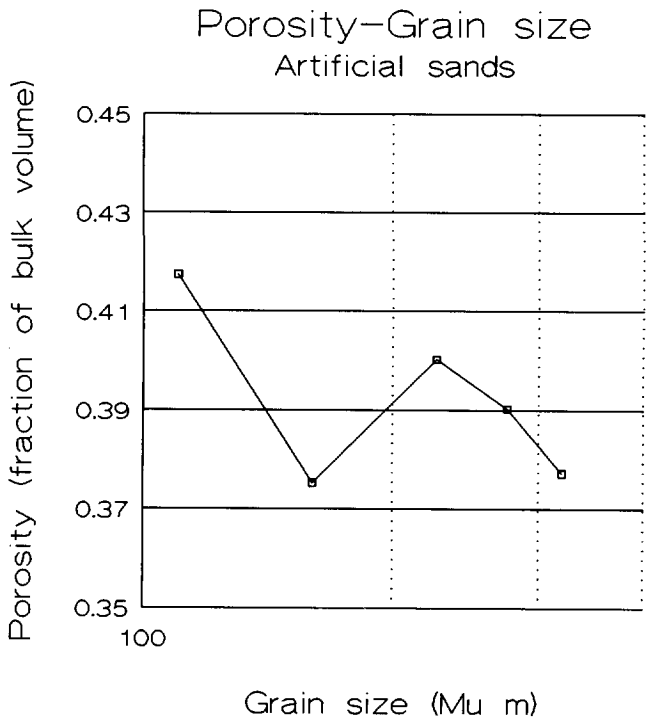

Fig. C.2 Crossplot of porosity versus grain size of the artificial sandstone samples.

porosity) shows a contrast of 8.46. Differences in contrasts are generally a factor 2 between the liquid and real porosity estimated curves (A and B) and a factor 3.3 between liquid and constant porosity estimated curves (A and C).

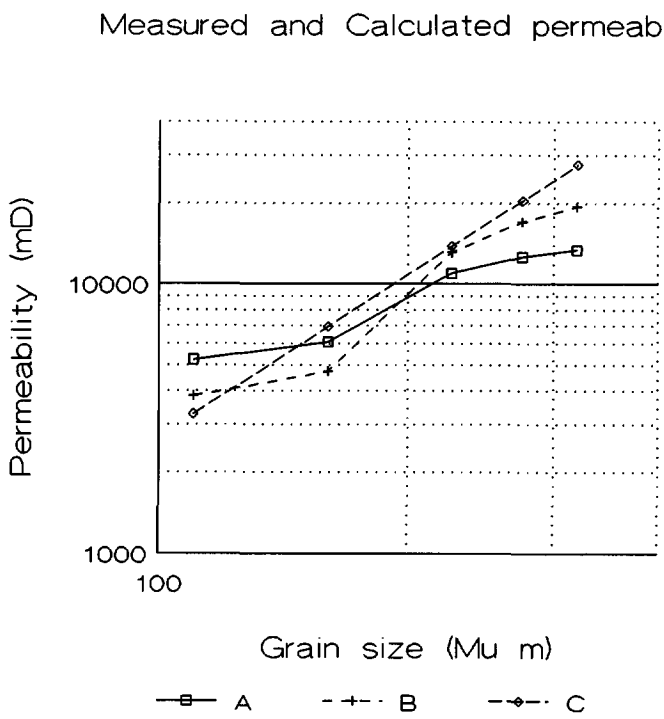

Fig. C.3 Crossplot of measured and calculated permeabilities versus grain size of artificial sandstone samples. Curve A shows the measured liquid curve. Curves B is similar to curve D in Figure 1 (C = 0.77 and m = 1.4). Curve C shows the van Baaren estimated permeabilities in the case of a constant porosity (39.2%).

C.4 COMPARISON OF PERMEABILITY CONTRASTS DETERMINED BY VAN BAAREN METHOD AND MINIPERMEAMETER

Although estimated permeability contrasts are expected to be larger than the liquid permeability contrasts, the quick-look method was used in comparing contrasts determination by minipermeameter of different sub-facies in a cross-bed. In chapter IIIB,

Table C.IV, Samples corresponding to chapter IIIB (Table I) together with van Baaren estimates in comparison with measured average permeability.

Nr.	Grain size (μm)	Sorting	Porosity (%)	Permeability (Darcy)		
				BAAREN binocular porosity	BAAREN constant poros. 37%	MINIPERM average
CFL						
1	373.71	0.80	32	5.92	12.66	10.72
2	351.11	0.20	34.6	7.87	11.18	8.49
3	297.3	0.81	31.8	3.62	8.02	8.59
4	260.62	0.79	31	2.44	6.16	4.38
5	246.56	0.72	27.8	1.23	5.51	4.9
6	200.27	0.99	18.6	0.1	3.64	10.63
7	336.81	0.74	29.6	3.2	10.29	5.73
8	154.96	0.69	19.8	0.08	2.18	9.97
9	217.64	0.82	25.4	0.6	4.3	12.68
FFL						
1	196.15	0.69	25.2	0.47	3.49	7.07
2	211.69	0.71	29.2	1.18	4.06	4.93
3	157.13	0.82	21	0.12	2.24	5.51
4	204.48	0.69	27.4	0.79	3.79	3.92
5	117.44	0.76	24.4	0.14	1.25	3.39
6	171.94	0.92	23.6	0.25	2.68	6.07
9	183.01	0.78	27.8	0.68	3.04	5.99
BL						
1	226.88	0.67	26.8	0.8	4.67	7.28
2	173.14	0.72	27.2	0.54	2.72	3.74
4	132.13	0.74	26.8	0.29	1.58	3.95
5	127.63	0.71	26.2	0.24	1.48	3.72
6	129.41	0.78	28	0.35	1.52	6
7-C	170.76	0.95	19.8	0.1	2.64	3.73
7-F	203.06	1.05	23	0.35	3.74	4.77
8-C	151.77	0.86	25	0.27	2.09	6.06
8-F	104.39	0.96	26.2	0.1	0.99	3.84

thin-section studies of cross-bedded outcrop samples provided us with detailed information about grain size, sorting and porosity of the different cross-bed sub-facies (Chapter IIIB, Table IIIB.I). Table C.IV shows average, grain size, sorting and binocular porosity of the different sub-facies together with van Baaren permeability estimates (estimated with binocular porosity and constant porosity of 37%) and average permeabilities derived by minipermeameter.

The estimated permeabilities with binocular porosity show very large differences

with the average minipermeameter measurements. This may be a result of the secondary porosity in the samples, creating larger pore throats that determine higher measured permeability values. The estimated permeabilities using a constant porosity of 37% are in better agreement with the average measured permeabilities.

In Table C.V, estimated and measured permeability contrasts of sub-facies (CFL: coarser-grained foreset laminae, FFL: finer-grained foreset laminae and BL: bottomset layers) of corresponding cross-bed samples are listed. The estimated contrasts with binocular porosity van Baaren estimates show the highest permeability contrasts. The van Baaren estimates determined with a constant porosity of 37% show permeability contrasts that are more or less a factor 2 higher than permeability contrasts determined by minipermeameter. In general, contrasts determined by minipermeameter show a same

Table C.V, Comparison of contrast in permeability. Those samples marked with (*) are contrasts between coarser- and finer-grained sub-facies.

	Binocular porosity	Constant porosity 37%	
Nr.	van Baaren	van Baaren	measured
1	6.9 : 0.5 : 1	2.7 : 0.8 : 1	1.5 : 1 : 1
2	14.5 : 2.2 : 1	4.1 : 1.5 : 1	2.3 : 1.3 : 1
3 *	31.5 : 1	3.6 : 1	1.6 : 1
4	8.3 : 2.7 : 1	3.4 : 2.4 : 1	1.1 : 1 : 1
5	5.1 : 0.6 : 1	3.7 : 0.9 : 1	1.3 : 0.9 : 1
6	0.3 : 0.7 : 1	2.4 : 1.8 : 1	1.8 : 1 : 1
7	9 : 0.3 : 1	2.8 : 0.7 : 1	1.2 : 0.8 : 1
8	0.5 : 1.7 : 1	2.2 : 2.1 : 1	2.6 : 1.6 : 1
9 *	0.9 : 1	1.4 : 1	2.1 : 1

trend as the van Baaren estimated contrasts (e.g. samples 1, 5 and 7, show a lower average permeability in the FFL than in BL.

In the former section (C.3), van Baaren contrasts were determined to overestimate permeability contrasts, especially when a constant porosity was filled in. From Table C.V it is concluded that estimated permeability contrasts (at constant porosity) generally differ

a factor 2 with the average measured permeabilities. It therefore may be concluded that errors in contrast determination by minipermeameter are likely to be small.

C.5 COMPARISON OF VAN BAAREN METHOD WITH PLUG AND MINIPERMEAMETER PERMEABILITIES

C.5.1 Method

Twenty five core plugs from fifteen cored sections of the Ten Boer Claystone Member and Upper Slochteren Sandstone Member were used to test the sensitivity of the minipermeameter and the van Baaren equation. The porosities and permeabilities of the core plugs were determined[1]. In the cored sections, holes marked the places from where the plugs had been taken. Minipermeameter measurements near such a hole were averaged arithmetically and compared to the core plug permeability. Grain size was determined empirically and the dominant grain size was entered in the van Baaren equation. The sorting and cementation was considered constant (moderately sorted, C = 0.91 and hard cemented, m = 1.8).

C.5.2 Results

Table C.VI illustrates the effectiveness of the quick-look method for estimating permeability within the range of core plug and minipermeameter permeabilities. Fig. C.4 shows the permeabilities of core plugs, minipermeameter and Baaren estimates by plug number. The curves of the minipermeameter measurements and the core plugs are very similar, except for very low plug permeability measurements. This graph shows that the minipermeameter is not effective for permeabilities below the 10 mD.

---

[1]. Nederlandse Aardolie Maatschappij, Schepersmaat 1, Assen.

Table C.VI, Porosities and permeabilities of plugs, minipermeameter and van Baaren estimates of a number of cored sections of the Upper Slochteren Sandstone Member.

Core	Porosity (%)	Plug k (mD)	Mini k (mD)	van Baaren k (mD) C = 0.91, m = 1.8
CH1	16	200	229	92.8
	19	265	229	236.36
CH2	11	65	58.25	0.31
	17	276	173.93	3.3
CH3	17	103	123.43	32.27
	20	110	123.43	78.11
CH4	17	129	140.15	129.06
CH5	17	273	238.14	129.06
	13	42		29.99
CH6	18.6	76	64.62	52.63
	18.6	239	308.26	210.52
CH7	18.4	142	125.17	352.89
	18.1	382	243.1	80.68
CH8	18.6	222	144.49	93.57
	24.9	139.2	406.97	457.39
CH9	6.9	0	48.55	0.0016
CH10	9.7	0	38.1	0.04
CH11	15	7	43.6	1.67
CH12-1	20.1	5.7	112.39	321.02
	22.5	131	242.34	592.96
CH12-2	19.2	21.3	31.8	111.21
	17.2	2.4	33.46	61.13
	14.3	237.8	243.7	201.48
CH13	14.2	22.3	154.57	48.48
	24.9	112.7	238	1829.59

The van Baaren-estimated permeabilities generally follow the trend of the plug permeabilities. However, they seem to be less consistent than the minipermeameter permeabilities. Estimated values are in cases 100 to 200 mD higher or lower than

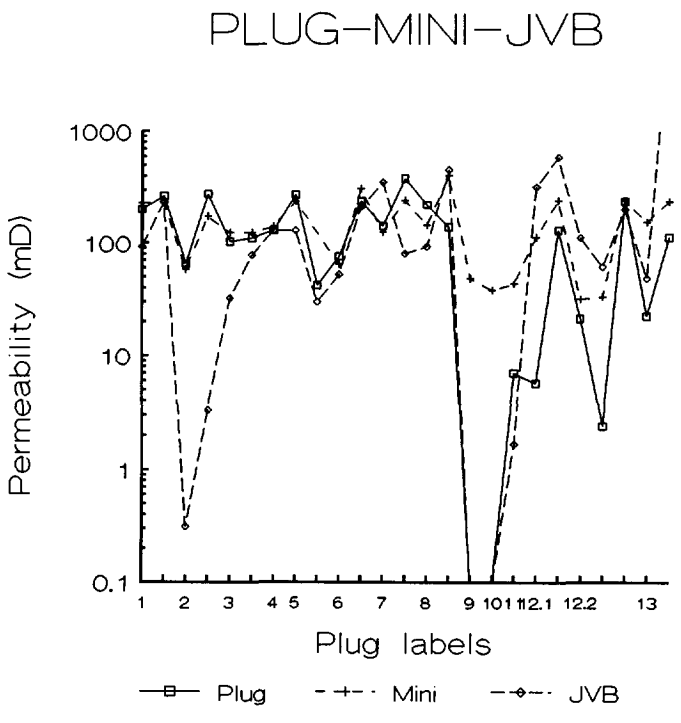

Fig. C.4 Graph showing core-plug permeabilities (Plug) of cored reservoir sections in comparison with average minipermeameter permeabilities (Mini) and van Baaren quick-look estimated permeabilities (JvB).

measured values. This is a result of errors in the determined dominant grain size, porosity or in the constants of sorting and cementation. Very low estimated values are clearly a result of low plug porosities (sample 2: 11% porosity).

C.6 DISCUSSION AND RECOMMENDATIONS

The reason that the van Baaren (1979) estimates are in the same range and show a similar trend as the determined permeabilities, but are not compatible with the liquid permeability lies perhaps in the grain-size factor. This factor is based on the assumption of a systematic packing of spherical grains (Slichter 1899, Kozeny 1927, Carman 1937). Natural sands show variations in packing and grain shapes. It is therefore recommended to determine a new factor based on shapes and packing of natural sands. For this purpose, the artificial sandstones would be ideal.

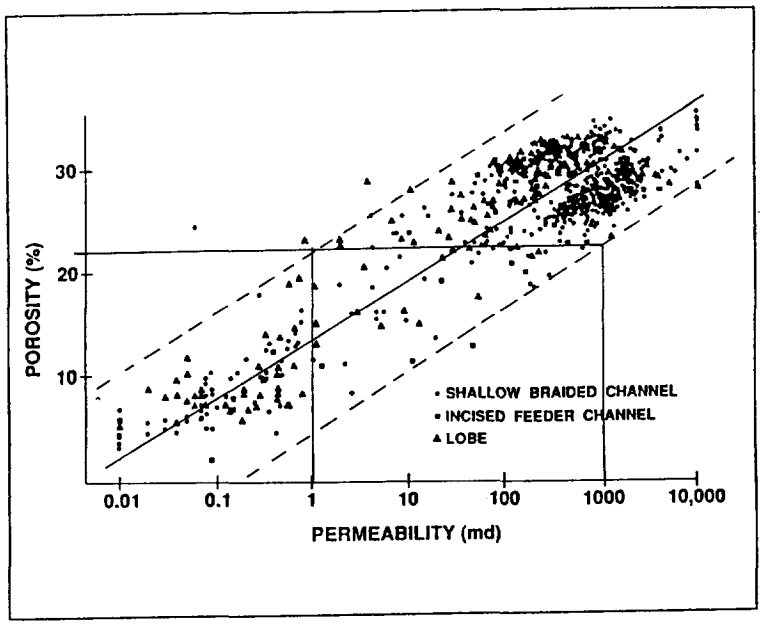

Fig. C.5 Crossplot of porosity versus permeability of 818 unstressed core-plugs of three different facies of the Balmoral Field, North Sea (after Slatt and Hopkins 1990). At a given porosity, permeability differs a factor 1000.

It is also recommended to determine a relationship between permeability and pore structure characteristics. The equation for estimating permeability is expected to be more

precise if pore diameter replaces grain size (more applicable if e.g. secondary porosity is present).

Slatt & Hopkins (1990) presented a crossplot of unstressed porosity versus permeability of 818 core plugs from 13 cored wells of Late Paleocene and younger deltaic, shelf and submarine fan deposits of Balmoral field, North Sea (Fig. C.5). Although they suggest that there is a good positive correlation between the two parameters, the spread of data is tremendous. At a constant porosity, permeability varies a factor 1000. It suggest that, since porosity is a strong parameter in the van Baaren equation ($\phi^{m+3.64}$), the estimated permeability will always show errors with respect to the apparent permeability. It is a valid method to quickly derive a general estimate of average permeability, but precise determination of permeability anisotropy in cross-bed laminae is ambiguous.

C.7 CONCLUSIONS

1) The van Baaren equation can be used for estimating a general "quick-look" permeability within a 20% accuracy.
2) The van Baaren estimated permeability is very sensitive to a change in one or more variables of the equation.
3) The van Baaren estimates of artificial sandstone samples of different grain sizes (110 to 320 μm) and carefully determined porosities (37.5% to 41.7%) generate a difference in contrast of a factor 2 with the experimentally determined liquid permeabilities. This contrast increases to a factor 3.3 in case of constant porosity estimated permeabilities.
4) It was found that the van Baaren equation is not suitable for general contrast determination in cross-bed laminae. Firstly, because the estimated contrasts are exaggerated and secondly, because small errors in determined variables may have large effects on individual estimates used for contrast determination.

REFERENCES

ABRAMS, A. (1975) The influence of fluid viscosity, interfacial tension, and flow velocity on residual oil saturation left by waterflood. *Soc. Petrol. Engineers Journ.*, **October**, 437-447.

AITCHISON, J AND BROWN, J.A.C. (1957) The lognormal distribution, Department of Applied Economics, University of Cambridge, U.K.

ALEXANDER, J. AND LEEDER, M.R. (1987) Active tectonic control on alluvial architecture. In: *Recent Developments in Fluvial Sedimentology* (Ed. by F.G. Etheridge, R.M. Flores and M.D. Harvey), *Spec. Publ. Soc. Econ. Paleont. Mineral.* **39.**, 243-252.

ALLEN, J.R.L. (1963) The classification of cross-stratified units. With notes to their origin. *Sedimentology*, **2**, 93-114.

ALLEN, J.R.L. (1970) *Physical Processes of Sedimentation*. George Allen & Unwin Ltd., London, pp. 248.

ALLEN, P.A AND ALLEN, J.R. (1990) *Basin Analysis, Principles and Applications.* Blackwell Scientific Publications, Oxford, pp. 451.

ALVAREZ-SIERRA, M.A., DAAMS, R., LACOMBA, J.I., LÓPEZ-MARTÍNEZ, N. AND SACRISTÁN-MARTÍN, M.A. (1987) Succession of micromammal faunas in the Oligocene of Spain. *Münchner Geowiss. Abh.*, **10**, 43-48.

ARCHER, J.S. AND WALL, C.G. (1986) *Petroleum Engineering; principles and practice.* Graham & Trotman, London, 362 pp.

ARRIBAS, J. AND ARRIBAS, M.E. (1991) Petrographic evidence of different provenance in two alluvial fan systems (Paleogene of the Northern Tajo basin, Spain). In: *Developments of Sedimentary Provenance Studies* (ed. by A.C. Morton, S.P. Todd and P.D.W. Haughton) *Geol. Soc. Spec. Publ.*, **57**, 263-271.

ASHLEY, G.M. (1990) Classification of large-scale subaqueous bedforms: A new look at an old problem. *Journ. of Sed. Petrol.*, **60-1**, 160-172.

BAAREN, J. VAN (1979) Quick-look permeability estimates using sidewall samples and porosity logs. *S.P.W.L.A. London, 6th Europ. Logging Conf.*, **March 26-29**, 11 pp.

BAKKEN, H. (1991) The effect of capillary forces in heterogeneous reservoirs, a streamline approach. *MSc Thesis*, Dietz Laboratory, Faculty of Mining and Petroleum Engineering, Delft University of Technology, The Netherland, **March**, 95 pp.

BAKKEN, H, BATENBURG, D. VAN, HARTKAMP-BAKKER, C.A. AND PALMGREN, C.T.S. (1991) The effect of capillary forces in heterogeneous reservoirs, a streamline approach. In: *Proceedings of the Lirkindel Petroleum Engineering Workshop*, Trondheim, Norway, 6-7 February.

BARWIS, J.H., MCPHERSON, J.G. AND STUDLICK, J.R.J. (1990) *Sandstone Petroleum Reservoirs.* Springer-Verlag, New York-Berlin, pp. 583.

BASUMALLICK, S. (1966) Size differentiation in a cross-stratified unit. *Sedimentology*, **6**, 35-68.

References

BATENBURG, D.W. VAN, BRUINING, J., BAKKEN, H. AND PALMGREN, C.T.S. (1991) The effect of capillary forces in heterogeneous "flow-units", a streamline approach. In: *Proceedings of the 66th Soc. Petrol. Engineers Annual Technical Conference and Exhibitions, Dallas*, SPE 22588, October 6-9.

BEARD, D.C. & WEYL, P.K. (1973) Influence of texture on porosity and permeability of unconsolidated sand. *Bull. Am. Assoc. Petrol. Geol.*, **57**, 349-369.

BERG, R.R. (1970) Method for determining permeability from reservoir rock properties. *Trans. Gulf Coast Ass. of Geol. Soc.*, **XX**, 303-317.

BERG, R.R. (1986) *Reservoir Sandstones*. Prentice-Hall Inc., Englewood Cliffs, New Jersey, pp. 481.

BERRUIN, N.A. AND MORSE, R.A. (1979) Waterflood performance of heterogeneous systems. *Journ. Petrol. Techn.*, **July**, 829-836.

BJØRLYKKE, K.O. (1984) Formation of secondary porosity: how important is it? In: *Clastic Diagenesis* (ed. by D.A.McDonald and R.C.Surdam) *Memoir of Am. Assoc. Petrol. Geol.*, **37**, 277-286.

BLACKBOURN, G.A. (1984) Diagenetic history and reservoir quality of a Brent sand sequence. *Clay Minerals*, **19**, 377-389.

BRELIH, D.A. AND KODL, E.J. (1990) Detailed mapping of fluvial sand bodies improves perforating strategy at Kern River Field. In: *Proceedings of SPE 60th California Regional Meeting, Paper 20080*, Ventura, California, **April 4-6**, 553-559.

BRETT FISCHBUCH, D. AND WATTENBARGER, R.A. (1991) Waterflood simulation of stratified sandstone reservoirs using dynamic pseudo curves. *Journ. of Petrol. Science and Engineering*, **5**, 219-235.

CARMAN, P.C. (1937) Fluid flow through granular beds. *Inst. Chem. Eng. Trans.*, **15**, 150-166.

CHANDLER, M.A., KOCUREK, G., GOGGIN, D.J. AND LAKE, L.W. (1989) Effects of stratigraphic heterogeneity on permeability in eolian sandstone sequence, Page Sandstone, Northern Arizona. *Bull. Am. Assoc. Petrol. Geol.*, **73**, 658-668.

CHATZIS, I. KUNTAMUKKULA, M.S. AND MORROW, N.R. (1988) Effect of capillary number on the microstructure of residual oil in strongly water-wet sandstones. *Soc. Petrol Engineers Reservoir Engineering*, **August**, 902-912.

CHATZIS, I. AND MORROW, N.R. (1984) Correlation of capillary number relationships for sandstones. *Soc. Petrol. Engineers Journal*, **October**, 555-562.

CHOUKROUNE, P., LE PICHON, X. & SEGURET, M. (1973) Bay of Biscay and Pyrenees. *Earth Planet. Sc. Lett.*, **18**, 109-118.

CLEVELAND, M.N. AND MOLINA, J. (1990) Deltaic Reservoirs of the Caño Limón Field, Colombia, South America. In: *Sandstone Petroleum Reservoirs* (Ed. by J.H. Barwis, J.G. McPherson and J.R.J. Studlick), Springer-Verlag, New York, 583 pp.

COLLINSON, J.D. AND LEWIN, J. (1983) *Modern and Ancient Fluvial Systems*. Blackwell Scientific Publications, Oxford, pp. 575.

COREY, A.T. AND RATHJENS, C.H. (1956) Effect of stratification on relative permeability. *Journ. of Petr. Techn.*, **December**, 69-71.

CORBETT, P.W.M. AND JENSEN, J.L. (1991) Estimating the mean permeability: how many measurements do you need? *Paper presented at the 3rd EAPG Meeting, Florence*, 34 pp.

CORBETT, P.W.M. AND JENSEN, J.L. (1993) Quantification of heterogeneity, a role for the minipermeameter in reservoir characterisation. Characterisation of Fluvial and Aeolian Reservoirs (eds. C.P. North and D.J. Prosser) Blackwell Scientific Publ., Oxford (in Press).

CUEVAS GOZALO, M.C. (1989) Sedimentary facies and sequential architecture of tide-influenced alluvial deposits. An example from the middle Eocene Capella Formation, South-Central Pyrenees, Spain. *Geologia Ultraiectina*, **61**, PhD Thesis; Rijks Universiteit Utrecht, 152 pp.

DAAMS, R. AND MEULEN, A.J. VAN DER (1984) Paleoenvironmental and paleoclimatic interpretation in the Upper Oligocene and Miocene of north central Spain. *Paléobiologie Continentale*, Montpellier, **14**, 241-257.

DAKE, (1978) *Fundamentals of Reservoir Engineering*, Elseviers Scientific Publishing Company, Amsterdam, 443 pp.

DARCY, H. (1856) Les Fontaines de la ville de Dijon Victor Dalmont, Paris, 590-594.

DAWE, R.A., WHEAT, M.R. AND BIDNER, M.S. (1992) Experimental investigation of capillary pressure effects on immiscible displacement in lensed and layered porous media. *Transport in Porous Media*, **7**, 83-101.

DESBARATS, A. (1988) Estimation of effective permeabilities in the Lower Stevens Formation of the Paloma Field, San Joaquin Valley, California. Soc. Petrol Eng. Reserv. Eng., November, 1301-1307.

DIAZ, C.E., CHATZIS, I. AND DULLIEN, F.A.L. (1987) Simulation of capillary pressure curves using bond correlated site percolation on a simple cubic network. *Transport in Porous Media*, **2**, 215-240.

DÍAZ MOLINA, M. (1979) Descripción del frente distal de un abanico fluvial húmedo en el Terciario continental situado al Este de la Sierra de Altomira. *Estudios Geologicos*, **35**, 119-129.

DÍAZ MOLINA, M. (1991) Geometry and lateral accertion patterns in meander loops. Examples from the Upper Oligocene-Lower Miocene, Loranca Basin, Central Spain. *IAS spec. publ.* (ed. by C. Puigdefabregas),

DÍAZ MOLINA, M., CAPOTE, R. & LOPEZ MARTINEZ, N. (1985) Wet fluvial fans of the Loranca Basin (Central Spain), channel models and distal bioturbated gypsum with chert. In: *6th I.A.S. Eur. Reg. Meeting, Excursion Guidebook.* (Ed. by Mila, M.D., and Rosell, J.), Institut d'Estudis Illerdencs (Lleida), pp. 149-185.

DÍAZ MOLINA, M., ARRIBAS MOCOROA J. AND BUSTILLO REVUELTA, A. (1989) The Tórtola and Villalba de la Sierra fluvial fans: late Oligocene-early Miocene, Loranca Basin, Central Spain. Field trip 7 of the 4th International Conference on Fluvial Sedimentology (Ed. by C. Puigdefabregas) Servei Geològic de Catalunya, Barcelona-Sitges, October.

DODGE, C.F., HOLLER, D.P. & MEYER, R.L. (1971) Reservoir heterogeneities of some Cretaceous sandstones. *Bull. Am. Assoc. Petrol. Geol.*, **55**, 1814-1828.

DREYER, T., SCHEIE, A. AND WALDERHAUG, O (1990) Minipermeameter based study of permeability trends in channel sandbodies. *Bull. Am. Assoc. Petrol. Geol.*, **74**, 359-374.

DULLIEN, F.A.L. (1988) Two-phase flow in porous media. *Chem. Eng. Techn.*, **11**, 407-424.

DYKSTRA, H. AND PARSONS, R.L. (1950) The prediction of oil recovery by waterflood. In: *Secondary recovery in the USA*, American Petroleum Institute, New York, 160-174.

EHRENBERG, S.N. (1990) Relationship between diagenesis and reservoir quality in sandstones of the Garn Formation, Halterbanken, mid-Norwegian continental shelf. *Bull. Am. Ass. Petrol. Geol.*, **74**, 1538-1558.

EIJPE, R. AND WEBER, K.J. (1971) Minipermeameter for consolidated rock and unconsolidated sand. *Bull. Am. Assoc. Petrol. Geol.*, **55**, 307-309.

FRIEND, P.F. (1983) Towards the field classification of alluvial architecture or sequence. In: *Modern and Ancient Fluvial Systems* (Ed. by J.D.Collison and J.Lewin), 345-354, *Spec. Publ. Int. Assoc. Sediment.*, **6**, Blackwell Scientific Publ., Oxford.

FOLK, R.L. (1980) *Petrology of Sedimentary Rocks*, Emphill Publishing Company, Austin, Texas, 182 pp.

GALLOWAY, W.E. AND HOBDAY, D.K. (1983) *Terrigenous Clastic Depositional Systems, Applications to Petroleum, Coal and Uranium Exploration*. Springer-Verlag, New York, pp. 423.

GARDINER, S., THOMAS, D.V., BOWERING, E.D. AND MCMINN L.S. (1990) A braided fluvial reservoir, Peco Field, Alberta, Canada. In: *Sandstone Petroleum Reservoirs* (Ed. by J.H. Barwis, J.G. McPherson and J.R.J. Studlick), Springer-Verlag, New York, 583 pp.

GARNES, J.M., MATHISEN, A.M., SCHEIE, A. AND SKAUGE, A. (1990) Capillary number relations for some North Sea reservoir sandstones. In: *Proceedings of the SPE/DOE Seventh Symposium on Enhanced Oil Recovery, Tulsa*, SPE/DOE 20264, April 22-25.

GIBBONS, K.; HALVORSEN, C. AND SIRING, E. (1991) Vertical and horizontal permeability variation within a sandstone reservoir based on minipermeameter data. *Paper presented at the Minipermeatry in Reserv. Studies Conference, Edinburgh*, **June 27-28**, 9 pp.

GLASMANN, J.R., CLARK, R.A., LARTER, S., BRIEDIS, N.A. AND LUNDEGARD, P.D. (1989) Diagenesis and hydrocarbon accumulation, Brent sandstone (Jurassic), Bergen high Area, North Sea. *Bull. Am. Assoc. Petrol. Geol.*, **73**, 1341-1360.

GLENNIE, K.W. (1990) *Introduction to the Petroleum Geology of the North Sea.* Blackwell Scientific Publ., Oxford, 402 pp.

GOGGIN, D.J., TRASHER, R.L. AND LAKE, L.W. (1988) A theoretical and experimental analysis of minipermeameter response, including gas slippage and high velocity flow effects. *In Situ*, **12**, 79-116.

GRAAFF, W.J.E. VAN DE AND EALEY, P.J. (1989) Geological modeling for simulation studies. *Bull. Am. Assoc. Petrol. Geol.*, **73**, 1436-1444.

GRINDHEIM, A.O. AND AASEN, J.O. (1991) An evaluation of homogenization techniques for absolute permeability. Lerkendal Petroleum Engineering Workshop, Trondheim, Februari.

GUSTAVSON, T.C. (1978) Bed forms and stratification types of modern gravel meander lobes, Nueces River, Texas. *Sedimentology*, **25**, 401-426.

HALDORSEN, H.H. AND CHANG, D.M. (1986) Notes on stochastic shales; from outcrop to simulation model. In: *Reservoir Characterization* (Ed. by L.W.Lake and H.B.Jr. Caroll), Academic Press inc., 445-486.

HALDORSEN, H.H. AND LAKE, L.W. (1984) A new approach to shale management in field-scale models. *Soc. Petrol. Eng. Journ.*, **24**, 447-457.

HALVORSEN, C. AND HURST, A. (1990) Principles, practice and applications of laboratory minipermeametry. In: *Advances in Core Evaluation, Accuracy and Precision in Reserves Estimation*, (ed. by P.F. Worthington), Gordon & Breach, 521-549.

HARMS, J.C.; MACKENZIE, D.B. AND MCCUBBIN, D.G. (1963) Stratification in modern sands of the Red River, Louisiana. *Journ. of Geology*, **71**, 566-580.

HARTKAMP, C.A.; ARRIBAS, J. AND TORTOSA, A. (1993) Grain size, composition, porosity and permeability variations within cross-bedded sandstones in Tertiary fluvial deposits, Central Spain, *Sedimentology*, in press.

HARTKAMP, C.A. AND DONSELAAR, M.E. (1993) Permeability patterns in point-bar deposits: Tertiary Loranca Basin, Central Spain. In: *The Geological Modelling of Hydrocarbon Reservoirs* (Ed. by S. Flint and I. Bryant), Spec. Publs Int. Ass. Sediment., Blackwell Scientific Publ., Oxford, **15**, 157-168.

HEWETT, T.A. AND BEHRENS, R.A. (1990) Considerations affecting the scaling of displacements in heterogeneous permeability distributions. *Paper presented at the Soc. of Petrol Eng. Annual Techn. Conf., New Orleans*, Paper SPE 20739, **September 23-26.**

HJELMELAND, O.S. AND LARRONDO, L.E. (1986) Experimental investigation of the effects of temperature, pressure, and crude oil composition on interfacial properties. *Soc. Petrol. Engineering Reservoir Engineering*, **July**, 321-328.

HÖCKER, C., EASTWOOD, K.M., HERWEIJER, J.C. AND ADAMS, J.T. (1990) Use of dipmeter data in clastic sedimentological studies. *Bull. Am. Assoc. Petrol. Geol.*, **74**, 105-118.

HOPKINS, J.C., WOOD, J.M. AND KRAUSE, F.F. (1991) Waterflood response of reservoirs in an estuarine valley fill: Upper Manville G, U, and W Pools, Little Bow Field, Alberta, Canada. *Bull. Am. Assoc. Petrol. Geol.*, **75**, 1064-1088.

HURST, A. AND ROSSVOLL, K.J. (1991) Permeability variations in sandstones and their relationship to sedimentary structures. *Reservoir Characterisation II* (Ed. by L.W. Lake, H.B. Carroll Jr. and T.C. Wesson), Academic Press, San Diego, California, 166-196.

INGERSOLL, R.V. (1983) Petrofacies and provenance of a late Mesozoic forearc basin, northern and central California. *Bull. Am. Ass. Petrol. Geol.*, **67**, 1125-1142.

ISAAKS, E.H. AND SHIVASTAVA, R.M. (1989) Applied Geostatistics, Oxford University Press., 561 pp.

JACOBSEN, T. & RENDALL, H. (1989) Permeability patterns in some fluvial sandstones. An outcrop study from Yorkshire, North East England. *Paper presented at the Niper conference, Dallas, 1989.*

JACQUIN, C.G., HENRIETTE, A. AND GUERILLOT, D. (1991) Heterogeneity and effective permeability of porous rocks: experimental and numerical investigations. In: *Reservoir Characterization II* (Ed. by L.W. Lake, H.B. Carroll Jr. and T.C. Wesson), Academic Press, San Diego, California, 662-664.

JENSEN, J.L. (1990) A model for small-scale permeability measurement with applications to reservoir characterization. In: *Proceedings of Seventh Symposium on Enhanced Oil Recovery, Tulsa*, SPE/DOE 20265, April 22-25.

JENSEN, L.J.; HINKLEY, D.V. AND LAKE, L.W. (1987) A statistical study of reservoir permeability: Distributions, correlations and averages, Soc. of Petrol. Eng. Form. Eval., December, 461-468.

JOHNSON, H.D. AND KROL, D.E. (1984) Geological modeling of a heterogeneous sandstone reservoir: Lower Jurassic Statfjord Formation, Brent Field. In: *Proceedings of SPE 59th Annual Technical Conference and Exhibition, Paper 13050*, Houston, Texas, september 16-19, 1-6.

JONES, S.C. (1972) A rapid accurate unsteady-state klinkenberg permeameter, *Soc. Petrol. Eng. Journ.*, **October**, 383.

JONES, J.R. JR., SCOTT, A.J. AND LAKE, L.W. (1984) Reservoir Characterization for numerical simulation of Mesaverde Meanderbelt Sandstone, Northwestern Colorado. In: *Proceedings of SPE 59th Annual Technical Conference and Exhibition, Paper 13052*, Houston, Texas, 14.

JONES, J.R. JR., SCOTT, A.J. AND LAKE, L.W. (1987) The geologic aspect of reservoir Characterization for numerical simulation: Mesaverde Meanderbelt Sandstone, Northwestern Colorado. *Soc. of Petrol. Eng. Formation Evaluation*, **March**, 97-106.

JOPLIN, A.V. (1965) Laboratory study of the distribution of grain sizes in cross-bedded deposits. In: Primary Sedimentary Structures and Their Hydrodynamic Interpretation (Ed. by Middleton, G.V.) *Soc. Economic Paleontol. Mineral. Spec. Publ.*, **12**, 53-65.

JOPLIN, A.V. (1967) Origin of laminae deposited by the movement of ripples along a streambed: A laboratory study. *Journ. of Geology*, **75**, 287-305.

JORDAN, D.W. AND PRYOR, W.A. (1992) Hierarchical levels of heterogeneity in a Mississippi river meander belt and application to reservoir systems. *Am. Assoc. Petrol Geol. Bull.*, **76**, 1601-1624.

KASAP, E. AND LAKE, L.W. (1990)[1] Calculating the effective permeability tensor of a gridblock. *Soc. of Petrol. Eng. Formation Evaluation*, **June**, 192-200.

KASAP, E. AND LAKE, L.W. (1990)[2] Dynamic effective relative permeabilities for crossbedded flow units. *Paper presented at Soc. of Petrol. Eng. DOE seventh Symposium on Enhanced Recovery, Tulsa*, Paper SPE/DOE 20179, **April 22-25.**

KEIJZER, P.P.M. AND VRIES, A.S. DE (1990) Imbibition of surfactant solutions. *Paper presented at the Soc. of Petrol. Eng. DOE Seventh Symposium on Enhanced Recovery*, Tulsa, Paper SPE/DOE 20222, **April 22-25.**

KEIJZER, J.H. AND KORTEKAAS, T.F.M. (1990) Comparison of deterministic and probabilistic simulation models of channel sands in the Statfjord Reservoir, Brent Field. In: *Proceedings of Soc of Petrol Eng. EUROPEC 90*, The Hague, The Netherlands. SPE 20947, October, 255-261.

KING, M.J. (1987) Viscous fingering and probabilistic simulation. In:*Proceedings of the 62th Soc. Petrol. Engineers Annual Technical Conference and Exhibitions, Dallas*, SPE 16708, September 27-30.

KING, M.J. AND SCHER, H. (1985) Probabilistic stability analysis of multiphase flow in porous media. In: *Proceedings of the 60th Soc. Petrol. Engineers Annual Technical Conference and Exhibitions, Las Vegas*, SPE 14366, September 22-25.

KIRSCHBAUM, M.A. AND MCCABE, P.J. (1992) Controls on the accumulation of coal and on the development of anastomosed fluvial systems in the Cretaceous Dakota Formation of Southern Utah. *Sedimentology*, **39-4**, 581-598.

KLINKENBERG, L.J. (1941) The permeability of porous media to liquids and gasses. *Drilling and Production Practices*, API, 200 pp.

KOCBERBER, S. AND COLLINS, R.E. (1990) Impact of reservoir heterogeneity on initial distributions of hydrocarbons. In: *Proceedings of 65th Soc. Petrol Engineers Annual Techn. Conference and Exhibitions, New Orleans*, SPE 20547, September 23-26.

KOK, W. (1982) De bepaling van de permeabiliteit van kernen van de Rijks Geologische Dienst en de ontwikkeling van een vloeistofpermeameter aan de TH Delft. *MSc Thesis*, Delft University of Technology.

KORTEKAAS, T.F.M. (1985) Water/oil displacement characteristics in cross-bedded reservoir zones. *Soc. Petrol. Engineers Journ.*, **December**, 917-926.

KOZENY, J. (1927) Uber kapillaire leitung des wassers in boden. *Sitzber Akad. Wiss. Wien, Math. Naturw. Klasse, Abt. IIa*, **136**, 271-306.

KRUIT, C. (1987) Sedimentologic reservoir study of a steam-drive project in deltaic river sands, East Tia Juana Field, Venezuela. In: *Reservoir Sedimentology* (ed. by R.W. Tillman and K.J. Weber) *SEPM spec. publ.*, **40**, 294-310.

KRUMBEIN, W.C. AND MONK, G.D. (1942) Permeability as a function of the size parameters of unconsolidated sand. *Am. Inst. Min. Met. Eng. Trans.*, **151**, 153-162.

LAKE, L.W. (1989) *Enhanced Oil Recovery*, Prentice hall, Englewood Cliffs, New Jersey, 46 pp.

LE BLANC, R.J. (1977) Distribution and continuity of sandstone reservoirs - part 1. *Journ. of Petr. Techn.*, **July**, 776-804.

LEDEBOER, R.C. (1992) Capillary entrapment in small scale heterogeneous porous media. *MSc Thesis*, Faculty of Mining and Petroleum Engineering, Delft University of Technology, The Netherlands. **May**, 160 pp.

LEEDER, M.R. (1982) *Sedimentology, Process and Product*. George Allen and Unwin, London, pp. 344.

LEEDER, M.R. AND ALEXANDER, J. (1987) The origin and tectonic significance of asymmetrical meander-belts. *Sedimentology*, **34**, 217-226.

LEOPOLD, L.B. AND MILLER, J.P. (1964) *Fluvial Processes in Geomorphology*. Freeman, San Fransisco, pp. 522.

LEOPOLD, L.B. AND WOLMAN, M.G. (1957) River channel patterns: braided, meandering and straight. *Prof. pap. U.S.geol. Surv.*, **282-B**, pp. 85.

LEVERETT, M.C. (1941) Capillary behaviour in porous solids. *Transactions AIME*, **155**, 155-175.

LEWIS, J.J.M. (1988) Outcrop-derived quantitative models of permeability heterogeneity for genetically different sand bodies. *S.P.E. Paper 18153 presented at the 63rd Ann. Techn. Conf., Houston, Oct. 25,*

LOWE, D. (1975) Water escape structures in coarse grained sediments. *Sedimentology*, **22**, 157-204.

LYELL, C. (1837) *Principles of Geology*. John Murray, London, 4 volumes.

Martinius, A.W. and Nieuwenhuijs, R. (1993) Flow-unit Characterization of permeability distribution and heterogeneities of distal fluvial fan deposits, Loranca Basin, Spain. (in prep.).

MARZO, M., NIJMAN, W. AND PUIGDEFABREGAS, C. (1988) Architecture of the Castissent fluvial sheet sandstones, Eocene, South Pyrenees, Spain. *Sedimentology*, **35**, 719-738.

MELROSE, J.C. AND BRANDNER, C.F. (1974) The role of capillary forces in determining microscopic displacement efficiency for oil recovery by water flooding. *Canadian Petr. Eng.*, **October**, 54-62.

MIALL, A.D. (1978) *Fluvial Sedimentology*. Canadian Society of Petroleum Geologists, Calgary, Alberta, Canada, **August**, pp. 869.

MILLER, D.D., MCPHERSON, J.G. AND COVINGTON, T.E. (1990) Fluviodeltaic Reservoir, South Belridge Field, San Joaquin Valley, California. In: *Sandstone Petroleum Reservoirs* (Ed. by J.H. Barwis, J.G. McPherson and J.R.J. Studlick), Springer-Verlag, New York, 583 pp.

MITRA, S., BEARD, W.E. (1980) Theoretical models of porosity reduction by pressure solution for well-sorted sandstones. *J. Sedim. Petrol.*, **50**, 1347-1360.

MOHANTY, K.K., DAVIS, H.T. AND SCRIVEN, L.E. (1987) Physics of oil entrapment in water-wet rock. *Soc. Petrol. Engineers Reservoir Engineering*, **Februari**, 113-128.

MORINEAU, Y., SIMANDOUX, P. AND DUPUY, M. (1965) Etude des heterogeneities de permeabilities dans les milieux poreux. In: *Compte Rendu du Ileme Colloque de l'Association de Recherche sur les Techniques de Forage et de Production*, May 31-June 4, Rueil, 273 pp.

MORROW, N.R. (1971) Small-scale packing heterogeneities in porous sedimentary rocks. *Bull. Am. Assoc. Petrol. Geol.*, **55**, 514-522.

MORROW, N.R. (1990) Wettability and its effect on oil recovery. *Journ. Petrol. Techn.*, **December**, 1476-1484.

MOWBRAY, T. DE AND VISSER, M.J. (1984) Reactivation surfaces in subtidal channel deposits, Oosterschelde, SW Netherlands. *Journ. of Sed. Petrol.*, **54**, 811-824.

MYROW, P.M. AND SOUTHARD, J.B. (1990) Combined-flow model for vertical stratification sequences in shallow marine storm deposited beds. *Journ. of Sed. Petrol.*, **61-2**, 202-210.

NADEAU, P.H. AND HURST, A. (1991) Application of back-scattered electron microscopy to the quantification of clay mineral microporosity in sandstones. *Journ. of Sed. Petrol.*, **61**, 921-925.

NAGTEGAAL, P.J.C. (1980) Diagenetic models for predicting clastic reservoir quality. *Revista del Instituto de Investigaciones Geologicas*, **34**, 5-19.

NEASHAM, J.W. (1977) The morphology of dispersed clay in sandstone reservoirs and its effect on sandstone shaliness, pore space and fluid flow properties. In: *Proceedings of the 52nd Soc. Petrol Engineers Annual Technical Conference and Exhibitions, Denver,* SPE 6858, October 9-12.

NEDERLANDSE AARDOLIE MAATSCHAPPIJ B.V. (NAM) AND RIJKS GEOLOGISCHE DIENST (RGD) (1980) *Stratigraphic Nomenclature of The Netherlands*, Verhandelingen van het K.N.G.M.G., **32**, 77 pp.

NIO, S.D. AND HUSSAIN, S.T. (1984) Sedimentological framework of Late Pliocene and Pleistocene alluvial deposits in the Bhittani range, Pakistan. *Geologie en Mijnbouw*, **63**, 55-70

NORTH, C.P. (1990) Characterization of mixed fluvial-aeolian reservoirs: Outcrop studies on the Cutler Formation (Permian) in S.E.Utah, U.S.A. *Report*, Faculty of Mining and Petroleum Engineering, Delft University of Technology, The Netherlands, **October**.

OLSEN, H. (1988) The architecture of a sandy braided-meandering river system: An example from the Lower Triassic Solling Formation (M. Buntsandstein) in West Germany. *Geologische Rundschau*, **77**, 797-814.

OLSEN, H. (1989) Sandstone-body structures and emphemeral stream processes in the Dinosaur Canyon Member, Moenave Formation (lower Jurassic), Utah, U.S.A. *Sediment. Geol.* **61**, 207-221.

PALLATT, N., WILSON, M.J. AND MCHARDY, W.J. (1984) The relationship between permeability and the morphology of diagenetic illite in reservoir rocks. *Journal of Petroleum Technology*, **36**, 2225-2227.

PETTIJOHN, F.J., POTTER, P.E. AND SIEVER, R. (1973) *Sand and Sandstone*, Springer-Verlag, New York, 618 pp.

PICKELL, J.J., SWANSON, B.F. AND HICKMAN W.B. (1966) Application of air-mercury and oil-air capillary pressure data in the study of pore structure and fluid distribution. *Soc. Petrol Engineers Journ.*, **March**, 55-61.

PITTMAN, E.D. (1979) Porosity, diagenesis and productive capability of sandstone reservoirs. In: *Aspects of Diagenesis* (Ed. by P.A. Scholle and P.R. Schluger, *Spec. Publs Soc. Econ. Paleont. Miner.*, **26**, 159-173.

PRYOR, W.A. (1973) Permeability-porosity patterns and variations in some Holocene sand bodies. *Bull. Am. Assoc. Petrol. Geol.*, **57**, 162-189.

PURCELL, W.R. (1949) Capillary pressures - Their measurement using mercury and the calculation of permeability therefrom. *Petrol. Transactions AIME*, **February**, 39-48.

QUI YINAN, CHEN ZIQI AND XU SHICE (1982) Waterflooding of channel sandstone reservoirs. In: *Proceedings of SPE Internat. Meeting on Petroleum Engineering, Paper 10559*, Beijing, China, **march 19-22**, 15-42.

RAVENNE, C., ESCHARD, R., MATHIEU, Y., MONTADERT, L. AND RUDKIEWICZ, J-L. (1987) Heterogeneities and geometry of sedimentary bodies in a Fluvio-Deltaic Reservoir. In: *Proceedings of SPE 62nd Annual Technical Conference and Exhibition, Paper* 16752, Dallas, Texas, september 27-30, 115-122.

RENDU J.M. (1979) Normal and Lognormal Estimation. *Mathematical Geology*, **11-4**, 407-422.

RHIJN, D. VAN (1990) The residual oil distribution in water flooded fluviatile cross-bedding, *MSc Thesis*, Faculty of Mining and Petroleum Engineering, Delft University of Technology, The Netherlands, **April**, 107 pp.

RIJN, F.C.M. VAN (1992) Minipermeametry; A calibration of two steady-state minipermeameters. *MSc Thesis*, Mining and Petroleum Engineering, Delft University of Technology, The Netherlands, **April**, 132 pp.

RINGROSE, P.S., SORBIE, K.S., CORBETT, P.W.M. AND JENSEN, J.L. (1993) Immiscible flow behaviour in laminated and cross-bedded sandstones. *Journ. of Petrol. Science and Engineering*, **9/2**, 103-124.

RITTENHOUSE, G. (1971) Mechanical compaction of sands containing different percentages of ductile grains: a theoretical approach. *Bull. Am. Ass. Petrol. Geol.*, **55**, 92-96

ROBERTSON RESEARCH INTERNATIONAL LTD, ENERGY RESOURCE CONSULTANTS LTD AND SCOTT, PICKFORD AND ASSOCIATES LTD. (1985) *The Permian, Triassic and Carboniferous Reservoirs of the Dutch North Sea: A Petroleum Geology and Engineering Evaluation.* 5 volumes incl. maps and well logs.

ROOS, B.M. AND SMITH, B.J. (1983) Rotliegend and Main Buntsandstein gas fields in block K/13 - a case history. *Geologie en Mijnbouw*, **62**, 75-83.

RUBIN, D.M. (1988) *Cross-bedding, Bedforms and Paleocurrents*. Soc. Econ. Paleont. Mineral., Tulsa, pp.187.

RUST, B.R. (1978) Depositional models for braided alluvium. In: *Fluvial Sedimentology* (Ed. by A.D. Miall), *Can. Soc. Petrol. Geol. Mem.* **5**, Calgary, 605-625.

SALATHIEL, R.A. (1972) Oil recovery by surface film drainage in mixed wettability rocks, In: *Proceedings of Soc. of Petrol Engineers 47th Annual FALL Meeting*, SPE 4104, 12 pp.

SCHMIDT, V. AND MCDONALD, D.A. (1979) The role of secondary porosity in the course of sandstone diagenesis. In: *Aspects of Diagenesis* (Ed. by P.A. Scholle and P.R. Schluger), *Spec. Publs Soc. Econ. Paleont. Miner.*, **26**, 175-207.

SCHOWALTER, T.T. (1979) Mechanics of secondary hydrocarbon migration and entrapment. *Bull. Am. Ass. Petrol. Geol.*, **63**, 723-760.

SCHUMM, S.A. (1968) Speculations concerning paleohydrologic controls of terrestrial sedimentation. *Geol. Soc. Am. Bull.*, **79**, 1573-1588.

SCHUMM, S.A. (1977) *The Fluvial System*. John Wiley & Sons, New York, pp. 338.

SHANLEY, K.W., MCCABE, P.J. AND HETTINGER, R.D. (1992) Tidal influence in Cretaceous fluvial strata from Utah, USA: a key to sequence stratigraphic interpretation. *Sedimentology*, **39**, 905-930.

SMITH, D.G. AND SMITH, N.D. (1980) Sedimentation in anastomosed river systems : examples from alluvial valleys near Banff, Alberta. *Journ. Sedim. Petrol.*, **50**, 157-164.

Smith, S.A. (1990) The sedimentology and accretionary styles of an ancient gravel-bed stream: the Budleigh Salterton Pebble Beds (Lower Triassic), southwest England. *Sedimentary Geology*, **67**, 199-219.

SHANMUGAM, G. (1985) Significance of secondary porosity in interpreting sandstone composition. *Bull. Am. Assoc. Petrol. Geol.*, **69**, 378-384.

SINGH, L., AHMED, A.E., VERMA, R.P. AND MURTHY, R.V.S. (1991) Depositional pattern and reservoir heterogeneity of Tipam Sand-2, Lakwa Field, India. *Geologie en Mijnbouw*, **70**, 355-371.

SLATT, R.M. AND HOPKINS, G.L. (1990) Scaling geologic reservoir description to engineering needs. *Journ. Petrol. Techn.*, **Februari**, 202-210.

SLICHTER, C.S. (1899) Theoretical investigation of the motion of ground waters. *U.S. Geol. Survey 19th Ann. Report*, **2**, 295-384.

SOETERS, M.M. (1992) Statistical analysis of small-scale permeability measurements at fluvial deposits in the Loranca Basin, Spain. *MSc thesis*, Faculty of Mining and Petroleum Engineering, Delft University of Technology, The Netherlands, 48 pp.

SOUTHARD, J.B. AND BOGUCHWAL, L.A. (1990) Bed configurations in steady unidirectional water flows. Part 1. Scale model study using fine sands, Part 2. Synthesis of flume data, Part 3. Effects of temperature and gravity. *Journal of Sed. Petrol.*, **60-5**, 649-686.

STALKUP, F.I. (1986) Permeability variations observed at faces of crossbedded sandstone outcrops. In: *Reservoir Characterization* (Ed. by L.W.Lake & H.B.Carroll Jr.), pp. 141-175, Academic Press, Inc., London, 650 pp.

STOUT, J.L. (1964) Pore geometry as related to carbonate stratigraphic traps. *Bull Am. Ass. Petrol. Geol.*, **48**, 329-337.

SUTHERLAND, W.J., HALVORSEN, C., HURST, A., MCPHEE, C.A., ROBERTSON, G., WHATTLER, P.R. AND WORTHINGTON, P.F. (1991) Recommended practice for probe permeametry. *Paper presented at the Minipermeatry in Reserv. Studies Conference, Edinburgh*, **June 27-28**, 26 pp.

SZPAKIEWICZ, M., MCGEE, K. AND SHARMA, B. (1987) Geological problems related to characterization of clastic reservoirs for EOR. *SPE Formation Evaluation*, **December**, 449-460.

THOMAS, C.E., MAHONEY, C.F. AND WINTER, G.W. (1987) Water-injection pressure maintenance and waterflood processes. *Petroleum Engineering Handbook* (ed. by H.B. Bradley), Richardson, U.S.A., 44/1-52.

THOMEER, J.H.M. (1960) Introduction of a pore geometrical factor defined by the capillary pressure curve. *Petroleum Transactions, AIME*, **219**, 354-358.

TYLER, N., BARTON, M.D. AND FINLEY, R.J. (1991) Outcrop Characterization of flow unit and seal properties and geometries, Ferron Sandstone, Utah. In: *Proceedings of SPE Annual Technical Conference and Exhibition*, Paper 22670, Dallas, Texas, october 6-9, 127-134.

TYLER, N. (1988) New oil from old fields. *Geotimes*, **July**, 8-10.

VEEN, F.R. VAN (1977) Prediction of permeability trends for water-injection in a channel-type reservoir, Lake Maracaibo, Venezuela. *S.P.E. Paper 6703.*

VISSER, M.J. (1980) Neap-spring cycles reflected in Holocene subtidal large-scale bedform deposits: a preliminary note. *Geology*, **8**, 543-546.

WAAL, J.A. DE, BIL, K.J., KANTOROWICZ, J.D. AND DICKER, A.I.M. (1988) Petrophysical core analysis of sandstones containing delicate illite, *Log Analyst*, **september-october**, 317-331.

WARDLAW, N.C. AND CASSAN, J.P. (1978) Estimation of recovery efficiency by visual observation of pore systems in reservoir rocks. *Bull. of Canadian Petrol. Geol.*, **26**, 572-585.

WARDLAW, N.C. AND CASSAN, J.P. (1979) Oil recovery efficiency and the rock-pore properties of some sandstone reservoirs. *Bull of Canadian Petrol. Geol.*, **27**, 117-138.

References

WARDLAW, N.C. AND TAYLOR, R.P. (1976) Mercury capillary pressure curves and the interpretation of pore structure and capillary behaviour in reservoir rocks. *Bull. Canadian Petrol. Geol.*, **24**, 225-262.

WEBER, K.J. (1971) Sedimentological aspects of oil fields in the Niger delta. *Geologie en Mijnbouw*, **50**, 559-576.

WEBER, K.J. (1982) Influences of common sedimentary structures on fluid flow in reservoir models. *Journ. Petrol. Techn.*, **273**, 665-672.

WEBER, K.J. (1986) How heterogeneities affects oil recovery. In: *Reservoir Characterization* (Ed. by L.W. Lake and H.B.Jr. Carroll), Academic Press Inc., 487-544.

WEBER, K.J., EIJPE, R., LEIJNSE, D. AND MOENS, C. (1972) Permeability distribution in a holocene distributary channel-fill near Leerdam (The Netherlands). *Geologie en Mijnbouw*, **51-1**, 53-62.

WEBER, K.J. & GEUNS, L.C. VAN (1990) Framework for constructing clastic reservoir simulation models. *Journ. of Petrol. Techn.*, **October**, 1248-1297.

WERREN, E.G., SHEW, R.D., ADAMS, E.R. AND STANCLIFFE, R.J. (1990) Meander-belt reservoir geology, Mid-Dip Tuscaloosa, Little Creek Field, Mississippi. In: *Sandstone Petroleum Reservoirs* (Ed. by J.H. Barwis, J.G. McPherson and J.R.J. Studlick), Springer-Verlag, New York, 583 pp.

WIJHE, D.H. VAN; LUTZ, M. AND KAASSCHIETER, J.P.H. (1980) The Rotliegend in The Netherlandst and its gas accumulations. *Geologie en Mijnbouw*, **March**, 3-24.

XUE PEIHUA (1986) A point bar facies reservoir model - semi-communicated sandbody. In: *Proceedings of SPE International Meeting on Petroleum Engineering, Paper 14837*, Beijing, China, march 17-20, p. 103-115.

YADAV, G.D., DULLIEN, F.A.L., CHATZIS, I. AND MACDONALD, I.F. (1987) Microscopic distribution of wetting and nonwetting phases in sandstones during immiscible displacements. *Soc. Petrol. Engineers Reservoir Engineering*, **may**, 137-147.

ZUFFA, G.G. (1980) Hybrid arenites: their composition and classification. *J. Sedim. Petrol.*, **50**, 21-29.

ACKNOWLEDGEMENTS

Firstly, I wish to express my gratitude to Prof.ir. K.J. Weber for his continuous support, enthusiasm and stimulating ideas.

A matter of utmost importance was the financial support given by oil companies (Shell, Texaco and B.P.) and the Technical University in Delft for fieldwork and for the acquisition of the minipermeameter equipment.

The Geological Survey of the Netherlands (RGD) in Haarlem as well as the Nederlandse Aardolie Maatschappij (NAM) in Assen (the Netherlands) are kindly thanked for permitting me to measure permeability at cored sections of gas-reservoir rock. Special thanks are due to drs. D. van Doorn (RGD) and dr. T.J.A. Reyers and drs. M. Brolsma (NAM) for their interest and support. P. van de Heuvel and J. Penninga are thanked for their help in the NAM laboratory. T. Robson of GAPS Nederland bv. is thanked for his support in the GAPS laboratory.

I am indebted to Margarita Díaz Molina for all her lessons in the fluvial sedimentology of the Loranca Basin, Central Spain and for her valuable discussions in the field. José Arribas Mocoroa and Amparo Tortosa Lopez are thanked for their guidance, help and companionship during the two years fieldwork and during the preparation of our paper. ¿Somos amigos ò no?

I am grateful to all members of the GEORES group in Delft for making work so pleasant. Drs. Rick Donselaar is thanked for his encouragement and support, especially during my first years in Delft and the fieldwork in 1989.

I appreciated the help of many colleagues at the Mining Faculty, who even helped me during the weekend if it was necessary. Special thanks are due to Rudy Ephraïm and Aad van Dijk.

I am specially thankful to dr.ir. Diederik van Batenburg and dr. Hans Bruining for their interest in the subject of two-phase fluid flow through cross-beds and for their never ending enthusiasm for modelling and discussing results.

I thank ir. Dick van Rijn (Multiflood simulator), ir. Frank van Rhijn (Minipermeametry), ir. Mireille Soeters (Statistics) for their M.Sc. work, which was carried out in the framework of this study. Ir. Hilde Bakken from Stavanger, Norway and ir. Robbert Ledeboer are thanked for their M.Sc. study in Reservoir Engineering. Their results form significant contributions to this thesis.

Frieda Gogelein is thanked for her comradeship during the fieldwork in 1990, which made that fieldseason very enjoyable.

Last but not least I like to thank Peter for his enormous support and patience during the years. Willemijn is thanked for having been a joyful distraction during the writing of this thesis.

SAMENVATTING

Als gevolg van onregelmatigheden in een reservoirgesteente zal een hoeveelheid winbare olie achterblijven. Deze onregelmatigheden, ook wel heterogeniteiten genoemd, worden voor een belangrijk deel gevormd gedurende de afzetting van sedimenten, welke later het reservoirgesteente vormen. Olie wordt dikwijls uit een reservoir gedreven met behulp van water. Hierna blijft in fossiele rivierafzettingen vaak een onverwacht hoog percentage olie achter in vergelijking met fossiele kustafzettingen met identieke reservoir eigenschappen. In rivier zanden (fluviatiele zanden) komt één type heterogeniteit in zeer hoge mate voor, namelijk scheve gelaagdheid. Tot nog toe was er erg weinig bekend over de werkelijke invloed van deze scheve gelaagdheid op het achterblijven van winbare olie. Het doel van de hier gepresenteerde studie is om de kennis te vergroten over de invloed van deze scheve gelaagdheid op de water/olie verplaatsing en op het achterblijven van hoeveelheden winbare olie in een fluviatiel reservoir.

Scheve gelaagdheid ontstaat door de afzetting van ribbels op de rivierbodem. Deze ribbels bewegen met de stroomrichting mee en verplaatsen zich door een continu proces van afzetting van zand aan de lijzijde van de ribbel. Het zand accumuleert aan de top en glijdt vervolgens met enige tussenpozen aan de lijzijde naar beneden. Hierdoor ontstaan dunne laagjes van gegroepeerde korrels die onder een hoek van zo'n 30° ten opzichte van het horizontale vlak staan, de scheve gelaagdheid. De laagjes lopen aan de onderzijde uit in een bodemlaag met meer fijnkorrelig sediment, dat uit suspensie is neergedwarreld. Deze bodemlaag bedekt het oorspronkelijke reliëf van de rivierbodem waar de ribbel overheen beweegt. Vaak is het reliëf door turbulente stromingen vlak voor de ribbel in een soort komvorm uitgesleten en heeft de ribbel zelf de vorm van een halve maan. In dit geval spreken we van trogvormige ribbels. Door een meer gelijkmatige stroming van het water zouden ribbels ook een meer rechtkammige structuur kunnen bezitten. Trogvormige scheefgelaagde sets hebben een gemiddelde dikte:breedte:lengte verhouding van 1 : 6.5 : 20. De dikte die in fossiele afzettingen gemeten wordt varieert van 0.2 tot 1 meter. De bodemlaag beslaat 10 tot 30% van de totale dikte van de scheefgelaagde set. De diktes van individuele laagjes in de scheefgelaagde set variëren tussen de 0.1 and 1.5 cm.

De trogvormige structuur en het gelamineerde karakter van de scheve gelaagdheid maakt het tot een belangrijke sedimentaire heterogeniteit in een reservoirgesteente. Doordat de bodemlaag uit fijne korrels bestaat en de scheefgelaagde set uit een afwisseling van laagjes met grovere en laagjes met fijnere korrels, is een niet continue doorlaatbaarheid voor olie en water te verwachten. Deze doorlaatbaarheid, ook wel permeabiliteit genoemd, wordt immers bepaald door de doorgangen tussen de korrels. Hoe groter de korrels, des te groter de doorgang tussen de korrels. De gemiddelde korrelgrootte in de scheefgelaagde sets varieert van fijn silt tot medium/grof zand. Het verschil in korrelgrootte in de scheefgelaagde set tussen de groverkorrelige laagjes en de fijnerkorrelige laagjes bedraagd gemiddeld een factor 1.5, waarbij het groverkorrelige laagje slechter gesorteerd is (korrelgroottes lopen meer uiteen).

Met behulp van een minipermeameter zijn zeer nauwkeurig permeabiliteiten gemeten binnen een kubieke centimeter gesteente. Metingen aan fluviatiele gesteenten in centraal Spanje gaven waarden tussen de 0.5 en de 20 Darcy. Permeabiliteiten gemeten aan kernen van reservoirgesteenten uit de Nederlandse ondergrond gaven waarden tussen de 10 millidarcy tot enkele honderden millidarcy te zien. Gemiddelde contrasten in permeabiliteit tussen de bodemlaag en de grovere lagen uit de scheefgelaagde set varieerden met een factor 2 in oppervlakte gesteenten, en met een factor 2 tot 30 in reservoir kernen. De grotere contrasten in de reservoir kernen zijn het gevolg van een verschillende mate van dichtgroei van poriën tussen afzonderlijke laagjes in de scheefgelaagde set en de bodemlaag. Deze dichtgroei van poriën werd veroorzaakt door poriënvullende mineralen (kaoliniet) en cement (anhydriet).

Korrelgrootte en sortering van een sediment bepalen de gemiddelde poriën grootte en de mate waarin de poriëngrootte varieert (sortering van poriëngrootte), en daarmee de capillaire kracht karakteristiek van het sediment. In een reservoir waar water sterker gebonden wordt aan het korreloppervlak dan olie, zal aan het water/olie front het water het sterkst opgezogen worden (imbiberen) in die delen van het reservoir waar korrelgrootte en poriënruimte het kleinst is. Dit betekent dat in scheefgelaagde sets imbibitie van water het sterkst zal zijn in de fijnkorrelige bodemlaag en de fijnkorrelige laagjes van de scheefgelaagde set. De mate van capillaire werking is het sterkst op het grensvlak van de twee verschillende fasen, bij lage waterdruk. Bij hogere waterdrukken krijgt de vloeistofdruk (visceuse kracht) de overhand. Achter het grensvlak neemt de

verzadiging van olie af ten opzichte van het voortschrijdende water en zal een steeds mindere invloed van de capillaire kracht merkbaar zijn. In twee aangrenzende laagjes met verschillende poriëngrootte en sortering, zal door een verschillende capillaire kracht karakteristiek de begin verzadiging en eind verzadiging van olie/water ongelijk zijn.

Computer simulaties en laboratorium experimenten hebben uitgewezen dat winbare hoeveelheden olie aanvankelijk achterblijven in de groverkorrelige laagjes van de scheefgelaagde sets op het moment dat de omliggende fijnerkorrelige laagjes en bodemlaag een hoge water verzadiging bereikt hebben, waarbij de capillaire kracht nog niet tot nul gereduceerd is. De verzadigingsgraad van de winbare olie die aanvankelijk achterblijft in de groverkorrelige laagjes wordt bepaald door de variatie in poriënruimte (sortering) in die laag, waarbij een slechtere sortering leidt tot een niet-maximale olie verzadiging.

In de experimentele en numerische modellen van water/olie verplaatsing door een scheefgelaagde heterogeniteit, werd een contrast in permeabiliteit van een factor 25 vastgesteld tussen de bodemlaag en de groverkorrelige laagjes van de scheefgelaagde set. In de laboratorium experimenten werden bijna identieke viscositeiten voor olie en water gekozen om een stabiel water/olie front te verwezenlijken. Na een waterinjectie van 0.77 poriënvolume in het model bleef winbare olie aanvankelijk achter in de groverkorrelige laagjes. De achtergebleven winbare olie werd na een doorgaande waterinjectie van 5-7 poriënvolumes uiteindelijk geheel geproduceerd en er bleef in alle verschillende zones in het model een residuale verzadiging over (niet-winbare verzadiging). De richting van waterverplaatsing ten opzichte van de stand en de geometrische karakteristieken van de heterogeniteit, bleek niet van invloed te zijn op het aanvankelijk achterblijven van olie (onder de aanname dat gravitatie geen invloed uitoefent). De snelheid waarmee water geïnjecteerd werd in het model bleek een positieve invloed te hebben op de snelheid waarmee de aanvankelijk achtergebleven olie uiteindelijk geheel geproduceerd werd.

Er kan uit de resultaten van het onderzoek geconcludeerd worden dat, in theorie, winbare olie achter kan blijven in groverkorrelige laagjes van scheefgelaagde sets in fluviatiele reservoirs. Een voorwaarde is dat de permeabiliteits contrasten in het betreffende reservoir groot zijn (bv. door diagenese). Dit effect wordt echter kleiner bij zeer langdurig verdringen van olie met water.